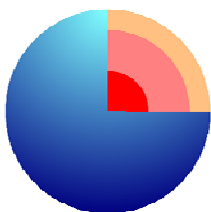# Depositional Control on Diagenetically-induced Heterogeneity in

Triassic Red Beds Sandstones

Tesis doctoral – PhD Thesis –

Saturnina Henares Ladrón de Guevara

Junio/June 2016

ugr | Universidad de Granada

Programa Doctorado
Ciencias de la Tierra

SEDIMENTARY
RESERVOIRS
WORKGROUP

El doctorando Saturnina Henares Ladrón de Guevara y los directores de la tesis César Viseras Alarcón y Giuseppe Cultrone Garantizamos, al firmar esta tesis doctoral, que el trabajo ha sido realizado por el doctorando bajo la dirección de los directores de la tesis y hasta donde nuestro conocimiento alcanza, en la realización del trabajo, se han respetado los derechos de otros autores a ser citados, cuando se han utilizado sus resultados o publicaciones.

Granada, 19 de Mayo de 2016

Director/es de la Tesis

Fdo.:

Doctorando

Fdo.:

Contents

4.1 Part I

4.2 Part II

5. Complementary contribution

LIST OF ACRONYMS

aK^+/aH^+, potassium ion activity/hydrogen ion activity

BSE, Back-Scattered Electrons

Ca^+, calcium ion

CCS, Carbon Capture and Storage

CEPL, Cementation Porosity Loss

CIC, Centro de Instrumentación Científica

CL, Cold-cathodoluminescence

COPL, Compaction Porosity Loss

EDX, Energy Dispersive X-ray Spectrometer

F, Feldspars

Fe^{2+}, iron (II) ion

FESEM, Field Emission Scanning Electron Microscope

H^+, hydrogen ion

I/S, mixed-layer smectite-illite

$I_{compact}$, Compaction Index

IGV, Intergranular Volume

IOR/EOR, Improved/Enhanced Oil Recovery

K, Kf, potassium feldspar

k, Permeability

K^+, potassium ion

Kv/Kh, vertical-to-horizontal permeability

Ln{S/Si}, log-log ratio plot S-Si

Lt, Lithic fragments

mD, mili-Darcy

Mg^+, magnesium ion

MICP, Mercury Injection-Capillary Pressure

Mn^{2+}, manganese (II) ion

Mx, Matrix

Na^+, sodium ion

O/BO, outcrop/behind outcrop characterization

OP, Open Porosity

P, Plagioclase

P1, Primary porosity

P2, Secondary porosity

PPL, Plane-Polarized Light

P-T, Pressure-Temperature

Q, Quartz

Qm, Quartz monocrystalline

Qp, Quartz polycrystalline

R^2, coefficient of determination

Rf, R, r.f., Rock fragments

RQ, Reservoir Quality

RQI, Reservoir Quality Index

RuC, Rip-up clast

SEM, Scanning Electron Microscope

SPB, South Permian Basin

TAGI, Trias Argilo-Gréseux Inférieur

TC, Total Composition

TFC, Total Framework Composition

TIBEM, Triassic red beds of the Tabular Cover of Iberian Meseta

TM, Total Matrix

TYH, Texel-Ijsselmeer High

WAG, Water-Alternating-Gas

XPL, Crossed- Polarized Light

XRD, X-ray Diffraction

XRF, X-ray Fluorescence

EXTENDEND ABSTRACT

Analysis of the spa tial and tem poral ev olution of diagenetic features is of paramount importance f or th e evaluation and modelling o f petrophys ical p arameter distribution in silicic lastic res ervoir ro cks. T he rec ent p roliferation of sof tware f or reservoir quality prediction and m odelling has changed the approach of the industry to the appraisal and recovery phases of hydrocar bons exploration and production. Most of these software focus on specific asp ects as for instance quartz cem entation m odelling which is much more easily pr edictable due to th e chemical conditions of the diagene tic environment in which it develops. A com pletely different task could be to forecast the occurrence and am ount of clay minerals and their im pact on reservoir quality by understanding their distribution within a depo sitional system and their subsequent post-depositional modifications.

Diagenetic patterns are linked to an array of depositional-dependant (depositional fabric, pore-water chem istry, intrabasinal components and bioturbation) and independent (burial-therm al evolution of the basin, res idence tim e in specific P-T conditions) factors which control the furthe r sedim ent modification, from shallow (early) to d eeper bur ial condition s. These ear ly m echanical and che mical proce sses proceed along different pathways directly related to depositionally-governed differences in textu re and com position. Mutual interact ion of depositio nal features and sandstone framework composition with diagenetic proc esses and flu ids determine the com paction intensity, the am ount and types of cem ents, the extent of dissolution and, therefore, the amount of residual prim ary porosity or genera tion of secondary porosity, so eventually permeability and reservoir quality.

All these factors (e.g. depositional envir onment, provenance, clim ate, tectonic) are intimately connected and represent – among others – the n ecessary input parameters to predict and m odel reser voir quality. However, in m any cases inform ation about depositional facies or environment is not fully captured from subsurface core samples. It is therefore of key im portance the use of outcrop rese rvoir analogue studies which provide quantitative, geo-refere nced data sets that serve as input in state-of-the-art forward modelling software of sandstone diagenesis and petrophysical properties.

The aforementioned facts constitute the starting point of this PhD project and the rationale behind the selection of both the st udy areas and the analytical approach. The aim of this Thesis is to redu ce the unc ertainty on RQ m odelling thro ugh a multidisciplinary approach integrating the study of depositional facies and the analysis of early diagenetic process in reservoir-ana logue outcrops and behi nd-outcrop core data analysis. The latter is of particular interest for the hydrocarbon indus try as it remarkably enhances the relatively limited interpretations obtained from traditional core descrip tion by direct outcrop-faced contrast.

The study areas have b een selected according to the relevance of both (i) the represented sedimentary environm ents of in terest for the hydro carbon exploration and (ii) featu res of the outcrops in term s of reservoir an alogues. The selected fluvial depositional environm ents are exposed in th e Triassic succession of C entral SE S pain (herein refe rred as TIBEM) and in the Argana Basin (W estern High Atlas, S W

Morocco) and correspond to: braidplain and floodplain (incl uding overbank and channelized deposits) environm ents in Spanis h area; and braided an d s traight fl uvial systems in Moroccan a rea. Due to for mation geological conditions, such areas are ideal outcrop analogues of a num ber of well-known Triassic rese rvoirs including the T AGI (Trias Argilo-Gréseux Inférieur) reservoirs of North Africa and the Bay of Fundy (Nova Scotia, Canada).

The methodology adopted for the developm ent of this research encom passes: a thorough selection of sam ples accord ing to pre-ex isting and newly acquired sedimentological criteria from outcrop and behind-outcrop core analysis; high-resolution p etrological analys is f ollowing th e up-to-date technique s (e.g. optical and electron m icroscopes, XRD, cathodolum inescence, m icroprobe) and developing done-on-purpose characterization m ethodologies; de termination of the m ain petrophysical parameters (porosity, perm eability and pore size distr ibution) by m ercury inje ction-capillary pressure.

The first part of this res earch has been focused on the Trias sic succession from Central SE Spain aim ing at (i) recognising vertical com positional and textural changes in sandstone samples from the fluvial deposits of floodplain environment of Sequence II to the braided environm ent of Se quence IV and (ii) evaluating th e im pact of such compositional and textural features on diag enetic processes and pore network evolution to (iii) eve ntually clas ify the s tudied sedimentary environm ents according to their potential as reservo ir ro cks. Obtain ed resu lts docum ent a significant matur ity incr ease up-section from floodplain to braidplain environm ent m arked by changes in depositional texture and detr ital com position. Petrograph ic evidences suggest that porosity loss happened during the very ear ly diagenetic stag es through different diagenetic processes according to facies. In floodplain environment, overbank sandstone deposits have been m ainly affected by m echanical com paction and gypsum cementation. The channelized deposits from floodplain include meandering and straight fluvial system s and dis play interm ediate m echanical com paction degree and variable amount and type of dom inant authigenic ph ases depending on targeted depositional facies. In the braidplain environm ent, prim ary porosity is s till well-p reserved with K-feldspar ov ergrowths as the prev ailing cem enting ph ase. Occurren ce of gypsu m-cemented slough channel facies and carbonate -cemented post-sedim entary fractures, where poro sity d rastically drop s, in the br aidplain, de teriorates the p otential of this depositional environment as reservoir rock.

The link between depositionally-controlled pa rameters (i.e. textural features and abundance of intrabasinal com ponents) a nd spatial and tem poral distribution of diagenetic processes has been further inves tigated in meandering channel deposits from Sequence II (Central SE Spain) and braide d and straight fluvial dep osits f rom the Argana Basin (Western High Atlas, SE Morocco).

In the meandering example, the study has been performed on core samples from 4 behind-outcrop wells targeti ng the main depositional facies: channel, point bar, scroll bar and ch ute channel. Besides to trad itional petrographic point cou nt, a done-on-purpose petrographic s emi-quantitative cha racterization of pore spac es has bee n developed. The statistical inte gration of petrographic and pe trophysical data revealed a

major role played by hydraulic sorting proc esses and its effects on the diagenetic evolution and reservoir properties. Obtain ed results show the direct relationship between depositional facies and the abundance and distribution of detrital matrix, which favours m echanical co mpaction b ut inhib its early cem ent precipitation. Multiv ariate statistical pr ocessing of the in tegrated data d emonstrates that larg e (>1 μm) and well-connected primary intergranular pores are th e main contributors to pe rmeability in the more heterogeneous samples. Secondary porosit y seems to be m ostly related to sm aller (<1 μm) and random ly distributed dissoluti on pores. Sedim entological, petrographic and petrophysical data have been integrated to calcu late the Reservoir Quality Index which was then used as input for a determ inistic facies 3D PETREL $^®$ model. Remarkably, the RQI model works perf ectly, enhancing the relationships betw een reservoir properties and facies distribution and identifying both the channel m argin and the scroll bar as the dep ositional facies having the best res ervoir qua lity. The obtain ed model can be therefore used to id entify poten tial pref erential-flow pathways and be successfully applied to Enhanced Oil Rec overy (EOR) stra tegies (water or s team injection).

In braided and straight fluvial deposits from the Argana Basin, occurrence and amount of different types of rip-clasts have a direct a nd substantial control on early diagenetic evolution and subsequent re servoir deterioration. A done-on-purpose classification of these g rains acco rding to the ir composition and m echanical behav iour leads to three m ain types, nam ely: muddy ri p-up clasts; dolom itic muddy rip-up clasts and dolomite crystalline rip-up clasts. Muddy ri p-up clasts behave as ductile grains and their presence in sandstone framework results in a significant early reduction of primary porosity and irreversible loss of IGV. Conversely, dolom ite crystalline rip-up clasts act as rigid grains against m echanical com paction but favour prec ipitation of early pervasive dolomite cement that occlude pr imary porosity and preserves IGV. At pore- and depositional-scales, spatial distribution of rip-up clasts in continuous layers (e.g. muddy rip-up clasts) or in spec ific depositional facies (e.g. dolomite crystalline rip-up clasts) and their asso ciated diag enetic pr ocesses m ay im pact re servoir quality by generation of vertical and 3D fluid flow ba rriers and baf fles that com partmentalize the reservoir. O btained qu antitative es timation of e arly reduction of prim ary porosity by compaction and cem entation on the basis of th e abundance of these t ype of grains can provide useful data for the better understanding of reservoir quality in analogous basins.

An additional case stud y is presented as part o f this Thesis, following the same approach of linking d epositional f eatures to e arly diagen etic p rocesses in orde r to predict their im pact on reservoir qualit y. This study was encouraged by the understanding of low-than-expect ed flow rates occurring at a geothermal well from the aeolian facies of the Rotlieg end re servoir (Upper Perm ian; The Netherlands). In this case, the diagenetic study incorporates petrophysical and high-resolution X-Ray Fluorescence (XRF) co re scann ing data and is integrated in a solid sedim entological framework constra ined by seism ic, well-log and core re cords. The depo sitional tex ture was characterized at co re- and thin-section scales consisting on altern ation of very fine- and very coarse-grained sandst one lam inae, with the latter system atically cem ented by anhydrite pore-filling cem ent. The identifica tion of detrital anhydrite/gypsum grains pointed out to these grains as potent ial local source f or anhydrite cem ent that precipitated in the coarser-grained, more permeable laminae. Due to the mechanical and

chemical instability of anhydrite/gypsum detrital particles, their grain size may be used as an indicator of source distance, interpreted as nearby gypscretes. By combining these results with the prevailing west-southwest aeolian transport direction, a conceptual predictive model is proposed for distribution of these low-permeability streaks which reduce uncertainty in reservoir quality prediction.

The multidisciplinary analytical workflow developed in this Thesis highlights the significance of diagenetic studies in reservoir quality prediction models. By using of outcrop-derived data, diagenetic analysis can be stressed to utmost when placed in a well-constrained depositional framework maximizing its use as input in upscaling reservoir properties.

RESUMEN EXTENDIDO

El análisis de la evolución espacial y temporal de los rasgos diagenéticos es de vital importancia para la evaluación y modelización de la distribución de parámetros petrofísicos en rocas almacén siliciclásticas. La reciente proliferación de software específico para la predicción y modelización de la calidad del almacén (*reservoir quality*) ha cambiado el enfoque de la industria en lo referente a la evaluación y recuperación de hidrocarburos durante las fases de exploración y producción. La mayoría de estos softwares se centran en aspectos específicos como o, por ejemplo, la modelización de la cementación de cuarzo la cual es fácilmente predecible dadas las condiciones químicas del ambiente diagenético donde se desarrolla. Una tarea completamente diferente es la de predecir la presencia y cantidad de minerales de la arcilla y su impacto en la calidad del almacén mediante la comprensión de su distribución dentro del sistema deposicional y sus posteriores alteraciones postdeposicionales.

Los variaciones diagenéticas están ligadas a un conjunto de factores tanto relacionados con el ambiente deposicional (fábrica deposicional, geoquímica del agua intersticial, componentes intracuencales y bioturbación) como o independientes del mismo (evolución térmica y de enterramiento de la cuenca, tiempo de residencia bajo unas condiciones específicas de P-T), todos los cuales afectan a la posterior modificación del sedimento, desde condiciones superficiales (tempranas) hasta de mayor profundidad. Son, precisamente, estos procesos mecánicos y químicos tempranos los que presentan trayectorias diferentes las cuales están directamente relacionadas con diferencias texturales y composicionales controladas deposicionalmente. La interacción mutua entre los rasgos deposicionales y la composición de la arenisca con los procesos y fluidos diagenéticos es lo que determina el grado de compactación, la cantidad y tipo de cementos, la intensidad de la disolución y, por tanto, la cantidad de porosidad primaria residual y/o la generación de porosidad secundaria que es lo que finalmente controla la permeabilidad y la calidad del almacén.

Todos estos factores (p.e. ambiente deposicional, procedencia, clima, tectónica) están íntimamente relacionados y representan – entre otros – datos de entrada necesarios para predecir y modelizar la calidad del almacén. Sin embargo, en muchos casos la información sobre las facies deposicionales o el ambiente sedimentario no puede ser completamente entendida si las muestra de rivan de testigos en profundidad. Por lo tanto, el uso de estudios de análogos de afloramiento es de crucial importancia ya que éstos proporcionan datos cuantitativos y georreferenciados que pueden servir como datos de entrada para los softwares más actuales de modelización de diagénesis y de propiedades petrofísicas en areniscas.

Todos los hechos mencionados anteriormente constituyen el punto de partida de este proyecto de Tesis y sientan las bases para la selección tanto de las áreas de estudio como del enfoque analítico seguido. El objetivo de esta Tesis es el de contribuir a reducir la incertidumbre en modelos de calidad de almacenes mediante un estudio multidisciplinar que integra el análisis de facies deposicionales con el análisis de los procesos diagenéticos tempranos tanto en análogos de afloramiento como en testigos de

tras-afloramiento. Este últim o caso es de particular interés pa ra la industria de hidrocarburos ya que m ejora considerablem ente las relativam ente lim itadas interpretaciones que se obtienen de la trad icional desc ripción de tes tigos m ediante el contraste directo de estos últimos con el afloramiento.

Las áreas de estudio han sido seleccionada s de acuerdo a su relevancia tanto en (i) los ambientes sedimentarios representados en ellas e in teresantes para la exploración de hidrocarburos y (ii) los rasgos que pr esenten los aflo ramientos com a análog os aflorantes. Los am bientes fluviales seleccion ados se en cuentran ex puestos en la sucesión triásica de la parte SE del centro de E spaña (aquí referida como TIBEM) así como en la cuenca d e Argana (Alto A tlas occidental, SW de Marruecos) y se corresponden con: ambiente de llanura de inundación (que incluye depósitos de desbordamiento y canalizados) y ambiente de llanu ra tren zada en la parte españ ola; sistemas fluvial trenzado y rectilíneo en la parte m arroquí. Debido a sus m utuas condiciones geológicas de for mación, am bas áreas se consideran análogos de afloramiento ideales de una serie d e conoc idos alm acenes triásico s entre los qu e se incluyen los depósitos del TAGI (Trias Arg ilo-Gréseux Inférieur) por todo el norte de África así como los depósitos triásicos en Bay of Fundy (Nova Scotia, Canadá).

La m etodología adoptada para el desarrollo de esta investigación abarca: una exhaustiva selección de muestr as en base a criterios sedim entológicos ya existentes y otros de nueva adquisición m ediante análisis de afloram ientos y de testigos; un análisis petrológico de alta resoluci ón utilizando las técnicas m ás actuales (p.e. m icroscopio óptico y electrónico, DRX, catodolum iniscencia, m icrosonda de electrones) y desarrollando nuevas m etodologías de caract erización; la determ inación de los parámetros petrofísicos principales (porosidad, permeabilidad y distribución de tamaños de poro) mediante porosimetría de inyección de mercurio.

La primera parte de esta investigación se ha centrado en la sucesión triásica de la parte SE del centro de España para tratar de (i) reconocer cam bios verticales en la composición y textura de las areniscas del ambiente de llanura de inundación de la Secuencia II hasta las del am biente de llanura trenzada de la secuencia IV y (ii) evaluar el im pacto de dichos rasgos composici onales y texturales sobre los procesos diagenéticos y sobre la evolución del sistem a de poros para, finalm ente, (iii) c lasificar los ambientes sedimentarios estudiados en función de su potencial com o roca almacén. Los resultados obtenidos docum entan un sign ificante increm ento de m adurez hacia arriba en la sucesión desde la llanura de inundación hasta la llanura trenzada m arcado por cam bios en la textura deposicional y la com posición detrítica. El estudio petrográfico sugiere que la pé rdida de porosidad m ás importante tuvo luga r durante las etapas diag enéticas m ás tem pranas a través de diferentes procesos diag enéticos seg ún las facies. E n la llanura de inundación, los de pósitos de arenisca de desbordam iento se han visto principalmente afectados por compactación mecánica y cem entación de yeso. Los depósitos canalizados de este m ismo a mbiente de llanura, que incluyen sistem as fluviales de estilo m eandriforme y recti líneo, m uestran grados de com pactación mecánica intermedia así como cantidades y tip o de fase autigénica d ominante variables en función de las facies depos icional. En la llanura trenza da, la porosidad prim aria aún se conserva bastante bien siendo el recrecimiento de feldespato potásico la principal fase cementante. La presencia de facies de can al abandonado cementadas por yeso así como

de fracturas postdeposicionales cem entadas por carbonato, donde la porosidad disminuye drásticam ente, reducen considerab lemente el potencial como roca alm acén de la llanura trenzada.

La relación entre los parám etros cont rolados deposicionalm ente (i.e. rasgos texturales y abundancia de com ponentes intr acuencales) y la distribución espacial y temporal de los procesos diagenéticos ha sido investigada c on m ás detalle en los depósitos de canal m eandriforme de la secuen cia II (parte SE del centro de España) así como en los depósitos d e los sistemas fluvial es trenzado y rectilíneo de la cuenca de Argana (Alto Atlas occidental, SW de Marruecos).

En el ejemplo m eandriforme, el estu dio se ha realizado sobre muestras procedentes de testigos de 4 pozos realizados tras-afloramiento los cuales atrav iesan las principales facies deposicionale s: canal, barra de m eandro (*point bar*), barra de *scroll* y canal de ch ute. Adem ás del contaje petrogr áfico tradic ional s e ha de sarrollado u na caracterización sem icuantitativa propia pa ra el sistem a poroso. La integración estadística de los datos petrográficos y pe trofísicos pone de m anifiesto el papel desempeñado por la selección h idráulica y su efecto sobre la evolu ción diagenética y sobre las propiedades d el alm acén. Los result ados obtenidos m uestran la relación directa entre las facies deposicionales y la a bundancia y distribución de matriz detrítica, la cual favorece la com pactación mecánica pero inhibe la precip itación tem prana de cementos. El proc esamiento estadístico multivariante de los datos integ rados demuestra que los poro s primarios inter granulares, mejor interconectados y de m ayor tamaño (>1 μm) son los principales cont ribuyentes d e la perm eabilidad en las m uestras más heterogéneas. La porosidad secundaria parece estar más relacionada con poros de menor tamaño (<1 μm) e irregularm ente dist ribuidos. L os datos sedim entológicos, petrográficos y petrofísicos han sido integra dos para calcu lar el índice de calidad d el almacén el cual ha sido usado com o dato de entrada para un modelo determinístico 3D de facies en PETREL[®]. Notablem ente, dicho modelo encaja perfectam ente, poni endo así de relieve las relaciones existentes entre las propiedades del alm acén y la distribución de facies e identifi cando las facies d e barra d e *scroll* y de m argen de canal como las que tien en la mejor calidad. Por lo tanto, este modelo puede ser utilizado para identificar potenciales trayectorias preferentes de fluidos y ser aplicado con éxito en las estrategias de recuperación mejora de petróleo (ya sea por inyección de agua o espuma).

En los depósitos fluviales trenzado y rec tilíneo de la cuenca de Argana, la presencia y abundancia de diferentes tipos de *rip-clasts* tiene un con trol d irecto y sustancial s obre la evo lución d iagenética temprana y el consecu ente deterioro del almacén. Una clasificación prop ia de es tos granos de acuerdo a su com posición y comportamiento m ecánico resulta en tres tipos prin cipales denom inados: rip-clasts arcillosos, rip-clas ts a rcilloso-dolomíticos y rip -clasts dolom íticos crista linos. Los rip - clasts arcillosos se com portan como granos dúc tiles y su pres encia en el esqueleto de la arenisca resulta en una reducción temprana importante de la porosidad primaria con una pérdida irreversible del volum en intergranular (*IGV*). Contrariam ente, los rip-clasts dolomíticos cris talinos actúan com o granos ríg idos contra la com pactación m ecánica pero favorecen la precipitación de cemento temprano de dolomita el ocluye la porosidad primaria pero preserva el IGV. A escala de posicional y de poro, la distribución espacial de los rip-clasts en lám inas continuas (p.e . los rip-clas ts arcillosos) o en facies

deposicionales específ icas (p.e. los rip-c lasts dolom íticos cristalino s) junto con sus procesos d iagenéticos asociados pu eden afect ar a la calidad del alm acén m ediante la generación de barreras o ba fles para la m igración de fluidos, verticales y 3D, provocando así su compartimentación. Las estimaciones cuantitativas obtenidas sobre la reducción de la porosidad prim aria por co mpactación y cementación en función de la abundancia de estos tipos de granos pr oporcionan datos útiles para un m ejor entendimiento de la calidad del almacén en cuencas análogas.

Un caso de estudio ad icional se p resenta como parte de esta Tesis, en e l cual se sigue el mismo enfoque de re lación entre rasgos deposiciona les y procesos diagenéticos tempranos para predecir su im pacto en la calidad del alm acén. Este estudio estuvo motivado por la necesidad de entender una s tasas de pro ducción m ás bajas de lo esperado en un pozo geotérm ico en facies eó licas del almacén del Rotlie gend (Pérmico Superior, H olanda). En este caso, el estudi o diagenético incorpora datos petrofísicos y de fluorescencia de rayos-X de alta resolución en escaneo de testigos y se integra en u n sólido m arco sedim entológico caracterizado mediante sísm ica, registros de pozo y testigos de subsuelo. La textura deposicion al fue caracterizad a a escala d e testigo y de lámina delgada consistiendo en una alternanci a de láminas de grano m uy fino y grueso, con estas ú ltimas siste máticamente cem entadas por anhid rita. La ide ntificación de granos detríticos de anhidrita/ yeso apunta a éstos com o la potencial fuente local para e l cemento de anhidrita el cual habría precipitado las láminas de mayor tamaño de grano y por tanto m ás permeables. Debido a la inestabi lidad de las partículas de anhidrita/yeso, su tamaño de grano puede usarse como indica dor de distancia hasta el área fuente, en este caso in terpretada c omo unas g ypsicretas c ercanas. Me diante la co mbinación de estos resultados con la dirección oeste-suroes te preferen te de transp orte eó lico, se propone un modelo conceptual pr edictivo para la distribución de estas lám inas de baja permeabilidad el cual ayuda a reducir la incertidumbre en la predicción de la calidad del almacén.

El flujo de trabajo m ultidisciplinar desarrollado en esta Tesis pone de relieve la importancia de los e studios d iagenéticos en los m odelos de predicción de calidad de almacenes. Mediante el uso de datos de rivados de afloram iento, los anális is diagenéticos pueden ser exprim idos al m áximo cuando se enm arcan dentro de un contexto deposicional bien caracterizado maximizando así su uso como datos de entrada para el *upscaling* de las propiedades del almacén.

CHAPTER **1**

Introduction

1. Introduction

The depositional facies characteristics of siliciclastic sediments play a major role into determining the evolution in space and time of diagenetic processes that change original physical, mineralogical and chemical signatures of the sediment. Diagenetic processes affect the original texture and composition and so the primary porosity and permeability from the moment of deposition onward, resulting in either its deterioration by compaction and cementation, or enhancement by selective dissolution.

The analysis of the spatial and temporal evolution of the diagenetic features and their interaction with the depositional setting is of paramount importance for the evaluation and modelling of the petrophysical parameter distribution in siliciclastic reservoir rocks at burial depth. The importance of reservoir quality (RQ) analysis is reflected in the shift over time of the focus of diagenetic studies from (*a*) purely descriptive petrography aiming to unravel the chronology of compaction, cementation and dissolution, to (*b*) quantitative diagenetic studies tentatively integrated with their response in seismic, well-log and core records in order to construct predictive three-dimensional RQ models to steer reservoir operational strategies in a proactive manner. However, RQ models still have inherent uncertainty originating from the combination of the one-dimensional nature of the core data and the stochastic interpolation algorithms to construct the reservoir architecture model from widely-spaced wells. The way forward to reliable RQ prediction in sandstones is to develop fully coupled diagenetic, depositional and 3D basin models that integrate processes operating on a broad range of length scales (Giles, 1997; Tuncay and Ortoleva, 2004).

Triassic rift basins dislocated along the northern Atlantic margins are well-known exploration targets. Some examples of currently productive Triassic reservoirs are: TAGI reservoir (Trias Argilo-Gréseux Inférieur) in the Ghadames petroleum province (Algeria, Lybia, Tunisia); Triassic levels from Essaouira basin (Morocco); Wolfville Formation, Fundy basin (Nova Scotia, Canada); Sherwood Sandstone Group in Lennox and Corrib fields (Slyne basin, West Ireland); and Skagerrak Formation (Central North Sea, UK and Norway), among others. The considerable literature available for both onshore and offshore regions constrains the understanding of depositional geometries and sedimentary architectures. Deposition during the whole Triassic developed during similar tectonic and climatic conditions as testified by the Carnian interval, documented from eastern North America (USA and Canada) to Northwest Africa (Morocco and Algeria) and Europe (SE Spain, Portugal, France, Germany and Great Britain) (Arche and López-Gómez, 2014). Such geological conditions favoured the generation of hydrocarbons which are nowadays stored mostly in Triassic fluvio-deltaic deposits found throughout the (paleo-) Atlantic margins. Hence, the doubly interest of both the oil industry and the academia for the thorough characterization of such Triassic deposits has promoted a multi-scale approach to build a comprehensive picture of the three-dimensional distribution of rocks-pores-fluids in the reservoir by using all available data sources (e.g. reservoir-analogue outcrops).
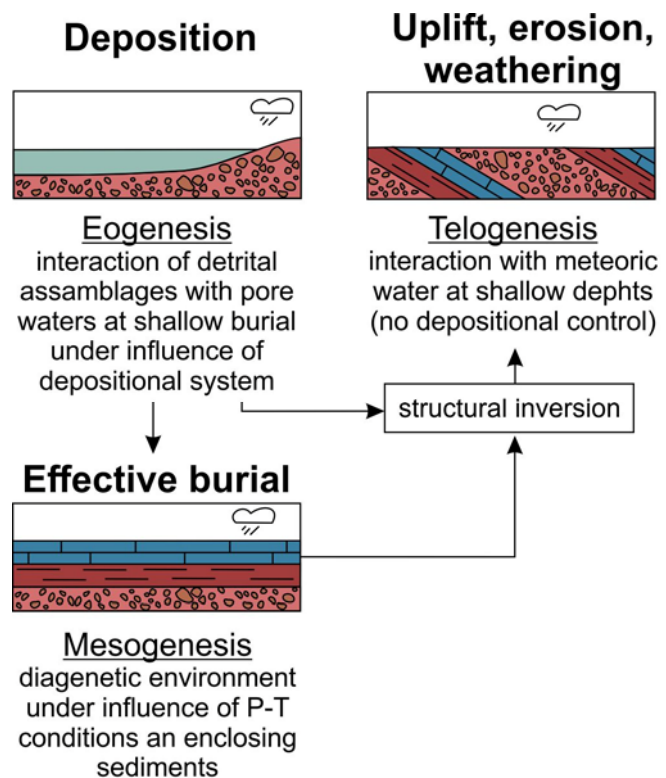
The aim of this Thesis is to reduce the uncertainty on RQ modelling through a multidisciplinary approach integrating the study of depositional facies and the analysis of early diagenetic process in reservoir-analogue outcrops and behind-outcrop core data analysis (outcrop/behind outcrop characterization workflow; O/BO; Donselaar and Schmidt, 2005; Slatt et al., 2011; Viseras et al., 2013; Viseras et al., 2015). This approach offers the possibility to construct 3D diagenetic architecture models directly from outcrop settings, which can then be used to validate and quality-control the RQ models.

The rationale behind this thesis founds on 3 fundamental questions: (1) (What?) depositional control on diagenetic processes, (2) (Why?) evaluation and prediction of reservoir quality through diagenetic studies, (3) (Where?) reservoir-analogue outcrops as valuable information sources.

1.1 Depositional control on diagenetic processes

It is widely accepted that diagenetic evolution can be subdivided in conceptual regimes according to depth and so to pressure and temperature conditions: eogenesis, mesogenesis and telogenesis, related to shallow burial, deep burial and late-stage erosion during uplift and denudation, respectively (Fig. 1; Choquette and Pray, 1970; Worden and Burley, 2003). The eogenetic realm operating at or near sediment surface is where depositionally-influenced diagenesis takes place by the particular combination of physical and (bio-) chemical processes. Consequently, significant diagenetic heterogeneity arises from heterogeneity in the depositional features of the sediment at different scales (Milliken, 2001).

Fig. 1. Flow chart showing the links between the regimes of diagenesis. The change from mesogenesis (burial diagenesis) to telogenesis can occur at any stage during burial (modified after Worden and Burley, 2003).

Deposition

Eogenesis
interaction of detrital assamblages with pore waters at shallow burial under influence of depositional system

Uplift, erosion, weathering

Telogenesis
interaction with meteoric water at shallow dephts (no depositional control)

structural inversion

Effective burial

Mesogenesis
diagenetic environment under influence of P-T conditions an enclosing sediments

Weber (1986) defined the scales of reservoir heterogeneity (Fig. 2), ranging from: (*a*) micro-scale pores (10 to 110s μm), laminae and sedimentary structures (10 to 100s mm) and cross-bed sets (1 to 10s m), to (*b*) meso-scale sediment body shape and size

(order of 100s m wide by 10s m thickness), to (*c*) macro-scale sedimentary stacking patterns (field scale, order of 1 to 10 km wide by 100s m thickness). Each of these scales has its own specific interaction between diagenetic processes and depositional facies. At the micro-scale, bioturbation, near surface pore-water chemistry, hydraulic sorting effect and grain-size distribution determine the initial sediment properties such as detrital composition (e.g. intrabasinal components) and primary pore network as well as chemical conditions of pH, Eh and salinity (Beard and Weyle, 1973; De Ros, 1998; Morad et al., 2000; Bjørlykke, 2014). At the meso- and macro-scale(s) sand-body geometry, vertical and lateral facies stacking patterns, lithofacies associations and sedimentary structures influence distribution of the mud/sand ratio, the connectivity between architectural elements and potential fluid flow pathways via laminae, bedding and stratification (Weber, 1986; Miall, 1988; Brayshaw et al., 1996; Sharp et al., 2003). In meandering fluvial systems for example, facies-induced heterogeneities related to internal depositional features - such as lateral accretion units with associated mud drapes and internal facies variations like vertical change from trough cross-bedding to ripple lamination -, produce fining upward grain size trends with the corresponding decrease of primary porosity and increase of permeability anisotropy (Hartkamp-Bakker and Donselaar, 1993; Pranter et al., 2007).
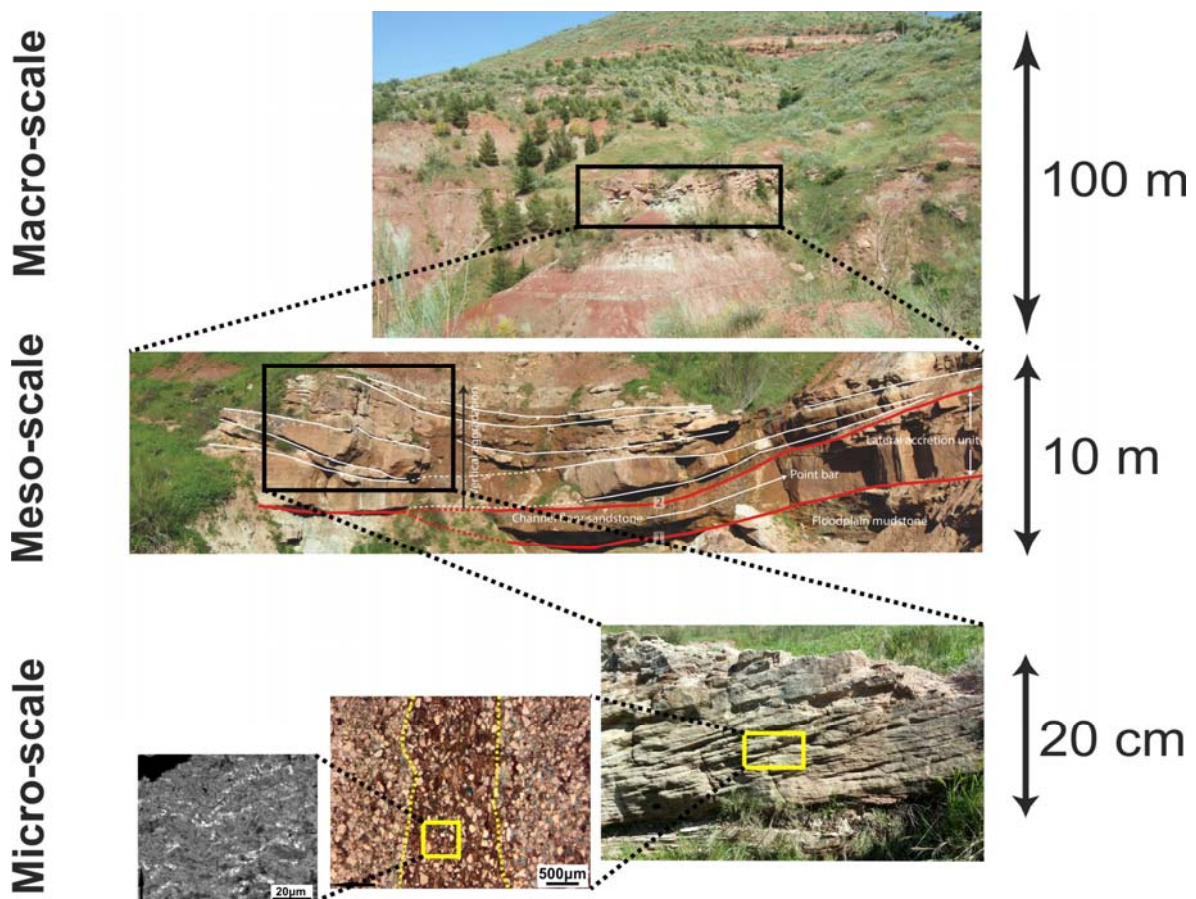

Fig. 2. Scales of reservoir heterogeneity (after Weber, 1986).

Variations in diagenetic patterns are linked to a suite of depositional-dependant (depositional fabric - primary porosity and permeability-, pore-water chemistry, types and amounts of intrabasinal components and extent of bioturbation) and independent factors

3

(burial-thermal evolution of the basin, residence time in specific P-T conditions). This large variety of parameters can then result in complex spatial and temporal distribution of diagenetically-induced heterogeneities within geobodies. Nevertheless, near-surface and shallow-burial diagenetic processes (eogenesis) are of key importance as they have a substantial control on ulterior deep-burial diagenesis, constrained by remaining porosity and permeability (Morad et al., 2010; Ajdukiewicz and Lander, 2010). Once the depositional controls on diagenesis have been established, it is possible to relate the inferred eogenetic mineral assemblages to exact geochemical sedimentary environments (Burley et al., 1985). These early mechanical and chemical processes proceed along different pathways directly related to depositionally-governed differences in textural and compositional parameters which makes them potentially predictable (Bloch and McGowen, 1994; De Ros et al., 1994; Salem et al., 2000; Milliken, 2001; Worden and Morad, 2003). Consequently, the analysis of early diagenetic processes within a well-constrained depositional framework becomes a basic approach for a thorough understanding of what Ehrenberg (1997) defined as "the *depositional sand quality*". Proof of that is also the new emerging trend on linking diagenesis and sequence stratigraphy. This approach aims at inferring facies distribution from sequence stratigraphic models, especially in deltaic, coastal and shallow marine deposits, for predicting occurrence and distribution of (early) diagenetic processes controlled by depositional conditions (Morad et al., 2013).

1.2 Evaluation and prediction of reservoir quality through diagenetic studies

Diagenetic studies have a huge variety of applications, such as rock mechanics, structural geology, ore mining or hydrogeology. Research on sandstone diagenesis was largely driven by the petroleum industry through the 80's and 90's because of the diagenetic control on the amount and distribution of porosity regulating hydrocarbon migration pathways in the subsurface and ultimately the production rates of oil and gas. In recent decades the increasing emphasis on maximizing recovery from existing oil and gas fields by IOR/EOR (Improved/Enhanced Oil Recovery) technologies such as WAG (water-alternating-gas) injection (Kulkarni and Rao, 2005), polymer flooding (Maia et al., 2009) or CO_2 injection (Bennion and Bachu, 2008) as well as further advances in Carbon Capture and Storage (CCS) technologies (Bennion and Bachu, 2008; Issautier et al., 2014) and geothermal energy production have prompted a renewed interest in the qualitative and quantitative characterization of reservoirs. Evaluation and prediction of RQ (i.e. porosity and permeability values) have then blossomed into a main task for reducing geological risk and raising success rates in the different phases of the play life (exploration, appraisal, planning, development and surveillance *sensu* Sneider, 1990).

Over the last 20 years diagenetic studies have evolved from routine petrographic analysis to a more sophisticated discipline of quantitative diagenesis based on geochemistry, isotopes and chemical thermodynamics and kinetics (Burley, 1985; Worden and Burley, 2003). Currently, diagenetic modelling software (e.g. Exemplar, Touchstone^{TM}) represents the state-of-the-art for quantitative RQ prediction and characterization (Taylor et al., 2010). These software systems generate calibrated models to forecast sandstone porosity and permeability by modelling mechanical compaction and

quartz cementation as a function of thermal and effective stress histories (Walderhaug, 2000; Lander et al., 2008). The evolution of the approach to diagenesis in time has been partially promoted by recent research on upscaling of reservoir properties which highlights the importance placed on the small-scale (pore-scale) property variation for accurate field-scale reservoir modelling (Pickup et al., 1995; Pringle et al., 2006). This lead to a re-evaluation of internal reservoir unit heterogeneity, which previously was not taken into account and often resulted in an overestimation of the recovery factor (Stanley et al., 1989; Teles et al., 1998; Dutton et al., 2002; Dutton, 2008). In this context the pore-to-field modelling philosophy has become of great interest in the petroleum community as a multi-scale approach that explicitly represents the flow properties within a reservoir (Ringrose and Bentley, 2015).

1.3 Reservoir-analogue outcrops as information sources

Most of recent publications dealing with the relationship between depositional facies and diagenetic evolution are based on core sample analyses (e.g. Luo et al., 2009; De Ros and Scherer, 2012; Carvahlo et al., 2014; El-Khatri et al., 2015; Khalifa and Morad, 2015; Lai et al., 2015; Olivarius et al., 2015; Zhang et al., 2015), in which depositional facies are interpreted and differentiated in terms of major sedimentary environments (meander belts, braided systems, floodplain deposits, and so on). This approach deals with limited spot measurements on one-dimensional core data and therefore suffers from operator bias in terms of interpretation of depositional features and spot analysis interpolation.

Flaws of the 1D approach point out to the need for a methodology in which the spatial distribution of lithofacies and its relation with diagenetic features can be directly observed in three dimensions. In this sense, outcrop analogue studies have been demonstrated to be a powerful tool, supplementing sparse subsurface data with outcrop-derived measurements (Bryant and Flint, 1993; Eschard and Doligez, 1993; Geehan and Underwood, 1993; Pringle et al., 2004; Ajdukiewicz and Lander, 2010; McKinley et al., 2011). The key factors that influence the modelled evolution of porosity and permeability (e.g. sand character *sensu* Heins and Kairo, 2007; Fig. 3) are important model input parameters which cannot fully be captured in subsurface samples, yet can easily be constrained via use of outcrop analogues. Outcrop studies yield quantitative geo-referenced data sets which serve as input in state-of-the-art forward modelling software packages of sandstone diagenesis and petrophysical properties in undrilled areas.

5
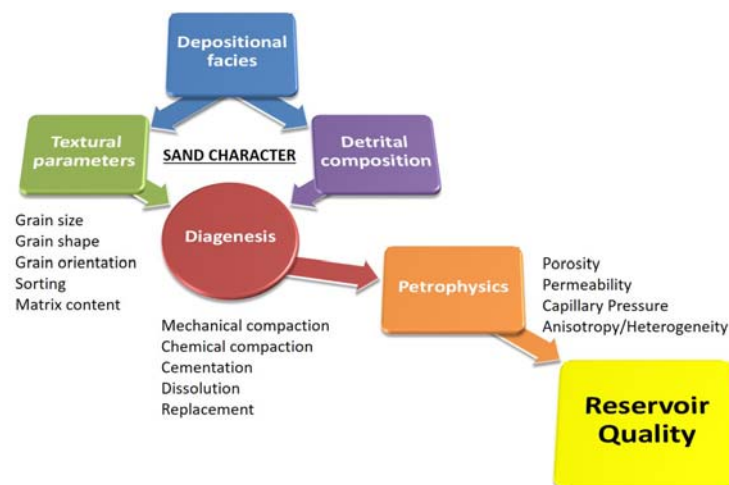
Fig. 3. Flow chart showing the relationship between the different concepts exposed.

The research approach of this Thesis (i.e. depositional contextualization of diagenetic processes by reservoir-analogue outcrop studies) complemented with behind-outcrop core data, provides an accurate control on the targeted depositional facies and sub-facies (e.g. lower, middle and upper point bar; Henares et al., 2016a) by direct validation of 1D cored material with 3D outcrop-based sediment-body size, shape, stacking patterns, sedimentary structures and internal facies heterogeneity. The outcrop/behind outcrop characterization workflow (O/BO; Donselaar and Schmidt, 2005; Slatt et al., 2011; Viseras et al., 2013; Viseras et al., 2015) therefore provides an added value by placing outcrop characteristics in the context of typical subsurface data types which can be used as diagnostic criteria for further interpretations at core scale.

Given that no two systems are identical, the "perfect" analogue does not exist. The key issue is to understand the purpose on the reservoir model to select an appropriate analogue or aspects of multiple of them (Howell et al., 2014). In general sense, an appropriate analogue selection includes similar tectonic setting, geological age, subsidence rates and sedimentary environments (Bryant and Flint, 1993; Bjørlykke and Jahren, 2010). From a diagenetic point of view, differences in burial history or tectonic setting (i.e. P-T conditions) may result in different burial diagenetic evolution between the subsurface reservoir and its outcrop analogue (Howell et al., 2014). However, if the selected outcrop analogue fits the depositional environment (i.e. depositional fabric), detrital composition and age, it can provides useful information on the comparative and relative properties of facies, trends within architectural elements and early diagenetic control on reservoir properties (Burley, 1984; Schmid et al., 2004; Dowey et al., 2012). In addition, a suitable outcrop must exhibit well-exposed lateral facies relationships, no structural deformation and relative three-dimensionality. All this together can contribute to a better understanding of linkages between depositionally-predictable features and diagenetically-induced heterogeneity resulting into more realistic reservoir models.

In this context the studied Triassic deposits can be considered as outcrop analogues of several currently productive subsurface reservoirs. The Triassic red beds of the Tabular Cover (TIBEM; Iberian Meseta, Central SE Spain; Fig. 4A) resemble the TAGI reservoirs in Algeria. Both formations result from the erosion of Paleozoic granitic and metamorphic terrains during the Tethyan rifting (Middle-Upper Triassic) and deposited in a peri-intracratonic basin under similar climatic, base level and tectonic conditions. Basin architectures show similar fluvial facies stacking patterns, varying from moderately-sinuous meandering river, to low-sinuous braided fluvial-channel deposits (associated with fine-grained floodplain sediments and palaeosol development) evolving upsection to tidally-influenced facies (Fernández and Dabrio, 1985; Turner et al., 2001; Rossi et al., 2002; Ratcliffe et al., 2006). Another excellent analogue of Triassic red beds is the Argana Basin (Western High Atlas, SW Morocco; Fig. 4B) which forms the eastward extension of the hydrocarbon-bearing Essaouira Basin (Medina, 1988; Broughton and Trépanier, 1993; Ellouz et al., 2003) and corresponds to the conjugate Atlantic passive continental margin of the Bay of Fundy Basin in Nova Scotia, Canada (Calder et al., 1998; Olsen et al., 2000; Letourneau and Olsen, 2003). Both basins have already been equated in the literature (Olsen, 1997; Olsen et al., 2000) on the basis of remarkable similarities in sedimentary

facies and stratigraphy throughout their thick, Late Permian-Early Jurassic successions (Smoot and Castens-Seidell, 1994; Kent et al., 1995; Hofmann et al., 2000).

Fig. 4. Location of study areas. A) Triassic red beds of the Tabular Cover (TIBEM; Iberian Meseta, Central SE Spain). B) Argana Basin (Western High Atlas, SW Morocco).

1.4 Objectives

Forward-modelling methodologies to predicting diagenetic effects on RQ require information about the character of deposited sand, including mean grain size, sorting,

matrix content, and composition of diagenetically relevant particles (i.e., intrabasinal components and all rock fragments, not just lithic fragments). Early mechanical and (bio-) chemical modifications develop as a function of deposition driven differences in texture and composition (i.e. detrital fabric). The latter is dominantly controlled by provenance and weathering whereas the depositional environment determines sediment distribution, grain size and sorting. To understand and model the influence of the above-mentioned parameters on diagenetic evolution it is therefore necessary to constrain all factors and processes exerting critical controls on their formation prior and subsequent to deposition.

This thesis aims at providing the information necessary to decipher the way depositional features influence sediment diagenetic history through the study of two Triassic red bed successions exposed in Central SE Spain and Western High Atlas (SW Morocco), and ultimately provide an analytical approach to estimate and predict reservoir properties from the study of outcrop analogues. To reach these goals, the following objectives have been defined:

1. **Refinement** of previous depositional and facies models by identifying diagnostic vertical and lateral lithofacies associations in outcrop.

2. **Application** of outcrop/behind-outcrop characterization workflow at meso- and microscale in a selected portion of the Triassic deposits of Central SE Spain by comparison and correlation of depositional and diagenetic characteristics in outcrop and behind-outcrop cores.

3. **Valorisation** of the Triassic sedimentary successions of Central SE Spain and SW Morocco (Western High Atlas) to be used as outcrop analogues for similar fluvial Triassic reservoirs of North Africa, Northeast America and Northwest Europe.

4. **Recognition** of vertical variations in detrital and diagenetic fabrics.

5. **Determination** of lateral variation patterns in sandstone composition and diagenetic processes within selected depositional environments (i.e. meandering channel and braided system).

6. **Characterization** of pore network and sandstone petrophysical properties (i.e. porosity and permeability).

7. **Identification** of fundamental linkages between depositional processes (e.g. hydraulic sorting), sediment composition (e.g. extrabasinal and intrabasinal components) and distribution of diagenetically-induced heterogeneity (e.g. compaction, cementation and dissolution), and their collective effect on RQ (e.g. porosity and permeability).

8. **Provision** of input data for 3D modelling of reservoir quality index (RQI).

1.5 Research outline

The structure of the Thesis is organised according to the objectives previously outlined:

Chapter 2 provides a **geological framework** of the studied Triassic sedimentary deposits from Central SE Spain and SW Morocco (Western High Atlas). The Triassic break-up of the Pangea triggered the formation of the Tethyan-prone and Atlantic-prone rift basins where thick continental red bed successions were accumulated. The summarized stratigraphy and the depositional facies characterization highlight their suitability as reservoir-analogue outcrops and supplies the key parameters to understand the depositional influence on diagenetic evolution.

Chapter 3 includes a detailed description of the **methodological procedures** as well as the **technical specifications** adopted for the development and completion of this PhD project, encompassing: sample selection according to sedimentological criteria based on outcrop and core analysis; petrological analysis following the up-to-date techniques and developing own (done-on-purpose) characterization methodologies; determination of the main petrophysical parameters.

Chapter 4 embraces the "**Results and Discussion**" section where the main results achieved are presented and discussed in the same way they have been published. This chapter is subdivided in two parts (I and II) according to related aims and concluding remarks.

- **Part I** presents a comprehensive picture of differences in diagenetic evolution and petrophysical properties (porosity, permeability and pore size distribution) according to general differences in depositional environments. It incorporates the first sandstone compositional data set ever produced on the Triassic succession in the region (Central SE Spain). The selection at outcrop of fluvial sedimentary bodies (sequences II and IV of the Triassic succession) was also based on their suitability as outcrop analogue facies of the TAGI reservoir of northern Africa.

- **Part II** deepens on the depositional-driven controls (e.g. hydraulic sorting effect and type and amount of intrabasinal components) on the internal distribution of early diagenetic processes within a given depositional system as well as their effect on depositional porosity. The integration of produced data through the analysis of three different fluvial examples (i.e. meandering system from Central SE Spain and braided and straight fluvial systems from Western High Atlas, SW Morocco) allows to establish a sound foundation of linkages between depositionally-predictable and diagenetically-induced features. In addition, the application of O/BO characterization workflow on the meandering example provides input data for a 3D modelling of RQ. The adopted approach highlights the value of the results for a better understanding of analogous reservoir properties such as those in the Fundy Basin (Nova Scotia, Canada).

The **complementary contribution** of **Chapter 5** includes the results from Henares et al. (2014b). This chapter deals with the depositional controls (i.e. intrabasinal components and depositional texture) on both diagenetic processes and reservoir quality in **aeolian depositional facies**. Samples are from selected cores from the Rotliegend (Upper Permian) geothermal reservoir in The Netherlands. The diagenetic study incorporates petrophysical and high-resolution X-Ray Fluorescence (XRF) core scanning data and is integrated in a solid sedimentological framework constrained by seismic, well-log and core records. A

conceptual model is proposed to predict reservoir deterioration by diagenetic alterations according to facies distribution, which reinforces and broadens the conclusions reached in this Thesis.

Chapter 6 is devoted to the general **conclusions** along with a summary of the future research **perspectives** in a short- and medium-term.

CHAPTER **2**

Triassic Geological Setting of Study Areas

2. Triassic Geological Setting of Study Areas

## 2.1. Triassic continental sedimentation during Pangea *break-up*

The Permo-Triassic *break-up* of the Pangea determined the onset of numerous rift systems in the southern Iberian Peninsula and northern Africa – with both Tethyan and Atlantic branches, respectively – and consequently the formation of several depocentres that caused the channeling of rivers to the sea (Fig. 2.1; Sánchez-Moya et al., 2004).

In the southern Iberian Peninsula, the Lower Triassic extensional phase (Tethyan rifting branch) was followed by a thermal subsidence event that widened the accommodation space in continental areas. Such event is recorded in the thick series of alluvial red beds forming the Buntsandstein facies. The protraction of the *break-up* of the Pangea through the Middle Triassic resulted in important crustal thinning and subsidence, with local basic volcanism in the proto-Internal Domain of the Betic Cordillera (Martín-Algarra and Vera, 2004) and the first marine incursion from the NE and the E without covering the entire Iberian rift (Sánchez-Moya et al., 2004). In the Internal and External Domains of the Betic Cordillera, the Triassic sedimentary successions consist of Ladinian by coastal and shallow marine evaporites and carbonates at the top of the Buntsandstein (Muschelkalk facies; Martín-Algarra and Vera, 2004). In the Tabular Cover the fluvial sedimentation continued until the Upper Triassic without deposition of Muschelkalk facies (Fernández y Pérez López, 2004). The overlying Keuper facies testifies to the significant marine regression occurred during the Upper Triassic (Carnian) that marked the onset of a new cycle of continental (argillaceous-sandy-evaporitic sediments) and coastal (carbonates) sedimentary environments on top of underlying sediments (Fernández, 1977; Fernández and Gil, 1989; Martín-Algarra and Vera, 2004; Sánchez-Moya et al., 2004; Fernández et al., 2005).

The red beds related to the Atlantic rifting branch formed from the Late Permian throughout the Triassic on both sides of the conjugate Atlantic margins, on the western margin of North Africa and on the eastern margin of North America. Triassic red beds were accumulated in the Argana and Ourika successions (High Atlas, SW Morocco) and in the Bay of Fundy basin (Nova Scotia, Canada). Sedimentation in the Argana basin was controlled by two main extensional phases – in Late Permian and during Triassic – that influenced paleodrainage patterns and consequently sediment dispersal pathways. The nature of the second extensional phase is still matter of debate, with authors describing it as synchronous to Triassic deposition (Brown, 1980; Laville and Petit, 1984; Medina, 1991, 1995) and other attributing it to post-rift phases (Hofmann et al., 2000; Baudon et al., 2012). This extensional phase created a number of WSW-ENE trending rift basins filled by continental (Argana Basin) and continental-marine sediments (Essaouira and Agadir Basins) separated by the Paleozoic Moroccan Arch (Medina, 1991; Tourani et al., 2000; El Arabi et al., 2006; Frizon de Lamotte et al., 2008; Klein et al., 2011, Arche and López-Gómez, 2014). East of Morocco, the Upper Triassic is found in the Ghadames basin – across East Algeria; West Libya and South Tunisia – and consists of the TAGI (Trias Argileux–Gréseux Inférieur) sandstone (Turner et al., 2001; Rossi et al., 2002). Fluvial

deposits of the upper TAGI filled a series of linked NE–SW trending grabens, related to the early phases of the North Atlantic opening.

Along with similar age, depositional styles and tectonic setting, further analogies between the southern Iberian Peninsula, Northwest Africa and Eastern Canada, are represented by the regional so-called Manuel Formation (herein referred as K2; Fernandez, 1977), a 20-m-thick sandy fluvial body deposited during the Carnian Pluvial event (Arche and Lopez-Gomez, 2014). The K2 is clearly documented in the entire Iberian Peninsula – from La Mancha to the Algarve in the South (Pérez-López and Sanz de Galdeano, 1994; Suárez-Alba, 2007), the Central System (Hernando, 1977a, b) and in the Lusitanian Basin (Uphoff, 2005) – and has been correlated with the Oukaimeden, Bigoudine (Argana Basin) and TAGI formations from Northwest Africa as well as with the Wolfville formation (Bay of Fundy, Nova Scotia Canada), among others (Fig. 1; Arche and Lopez-Gomez, 2014).
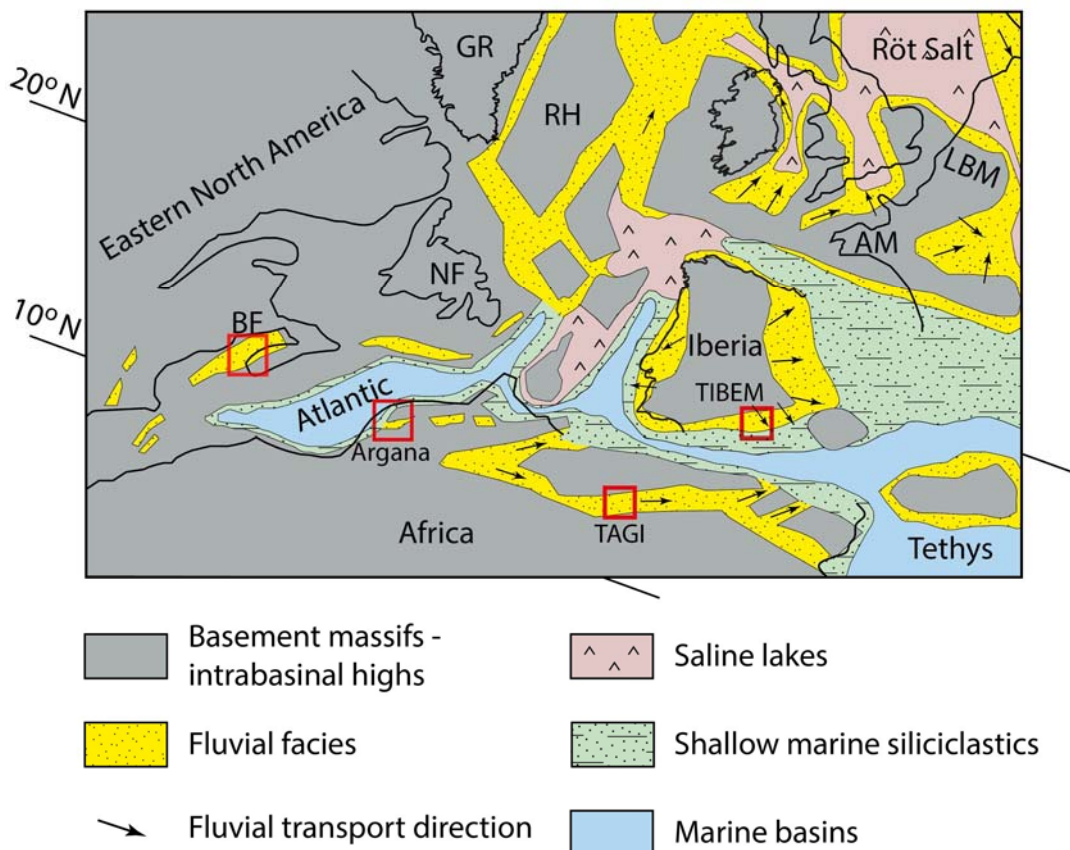
Fig. 1. Paleogeographic map of the North Atlantic and Tethyan rift basins in the middle Carnian. Triassic study areas and analogous Triassic basins indicated in red boxes. AM: Armorican Massif; BF: Bay of Fundy; GR: Greenland; LBM: London-Brabant Massif; NF: Newfoundland; RH: Rockall High. Modified from: Arche and López-Gómez (2014) with additional information from Ziegler (1990); McKie and Williams (2009).

2.2. Triassic stratigraphy: the Tabular Cover of Iberian Meseta (Central SE Spain) and the Argana Basin (Western High Atlas, SW Morocco)

Tabular Cover of the Iberian Meseta (Central SE Spain)

Triassic red beds of the Tabular Cover of the Iberian Meseta (Central SE Spain; herein referred as TIBEM; Henares et al., 2011; Viseras et al., 2011; Fig. 4A of Chapter 1) - originally defined as *Chiclana de Segura* Formation (López-Garrido, 1971) - cover *ca.* 4000 km^2 and range in thicknesses between 250 m and 600 m (Fernández, 1977). It corresponds to the southeast border of the Iberian Massif and constitutes an extensive continental non-deformed domain of red beds. It is organised in 4 different sequences (from I to IV, *sensu* Fernández and Gil, 1989) determined according to the fluctuation of the sea level – and its fingerprint in the alluvial record – recognised in the Prebetic zone (Gil et al., 1987; Fernández and Gil, 1989; Fernández et al., 1994). However, other authors divide the succession in three units according to minor regressive-transgressive events (Arche et al., 2002). As indicated by paleocurrent data, the main drainage directions were W-E (in the northern fluvial branch) and SW-NE (in the southern fluvial branch) with the studied section of Alcaraz (Albacete Province) being the most distal part of the TIBEM outcrops (Fernández and Dabrio, 1985; Henares et al., 2011). The succession in this area is about 160 m thick and only includes, from the base to the top, sequences II, III (Buntsandstein facies) and IV (Keuper facies) (Fernandez, 1977; Fernández and Dabrio, 1985; Fernández and Viseras, 2004) (see 4.1.1 section for further illustrations).

- Sequence I (Lower Ladinian) is a fining upward succession unconformably overlying the Paleozoic quartzite basement, with coarse sediments of alluvial fan and braided rivers passing up-section to sandy and silty sediments formed in sand flat and playa-lake environments. Deposition of this sequence is consistent with a drop of the base level caused by the subsidence associated to the first Triassic rifting stage.

- Sequence II (Ladinian) includes the Buntsandstein and Muschelkalk facies in the Prebetic Zone and most of the Buntsandstein in the Tabular Cover. The latter is made of mostly silty sediments with interbedded sandstone bodies deposited during a general base level rise which resulted in a lack of channel encasement and relatively high vertical accretion rates in floodplain. Sandstone bodies correspond to ribbon-like (Friend, 1983) straight and more frequently meandering channels along with lenticular, convex-up crevasse splay lobes and extensive tabular cm-thick horizontal sheetflood-like deposits, (Viseras and Fernández, 1994). Floodplain deposits include micritic carbonate paleosols, displacive gypsum nodules, and locally lignite layers.

- Sequence III (Ladinian-Carnian) approximately corresponds to the K1 unit defined by Ortí-Cabo (1974) in the Triassic of the Iberian Range and is regionally capped by the overlying K2 unit. In the Prebetic zone, the sequence overlies a karstified surface at the top of the Muschelkalk and consists of silt-gypsum-carbonate elementary sequences, while at the Tabular Cover it includes sandstone levels

15

embedded in silty sediments with calcrete paleosols. The channel fills observed in this succession include ripples and megaripples. Facies associations suggest that sediment was deposited during quiescent (or slightly decreasing) base level conditions in a fluvial environment connected to an evaporitic coastal plain (Fernández et al., 1993).

- Sequence IV (Carnian-Rethian) includes the Keuper units K2, K3, K4 and K5 as well as the dolomitic Imón Formation (Upper Triassic-Lower Jurassic; Goy and Yébenes, 1977). A 20-m-thick and hundred kilometers long continuous sandstone unit (the aforementioned K2 unit) formed as a braidplain depositional system marks the deposition of sequence IV. The overlying lutitic K3 unit evolves upward to argillaceous levels comprising nodular gypsum and carbonates (K4 and K5 units, respectively). Facies associations indicate a coastal alluvial system passing to an evaporite and carbonate tidal flat under rising base level conditions. At the time of the deposition of the K2 the base level was still stable so that sediment dispersal was mainly concentrated in coastal areas determining the retrogradation of both the coast line and the distal portion of fluvial systems. After that, a rapid base level rise marked the backstepping of the former coastal plain which was then converted into a coastal environment with sabkha evaporites overlain by marine carbonates.

The Argana Basin (Western High Atlas, SW Morocco)

Continental red beds of the Argana Basin (Fig. 4B of Chapter 1) - up to 20 km in width and extending over 85 km - consist of a *ca.* 5000-m-thick succession of Permo-Triassic sedimentary rocks (Tixeront, 1973, Brown, 1980) capped by the Argana basalt (205 ± 16 Ma; Fiechtner et al., 1992). This stratigraphic succession is subdivided into eight lithostratigraphic units or members (namely T1 to T8; Tixeront, 1973) grouped into three formations (Brown, 1980) (see 4.2.2 section for further illustrations).

- The lowermost Ikakern Formation (Late Permian, Brown, 1980; Jalil and Dutuit, 1996) rests unconformably on Palaeozoic basement and includes Ait Driss (T1) and Tourbihine (T2) Members. It typically consists of alluvial fan conglomerates from T1 grading vertically and laterally into cycles of conglomerate–sandstone–siltstone–mudstone from T2 interpreted as meandering river deposits intercalated with floodplain sediments (Brown, 1980).

- The intermediate Timesgadiouine Formation (Early–Middle Triassic; Klein et al., 2011) unconformably overlies the Ikakern Formation and consists at its base of the Tanameurt Member (T3), a volcanoclastic sheet-like conglomerate body of braided river origin (Brown, 1980). The Aglegal Member (T4) is conformable with both the underlying T3 and overlying T5 and is dominated by clayey mudstones, siltstones and minor fine-grained sandstones deposited in a flood plain environment with development of vertisols and intercalations of meandering fluvial deposits (Brown, 1980) or in a playa environment with intercalations of sheetflood and ephemeral streams (Hofmann et al., 2000). The Irohalene Member (T5) is a coarsening-upward sequence characterized by sandstones cyclically intercalated with massive mudstones, generated on an alluvial plain setting with meandering ephemeral rivers (Hofmann et al., 2000).

- The uppermost Bigoudine Formation (Late Triassic, Fiechtner et al., 1992) encompasses the Tadrart Ouadou Member (T6) at the base, the Sidi Mansour (T7) and the Hasseine Members (T8) (Tixeront, 1973; Brown, 1980). The Tadrart Ouadou sandstone is interpreted as the result of the aforementioned Carnian Pluvial Event (Arche and López-Gómez, 2014) and is continuous throughout the Argana Basin. The unit is up to 150 m thick and consists of proximal braided river conglomerates grading upward into sand-dominated, distal braided river deposits with intercalated aeolian sandstones (Hofmann et al., 2000; Mader and Redfern, 2011). Both T7 and T8 are composed of similar, cyclically arranged mud-rich facies which are difficult to separate into two distinctive members. T7/T8 strata formed in shallow ephemeral lakes and extensive saline mudflats with periodic fluvial and aeolian inputs of sand (Hofmann et al., 2000).

2.3. Depositional Environments

Tabular Cover of the Iberian Meseta (Central SE Spain)

From the Triassic sedimentary succession of the TIBEM in the area of Alcaraz, two major depositional environments were selected for further analysis of this thesis: floodplain (sequence II) and braidplain (K2 unit of sequence IV). Sedimentary deposits from the floodplain include: (i) overbank (crevasse splay lobe and sheetflood) and (ii) channelized (straight and meandering channels) deposits. The braidplain environment is characterized by three main depositional facies: (i) compound bar or "*sand flat*"; (ii) active channel area; and (iii) abandoned channel or "*slough channel*" (see 4.1.1 section for further illustrations).

Crevasse splay lobes are approximately 1-m-thick and extend over 30-70 m in the direction of progradation. They have a lenticular, convex-up morphology and are systematically associated to meandering channels (Dabrio and Fernández, 1986). Internally, sedimentary structures evolve upward from planar cross-bedding to low-angle cross-lamination or parallel lamination of lower flow regime (Dabrio and Fernández, 1986). Locally, mm-thick clay drapes separate successive prograding lobes (Fernández et al., 2005; Viseras and Fernández, 2010a).

Sheetflood deposits constitute tabular layers with a thickness around 1 m extending laterally for several hundred meters. They end wedging within floodplain clays (Dabrio and Fernández, 1986). Internally, energy decreases vertically and towards channel remote positions so that sedimentary structure evolves with the same pattern from parallel lamination of upper flow regime to parallel lamination of lower flow regime or cross-lamination (Dabrio and Fernández, 1986; Viseras and Fernández, 2010).

Straight channels are represented by lenticular, concave-up deposits which spread out toward the top forming the *expansion wings* (Friend et al., 1979; Stear, 1983). Their thickness is *ca.* 2 m and their lateral extension in transverse section of several tens of meters (30-50 m) (Fernández and Gil, 1989; Fernández et al., 2005). The internal organization consists of a thinning-upward succession made up of stacked, concave-up

sandstone layers, separated by clay laminae. From the base to top, trough cross-bedding evolves to cross- or parallel lamination (Fernández and Gil, 1989).

The meandering, ribbon-like, single-storey channel is of intermediate scale (70 m wide, 6.3 m thick, approximately; Fernández and Dabrio, 1985; Viseras and Fernández, 2010; Henares et al., 2014a; Henares et al., 2016a). Integrating depositional elements are: 1) main channel; 2) point bar; 3) scroll bar; and 4) chute channel. The main channel is represented by a thinning-upward succession with three different intervals: lowermost sandstone interval, which makes around the 75% of the total channel thickness and shows a concave-up morphology with cm-thick layers at the base comprising weakly imbricated mud intraclasts and trough cross-bedding; the overlying heterolithic interval characterized by alternating beds of silt/clay and very fine-grained sand with ripple lamination; and uppermost mud-dominated interval functioning as a clay plug. At the channel margin, sandstone layers with abundant mud intraclasts are overlain by sandstones beds with planar cross-bedding and wavy lamination. A wedge-shaped, asymmetric point bar sandstone body displays an internal mega cross-bedding which becomes asymptotic at the base and the top. Different sigmoidal sandstone beds within the point bar are separated by cm-thick clay drapes showing a fining upward succession from mud intraclasts lags deposit to fine and very fine-grained sand. From the base to the top, low-angle planar cross-bedding evolves to ripple lamination and eventually to horizontally laminated siltstone-claystone. Towards the floodplain, scroll bar facies show lower energy sedimentary structures such as horizontal lamination and climbing ripples. A lenticular-shaped, symmetrical chute channel sandstone body has basal and internal erosional surfaces with its infill dominated by ripple lamination (Viseras and Fernández, 2010).

The braided system constitutes a tabular 20-m-thick sandstone layer that is continuous over several hundred kilometres (Dabrio and Fernandez, 1986; Fernandez et al., 2005; Viseras and Fernandez, 2010). Individual braided channel sandstone is around 250-m-wide and consists of a thinning upward succession: on top of a flat base with horizontal lamination of upper flow regime, dunes and megaripples are hierarchically stacked resulting in trough cross-bedded and rippled sandstone layers. Locally, overturned cross-bedding are observed. Internal erosional surfaces are marked by lags of dm-scale mud intraclasts. Individual transverse compound bar sandstone body has an estimated width of 500 m and a length exceeding 1000 m, in the the main paleocurrent direction. Bar deposits are made of thinning-upwards lithofacies association with massive and horizontal lamination of upper flow regime at the base evolving to planar and trough cross-bedding. Arche and López-Gómez (2014) describe the occurrence of aeolian intervals of small dunes and interdune deposits with adhesion ripples, intercalated to these fluvial sediments. The transition between compound bar and the channel downstream (i.e. bar foreset or delta foreset *sensu* Cant and Walker, 1978) is characterized by sigmoidal cross-bedding with decreasing thickness towards the top. Abandoned channel shows a finning upwards succession with a cm-thick sandstone layer at the base with trough cross-bedding that passes to ripple lamination and finally to a clay plug.

The Argana Basin (Western High Atlas, SW Morocco)

Two fluvial systems were selected from the Triassic sedimentary succession of the Argana Basin: the braided system corresponding to the Tadrart Ouadou Mb (T6 unit) and a

straight channel from the Sidi Mansour-Hassein interval (T7/T8 unit) (see 4.2.2 section for further illustrations).

The deep perennial braided system (Cant and Walker, 1978; Ashmore, 1982) from the Tadrart Ouadou Member is a 25-40 m thick, 200-300 m wide sandstone body comprising four fluvial depositional elements (Viseras and Fernández, 2010; Mader and Redfern, 2011): main channel, lobate unit bars, compound bars and secondary channels. Asymmetric lobate unit bars (15-20 m long and up to 3 m high) display thick cross-bed sets separated by sharp, near horizontal bounding surfaces at the bar-tail with abundant rip-up clasts accumulated at the angular or tangential toesets. They correspond to foresets of megarriples and dunes developed at the bar-tail covering channel erosive bases (Lunt et al., 2004). Dominantly horizontal bedding is observed at the bar-head. Lateral and downstream accretion of lobate unit bars results in a larger-scale compound bar sandstone body (Bridge et al., 1998; Lunt et al., 2004). The lowermost part shows metre-thick sets of planar cross-bedded and horizontal laminated sandstones of several tens of metres in lateral extension. Mader and Redfern (2011) have interpreted part of these deposits as aeolian sediments. Top of compound bars can be truncated by a 2-3 m wide cross-bar channel which shows an erosional-base with abundant rip-up clasts (Bridge et al., 1998; Viseras and Fernández, 2010). A main channel segment may become partially disconnected due to bank attachment processes, when bars migrate obliquely respect to the main current direction, being reduced to a secondary channel (Lunt et al., 2004). The secondary channel fills mainly by lateral accretion and is characterized by a fining upward succession comprising epsilon cross-bedded sandstone with abundant rip-up clasts at the base, to cross- and ripple-laminated sandstone with flaser and wavy structures at the top.

Fluvial deposits from the T7/T8 interval are characterized by a 2 m-thick sandstone, with alternations of mudstone layers showing vertical aggradation. From the base to the top, a planar cross-bedding structure evolves to trough cross-bedding. Sedimentary architecture, dimension and internal structures suggest a straight channel as the fluvial depositional system (Viseras and Fernández, 2010, Viseras et al., 2011).

CHAPTER **3**

Methodology

3. Methodology

On the basis of a well-constrained sedimentological framework (see chapter 2 and references therein), the methodology followed on this thesis has three axial points: 1) sampling strategy; 2) high-resolution petrological analysis; and 3) petrophysical analysis.

3.1. Sampling strategy

Sampling was carried out to target the different sandy depositional facies integrating the studied depositional environments. Accordingly, the number of samples in each case study was determined to be representative as a function of defined number of architectural elements, their dimensions, lithofacies and spatial distribution. In all cases, samples correspond to the sand size interval (from 4 to -1Φ or from 0.063 to 2 mm) according to the Udden-Wentworth scale (Wentworth, 1922).

Core description

Outcrop sampling was based on pre-existing facies analysis and interpretation (Fernandez, 1977; Fernández and Dabrio, 1985 Fernández et al., 2005; Viseras and Fernandez, 2010a, b; Viseras et al., 2011). Samples were selected from unweathered portions of sandstone bodies.

Core sampling was based on the outcrop/behind outcrop characterization workflow (Slatt et al., 2011; Viseras et al., 2013; Viseras et al., 2015) which combines: 1) a high-detailed core description of four fully-cored behind-outcrop wells targeting the main depositional elements; and 2) the identification in core of sedimentary surfaces and facies boundaries by direct comparison and correlation with depositional geometries recognised in outcrop. A 1:20 scale core description, was performed according to a self-designed template which includes: driller's depth, grain-size log, main and secondary sedimentary structures, sediment colour (based on Munsell's colour chart), contacts, trends, fractures, lithofacies code as well as other remarks and environmental interpretation. Following correlation between outcrop and behind outcrop cored material was also validated with supplementary well log data (natural and spectral gamma ray logs) and borehole images (acoustic and optical televiewers).

3.2. High-resolution petrological analysis

Petrological analysis consisted of a detailed qualitative petrographic description and quantitative point count analysis to determine and characterize both depositional and diagenetic fabrics and mutual textural relationships. Chemical composition of mineral phases (e.g. clay and carbonate cements by back-scattered electrons – BSE – and microprobe analysis) was also determined in relevant cases. The depositional fabric was featured in terms of textural parameters such as grain size, sorting and roundness, detrital modal composition of sandstone framework and primary pore characteristics. Characterization of the diagenetic fabric included mineralogy and abundance of authigenic phases, habit and size of crystals and secondary pore features.

Sample preparation

Samples were thin sectioned oriented perpendicular to the bedding, etched and stained with hydrofluoric acid and Na-cobaltinitrite for plagioclase and K-feldspar identification (Chayes, 1952) as well as stained with alizarin red-S and potassium ferricyanide for carbonate type discrimination (Dickson, 1965). For pore system characterization, thin sections were vacuum-impregnated with blue epoxy resin. Samples were polished and carbon-coated for further investigation using scanning electron microscopy and determination of mineral chemical composition.

Techniques

Petrographic features were determined through optical and electron microscopy: a polarized optical microscope (model Carl Zeiss Jenapol-U; Department of Mineralogy and Petrology, University of Granada) equipped with a digital microphotography system (Nikon D7000) and two types of electron microscopes (operating at Centro de Instrumentación Científica – CIC –, University of Granada): scanning electron microscope (SEM Cambrigde Steresocan 360) and field emission scanning electron microscope which provides higher magnification than the first one (FESEM Leo-Gemini 1530, of Carl Zeiss SMT). Both are equipped with an energy dispersive X-ray spectrometer (EDX) for semiquantitative chemical analysis. Cold-cathodoluminescence (Citl MK4, conditions: 300-500 µA, 11-16 kV and 0.1-0.2 Torr; Department of Petrology and Geochemistry, Universidad Complutense de Madrid) coupled to an optical microscope was used for the characterization of carbonate cements by qualitative variations in Fe^{2+} (quencher element) and Mn^{2+} (activator element) contents (Hemmings et al., 1989).

In selected cases, bulk and clay-fraction mineralogy was determined by X-ray diffraction (XRD) in powders and oriented air-dried aggregates, respectively, using a Philips X'Pert PRO system (Department of Mineralogy and Petrology, University of Granada) and the XPowder© software (Martin Ramos, 2004) for interpretation of analytical results.

Chemical composition of carbonates (Ca, Mg, Mn, Fe, Sr and Ba) was obtained by using a Cameca SX100 electron microprobe (CIC, University of Granada) operating at 15 kV and 20 nA with an electron beam of 5 µm diameter.

Procedures

Standard:

- Petrographic point-count or "Gazzi-Dickinson" method (Dickinson, 1970; Gazzi et al., 1973; Ingersoll et al., 1984; Zuffa, 1985, 1987). This point-count technique (300-600 points per thin section), also called "modern method of textural approach", basically differs from traditional procedurres in to consider as monomineralic grains all crystals with size greater than 0.063 mm, including those in rock fragments. This approach reduces the grain-size dependency of modal composition and determines quantitatively the framework composition for sandstone classification and provenance discrimination. Proportions between

diagenetic products, intergranular components (i.e. matrix) and spaces are also determined.

- Grain size measurement. Mean grain (100 grains per thin section) and authigenic crystal sizes were digitally measured by using the open source software ImageJ (https://imagej.nih.gov/ij/).

- Diagenetic indexes (Ehrenberg, 1989; Lundegard, 1992). Following established conventions (Lundergard, 1992) and using Gazzi-Dickinson point-count data, intergranular volume (IGV), compaction (COPL) and cementation (CEPL) porosity loss and compaction index ($I_{compact}$) were calculated.

Done-on-purpose:

- Pore network characterization (Henares et al., 2016a). A point count (100 points per thin section) of pore spaces in the same area of the Gazzi-Dickinson point-counting allowed the semi-quantitative determination of both abundance and distribution of primary and secondary pore types and to relate them with petrophysical properties.

- Rip-up clast classification (Henares et al., 2016b). Specific characterization of rip-up clast grains was carried out according to their petrographic features (inclusion or not of dolomite crystals and, if so, its abundance and size) and mechanical behaviour during compaction in diagenesis (ductile, semi-ductile and rigid). Three main classes were determined: muddy, dolomitic muddy and dolomite crystalline rip-up clasts.

3.3. Petrophysical analysis

Petrophysical analysis focused on pore size distribution and open porosity (OP) and estimation of permeability (k).

Sample preparation

Samples of ca. 1 cm^3 were oven-dried for 24 h at 60º C before analysis. Two pieces were measured for each sample.

Techniques

Petrophysical parameters of OP and pore size distribution were determined by mercury injection-capillary pressure (MICP) with a Micromeritics Autopore III 9410 porosimeter, operating at Universidad de Granada. Technical limit ranges between pore sizes less than 0.003 and greater than 360 μm. Analysis with less than 15% mercury intrusion were discarded.

Procedures

- Permeability calculation (Pittman, 1992). On the basis of Pittman's (1992) work and MICP data, the following equation was used to estimate permeability values:

Log k = -1.221 + 1.415 Log (OP) + 1.512 Log r_{25}

where r_{25} is the pore aperture (µm) corresponding to the 25th percentile of saturation on a cumulative mercury injection plot. Correlation coefficient of this equation is 0.926.

CHAPTER **4**

Results and Discussion

4.1 Part I

Objectives

(i) To recognise vertical compositional and textural changes within sandstone samples from different fluvial environments of the TIBEM (sequence II and IV) and evaluate their impact on the development of diagenetic processes and pore network system.

(ii) To provide solid evidences supporting the TIBEM as the ideal outcrop analogue for the TAGI reservoirs (North Africa) and therefore enhance its value in estimating its microscale attributes as an important input for exploration, appraisal and enhanced oil recovery performance in this reservoir and in others with similar fluvial sandy facies throughout the Berkine-Ghadames basin.

4.1.1 The role of diagenesis and depositional facies on pore system evolution in a Triassic outcrop analogue (SE Spain)

S. Henares, L. Caracciolo, G. Cultrone, J. Fernández and C. Viseras

Abstract

This study aims at unravelling the diagenetic history and its effect on the pore system evolution of the Triassic redbeds exposed in SE Spain (TIBEM), an outcrop analogue of the TAGI (Trias Argilo-Gréseux Inférieur) reservoir (Berkine-Ghadames Basin, Algeria). Similar climatic, base level and tectonic conditions of aforementioned alluvial formations developed analogue fluvial facies stacking patterns. Furthermore, interplay of similar detrital composition and depositional facies in both formations resulted in analogue early diagenetic features. Petrographic observations indicate lithic subarkosic (floodplain facies) and subarkosic (braidplain facies) compositions which are considered suitable frameworks for potential reservoir rocks. Primary porosity is mainly reduced during early diagenesis through moderate mechanical compaction and formation of K-feldspar overgrowth, gypsum, dolomite and phyllosilicate cements. Early mesodiagenesis is testified by low chemical compaction and quartz cementation. Telodiagenetic calcite filling fractures and K-feldspar dissolution determined the final configuration of analysed sandstones. Mercury injection-capillary pressure technique reveals overbank deposits in the floodplain as the least suitable potential reservoirs because of their lowest open porosity (OP < 16%), permeability (k < 5 mD) and small dimensions. On the other hand, braidplain deposits show the highest values of such properties (OP up to 31.6% and k > 95 mD) and greater thickness and lateral continuity, so being considered the best potential reservoir. The accurate estimation of TIBEM microscale attributes can provide important input for appraisal and enhanced oil recovery performance in TAGI and in others reservoirs consisting on similar fluvial sandy facies.

INTRODUCTION

About 60% of petroleum reservoirs are sandstones (Bjørlykke and Jahren, 2010). In recent decades the increasing emphasis on maximizing recovery from existing oil and gas fields has prompted a renewed interest in the qualitative and quantitative characterization of reservoirs. Heterogeneity in continental sandstone bodies occurs at various levels and scales, ranging from micrometers to hundreds of meters, and is commonly attributed to variations in depositional facies, diagenesis and structural features such as the presence of fractures and faults (De Ros, 1998; Schulz-Rojahn et al., 1998). In this context, depositional system mainly controls: (i) sand-body geometry and architecture, sedimentary structures and mud/sand ratio, (ii) hydraulic sorting, (iii) primary porosity and permeability of sandstones, and (iv) near surface pore-water chemistry (Hartmann and Beaumont, 1999; Morad et al., 2000). Numerous interrelated factors such as detrital composition, textural parameters, tectonic setting, burial depth, composition and basinal fluid flow patterns determine type and development of physical and chemical diagenesis (Salem et al., 2000). Of particular relevance in reservoir quality assessment is porosity (primary and secondary), which varies according to the interplay of the main features mentioned above. Consequently, understanding the relationship between depositional facies and diagenesis is crucial in reservoir quality predictions (Bloch and McGowen, 1994).

Understanding reservoir evolution requires a relatively detailed reservoir 3D model, although its accuracy depends on the quantity and quality of available input data. In this sense, outcrop analogue studies have been demonstrated to be a powerful tool, supplementing sparse subsurface data with outcrop-derived measurements (Bryant and Flint, 1993; Ajdukiewicz and Lander, 2010). An appropriate analogue selection includes similar tectonic setting, geological age, subsidence rates and sedimentary environments (Bryant and Flint, 1993; Bjørlykke and Jahren, 2010). Triassic redbeds exposed in the Tabular Cover of the Iberian Meseta (SE Spain; herein referred to as TIBEM; Henares et al., 2011; Viseras et al., 2011) constitute an outcrop analogue of the TAGI (Trias Argilo-Gréseux Inférieur) reservoir (Rossi et al., 2002; Fernández et al., 2005; Viseras and Fernández, 2010). This Giant Field hosts the main oil reservoirs in the Berkine (Ghadames) Basin (Algeria) with reserves exceeding 250 million barrels of oil equivalent (MacGregor et al., 1998). TIBEM and TAGI developed result from the erosion of Paleozoic granitic and metamorphic terrains during the Tethyan rifting (Middle-Upper Triassic), and deposited in a peri-intracratonic basin during the Tethyan rifting process (Middle-Upper Triassic) and under similar climatic, base level and tectonic conditions. Hence, basin architectures show similar fluvial facies stacking patterns, varying from moderate sinuosity to braided fluvial channels (streaming over floodplain fine sediments, including palaeosol development) evolving upsection to tidal-influenced facies (Fernández and Dabrio, 1985; Turner et al., 2001; Rossi et al., 2002; Ratcliffe et al., 2006). However, rReservoir-scale TAGI sandstone correlation and modelling is hampered by marked vertical and lateral facies variations, plus sequences are biostratigraphically barren (Ratcliffe et al., 2006).

This study aims at determining the spatial variations and timing of diagenetic processes and their influence on the pore system among well-defined fluvial facies in sandstone bodies of TIBEM. Differences in the late burial history between TAGI and

TIBEM exist. However, mutual age, tectonic setting, detrital composition and depositional facies justify its comparison, and make the TIBEM a suitable analogue for the TAGI reservoir. Furthermore, Given that this formation can be considered as an outcrop analogue of the TAGI sandstones, the accurate estimation of its microscale attributes can provide important input for exploration, appraisal and enhanced oil recovery performance in this reservoir and in others with similar fluvial sandy facies throughout the Berkine-Ghadames basin.

GEOLOGICAL AND STRATIGRAFIC BACKGROUND

Triassic redbeds of the Tabular Cover of the Iberian Meseta (TIBEM) crop out between the Iberian Massif to the North (Central Iberian Zone) and the Betic Cordillera to the South (External Zones; Fig. 1). The basin is part of the continental realm developed during the Tethyan continental rifting process (Late Permian-Upper Triassic; Sánchez-Moya et al., 2004). The ca. 250 m thick Triassic (Anisian-Norian) sedimentary succession is organised in four subhorizontal depositional sequences (I to IV according to Fernández and Dabrio, 1985). The succession consists of siliciclastic alluvial-lacustrine and fluvial facies directly overlying the Paleozoic basement. Each sequence developed under the same base level conditions controlled by Tethys level fluctuations (Haq et al., 1987; Fernández et al., 1993, 2005). Basing on sedimentary structures and facies association, Arche et al. (2002) identify three stratigraphic units produced by minor regression-transgression cycles during a general sea level rise.
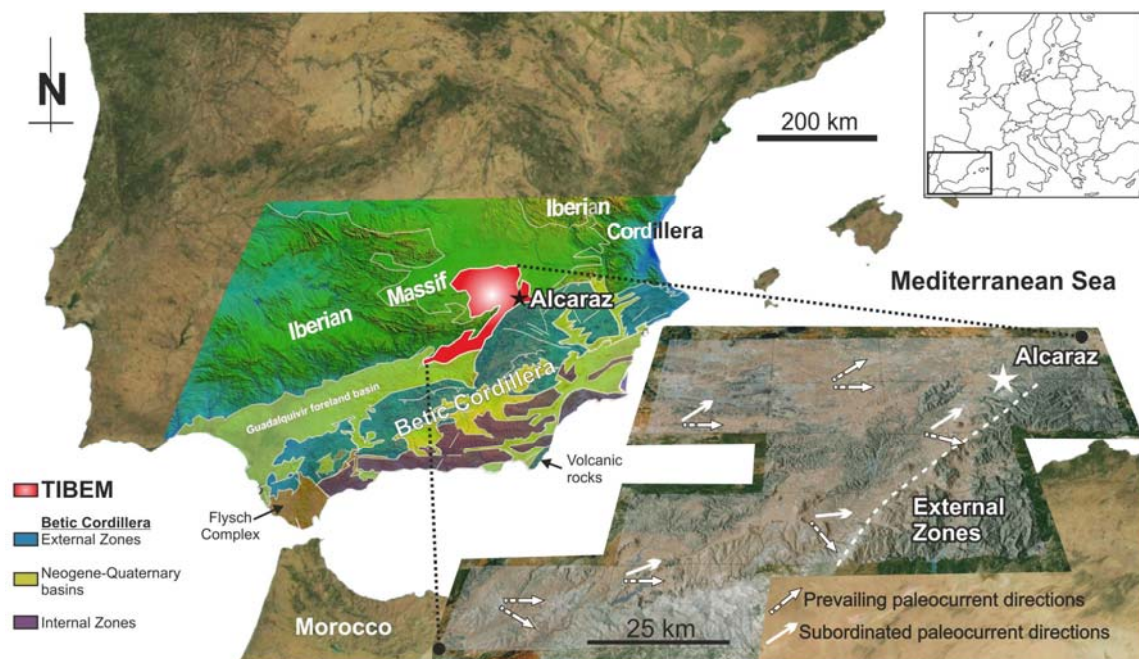

Fig. 1. Geographical and geological location of the TIBEM. Arrows show the paleocurrent directions of drainage near the study area (Alcaraz) (Henares et al., 2011; Viseras et al., 2011).

As indicated by paleocurrent data, the main drainage directions were W-E and SW-NE with the section in Alcaraz (Albacete, SE Spain) proving to be the most distal part of the TIBEM outcrop (Fernández and Dabrio, 1985; Henares et al., 2011) (Fig. 1). The succession is about 160 m thick and includes, from the base to the top, sequences II, III
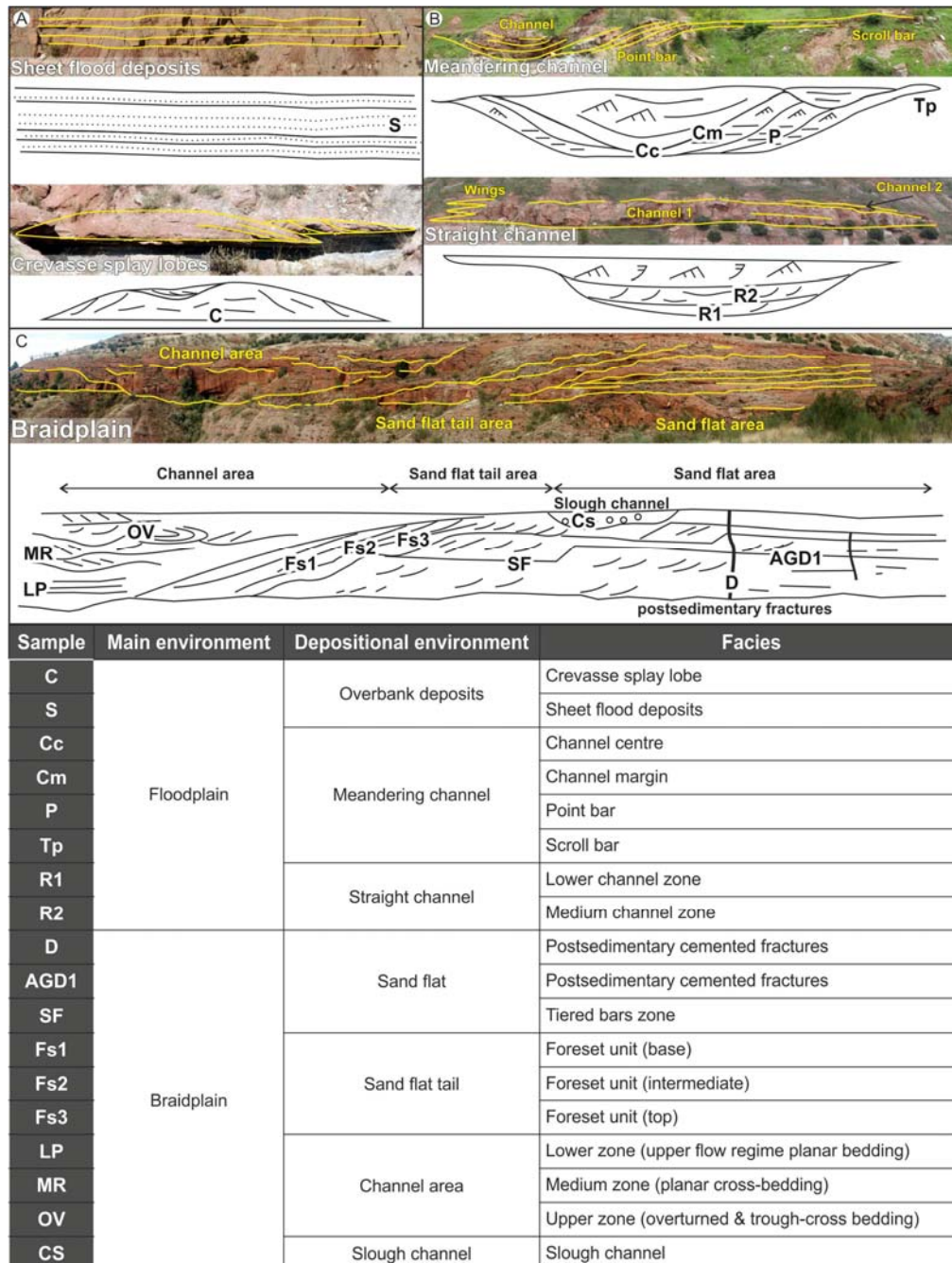
(Buntsandstein facies) and IV (Keuper facies) (Fig. 2). Sandstone bodies and micritic carbonate levels from silt-rich sequence II were deposited in a floodplain including channels (meandering and straight) and overbank deposits (crevasse splay lobes and sheet flood deposits) (Viseras and Fernández, 1994) during a general base level rise (Fig. 2). Channel bodies are 3 to 7 m thick and several decametres long, while overbank deposits vary from 1 to 3 m thick and 30 to several hundred meters long (Fernández and Dabrio, 1985). A widespread development of calcrete paleosols, consistent with a falling base level (Fernández et al., 1993), accompanies the deposition of sequence III. A 20 m thick and 100 km long sandstone bank from braidplain depositional system, marks the beginning of sequence IV (Fernández et al., 2005; Viseras and Fernández, 2010; Fig. 2). A progressively faster base level rise triggered the deposition of silt-rich coastal plain facies and intertidal sabkha evaporites. Shallow marine dolomites of the Imón Formation (Upper Triassic-Lower Jurassic) overlie and cap sequence IV.

Fig. 2. TIBEM stratigraphic succession in the Alcaraz area (modified after Dabrio and Férnandez, 1986).

33
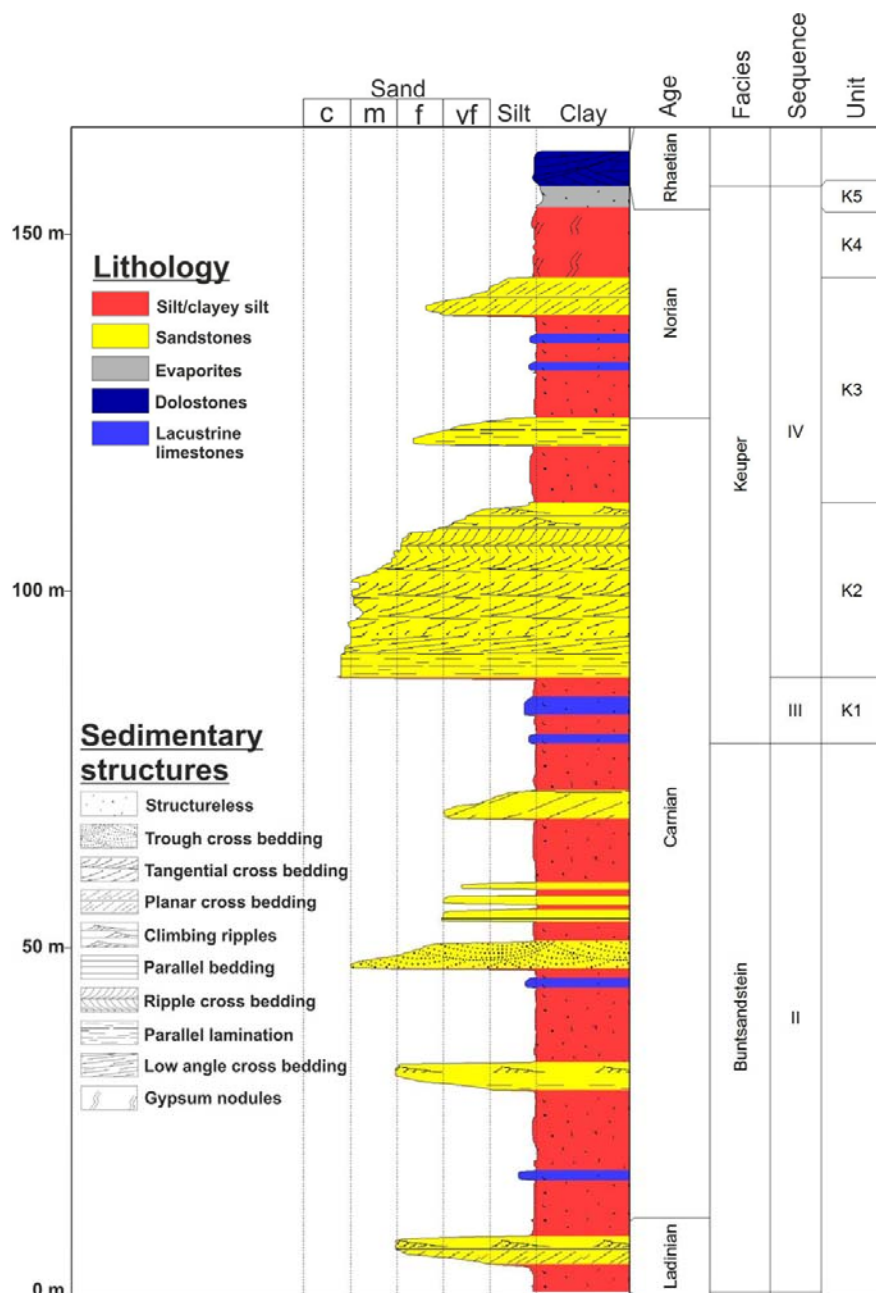
SAMPLING AND METHODS

Two principal sedimentary environments were studied: floodplain (sequence II; Fig. 3A, B) and braidplain (base of sequence IV: Fig. 3C). Samples from floodplain deposits were selected from: (i) overbank (crevasse splay lobe and sheet flood deposits) and (ii) channel facies (meandering and straight). Samples from the straight channel are from the lower and the medium part of the channel centre. The meandering channel has been sampled in its centre, margin, point bar and scroll bar sandy facies.

Sample	Main environment	Depositional environment	Facies
C	Floodplain	Overbank deposits	Crevasse splay lobe
S			Sheet flood deposits
Cc		Meandering channel	Channel centre
Cm			Channel margin
P			Point bar
Tp			Scroll bar
R1		Straight channel	Lower channel zone
R2			Medium channel zone
D	Braidplain	Sand flat	Postsedimentary cemented fractures
AGD1			Postsedimentary cemented fractures
SF			Tiered bars zone
Fs1		Sand flat tail	Foreset unit (base)
Fs2			Foreset unit (intermediate)
Fs3			Foreset unit (top)
LP		Channel area	Lower zone (upper flow regime planar bedding)
MR			Medium zone (planar cross-bedding)
OV			Upper zone (overturned & trough-cross bedding)
CS		Slough channel	Slough channel

Fig. 3. Outcrop photointerpretations and facies models of the analysed deposits, with letters indicating the name and the position of the samples. A) and B) Overbank and channel deposits from the floodplain environment. C) Braidplain environment. Note that the facies model corresponds to one aggradation cycle in the braidplain. Attached table shows the samples legend.

Four depositional environments were analysed from the braidplain: (i) sand flat area (tiered bars zone and vertical postsedimentary cemented fractures); (ii) sand flat tail area (foreset units); (iii) channel area (upper flow regime planar bedding, planar cross-bedding and overturned and trough-cross bedding zones); (iv) slough channel (see inset table in Fig. 3 for more detailed information about analysed facies).

Seventeen selected samples were thin sectioned and polished for petrographic study, including etching and staining, using hydrofluoric acid and Na-cobaltnitrite for plagioclase and K-feldspar identification respectively (Chayes, 1952). 340-561 points per thin section were determined, according to the Gazzi-Dickinson method (Ingersoll et al., 1984; Zuffa, 1987, 1985). Confidence regions of detrital-mode means were calculated according to Aitchison (1997). Confidence regions (90%) were computed using the log-ratio transformation of compositional data 'R' and the 'Composition' software package (Boogaart and Tolosana-Delgado, 2008).

Bulk and clay-fraction mineralogy identification was carried out by X-ray diffraction (XRD) in powders and oriented air-dried aggregates respectively. A Philips X'Pert PRO system was used, and the results were interpreted using the XPowder(C) software (Martin, 2004). The textural features of the cements were studied by examining freshly broken and polished sample surfaces using a field emission scanning electron microscope (FESEM Gemini, of Carl Zeiss SMT) and a scanning electron microscope (SEM Cambrigde Steresocan 360), both equipped with an energy dispersive X-ray spectrometer. Cold-cathodoluminescence was used for microscopic optical inspection of carbonate cements. In addition, mercury intrusion injection-capillary pressure porosimetry (MICP) was carried out on two fragments per sample of about 1 cm3 using a Micromeritics Autopore III porosimeter model 9410. Pores ranging between 0.003 and 360 μm were analysed to characterize the pore system of the sandstones.

RESULTS

Petrology

Depositional texture

Grain size of sandstones from floodplain varies from very fine-grained overbank to fine-grained channel deposits with moderately to well-sorted rounded grains. In some cases, sedimentary structure is highlighted by laminae showing a fine to slightly coarser grain size alternation (e.g. point bar; Fig. 4A), whereas others show higher concentrations of micas and Fe oxides (e.g. sheetflood deposit and crevasse splay lobe; Fig. 4B). Contacts between grains vary from punctual to elongated concave-convex in samples with a high compaction degree. Sandstones from braidplain are fine to medium-grained with well-sorted subrounded to rounded grains. Exceptions are represented by samples with abundant detrital matrix. Sutured contacts were observed in samples showing evidence of chemical compaction.
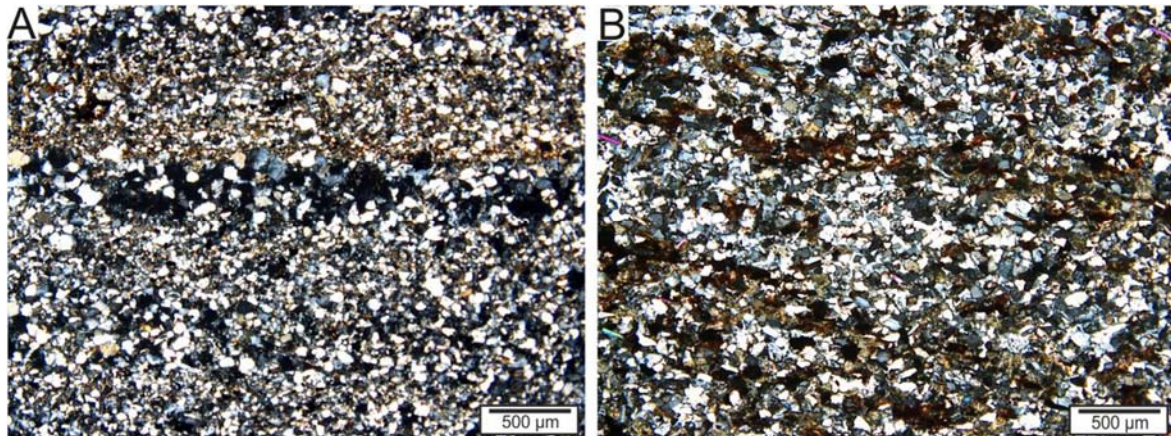
Fig. 4. A) Alternation of finer- and coarser-grained laminae in point bar facies. B) Laminae with higher mica and Fe-oxide contents in crevasse splay facies.

Arenite framework composition

The composition of the analysed sandstones varies from lithic arkose to lithic subarkose ($Q_{62}F_{27}Rf_{11}$) in sandstones from the floodplain (sequence II) to dominantly subarkose and subordinate lithic subarkoses ($Q_{74}F_{16}Rf_{10}$) in sandstones from the braidplain (base of sequence IV; Tables 1 and 2, Fig 5) (according to Pettijohn et al., 1975).
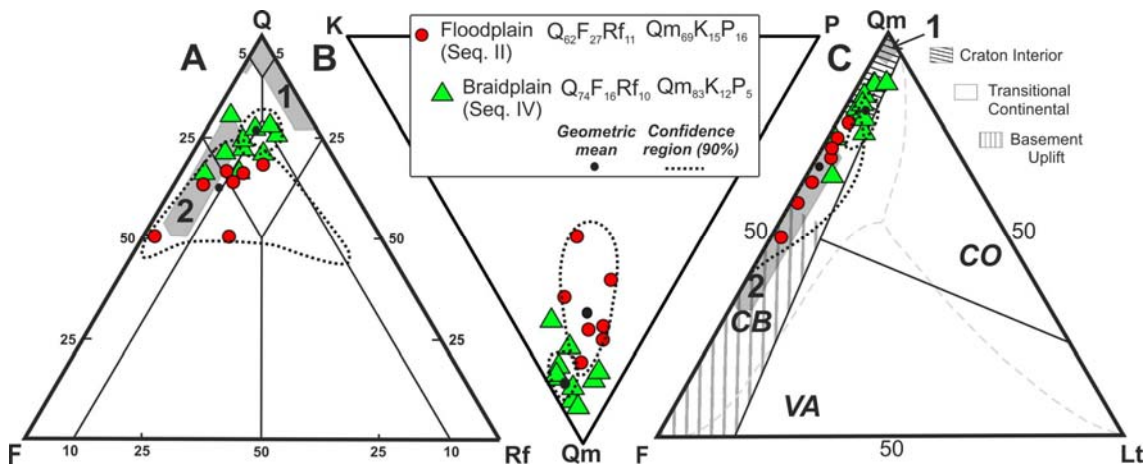
Fig. 5. Ternary plots of compositional parameters and tectonic discrimination. A) QFRf: quartz, feldspars and rock fragments (according to Pettijohn et al., 1975). B) QmKP: monocrystalline quartz, K-feldspars and plagioclase. C) QmFLt: monocrystalline quartz, feldspars and lithic fragments [according to Dickinson (1985) and Weltje (2006)]. CB: continental block; CO: collisional orogeny; VA: volcanic arc. Light grey dotted lines indicate Weltje's recalculated provenance fields. Grey-filled fields represent TAGI samples: 1= Lower TAGI, 2= Middle-Upper TAGI (after Rossi et al., 2002).

Quartz is the dominant grain. It occurs in both monocrystalline (Q_m) and polycrystalline form, with the latter being more abundant in braidplain deposits (Fig. 5A). A peculiar corrosion embayment alteration has been recognised on quartz grains from sand flat facies ("embayed quartz" from Clearly and Conolly, 1974; Fig. 6A). Feldspars are well represented: K-feldspars (K; mostly orthoclase and secondarily, microcline) dominate on

plagioclase (P; mainly albite) (Fig. 5A). Moreover, plagioclase content decreases upsection from the floodplain ($Qm_{69}K_{15}P_{16}$) to the braidplain deposits ($Qm_{83}K_{12}P_5$) (Fig. 5B). They are typically monocrystalline and their presence is scarce in rock fragments. Floodplain deposits show alteration of potassium feldspars by kaolinite and/or illite and plagioclase by sericite. Locally, feldspars show partial dissolution of the detrital grain (Fig. 6B, C). Rock fragments (Rf) encompass composite quartz (>63 µm monomineralic, polycrystalline rock fragment of plutonic or high grade metamorphic undeterminable origin) and lithic fragments, representing 2.7% of Total Framework Composition (TFC). Lithic fragments consist of fine-grained schists and minor phyllites. Micas (mainly muscovite) are rare (0.5% TFC) and mainly concentrated in sandstones from the floodplain. They are frequently altered and stained by Fe-oxides and show deformation due to mechanical compaction. Heavy ultrastable mineral assemblage (0.4% TFC) consists of zircon, tourmaline and rutile, and less frequently, opaque minerals. These grains typically concentrate in sandstones from the floodplain along preferential finer-grained laminae and are usually well rounded (Fig. 6D, E).

Matrix

Matrix content varies from 7% of the total composition in floodplain to 6.6% in braidplain sandstones. Detrital matrix, consisting of siliciclastic grains, i.e. quartz and feldspars of less than 63µm in size, is transported and deposited with the coarser sand-size grains above all in braidplain facies (Fig. 7A). Diagenetic matrix or pseudomatrix consists of clay minerals (size under 30 µm), frequently reddish-stained by adsorption of Fe-oxides (Fig 7B, C, D). Pedogenesis (sensu FitzPatrick, 1984 and Scarciglia, 2; Fig. 7A), replacement of feldspar grains by kaolinite and/or illite (Fig. 7B) and mechanical deformation of ductile grains (silty-clay intraclasts) (sensu Dickinson, 1970 and Arribas, 1984; Fig. 7C, D) are the processes responsible of pseudomatrix formation. Its occurrence has been documented in all deposits, though is more abundant in floodplain facies.

Diagenesis

Compaction

Mechanical compaction is manifested as deformation of ductile grains such as micas and silty-clay intraclast (Fig. 7C, D). This process, favoured by the occurrence of these grains and inhibited by early diagenetic cements, enhances a denser sediment packaging in floodplain sandstones. Ductile grains concentrate preferentially in the finer-grained laminae. Chemical compaction usually generates elongate concave-convex contacts and triple joints. Pressure solution (grain contact dissolution) processes also occur especially between quartz and plagioclase grains, sometimes favoured by the presence of clay coatings.

**Table 1.** Modal composition of selected representative floodplain facies.

	C	S	Cc	Cm	P	Tp	R1
	Crevasse splay	Sheetflood	Centre meand.	Margin meand.	Point bar	Scroll bar	Straight ch.
Quartz (single crystal)	148	209	195	184	194	162	192
Polycrystalline Q without tectonic fabric	1				5	2	
Q in plutonic r.f.				2		2	2
Q in sandstone							
Composite Q	3	17	40	24	48	52	26
Carbonate replacement on Q							
K-feldspar (single crystal)	80	71	22	26	25	38	34
Kf in plutonic r.f						2	2
Carbonate replacement on Kf							
Plagioclase (single crystal)	72	34	44	48	23	70	40
P in plutonic r.f.			2		1	4	
Carbonate replacement on P							
Mica (single crystal)	1	4	4		2		4
Mica in plutonic r.f.				4			
Opaque	1	2					
Tourmaline	1						
Rutile		1			1		
Zircon		3					
Slate lithic fragment							
Phyllite lithic fragment		1					
Fine grained schist		2		8	1	2	
Fe-oxides			2	1		2	
Matrix							
Siliciclastic/Detrital matrix	8	60	8	2	21	36	8
Pseudomatrix	6	6	18		13		8
Cements							
Carbonates							22
Phyllosilicate pore filling	7	8	4	12	24	20	28
Quartz overgrowth			2				
K-feldspar overgrowth	6				7	2	13
Gypsum	24	58	36	90	3		
Fe-oxides	2				2		
Carbonate replacement on undetermined grain							
Clay grain coats	4	8					3
Q % (2σ)	48.8 (0)	62.6 (0)	64.4 (0)	62.2 (0)	66.4 (0)	48.8 (0)	64.9 (0)
F % (2σ)	50.2 (5.6)	31.4 (26.1)	21.8 (15.5)	25.0 (15.5)	16.4 (1.4)	32.5 (22.6)	25 (4.2)
Rf % (2σ)	1 (0)	6 (8.9)	13.9 (26.9)	12.8 (9.9)	17.1 (27.1)	18.7 (22.1)	10.1 (13.8)
Qm % (2σ)	49.2 (0)	65.9 (0)	74.1 (0)	69.2 (0)	77.9 (0)	57.9 (0)	71.6 (0)
F % (2σ)	50.5 (5.7)	33.1 (18.4)	25.9 (21)	27.8 (15.6)	19.7 (13.3)	40.7 (32.2)	28.4 (20.4)
Lt % (2σ)	0.3 (0)	0.9 (0.7)	0 (0)	3.0 (0)	2.4 (2.8)	1.4 (0)	0 (0)

Table 2. Modal composition of selected representative braidplain facies

	D	SF	AGD1	Fs1	Fs2	Fs3	LP	MR	OV	CS
	Sand flat			Sand flat tail			Channel			Slough ch.
Quartz (single crystal)	185	236	220	192	209	258	214	277	220	242
Polycrystalline Q with tectonic fabric	2	2	2		1		2		4	2
Polycrystalline Q without tectonic fabric	12	10	6	2	9	9	4	9	6	10
Q in plutonic r.f.				1	3		6			
Q in sandstone		2					1			
Composite Q	13	20		32	15	30	34	56	23	32
Carbonate replacement on Q	12			8	15	6				2
K-feldspar (single crystal)	46	44	38	40	53	29	15	26	16	18
Kf in plutonic r.f			2	1		3	1			
Carbonate replacement on Kf	17				1					
Plagioclase (single crystal)	22	13	4	24	13	12	26	6	33	2
P in plutonic r.f.							2			
Carbonate replacement on P	2		2			3				
Mica (single crystal)					4			4		
Opaque					2				5	
Tourmaline	1									
Rutile								2		
Zircon							1	1		
Slate lithic fragment		4								
Phyllite lithic fragment		3			3					
Fine grained schist	1		2	1	2				1	2
Fe-oxides					2	3			2	
Matrix										
Siliciclastic/Detrital matrix	2	41	2	3	20	4	12	130	16	1
Pseudomatrix	5	6	4	1	1		1		2	16
Cements										
Carbonates	95		40	35	19	30		44	11	2
Phyllosilicate pore filling	9		2		2	1				
Quartz overgrowth										1
K-feldspar overgrowth	7	18	4	5	8	8	9		11	
Gypsum										104
Fe-oxides			4	3	1	8	6		5	
Carbonate replacement on undetermined grain	6		18	6	1	7		4		
Clay grain coats		9		1			6		7	
Q % (2σ)	66.1 (122.3)	66.1 (0)	82.1 (0)	66.9 (130.1)	71.3 (137.2)	77.4 (178.2)	71.6 (0)	75.9 (0)	75.1 (0)	81.9 (169.7)
F % (2σ)	29.2 (18.3)	29.2 (21.9)	16.4 (20.2)	21.4 (11.3)	21.3 (27.2)	12.9 (13.2)	13.7 (7.8)	8.8 (14.1)	16.7 (12)	6.7 (11.3)
Rf % (2σ)	4.7 (8.5)	4.7 (8.5)	1.5 (0)	11.7 (15.5)	7.3 (6.2)	9.7 (19.1)	14.7 (14.2)	15.3 (0)	8.2 (15.6)	11.4 (21.2)
Qm % (2σ)	64.5 (122.3)	75.6 (0)	79.7 (0)	73.8 (0)	71.8 (0)	82.2 (0)	81.1 (0)	87.1 (0)	78.6 (0)	87.7 (0)
F % (2σ)	30.3 (18.3)	18.3 (21.9)	16.7 (20.2)	25 (19.6)	23 (27.2)	15 (12.3)	16.7 (11.9)	10.1 (14.1)	17.5 (12)	7.2 (11.3)
Lt % (2σ)	5.2 (8.5)	6.1 (3.6)	3.6 (0)	1.2 (0.7)	5.2 (3.6)	2.9 (0)	2.3 (1.4)	2.8 (0)	3.9 (2.5)	5.1 (4.6)
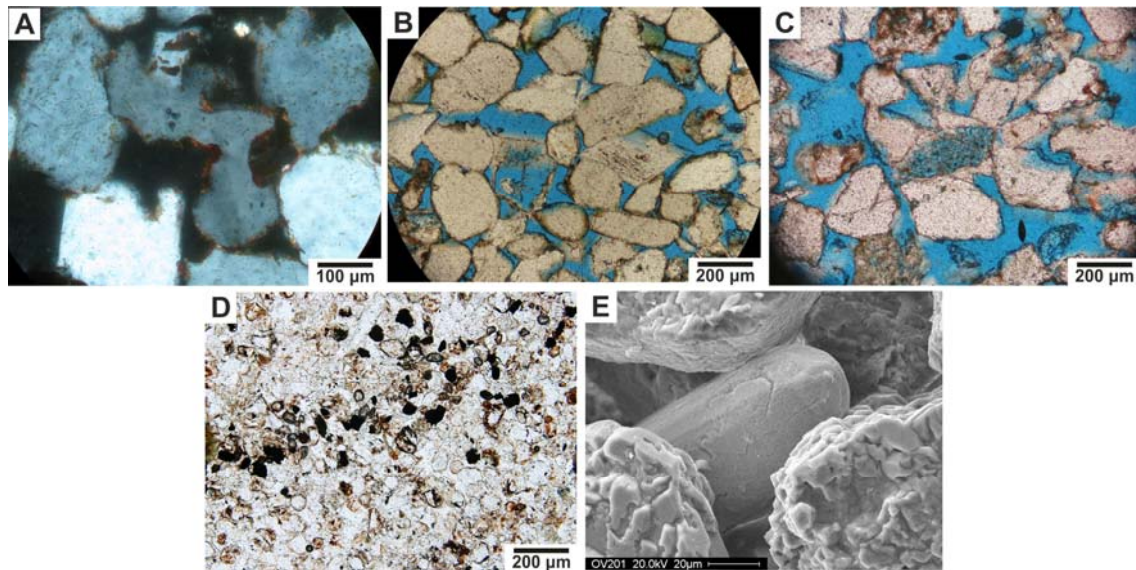
Fig. 6. A) Crossed-nicols photomicrograph showing corrosion embayment alteration in quartz grains from sand flat deposits. B) and C) One-nicol photomicrographs showing partial dissolution of detrital feldspar grains in sand flat deposits. D) One-nicol photomicrograph showing preferential concentration of heavy and opaque minerals along a discrete lamina in the crevasse splay deposit. Note the abundance of zircons. E) SEM image of a well-rounded zircon in a sample from the braidplain channel area.
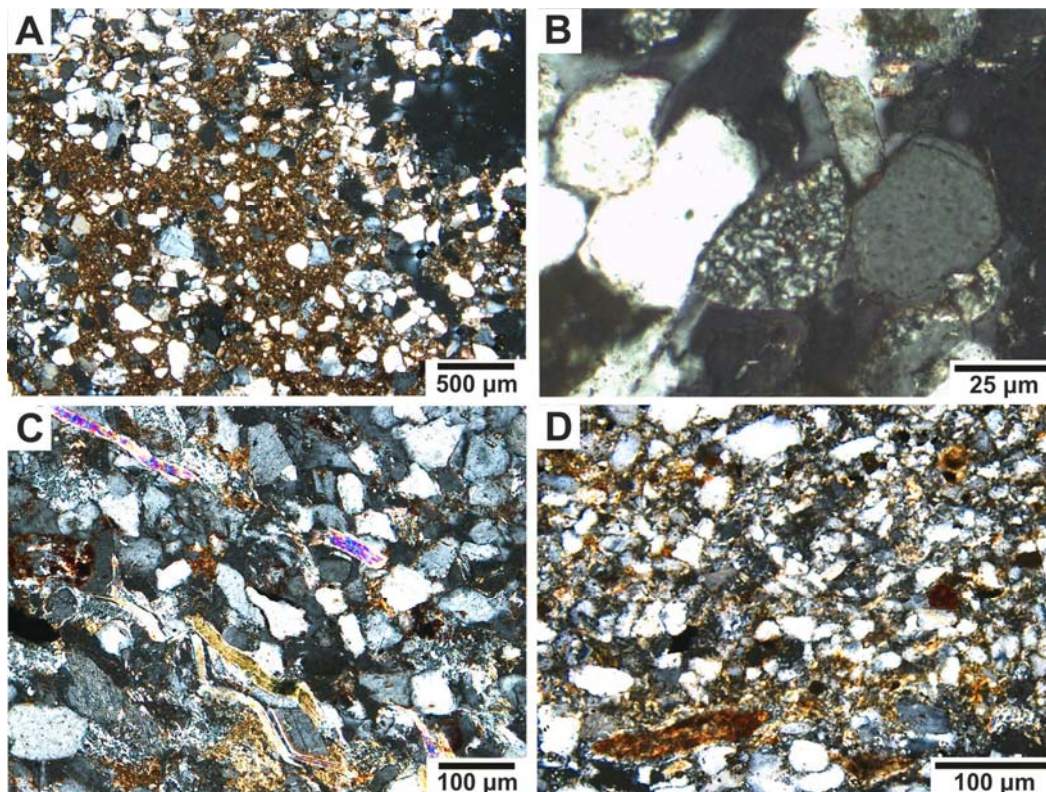
Fig. 7. Crossed-nicols microphotographs of matrix and pseudomatrix. A) Detrital with pedogenetic matrix in a sample from the braidplain channel area. B) Kaolinite completely replacing a feldspar grain in the sheet flood deposit. C) and D) Mechanically deformed muscovite (crevasse splay deposit) and silty-clay intraclast (point bar deposit) grains, respectively.

Cements

Fe-oxide cement: this occurs in low concentrations (0.4%), typically in braidplain samples. It mostly precipitates in veins and fractures, although it has been identified locally as a pore-filling type cement adjacent to detrital grains (Fig. 8A).

Illitic clay grain-coatings: this cement has been recognized in all of the studied environments (0.6%). Coatings consist of reddish-stained illitic platelets arranged tangentially to detrital grain surfaces (Fig. 8B). Usually the coats are thicker in braidplain samples (Fig. 9A), whereas in overbank samples they are usually thin and discontinuous. Sometimes, illite is associated with mixed-layer illite/smectite (Fig. 9A, B).

Kaolinite-illite pore fillings: this type of cement (1.7%) occurs preferentially in floodplain facies including abundant intraclasts. Kaolinite plates are typically less than 10 μm and normally occur bordering detrital framework grains. Gypsum and carbonate patches enclosed by this cement have been recognized (Fig. 8C). Locally, kaolin masses are reddish-stained due to admixed Fe-oxides. Some kaolinite is transformed into illite, forming face-to-face aggregates (Fig. 9C).

Quartz cement: This only occurs in minor amounts (<0.1%). Two different textures are recognized: (1) grain overgrowths and (2) microcrystalline growths. A large number of inherited abraded overgrowths are observed (Fig. 8D). Nevertheless, when authigenic syntaxial overgrowths form, they are discontinuous and thin around quartz detrital grains developing euhedral faces. This texture developed in samples with important chemical compaction features. Microcrystalline quartz growths, identified by FESEM, consist of subeuhedral crystals usually less than 5 μm (Fig. 9D).

K-feldspar overgrowths: this type of cement occurs in higher concentration than that of quartz (1.4%) and is especially well represented in braidplain facies. It consists of thick syntaxial overgrowths, forming euhedral prisms around detrital K-feldspar grains (Fig. 9E). Locally, its growth occludes primary pore spaces (Fig. 8E).

Carbonate cement: this cement is composed of dolomite and subordinate calcite (5%) and normally concentrates in fracture-associated braidplain facies. Poikilotopic crystals are the most common texture for both minerals, although locally mosaic-type textures have been recognized (Fig. 8F). Replacements of framework grains and kaolinite cement are pervasive (Fig. 8G, 9C). Zoned orange-yellowish luminescent dolomite and null luminescent calcite usually occur together in the same sample (Fig. 10A, B, C, D). Dolomite is more abundant whereas calcite precipitation occurred in small randomly distributed spots. Patches with regular borders of luminescent dolomite were also observed enclosed by gypsum cement in samples from the slough channel.

Gypsum cement: it was recognised (4.6%) exclusively in floodplain facies and in the braidplain slough channel. Usually it consists of poikilotopic crystals occluding the primary porosity (Fig. 8H, 9F). A drusy texture was observed in veins filled with gypsum.
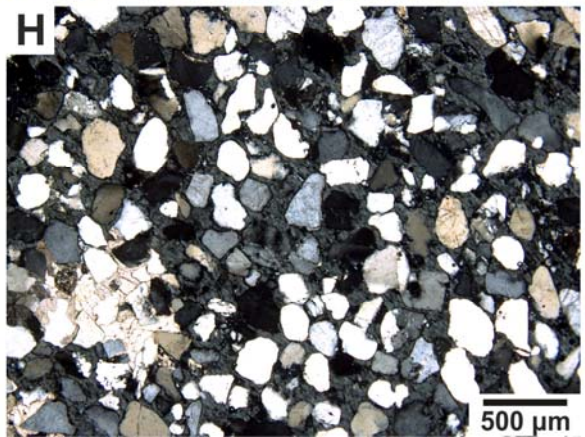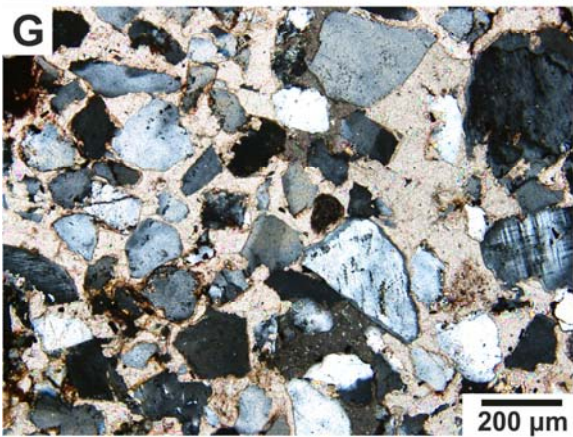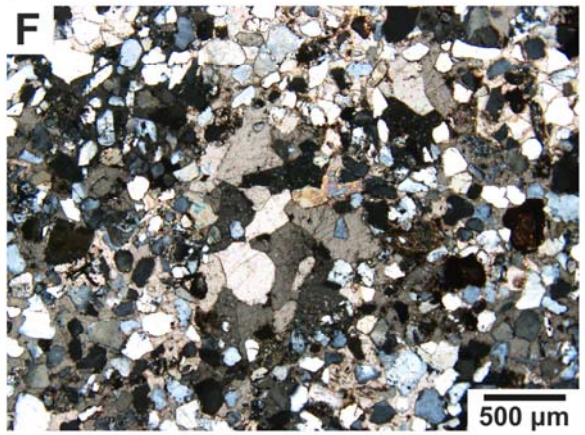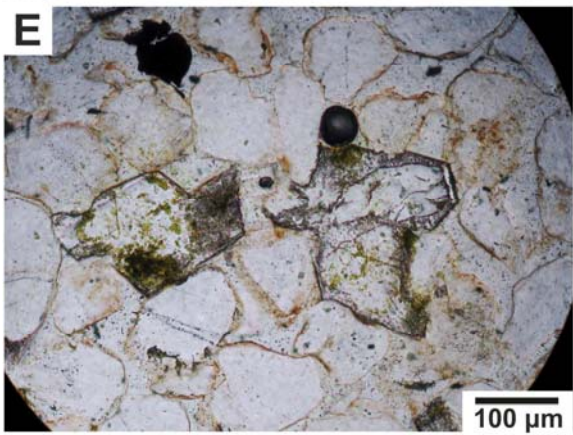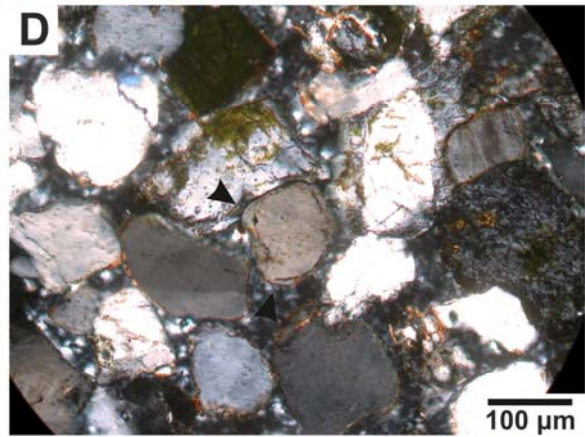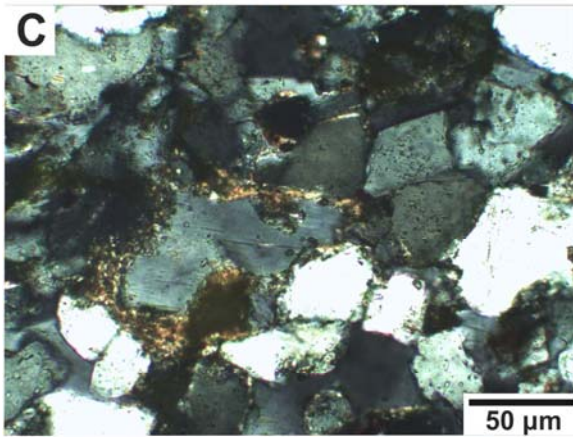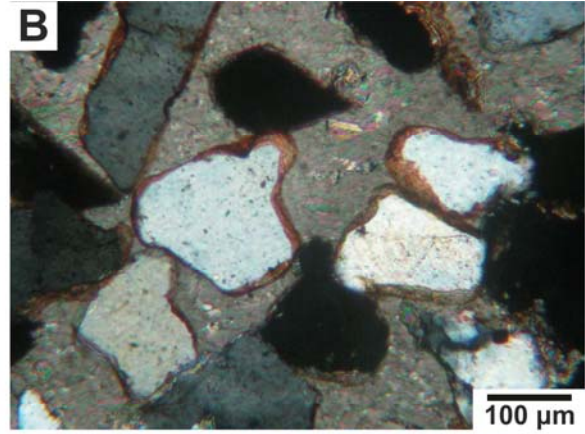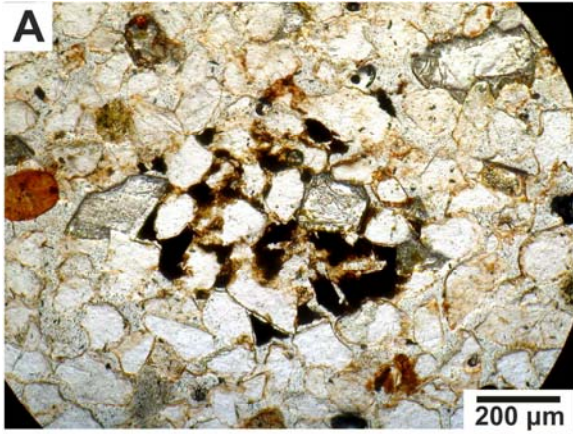
Dissolution

Secondary porosity is related to feldspars, carbonates and gypsum dissolution. Feldspar detrital grains preferentially dissolve following the cleavage planes and do not affect associated overgrowths (Fig. 6B, C). Secondary pores with irregular rims occur where dolomite and gypsum have been dissolved. Fractures are also observed within gypsum crystals.

Pore system

MICP data show considerable differences in open porosity (OP) values and pore size distribution between floodplain and braidplain facies (Table 3; Fig. 11). The lowest OP values are systematically related to the occurrence of carbonate and gypsum cements, finer grain sizes and, occasionally, higher mechanical compaction. The highest OP values are mostly associated with the occurrence of K-feldspar overgrowths and coarser grain sizes. Indicative permeability values (k) were obtained (Table 3) basing on MICP data and Pittman's equation (Pittman, 1992, 2001).

Open porosity

Overbank deposits in the floodplain show very uniform OP values with 15.6% (k = 2 mD) for crevasse splay lobe (C) and 15.7% (k = 3 mD) for sheet flood deposit (S) (Table 3). Gypsum cement, as well as a high mechanical compaction, has been documented in these facies. Straight channel shows OP values varying from 23.6% (k = 154 mD; medium part, R2) to 24.1% (k = 140 mD; lower part, R1). In the meandering channel, the different facies show variable OP values, from the lowest to the highest as follows: channel margin (Cm; 16%; k = 16 mD), point bar (P; 19.8%; k = 56 mD), scroll bar (Tp; 27.2%; k = 133 mD) and centre of the channel (Cc; 30.7%; k = 413 mD). In the channel margin, gypsum cement occurs, whereas the point bar facies shows significant mechanical compaction features.

Fig. 8. Photomicrographs of the petrography of TIBEM sandstones cements. A) Fe-oxide pore-filling cement in a sample from the braidplain channel area. Proximity to detrital grains and the textural relationship with K-feldspars reveal its early precipitation (one-nicol). B) Relatively thick and continuous illitic clay coatings in a sand flat tail sample. Textural relationships suggest an early formation (crossed-nicols). C) Gypsum cement patch enclosed by kaolinite-illite pore-filling cement in the sheet flood deposit. Note the high compaction degree highlighted by elongated concave-convex contacts and triple joints between detrital grains (crossed-nicols). D) Inherited abraded quartz overgrowth in a sample of braidplain channel area (crossed-nicols). E) Well-developed K-feldspar overgrowths in a sample from the braidplain channel area. Note the occlusion of primary pore spaces, avoiding a high mechanical compaction (one-nicol). F) Mosaic-type texture in carbonate cements of fracture-associated sand flat facies (crossed-nicols). G) Pervasive carbonate replacements on detrital grains in sand flat facies (crossed-nicols). H) Gypsum cement in slough channel facies. Early precipitation of this cement hinders a high compaction degree. Patches of early dolomite can also be observed (crossed-nicols).
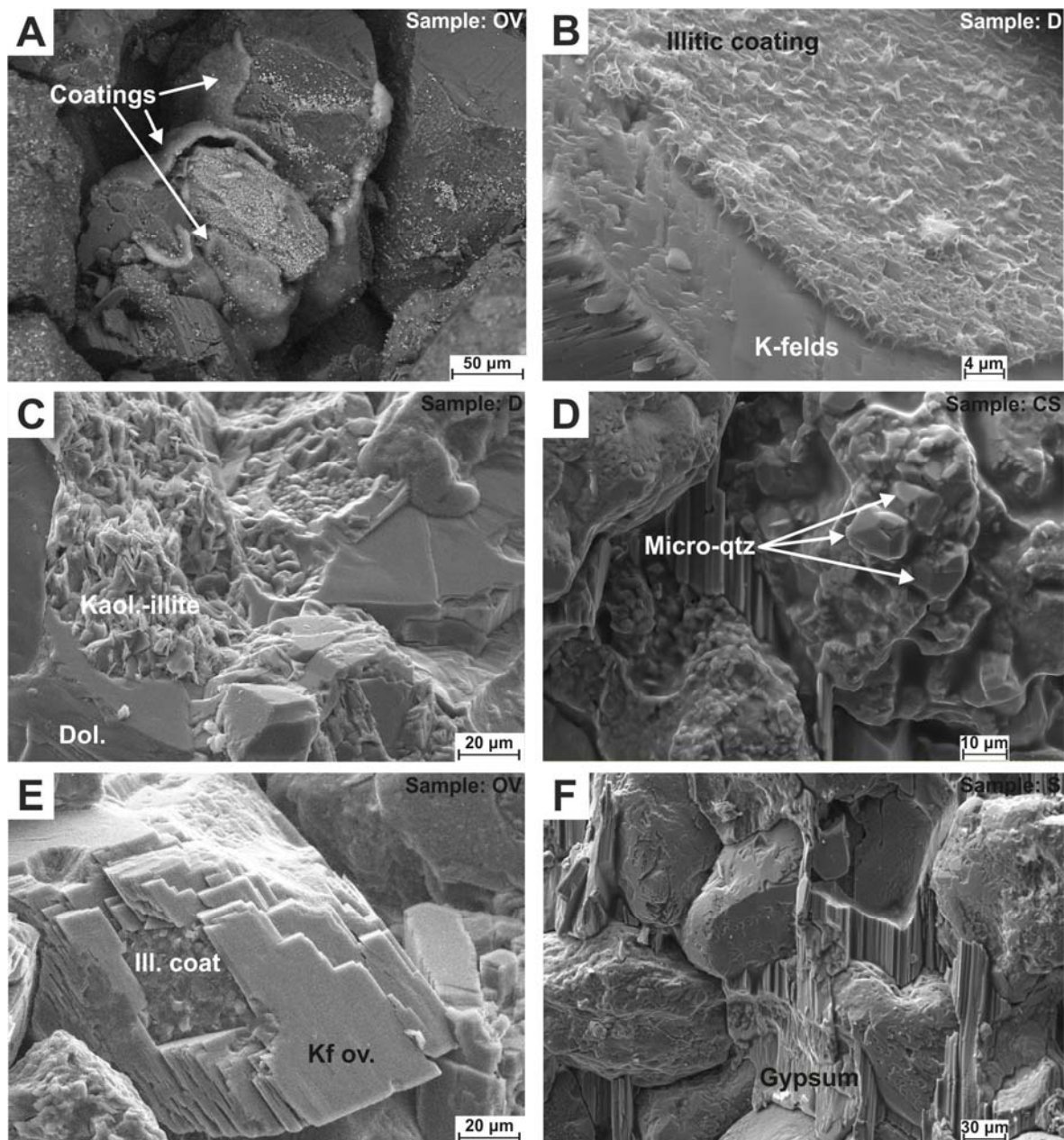
Fig. 9. SEM (left column) and FESEM (right column) images showing more-detailed petrographic features of TIBEM sandstone cements. A) Thick mixed-layer illite-smectite (I/S) grain coatings surrounding detrital grains in a sample from the braidplain channel area. Bright brownish dots on grain surfaces correspond to Fe-oxides. B) Mixed-layer illite- smectite (I/S) grain coating on feldspar grain (K-felds.) in fracture-associated sand flat facies. C) Kaolinite-illite (Kaol.-ill) pore-filling cement being replaced by the dolomite (Dol.) cement in fracture associated sand flat facies. D) Microcrystalline quartz growths (Micro-qtz) in the slough channel facies. E) K-feldspar overgrowth postdating illitic grain coating in a sample form the braidplain channel area. F) Gypsum cement occluding primary porosity in the slough channel facies.

Braidplain sand flat area shows the highest OP value (SF; 31.6%; k = 473 mD) in the tiered bars zone and the lowest OP value related to postsedimentary carbonate-cemented fractures (D; 4.9%; k = 2 mD; Table 3). Most of the braidplain facies include well-developed K-feldspar and, subordinately, quartz overgrowths. In the sand flat tail area (Fs1, Fs2 and Fs3), OP values range from 5.1% to 28.2% (k ranges between 45 and 536

mD, respectively). Carbonate cement is randomly distributed in this facies. In the channel area, OP evolves upward in the succession as follows: 29.4% (k = 419 mD; lower zone; LP), 24.4% (k = 325 mD; medium zone; MR) and 31.2% (k = 725 mD; upper zone; OV). In gypsum-cemented slough channel sandstone, OP decreases to 18.1% (k = 95 mD; CS).

MICP analysis was carried out on two samples from the sand flat area (AGD1) where postsedimentary carbonate-cemented fractures occur. The first 6 cm away from the fracture, shows OP value of 30% (k = 358 mD; AGD1 no cem.), whereas in the second, 1 cm away, OP value sharply decreases to 3.4% (k = 14 mD; AGD1 cem.).

Pore size distribution

Overbank deposits from the floodplain show a bimodal-type distribution of pore radii (Fig. 11A). 80.3% of OP corresponds to pores with a radius of less than 1 µm (ultramicropores according to Brewer, 1964) (Table 3). On the other hand, straight and meandering channels show a unimodal distribution of pore radii with only the meandering channel margin displaying a bimodal-type (Fig. 11B). 76.9% of OP in the straight channel and 67% in the meandering channel (margin, point bar and scroll bar facies) result from pores whose radii are within 1-10 µm (ultra- and micropores according to Brewer, 1964). Pores in the centre of the meandering channel are exception with radii between 10 and 100 µm (micro-, meso- and very fine macropores according to Brewer, 1964), making 70.9% of the OP of this facies.

In the braidplain, most of the sand flat, sand flat tail and channel facies show a unimodal distribution of pore radii (Fig. 11C). However, there are some exceptions in samples from: postsedimentary carbonate-cemented fractures in the sand flat area; base of the sand flat tail area; and the slough channel. The first two have an irregular pore size distribution whereas the slough channel is a bimodal-type. 70.8% of OP in all the braidplain samples results from pores whose radii are within 10-100 µm (micro-, meso- and very fine macropores according to Brewer, 1964; Table 3). Samples with pore radii between 1 and 10 µm correspond to the aforementioned exceptions (ultra- and micropores according to Brewer, 1964) representing 46.1% of the OP in postsedimentary carbonate-cemented fractures, 76% in the base of the sand flat tail area and 44.7% in the slough channel.

In addition, the samples from the sand flat area located at different distances (1 and 6 cm) from a carbonated-cemented fracture show a unimodal distribution of pore radii. However, lower peak height is recognised in the sample taken 6 cm away from the fracture (Fig. 11D). In the latter, 55.5% of OP corresponds to pores with radii of between 10 and 100 µm (micro-, meso- and very fine macropores according to Brewer, 1964), whereas in the sample taken closer to the fracture, 60.6% of OP is due to pores with radii in the 1-10 µm range (ultra- and micropores according to Brewer, 1964) (Table 3).

Table 3. Open porosity (OP) values for the analysed deposits, showing the distribution of pore sizes that originate this OP. Cake diagrams represent the distribution of pore sizes in the main sedimentary environments: overbank and channel deposits (floodplain) and braidplain. Note the dominant pore size increase, from 0.1-1 to 10-100 µm, in the same aforementioned environment order. The last diagram shows the distribution of pore sizes in carbonated- and gypsum-cemented braidplain samples, where the dominant pore size decreases to the 1-10 µm range.

Facies	Crevasse	Sheet flood	Centre meand.	Margin meand.	Point bar	Scroll bar	Straight ch.			Sand flat			Sand flat tail			Channel area			Slough ch.
Sample	C	S	Cc	Cm	P	Tp	R1	R2	D	SF	AGD1 (no cem.)	AGD1 (cem.)	Fs1	Fs2	Fs3	LP	MR	OV	CS
Porosity (%)	15.6	15.7	30.7	16	19.8	27.2	24.1	23.6	4.9	31.6	30	3.4	5.1	28.2	20.1	29.4	24.4	31.2	18.1
Permeability (mD)	2	3	413	16	56	133	140	154	2	473	358	14	45	536	105	419	325	725	95
>100 µm	0.7	1.2	0.52	2.6	0.7	0.7	0.9	0.6	3.2	0.8	1.1	1	4.1	1.3	1	0.8	1.1	0.8	1.4
100-10	3.8	3.6	70.9	8.4	4	4.5	8.2	15	8.4	78.3	55.5	34.8	49.6	61.5	8.9	72.3	56.6	85.2	19.4
10-1	13.8	16.1	23.3	40.6	77.5	82.9	77.7	76.1	46.1	17.9	32.9	60.6	22.3	29.3	76	23.3	34.2	9.7	44.7
1-0.1	46.5	52.1	2.4	28.8	8.7	5.4	5.7	4.2	34.2	2.4	7	3.7	14.9	4.7	10.4	2.6	5.6	2.8	20.7
<0.1	35.2	26.9	2.9	19.6	9.2	6.5	7.4	4	8.1	0.6	3.4	0	9.1	3.3	3.6	0.9	2.6	1.5	13.9

Legend:
- ■ >100
- ■ 100--10
- ■ 10--1
- ■ 1--0.1
- □ <0.1

Cemented (AGD1, CS, D, Fs3)
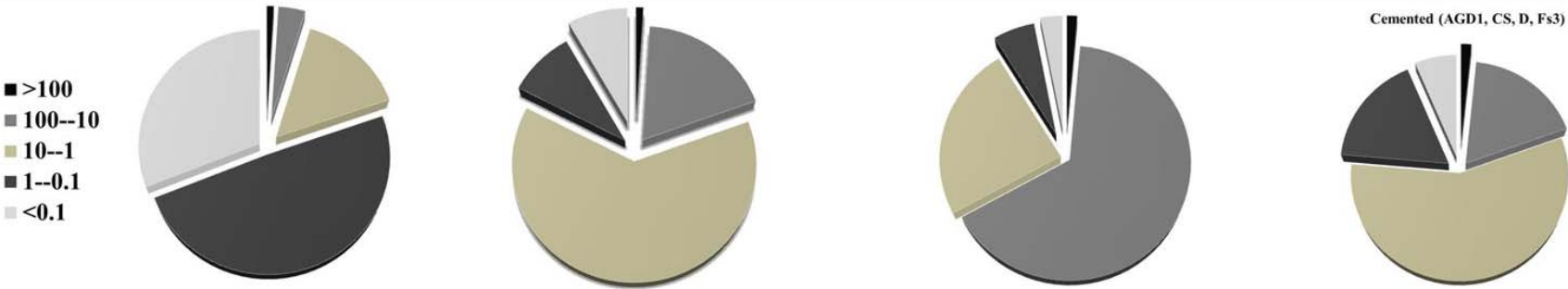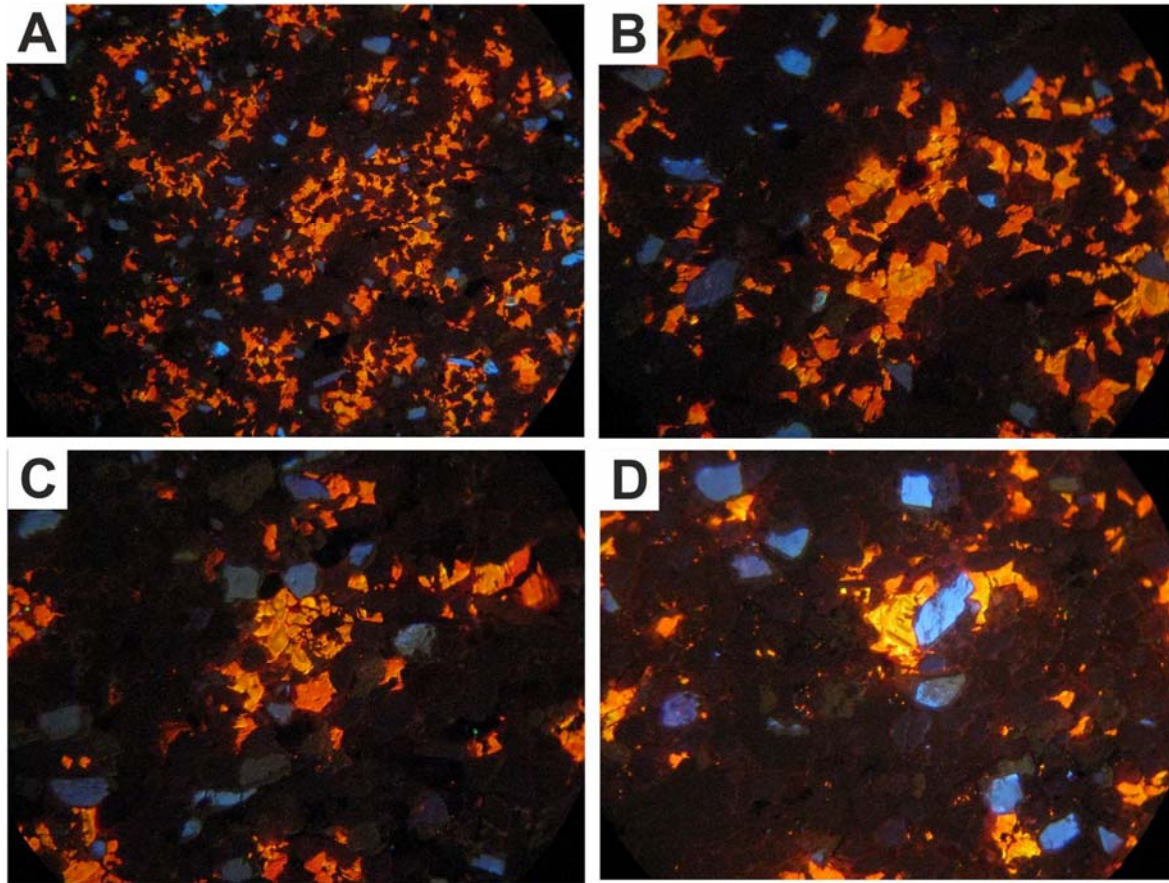
Fig. 10. Cathodoluminescence microphotographs of carbonate cement in fracture-associated sand flat facies. A) Luminescent dolomite and null luminescent calcite occurring in the same sample. Note the orange-yellowish dolomite dominance over the randomly distributed patches of null calcite. Blue luminescent grains correspond to detrital feldspars (magnification 4x). B), C) and D) Zonation in luminescent dolomite crystals (magnification 10x).
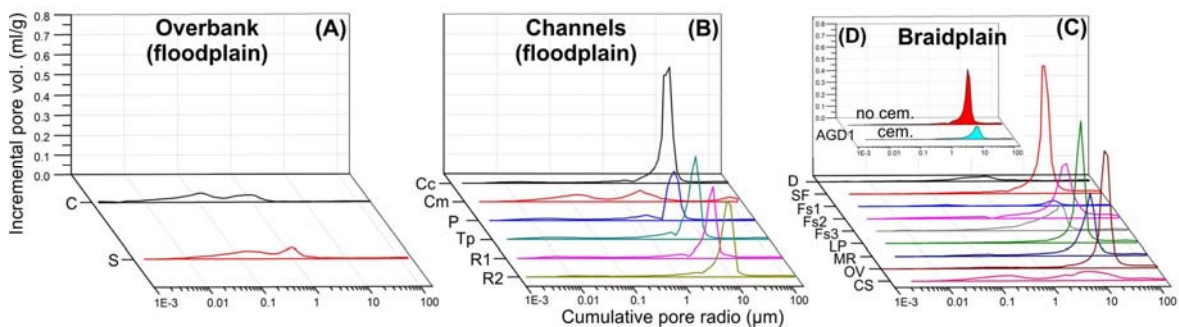
Fig. 11. Pore radii distributions of analysed deposits. A) C: crevasse splay; S: sheet flood. B) Cc: centre of meandering channel; Cm: margin of meandering channel; P: point bar; Tp: scroll bar; R1: lower part of straight channel; R2: medium part of straight channel. C) D: cemented fracture in sand flat facies; SF: sample from sand flat; Fs1-3: sand flat tail facies, from base to top; LP, MR and OV: channel area, from base to top; CS: slough channel. D) AGD1: sample from the sand flat, affected or not by a fracture.

DISCUSSION

Provenance and composition

TIBEM sandstones, i.e. floodplain and braidplain facies (sequence II and IV), are consistent with a provenance typical of 'transitional' to 'craton interior' tectonic setting according to the Dickinson (1985) classification scheme for tectonic setting discrimination (Fig. 5C). Nevertheless, differences in composition are observed between floodplain and braidplain environments (Fig. 5A, B). Upsection (from floodplain to braidplain), there is an increase in roundness of quartz grains, which commonly bears inherited overgrowths, and in monocrystalline quartz content. A decrease in plagioclase and pseudomatrix content is also observed. In addition, an ultrastable heavy mineral assemblage occurs, especially in floodplain facies, with a high roundness degree (Fig. 6D, E). These features suggest that analysed Triassic fluvial sediments were supplied from similar plutonic source rocks. However, compositional maturity, degree of roundness and the association of zircon-tourmaline-rutile ultrastable minerals clearly indicate recycling and possible cannibalization of Permo-Triassic siliciclastic successions (Suttner et al., 1981; Zuffa, 1987; Johnsson, 1988; Arribas et al., 1990).

Chronology of diagenetic processes

Textural features and relationships between cements and replacements suggest the chronology of eo-, meso- and telodiagenetic stages (Fig. 12). Near-surface and early diagenetic processes (eodiagenesis) consist of cementation by Fe-oxides, illite after smectite replacement (clay coats), kaolinite and K-feldspar overgrowths and mechanical compaction. Gypsum cementation developed dominantly in floodplain and to a lesser extent in slough channel facies where patches of dolomite were also recognised. The poikilotopic texture of dolomite indicates relatively high pore-network connectivity and it is therefore associated with an early mesodiagenetic stage which also includes moderate mechanical and chemical compaction and quartz overgrowths. Diagenetic processes related to exhumation and weathering (telodiagenesis) result in the formation of calcite cement and patches of late kaolinite, precipitated within carbonate crystals. The generation of secondary porosity is negligible and is related to feldspars, gypsum and/or carbonate dissolution.

The aforementioned diagenetic sequence reflects an evolution from meteoric to brackish-dominant porewaters. Since TIBEM sandstones are fluvial in origin, they were fluxed by freshwater immediately after deposition. Owing to kinetic constraints, illitic coatings are normally the transformation product of eodiagenetic smectite coatings during a shallow burial (Morad et al., 2000, 2010). In fact, Worden and Morad (2003) suggest that texture similar to those of Fig. 9A and 9B, illustrates the progressive burial diagenetic transformation of infiltrated smectite into illite, via a mixed-layer of smectite (80%)-illite (20%). Kaolinite pore-filling precipitation has likely been favoured by the occurrence of clay intraclasts and the abundance of altered K-feldspars. Leaching by acidic meteoric waters may supply the required oxidizing conditions for Fe-oxides formation (Bjørlykke, 1994; Bjørlykke and Aagaard 1992; Worden and Morad 2003). Under shallow burial conditions, the chemistry of porewaters is greatly affected by the evaporation-precipitation processes (Dutta and Suttner, 1986). Thus, porewater evolves during burial to more saline compositions, saturated in cations, resulting in gypsum and K-feldspar overgrowths

precipitation and minor dolomite patches (in slough channel facies). Internal K+ from K-feldspar dissolution by meteoric waters with a low (K+, Na+)/(H+) ratio, and refluxing of the upper evaporitic units and carbonate formation (units K4-K5 and Imón Formation) probably increase the K+/H+ ratio and constituted the source of Ca2+ (Rossi et al., 2002). Relatively deep burial (early mesodiagenesis) resulted into significant chemical compaction, highlighted by quartz dissolution features such as intergranular sutured contacts. This suggests that most of the silica required for quartz cementation was internally sourced by detrital grain contact pressure- or clay-induced dissolution. Also, transformation of smectite into illite frequently results in concomitant quartz cementation (McKinley et al., 2003). Carbonate cement distribution seems to be associated to braidplain areas where telodiagenetic fractures developed. These fractures may act as preferential conduits for density-driven brine refluxes, originated during the Upper Triassic marine-influence stage. Dolomite likely precipitates from such Mg-rich waters whereas calcite formed during the uplift and consequent introduction of meteoric waters following the dedolomitization process (Morad et al., 1990). Dissolution of gypsum also results in an increase of the calcium activity of the ground water, which raises the ion activity product of calcite and thus enhances the potential for calcite precipitation (Burt, 1993). Zonation in dolomite crystal luminiscence observed in Fig. 10 can be attributed to variations in the Fe/Mn ratio, with the more luminescent areas being richer in Mn content. Null luminescent calcite may therefore correspond to negligible Mn contents related to more oxidizing conditions, due to mixing between marine and meteoric water compositions (Lee and Harwood; 1989; Horbury and Adams, 1989; Morad et al., 1992, 1990).

Available sedimentological data indicate a 600 m maximum overburden (Fernández, 1977). Diagenetic signatures suggest a burial temperature between 40ºC and 70ºC. Quartz overgrowths usually require temperatures greater than 60ºC, although its occurrence can be influenced by several processes such as clay mineral transformations, grain to grain pressure solution, feldspar alteration, weathering, among others (McBride, 1989). Transformation of smectite into illite can take place at temperatures between 47ºC and 68ºC in a potassium-rich environment (Weibel, 1999).

Porosity evolution, diagenesis and depositional facies

Pore system evolution, i.e. open porosity and pore radii, strongly depend on the depositional and early diagenetic features of the analysed sandstones. Petrographic observations (well sorted textures and quartz- and feldspar-rich framework composition) would suggest high pore space preservation (Bloch, 1991) and, thus, high potential as reservoir rocks (Caracciolo et al., 2013). Nevertheless, in overbank deposits, the very fine grain size and the abundance of pseudomatrix, trigger a high compaction degree, resulting in low OP (< 16%) and the finest pore radii (0.1-1 µm; Table 3, Fig. 11A). Moreover, the low hydrodynamic regime in both overbank and braidplain slough channel facies, probably favours the early precipitation of gypsum, occluding the primary pore spaces. On the other hand, in braidplain sandstones, the medium grain size, the scarcity of pseudomatrix and other cements, except for early well-developed K-feldspar overgrowths, likely prevents a high compaction, preserving high OP (> 21%) and the highest pore radii (10-100 µm;

Table 3, Fig. 11C). Detrital matrix could also act as a mechanically-resistant component of the framework against the compaction. Fracture-associated carbonate-cemented samples are exceptions showing minimum OP (< 5%) and finer pore radii (1-10 μm; Table 3, Fig. 11C). They can therefore act as barriers for the lateral migration of fluids, which may compartmentalize the sandstone body. Floodplain channel deposits show intermediate grain size, matrix and cement content with respect to overbank and braidplain facies. OP and pore radii values vary considerably among the different analysed sub-environments, between 16 and 31% and corresponding to the 1-10 μm range (Table 3, Fig. 11B).

Fig. 12. Chronology of diagenetic processes, deduced by mutual textural relationships.

It is also worth noting that gypsum-cemented samples show systematically bimodal distribution of pore sizes, while carbonate-cemented samples display a unimodal distribution with lower peak heights (Fig. 11D). The effect of fluid density and pore size on crystallization process can be traced back through the literature (Putnis and Mauthe, 2001 and references herein). In very fine-grained deposits (e.g. overbanks) and/or in those with a high clayey content (e.g. the margin of the meandering channel and the braidplain slough channel), gypsum-saturated fluids likely precipitate into larger pores, resulting in smaller pore-throats and/or remaining supersaturated in the smallest spaces (Putnis and Mauthe, 2001). As a result, the pore size distribution appears as bimodal. On the other hand, given the different density of carbonate-saturated fluids, precipitation probably takes place in the larger pores of the braidplain deposits.

Permeability (k) strongly depends on the direction it is measured. Nevertheless, there are many examples in the literature using MICP data to deduce permeability values (e.g. Schowalter, 1979; Katz and Thompson, 1987; Kolodzie, 1980; Swanson, 1981; Pittman, 1992, 2001). In analysed sandstones, permeability is very sensitive to pore size distribution. k values vary greatly depending on the dominant pore size and on which proportion it dominates (Table 3). Samples S (sheet flood deposit) and Cm (meandering channel margin) show similar OP values (15.7% and 16%, respectively) but different dominant pore sizes (interval 1-0.1 μm and interval 10-1 μm, respectively) with k being higher in Cm. Samples SF (sand flat area) and OV (channel area) show similar OP values

(31.6% and 31.2%, respectively) and identical dominant pore size (100-10 μm) but in different proportions (78.3% and 85.2%, respectively) with k being higher in OV.

Analogue features

TIBEM and TAGI are both alluvial/fluvial formations that developed during Tethys rifting (Middle-Upper Triassic) and deposited on a coastal retrograding plain which onlap the Paleozoic eroded and deformed basement (Fernández and Dabrio, 1985; Turner et al., 2001; Rossi et al., 2002; Ratcliffe et al., 2006). Thus, similar paleogeography, tectonic regime and climatic conditions lead to analogous stacking associations of fluvial facies on their stratigraphic successions of 150-160 m thickness.

The base of the successions (not outcropping in the Alcaraz area) is characterised by coarse alluvial fan deposits which adjust to basement relief. Upwards, there is a rejuvenation of fluvial systems, resulting in relatively low sinuosity and isolated channels within floodplain siltstones, with crevasse and sheet-like splay deposition (Viseras and Fernández, 1994; Turner et al., 2001). Floodplain facies are red and/or green (secondarily reduced) with lacustrine calcretes, indicating paleosols development (Turner et al., 2001; Fernández et al., 2005). Nevertheless, the thickest sand body in TAGI corresponds to the deposition on an anastomosing system whereas in TIBEM it is interpreted as a braidplain depositional system. In both cases, this deposit is thought to be the best potential reservoir. Both successions end with silt- and evaporite-richer facies, culminating in the Liassic carbonate platform (Fernández and Dabrio, 1985; Viseras and Fernández, 1994; Turner et al., 2001; Ratcliffe et al., 2006).TIBEM and TAGI show similar detrital composition and depositonal facies (i.e. textural parameters). In TAGI, sandstone composition evolves upsection (from the Lower to the Middle-Upper TAGI) from quartz arenites to subarkoses (Fig. 5A) whereas TIBEM mainly resembles the Middle-Upper TAGI framework composition, albeit with a slightly higher feldspar content. The main difference between TIBEM and TAGI lies in the post-Triassic sedimentary evolution. In TAGI, overlaying sediments reach thickness up to 3000 m, whereas in TIBEM there is no evidence for an overburden greater than 600 m (Fernández and Dabrio, 1985; Viseras and Fernández, 1994; Turner et al., 2001; Ratcliffe et al., 2006). Although the nature of cements is similar in both cases, some of them occur as different mineral phases at a distinct diagenetic stage (Rossi et al., 2002). Carbonate precipitation in TAGI occurs early and results in magnesite-siderite and dolomite formation (Rossi et al., 2002). In TIBEM, dolomite precipitates as early cement, whereas calcite does it later. In TAGI, sulphate cements (anhydrite-barite) precipitated during the last diagenetic stage, whereas in TIBEM gypsum precipitates early. Porosity values of TAGI sandstones are systematically less than 20% increasing from Lower to Middle-Upper TAGI, due to the dissolution of detrital and authigenic feldspars. The same upward increase in porosity is documented in TIBEM (up to 30%) where feldspar dissolution also takes place, although in minor amount than in TAGI.

In TAGI, variation in diagenesis between Lower and Middle-Upper parts is related to differences in initial feldspar content and in syndepositional grain-coating illitic clays

(Rossi et al., 2002). Since sediment composition and depositional facies are primary controlling factors on early/shallow diagenesis and consequently on porosity and permeability reduction or increase, comparison between TIBEM and TAGI is justified.

CONCLUSIONS

Coupling the information from depositional facies, sandstone petrology and petrophysical analysis of TIBEM (Tabular Cover of the Iberian Meseta) sandstone bodies leads to the following conclusions:

1. There is a significant maturity increase up-section from flood- plain to braidplain environments, evidenced by changes in depositional texture and detrital composition. Grain size and roundness of quartz grains increase, whereas matrix content decreases. Detrital composition evolves from arkose ($Q_{62}F_{27}Rf_{11}$) in the floodplain to subarkose ($Q_{74}F_{16}Rf_{10}$) in the braidplain deposits, showing an important increase of monocrystalline quartz while feldspar content decreases, especially plagioclases.

2. Petrographic observations revealed that primary porosity has been mostly reduced and pore system affected during the early diagenetic stage (eodiagenesis) through cementation by Fe-oxides, illite coatings, kaolinite and K-feldspar overgrowths and mechanical compaction. Early gypsum cement also occurs, dominantly in floodplain and subordinately in slough channel facies. Poikilotopic dolomite has been attributed to an early mesodiagenetic stage, which also includes moderate mechanical and chemical compaction and quartz over- growths. Diagenetic processes related to exhumation and weathering (telodiagenesis) result in calcite formation and patches of late kaolinite, hosted by carbonate crystals. Negligible secondary porosity is related to feldspars, gypsum and/ or carbonate dissolution. The aforementioned diagenetic sequence reflects an evolution from meteoric to slightly saline porewaters, with a refluxing of acidic waters during the last diagenetic stage.

3. On the basis of open porosity values, pore size distribution pattern, permeability and sedimentary architecture, sandstone deposits can be classified as a function of their quality as potential reservoir. Overbank facies are considered the least suitable reservoirs due to their low open porosity and permeability, finest pore radii and small dimensions. Channel de- posits show better attributes such as higher open porosity values and dimensions, but the properties of their depositional sub-environments vary greatly. Braidplain sandstone body constitutes the highest-quality potential reservoir because of its high open porosity and permeability values as well as its thickness and lateral continuity. It is worth to note the occurrence of cemented fractures and facies-related heterogeneities, such as the slough channel, which may compartmentalize the potential reservoir, acting as barriers and/or baffles to fluid migration.

4. This study points out TIBEM as an outstanding outcrop analogue for the TAGI reservoir. The fact that TIBEM experienced telodiagenesis and that is currently subjected to weathering justifies the differences with TAGI. However, the evolution and the compositional signatures of the two successions were deter- mined by those mutual factor

(tectonic setting, source area and climatic conditions) known to exert a primary control on early diagenesis and thus porosity and permeability reduction (or enhancement). Comparison of both formations represents a valuable source of information to broaden the knowledge of TAGI reservoir.

Acknowledgements

Concluding remarks

A compositional and textural maturity increase is observed upwards in the succession from floodplain (sequence II) to braidplain (sequence IV) depositional environments. Early diagenetic processes have been the most important in reducing primary porosity and permeability and their distribution and magnitude is strongly related to depositional facies. In floodplain environment (including overbank and channelized deposits) mechanical compaction has been more intense with early pervasive poikilotopic gypsum being the main porosity-occluding cement. In braidplain environment, primary porosity still remains relatively high (up to 30%) with K-feldspar overgrowths being the prevailing authigenic phase. Gypsum-cemented slough channel facies and carbonate-cemented post-sedimentary fractures in the braidplain show an important reduction of porosity and permeability giving place to compartmentalization of the potential reservoir acting as barriers and/or baffles to fluid migration. Analysed depositional environments can be classified, from lower to greater quality as potential reservoir rocks, as follows: overbank deposits (crevasse splay lobes and sheetfloods); channelized deposits (meandering and straight channels); and braided fluvial system. Despite the differences in burial history, similarities in composition, age, source area and depositional characteristics justify satisfactorily the use of TIBEM as outcrop analogue for the TAGI reservoir.

4.2 Part II

Objectives

Once established in Part I that diagenetic differences exist among depositional environments developed under same allogenic (sedimentary deposits from sequence II) and autogenic factors (e.g. meandering system), the investigation on the most influential depositionally-controlled parameters on diagenesis becomes necessary.

On the one hand, multiscale heterogeneities within meandering fluvial deposits (example from Central SE Spain) provides an excellent opportunity to evaluate the effect of depositional fabric (i.e. matrix distribution) on early diagenetic processes and related pore spaces. On the other hand, understanding the mechanisms determining the occurrence and abundance of different types of intrabasinal components (i.e. muddy and dolomitic rip-up clasts) - whose distribution is strongly facies-related - in selected braided and straight fluvial deposits (Western High Atlas, SW Morocco) provide critical evidences to appraise their behaviour during compaction and cementation processes and therefore their impact on porosity reduction. In all cases, a well-constrained sedimentological framework exists. In the case of the meandering deposit, outcrop data were further complemented with behind-outcrop core data, by applying the O/BO characterization workflow, in order to produce a 3D reservoir quality model. Triassic deposits from SW High Atlas (Morocco) are presented as outcrop analogues of the hydrocarbon-bearing Fundy Basin (Nova Scotia, Canada).

4.2.1 Diagenetic constraints on heterogeneous reservoir quality assessment: a Triassic outcrop analogue of meandering fluvial reservoirs

S. Henares, L. Caracciolo, C. Viseras, J. Fernández and L.M. Yeste

Abstract

Reliable modeling of meandering fluvial reservoirs is challenging because of the heterogeneity in magnitude and pattern of porosity and permeability related to depositional and diagenetic features. Early mechanical and chemical alterations proceed along different pathways directly related to depositionally governed differences in textural and compositional parameters. In a well-constrained sedimentological framework and with relatively homogeneous conditions of detrital composition, this study aims to determine the effect of depositional fabric on early diagenetic processes and their collective effect on petrophysical properties (pore size distribution, open porosity, and permeability). A high-resolution qualitative and quantitative petrographic analysis is conducted on 22 fine- to very fine–grained sandstones from the main meandering fluvial facies of the channel (center and margin), point bar (lower, middle, and upper), scroll bar, and chute channel of a Triassic outcrop analog. The occurrence of small-scale internal heterogeneity associated with detrital matrix and suspension-settling laminae favors the compaction process and hinders early pore-filling cement precipitation that helps the preservation of primary porosity. Multivariate statistical treatment of data demonstrates that large (>1 μm) and well-connected primary intergranular pores are the main contributors to permeability in the more heterogeneous samples. The distribution of the finer-grained sediment fraction is strongly facies related as a result of hydraulic sorting. Better understanding of linkages between depositionally predictable features and diagenetically induced heterogeneity may lead to realistic reservoir models and enhanced effectiveness of exploitation and bypassed-oil recovery strategies.

INTRODUCTION

"Every reservoir is in some way unique" (Ringrose and Bentley, 2015, p. 173).

Fluvial sandstone reservoirs account for more than 20% of the world's remaining reserves of hydrocarbons (Keogh et al., 2007). However, reliable modelling of such reservoirs is challenging because different scales of bedding create the potential for heterogeneity in the magnitude and pattern of porosity and permeability (Miall, 1988; Brayshaw et al., 1996; Sharp et al., 2003). In meandering fluvial systems, facies-induced heterogeneity related to internal depositional features such as lateral accretion units with associated mud drapes as well as internal facies variations such as vertical change from trough cross-bedding to ripple lamination, produce fining upward grain size trends with the corresponding decrease in primary porosity and increase in permeability anisotropy (Hartkamp-Bakker and Donselaar, 1993; Pranter et al., 2007). Example of this may be found in the Lower Cretaceous McMurray Formation (Athabasca oil sands region, Alberta) where ultimate reservoir porosity and permeability patterns are a direct function of primary facies distribution as a single channel and point bar deposit (Strobl et al., 1991; Labrecque et al., 2011). Diagenetically-induced heterogeneity is rarely assessed, despite its major impact on reservoir quality, which often leads to an overestimation of the recovery factor due to the assumption that channel bodies are equivalent homogeneous medium (Stanley et al., 1989; Teles et al., 1998; Dutton et al., 2002; Dutton, 2008). In this context, the pore-to-field modelling philosophy is becoming of great interest in the petroleum community (Øren et al., 1998; Theting et al., 2005). Research on upscaling of reservoir properties highlights the importance placed on small-scale (pore scale) properties variation for accurate field-scale reservoir modelling by using subsurface and outcrop analogue data (Pickup et al., 1995; Pringle et al., 2006).

Near-surface and shallow-burial diagenetic processes (early diagenesis) have a substantial control on deep-burial diagenesis, constrained by remaining porosity, and consequently, on reservoir quality evolution (Morad et al., 2000, 2010; Ajdukiewicz et al., 2010). Early mechanical and chemical alterations proceed along different pathways directly related to depositionally-governed differences in textural and compositional parameters (Bloch and McGowen, 1994; De Ros et al., 1994; Milliken, 2001; Worden and Morad, 2003). Mineralogy is largely controlled by provenance and weathering but depositional environment determines sediment distribution, grain size and sorting (Bjørlykke, 2014). These parameters can be characterized qualitative and quantitatively, if a proper calibration data set is available. Therefore, understanding the relationship between depositionally- and early diagenetically-induced heterogeneities provides crucial for prediction of reservoir quality (Henares et al., 2014a).

Meandering river deposits in the Middle Triassic Sequence II of the Iberian Meseta (SE Spain) are studied as outcrop analogue of heterogeneous fluvial reservoirs. The outcrops feature: (i) well-exposed lateral facies relationships, (ii) no structural deformation, (iii) three dimensionality through behind-outcrop well data. In such well-constrained sedimentological framework, this study aims to determining the control of depositional fabric on early diagenetic processes by a high resolution qualitative and quantitative petrographic analysis. Collective effect of diagenesis on petrophysical properties (pore size

57

distribution, open porosity and permeability) is also evaluated to determine reservoir quality. The results may provide improved knowledge for the characterization, prediction and static reservoir modelling of pore-scale properties in similar heterogeneous fluvial reservoirs worldwide.

GEOLOGICAL SETTING

The Triassic redbeds of the Iberian Meseta (SE Spain) form part of the continental realm developed during the Tethyan rifting process (Sánchez-Moya et al., 2004). In the study area in Alcaraz (Albacete) (Figure 1A), the Triassic sedimentary succession (Anisian-Norian) consists of 160 m (525 ft) thick, siliciclastic alluvial-lacustrine and fluvial stacked facies organised in three subhorizontal depositional sequences (Figure 1B; Fernández and Dabrio, 1985; Fernández et al., 1993, 2005). Available sedimentological data indicate a maximum burial depth of 600 m (1969 ft) (Fernández and Dabrio, 1985). Paleocurrent data indicate main drainage directions in the Triassic basin to the East (Northern drainage branch) and Northeast (Southern drainage branch) so that studied outcrop location is at the confluence of both branches (Figure 1A; Fernández and Dabrio, 1985). The fluvial sandstone is part of Sequence II (Figure 1B) following Fernández and Dabrio (1985) together with other sandstone units corresponding to straight channel and overbank deposits. These sedimentary geobodies developed during a general base level rise and are embedded in floodplain mud sediments. Displacive lenticular gypsum nodules (cm to dm sized) and micritic carbonate paleosols are also present in the floodplain as a result of predominant arid climatic conditions. Arche et al. (2002) subdivide the stratigraphic succession into three stratigraphic units produced by minor regression-transgression cycles during a general sea level rise. The studied geobody is part of their Unit 3.
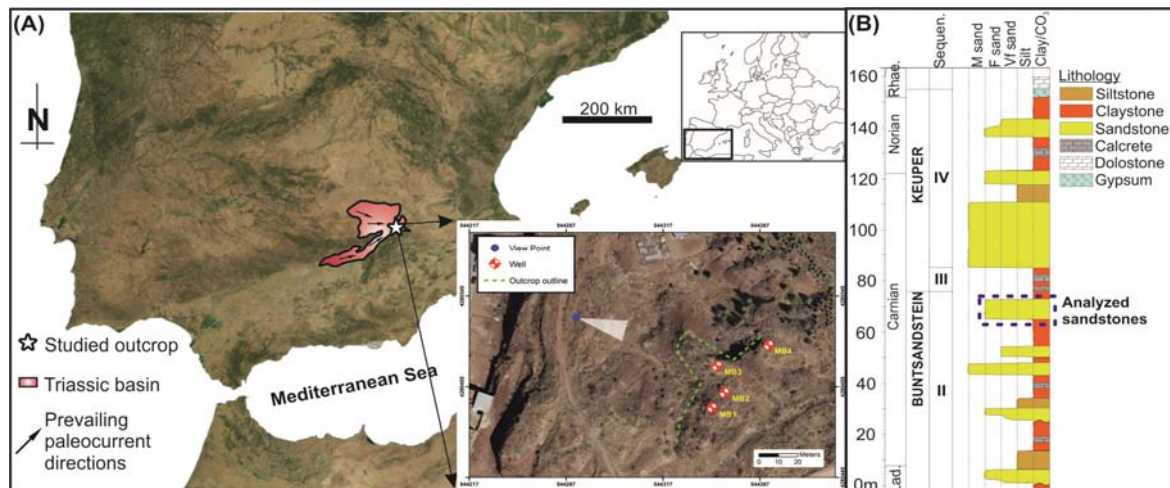
Fig. 1. (A) Location map of the Triassic basin (SE Spain). Insert: orthophoto of the studied area indicating the outcrop profile, the view point of photo panel in Fig. 2 and the well positions. (B) Simplified stratigraphic column of the Triassic succession in the study area (modified from Henares et al., 2014a).

DEPOSITIONAL FACIES

The studied composite sandstone geobody is an intermediate-scale (~ 70 m wide [230 ft], 5 m thick [16 ft]), ribbon-like depositional element that developed from a single

meandering channel within a low net-to-gross fluvial system (Figure 2; Fernández and Dabrio, 1985). The depositional facies elements in outcrop (Fernández et al., 2005; Viseras and Fernández, 2010; Henares et al., 2014b) and in the behind-outcrop wells are (Figure 3): main channel (center and margin), point bar (lower, mid- and upper part), scroll bar and chute channel. Sigmoidal sandstone beds formed during the active phase of channel deposition and show a typical fining upward succession from clay pebble lags to fine to very fine-grained sand with trough cross bedding, low-angle planar cross bedding and ripple lamination, to silt layers at the top. During the abandonment phase, the channel was filled with alternating beds of silt or clay (settling out of suspension in a standing body of oxbow lake water) and very fine-grained sand with ripple lamination (due to the reactivation of the channel during peak discharge). Flow deceleration at peak flow and high suspension load cause wavy lamination in the channel margin. Channel abandonment terminates with the formation of a clay plug. Towards the floodplain, upper point bar and scroll bar facies show lower energy sedimentary structures such as horizontal lamination and climbing ripples. The chute channel infill, dominated by ripple lamination, responds to its intermittent behaviour being active only during the peak-flow periods (Viseras and Fernández, 2010).
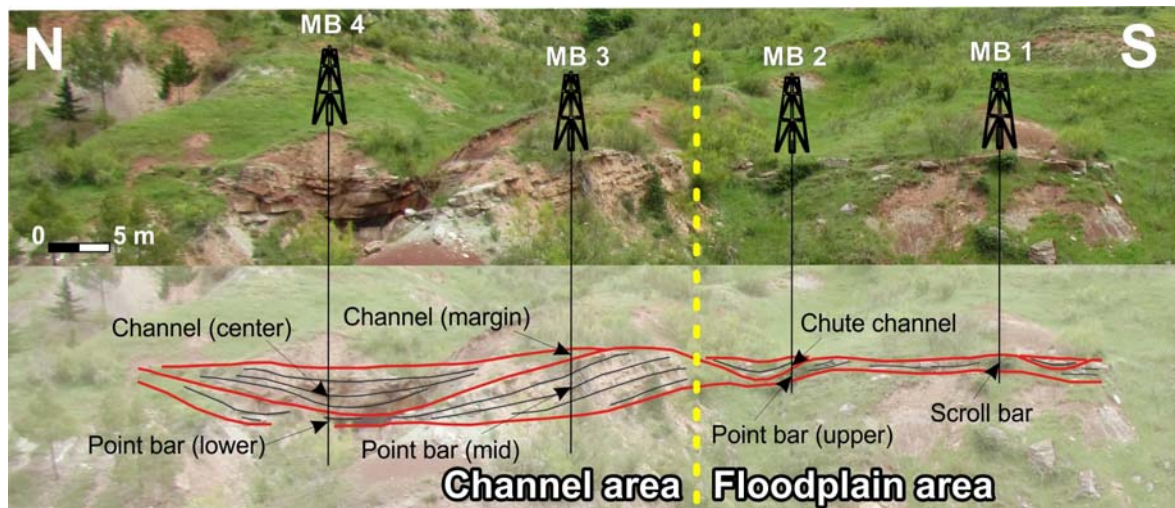
Fig. 2. Outcrop photo panel interpretation of the composite fluvial sandstone geobody, indicating the positions of wells and facies elements.

DATA AND METHODS

Four fully-cored slim-hole (16 cm - 6.2 in.) behind-outcrop wells (Figures 2 and 3) target the main depositional facies and provide the material for this study. The distribution of wells from north to south and from base to top is as follows: well MB4 includes samples from the lower point bar and the active part of the channel infill; well MB3 comprises samples from the mid-point bar and the channel margin; well MB2 corresponds to samples from the upper point bar and the chute-channel deposits; and well MB1 samples comprises samples from the scroll bar facies.

High-resolution petrographic analysis was performed on 22 selected samples using optical and scanning electron microscopes (SEM; equipped with an energy dispersive X-ray spectrometer [EDX]). Thin section orientation was perpendicular to the bedding. After
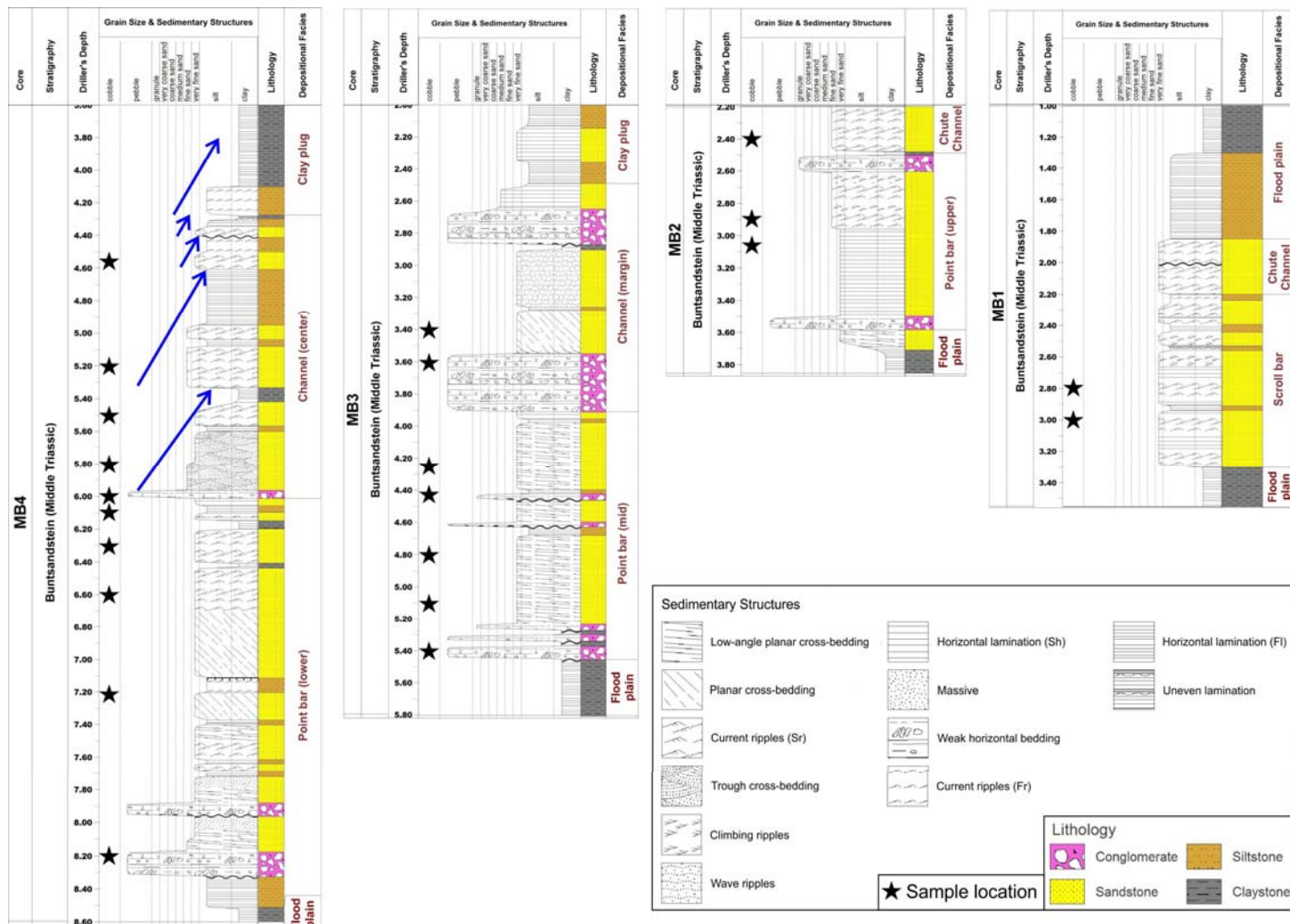
Fig. 3. Lithostratigraphic columns of the four wells. Arrows indicate the fining-upward successions that characterize the gradual infill of the channel depression and stars indicate the sample location. Depths are referenced to the same level as well MB1, but different depth intervals are represented to highlight the main depositional features in each well.

vacuum-impregnation with blue epoxy resin, samples were etched and stained with hydrofluoric acid and Na-cobaltnitrite for plagioclase and K-feldspar identification, respectively, and with alizarin red-S for carbonate type discrimination. Two types of point counting were performed: (1) Gazzi-Dickinson point-counting (500 points per thin section; Ingersoll et al., 1984; Zuffa, 1987, 1985) provided qualitative and quantitative data of framework composition and interstitial component (i.e., cements and matrix) to characterize depositional and diagenetic fabrics; (2) intentional diagenetic point-counting allowed semi-quantitative description (100 points per thin section) of the primary and secondary pore spaces in the same area of the Gazzi-Dickinson point-counting. Intergranular volume (IGV) and compaction and cementation indexes for porosity loss (COPL and CEPL, respectively) as well as compaction index ($I_{compact}$) were calculated following established conventions (Lundegard, 1992).

The OP and pore size distribution were determined for the same samples using mercury injection-capillary pressure (MICP) with a Micromeritics Autopore III porosimeter (model 9410). Permeability (k) was obtained from the MICP data and Pittman's equation (Pittman, 1992, 2001).

RESULTS

Depositional fabric

Texture

The grain size of the analyzed fluvial sandstone varies from very-fine to fine sand with well-sorted, subrounded to subangular grains. The depositional texture, which is far from uniform at the thin section scale, displays sedimentary structures such as cross and parallel lamination highlighted by laminae with higher mica and matrix content (suspension settling laminae; Figure 4A), alternation of laminae with fine-slightly coarser grain size (Figure 4B), laminae with preferential heavy minerals concentrations (Figure 4B) or rip-up clasts (lags; Figure 4C) and preferred orientation of elongate grains such as micas, lithic fragments or rip-up clasts. Detrital matrix dominates (88.7-100% of Total Matrix [TM]) over pseudomatrix (0-11.4% TM) and consists of silt-sized grains of quartz and feldspars locally embedded in a reddish-stained, clay-rich groundmass (Figure 4D). Matrix distribution is strongly facies-related. It is more abundant in the channel area at the channel margin (14.4% of Total Composition [TC]) and decreases towards the lower point bar (6.4% TC), passing through the mid-point bar (9.6% TC) and the channel center (9.5% TC). Detrital matrix content increases in the floodplain area from the upper point bar (4.1% TC) to the scroll bar (6.2% TC). The chute channel has a matrix content similar to the underlying upper point bar, with 4.2% TC.
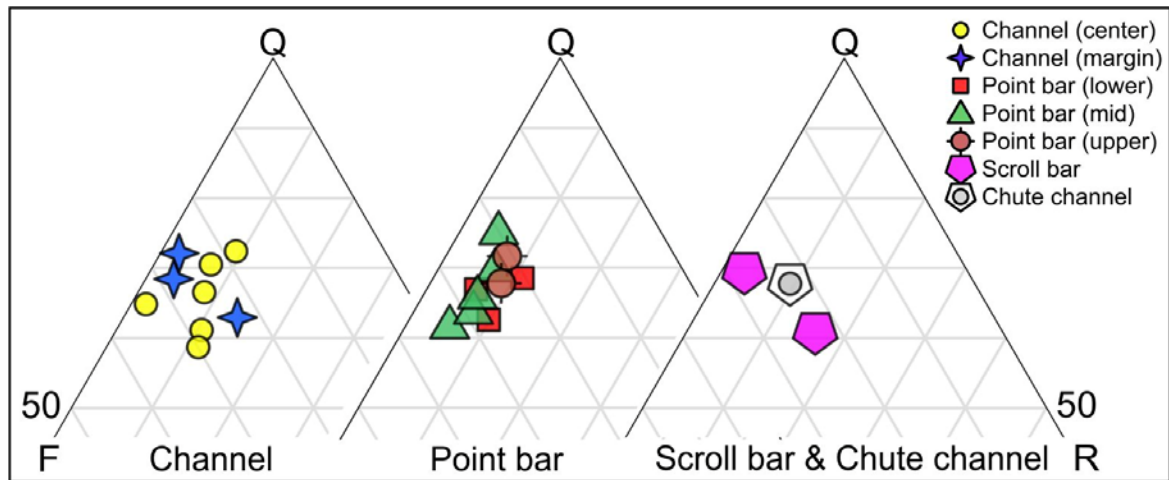
Composition

The sandstones in the study area display a homogeneous quartz-rich composition with appreciable amounts of feldspars and subordinate lithic fragments. They are classified as subarkoses to lithic subarkoses (*sensu* Pettijohn, 1975; $Q_{68.82}F_{25.31}R_{5.86}$ -

$Q_{60.18}F_{23.96}R_{15.86}$; average: $Q_{65.43}F_{24.59}R_{9.97}$; Figure 5; Table 1). Monocrystalline quartz is the dominant grain, followed by monocrystalline K-feldspar and, to a minor extent, plagioclase. Feldspars often show partial dissolution of the detrital grain and, occasionally, of its overgrowth. Locally, K-feldspars show replacement by kaolinite or illite. Lithic fragments are mostly low to medium-grade metamorphic fragments such as fine-grained schists and mica-schists. Rip-up clay clasts are also present as non-carbonate intrabasinal components representing up to 3.6% of Total Framework Composition (TFC; Zuffa, 1980). Mica flakes, mainly muscovite (1-2.2% TFC), usually are mechanically deformed. Heavy ultrastable mineral assemblage consists of well-rounded zircon, tourmaline, rutile and opaque minerals (0.5-4% TFC).
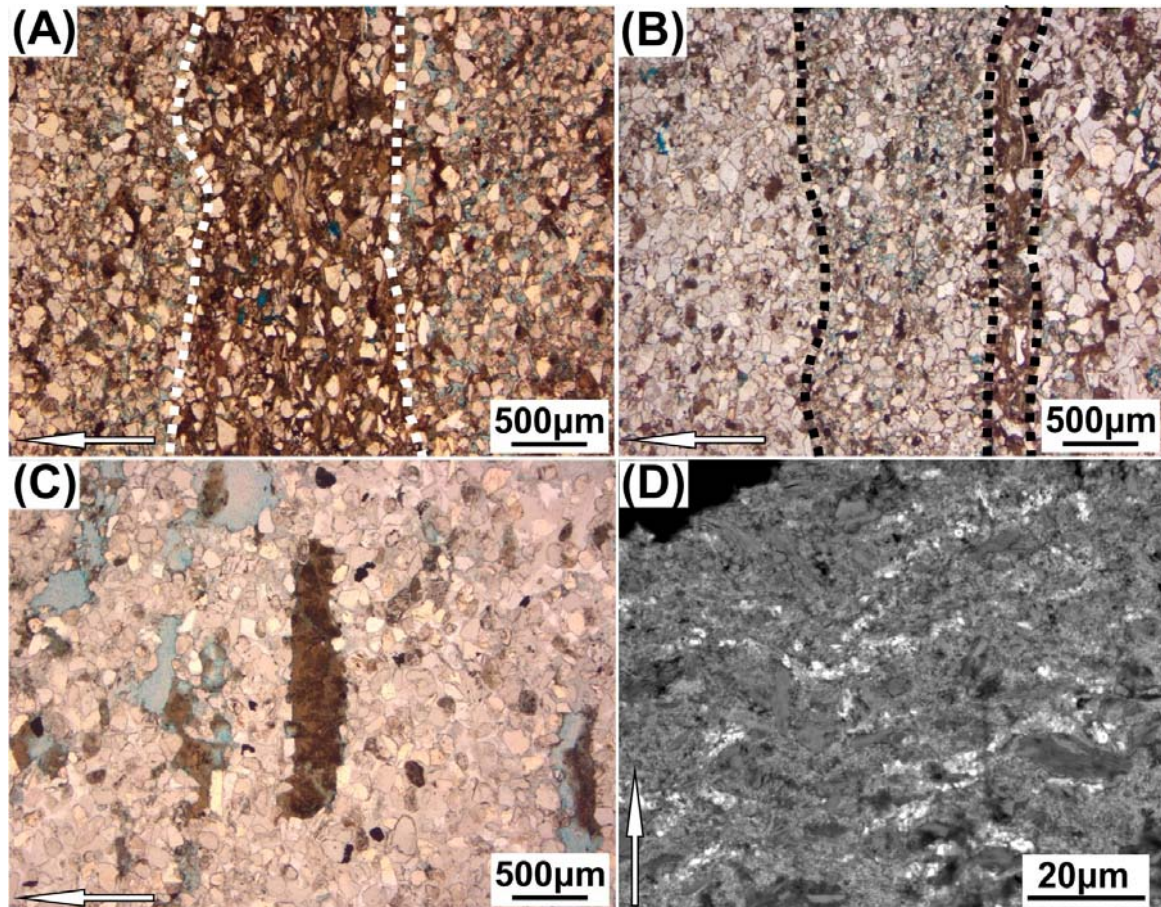
Fig. 4. Photomicrographs of the depositional texture highlighting the small-scale heterogeneity (arrow points out the stratigraphic polarity). (A) Lamina with higher mica and clay-rich matrix content. Note the absence of pervasive pore-filling cements above, within, and below such lamina (MB3, 3.40-m [11-ft] depth, plane-polarized light [PPL]). (B) Alternation of sand and silt-sized laminae with preferential clay-rich matrix and heavy-mineral concentrations (within dotted lines). Note that the matrix-rich, cement-free lamina at the center of the image is intercalated between coarser grained, gypsum-cemented laminae (MB4, 5.2-m [17-ft] depth, PPL). (C) Lamina of preferentially oriented rip-up clasts (at the center). Some of the rip-up clasts have been partially removed (gray) during thin section preparation (MB3, 4.40-m [14-ft] depth, PPL). (D) Scanning electron microscope image of the detrital matrix in detail, composed of silt-sized grains of quartz and feldspars locally embedded into a reddish-stained (in color version), clay-rich groundmass (MB4, 6.30 m [21 ft] depth).

Fig. 5. The Q-F-R diagrams displaying the compositional parameters of the analysed depositional facies.

Diagenetic fabric

Compaction & cementation

Compaction is manifested as mechanical deformation of ductile grains, mostly micas (Figure 6A, B) and rip-up clasts (Figure 6C), sometimes resulting in the formation of pseudomatrix. Compaction is favoured by the presence of these grains but inhibited by early diagenetic cements. Chemical compaction generates elongate concave-convex grain contacts.

The main early porosity-modifying cements include, in order of abundance, gypsum (6.7-19.9% TC), authigenic K-feldspar (3.8-6.3% TC), phyllosilicates (0.2-4.4% TC), carbonates (0-6.1% TC) and Fe-oxides (0.5-3.9% TC). Gypsum pore-filling cement with poikilotopic texture completely occludes primary porosity with single crystals up to 2 mm sized. A "floating-grain" texture is common (Figure 7A). Veins of drusy gypsum are especially abundant in the center of the channel (Figure 7B). Gypsum usually envelops K-feldspar overgrowths, thus postdating them (Figure 7C and E). Syntaxial K-feldspar overgrowths form continuous euhedral prisms around K-feldspar detrital grains with local obstruction of primary pore spaces and entrapment of other framework grains (Figures 7D and 8A). K-feldspar overgrowths are overgrown by dolomite rhombic crystals, so predate them (Figure 7E). Epitaxial K-feldspar outgrowths are present in minor amounts (Figure 8A). Phyllosilicate pore-filling cement is mainly composed by mixed-layer illite-smectite and, to a minor extent, kaolinite identified by SEM and EDX analysis (Figures 7F; 8B, C). Phyllosilicate cement is closely related with the occurrence of detrital matrix (Figure 8D) and be locally hosted by gypsum cement (Figures 8B; 9A). Carbonate cement encompasses Fe-dolomite and ferroan calcite. Dolomite precipitates as: (1) euhedral, poikilotopic, single rhombic crystals (up to 1.8 mm) that usually replace other framework grains and are hosted by gypsum cement (Figures 7E; 8E), (2) equant microcrystalline mosaics (10-15 μm) in contact with detrital grains (Figure 9B). Patches of replacive purple-stained calcite (for its Fe content) have been identified randomly distributed (Figure 9C). Fe-oxide cement mostly precipitates in veins and fractures associated to drusy gypsum (Figure 9D). Quartz cement

Table 1. Mean modal composition and compaction index, intergranular volume, and porosity loss by compaction of the analyzed meandering fluvial facies. Abbreviations: Cch = chute channel; Ch = channel; COPL = porosity loss by compaction; Fe=iron; I$_{compact}$ = compaction index; IGV = intergranular volume; K = potassium; PB = point bar; SB = scroll bar.

	PB (lower)	CH (center)	PB (mid)	CH (margin)	PB (upper)	SB	Cch
Q (single)	211	189	205	203	219	224	195
Polycrystalline Q with tectonic fabric	5	5	2	3	2	0	0
Polycrystalline Q without tectonic fabric	5	3	3	5	4	2	5
Q in plutonic r.f.	4	3	4	2	3	2	5
Composite Q	5	2	7	4	5	2	4
K-feldspar (single)	50	42	46	42	40	49	42
Plagioclase (single crystal)	30	34	35	35	30	33	35
P in plutonic r.f	3	1	3	1	3	2	4
Micas (single crystal)	5	7	7	7	5	6	4
Opaque minerals	3	1	1	2	1	5	7
Tourmaline	1		1	1		1	2
Rutile		1					
Zircon				1	1		5
Phyllite	5	5	6	5	7	10	35
Fine-grained schist	10	13	7	5	8	4	9
Muscovite schist	1		1	1	5		4
Fe-oxides	1	4			1		
Rip-up clasts	4	6	10	12	5		
Matrix							
Siliciclastic matrix	25	32	35	62	19	28	18
Phyllosilicate matrix	3	14	14	10		3	4
Pseudomatrix	4	1			2		
Cements							
Carbonate	3	3	2		8	31	4
Phyllosilicate	8	20	17	22	1	19	9
K-feldspar overgrowths	27	19	22	22	25	32	12
Gypsum	79	86	65	34	100	38	78
Fe-oxides	2	9	3	14	2	2	19
Quartz overgrowths	1	1	1	2	3	2	2
I$_{compact}$	0.51	0.43	0.56	0.64	0.42	0.48	0.50
IGV	24.8	27.6	23.0	20.1	28.0	26.4	25.0
COPL	20.2	17.1	22.1	24.9	16.6	18.5	20

is negligible but, when present, occurs as microcrystalline rims (<10 μm) intimately intergrown with illite (Figure 8F).
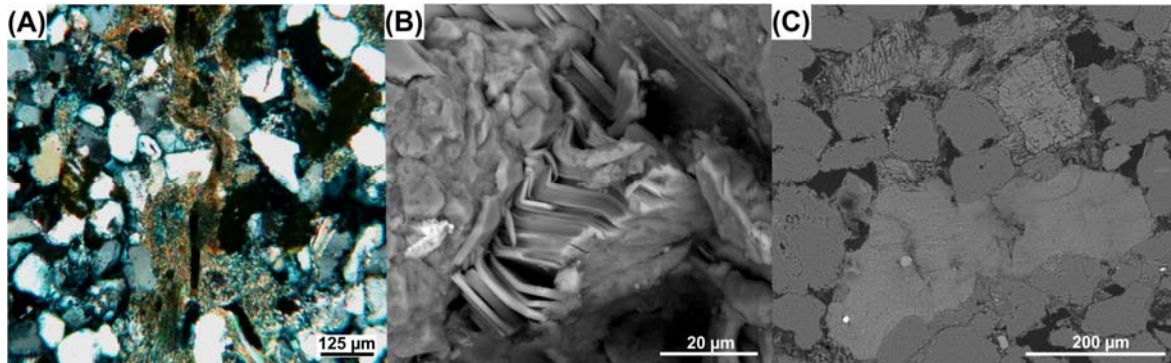
Fig. 6. Photomicrographs of mechanical compaction evidences. (A) Ductile yielding of clay-rich matrix lamina with associated mica deformation (MB3, 3.20-m [10.5-ft] depth, cross-polarized light). (B) Scanning electron microscope (SEM) image of mechanically deformed mica (MB3, 3.6-m [12-ft] depth). (C) An SEM image of pseudoplastic deformation of a rip-up clast (MB3, 3.6-m [12-ft] depth).

The spatial distribution of cements within the composite sandstone geobody is strongly facies-related (Figure 10A). In the channel area, gypsum content increases from the channel margin to the center and from the mid- to the lower point bar whereas phyllosilicate and Fe-oxide cements decrease with the same pattern. K-feldspar overgrowths show variable trends, decreasing from the channel margin to the center but increasing from the mid- to the lower point bar. Carbonate content is low and increases from the channel margin to the center and from the middle to the lower point bar. In the floodplain area from the upper point bar to the scroll bar, there is a general increase in all cement contents with the exceptions of gypsum, which decreases, and Fe-oxides that do not vary. The chute channel fill is mainly cemented by gypsum and, in minor amount, by Fe-oxides, K-feldspars, phyllosilicates and carbonates.

Intergranular volume analysis (Figure 10B; Table 1) reveals that compactional processes in the channel area have been more important than in the floodplain area. According to Lundegard (1992), $I_{compact}$ equals 1 when all porosity loss is by compaction whereas $I_{compact}$ equals 0 when all porosity loss is by cementation. Thus, highest compaction values are associated to the channel margin ($I_{compact} = 0.64$) whereas in the center of the channel early cementation prevails ($I_{compact} = 0.43$). The point bar facies in this area (lower and mid-point bar) display intermediate compaction-cementation values, slightly veering towards compaction processes ($I_{compact} = 0.51$ and $I_{compact} = 0.56$, respectively). In the floodplain area, porosity loss by compaction increases from the upper point bar ($I_{compact} = 0.42$) to the scroll bar ($I_{compact} = 0.48$), whereas cementation processes decrease in the same direction (Table 1). The chute channel differs from the underlying upper point bar according to a higher compaction index ($I_{compact} = 0.50$).

Primary and Secondary Porosity In the study area, sandstone pore types are related to either primary depositional fabric or secondary dissolution and grain deformation (Figures 11; 12). Primary pores are predominantly large intergranular pores between framework grains (Figures 7D; 9C) and,
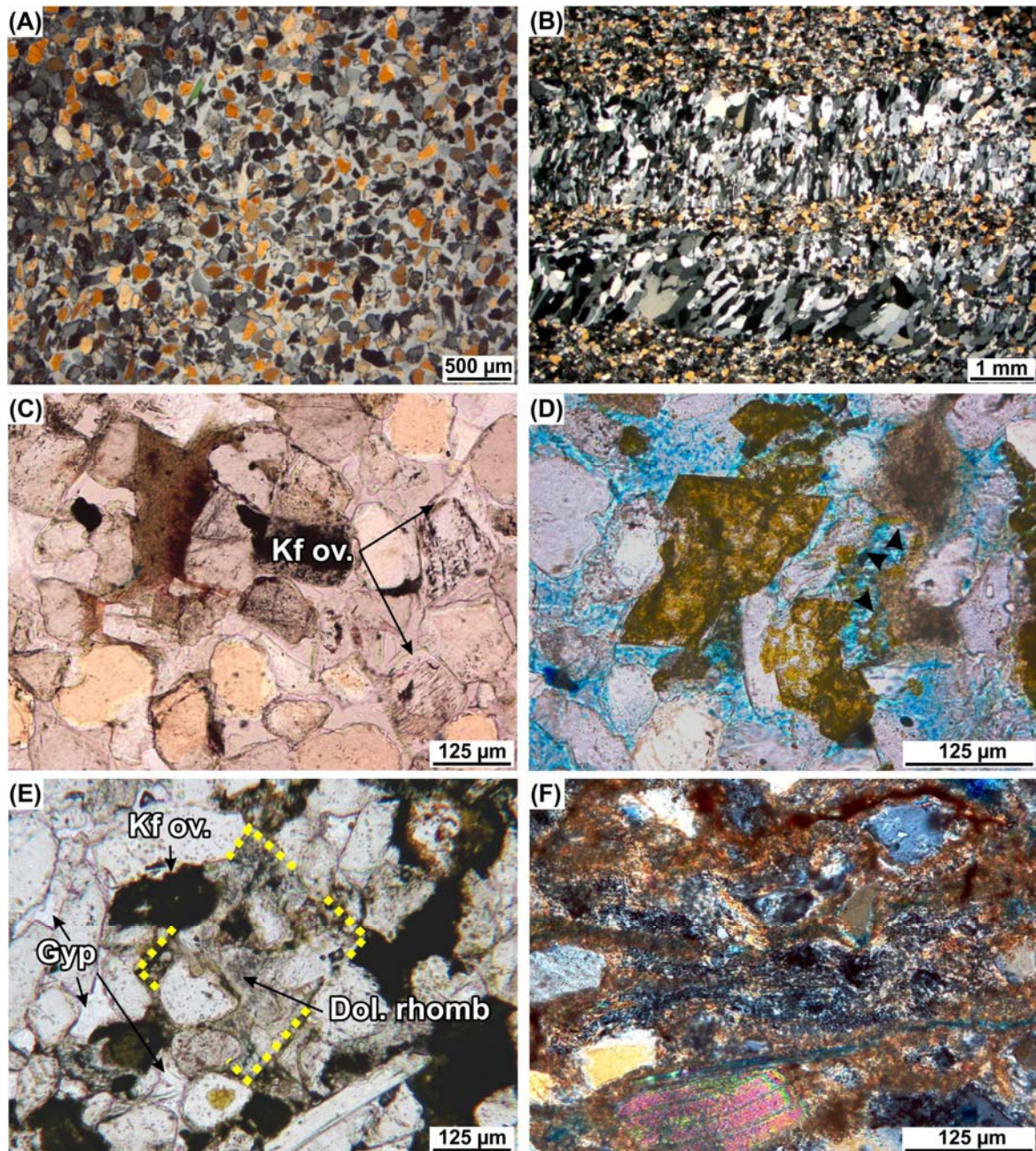
Fig. 7. Photomicrographs of the main porosity-modifying cements. (A) Pore-filling gypsum cement showing "floating-grain" texture (MB4, 5.8-m [19-ft] depth, cross-polarized light [XPL]). (B) Drusy gypsum precipitated in veins (MB4, 5.8-m [19-ft] depth, XPL). (C) Porefilling gypsum cement surrounding and postdating the potassium (K)-feldspar overgrowths (Kf ov.; MB4, 5.8-m [19-ft] depth, planepolarized light [PPL]). (D) Well-developed K-feldspar overgrowth (yellowish stained) partially overlying detrital quartz grain. Secondary pore results from detrital K-feldspar dissolution (black arrows). Note the abundance of preserved primary pore spaces (MB1, 3.0-m [10-ft] depth, PPL). (E) Euhedral iron (Fe)-dolomite rhombic crystal (Dol. rhomb; dotted line) partially overlying Kf ov. and completely surrounded by pore-filling gypsum cement (Gyp; MB3, 5.4-m [18-ft] depth, PPL). (F) Phyllosilicate pore-filling cement mainly composed of mixed-layer illite–smectite and, to a minor extent, kaolinite, reddish stained by Fe oxides (MB4, 7.2-m [23.5-ft] depth, XPL). Note: A color version can be seen in the online version.

to a minor extent, smaller void spaces within the matrix (Figure 4A, B). Preservation of primary porosity is more pronounced in samples with higher matrix and lower early-

precipitated cement contents (Table 2; Figure 11A). In the channel area, primary porosity and matrix abundance decrease from the channel margin towards the lower point bar whereas in the floodplain area these parameters increase from the upper point bar to the scroll bar facies. The chute channel fill shows similar primary porosity values of the underlying upper point bar except for slightly greater matrix content.
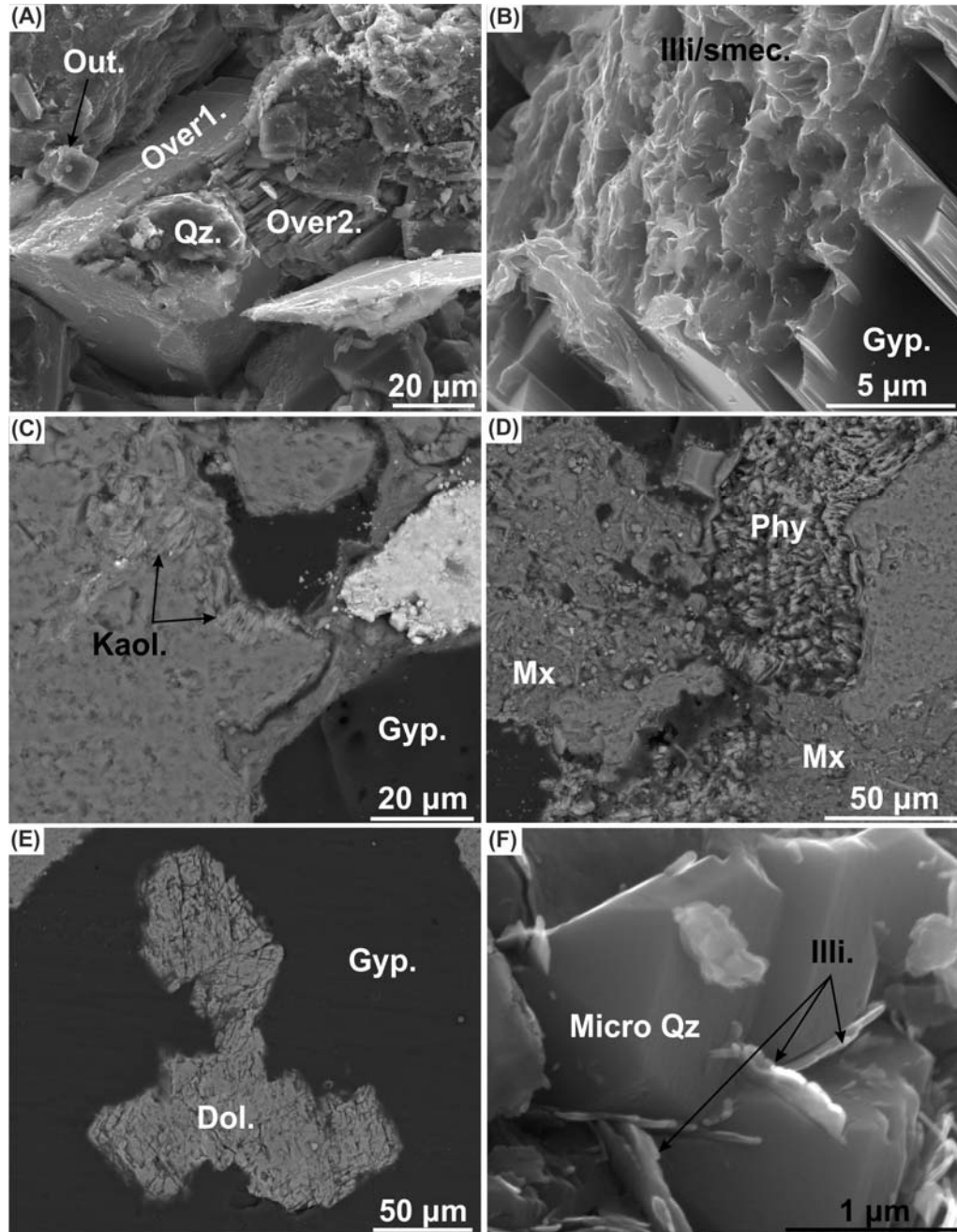
Fig. 8. Scanning electron microscope images of more-detailed diagenetic features. (A) potassium (K)-feldspar overgrowths (Over1. and Over2.) surrounding detrital quartz (Qz.). K-feldspar outgrowth (Out.) also occurs (MB4, 8.2-m [27-ft] depth). (B) Mixed-layer illite–smectite cement (Illi) trapped by gypsum crystal (Gyp.; MB4, 5.2-m [17-ft] depth). (C) Kaolinite (Kaol.) replacing detrital K-feldspar at the grain rim (MB4, 6.6-m [21.5-ft] depth). (D) Textural differences between detrital clay-rich matrix (Mx) and phyllosilicate pore-filling cement (Phy; MB1, 2.8-m [9-ft] depth). (E) Rhombohedral crystals of iron (Fe-dolomite (Dol.) enclosed by Gyp. (MB2, 2.9-m [9.5-

ft] depth). (F) Microcrystalline quartz (Micro Qz) intergrown with illite (Illi.; MB3, 5.4-m [18-ft] depth).
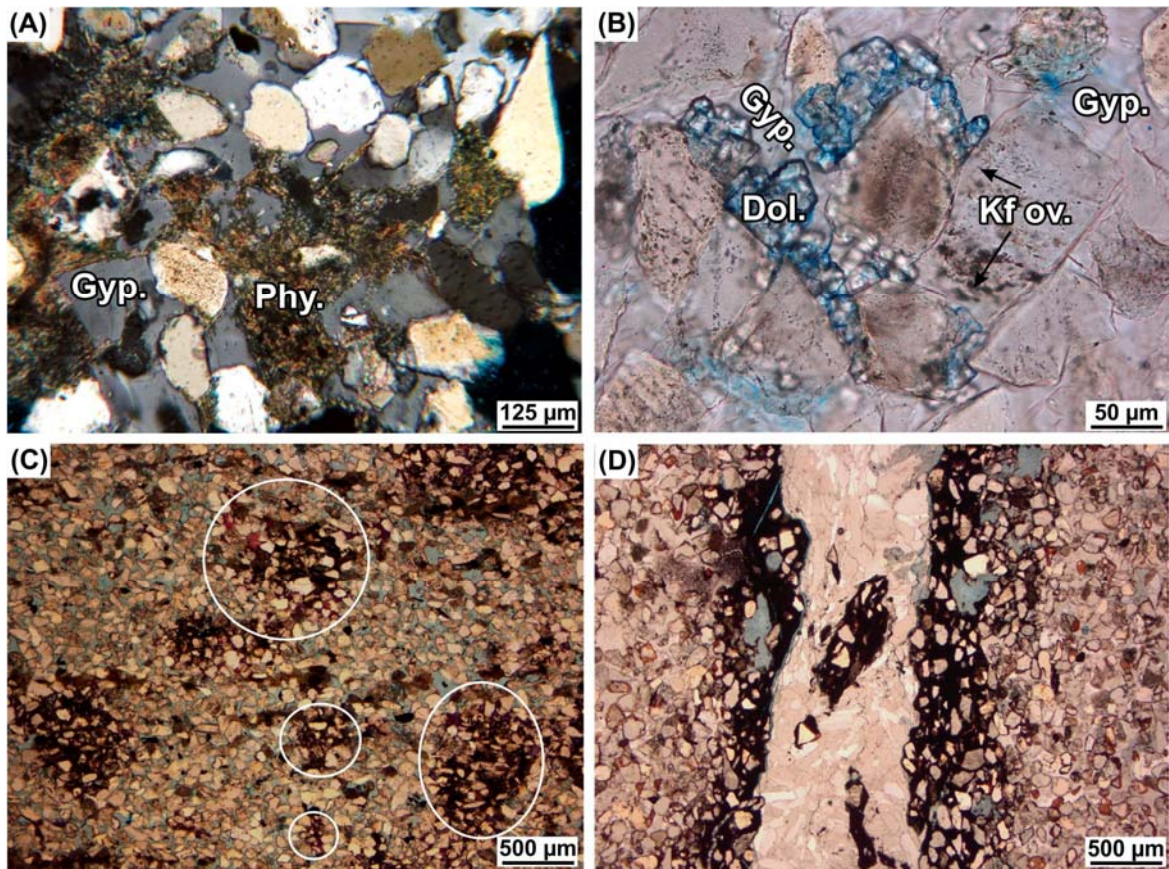
Fig. 9. Photomicrographs of the main porosity-modifying cements (continued). (A) Patch of phyllosilicate pore-filling cement (Phy.) hosted by gypsum (Gyp.) crystals (MB4, 6.6-m [21.5-ft] depth, cross-polarized light). (B) Equant microcrystalline mosaics of iron (Fe)-dolomite (Dol.) in contact with detrital grains, overgrown by Gyp. but overlying potassium (K)-feldspar overgrowths (Kf ov.; MB4, 8.2-m [27-ft] depth, plane-polarized light [PPL]). (C) Patches of replacive reddish-purple–stained (in color version), Fe-rich calcite (solid circles), randomly distributed (MB1, 2.8-m [9-ft] depth, PPL). Note the abundance of preserved primary pores. (D) Late Fe-oxide cement precipitated in a fracture and associated with drusy gypsum (MB4, 5.8-m [19-ft] depth, PPL).
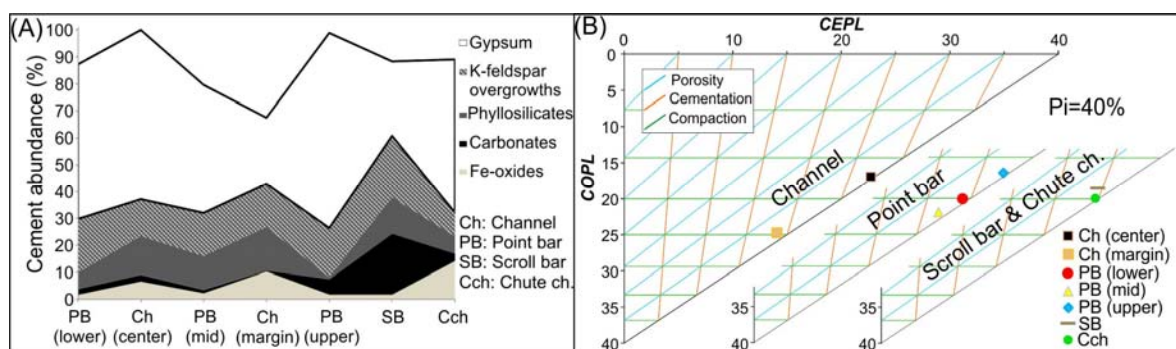
Fig. 10. Cementation and compaction features of the analyzed meandering fluvial facies. (A) Relative cement distribution within the different depositional facies (normalized to 100%). Note that gypsum is systematically the most abundant porosity-modifying cement, although its occurrence varies across facies. (B) Plots of compaction porosity loss (COPL) versus cementation porosity loss (CEPL) (after Lundegard, 1992) showing that compaction prevails on channel (ch.)

margin and scroll-bar facies, whereas cementation dominates on channel center and midpoint bar. Fe = iron; K = potassium; Pi = assumed initial porosity of 40%.

Table 2. Pore system characterization and petrophysical parameters of the analyzed meandering fluvial facies. Abbreviations: Carb = carbonates; Cch = chute channel; Ch = channel; Fk = K-feldspar; Fk-ov = K-feldspar overgrowths; Fp = plagioclase; full = whole undetermined feldspar; Gyp = gypsum; K = permeability; Ls = lithic fragments; Mica = micas; OP = open porosity; PB = point bar; Phy = phyllosilicates; P1 = total primary porosity; P1 Frw = primary porosity between framework grains; P1 Mx = primary porosity within the detrital matrix; P2 = total secondary porosity; P2 Cem. = secondary porosity by cement dissolution; P2 def. = secondary porosity by compaction; P2 Felds. = secondary porosity by detrital feldspar dissolution; SB = scroll bar.

	PB (lower)	CH (center)	PB (mid)	CH (margin)	PB (upper)	SB	Cch
P1	21	18	23	26	8	31	7
P1 Frw	15	9	11	11	6	28	4
P1 Mx	6	9	12	15	2	3	3
P2	79	82	77	73	92	69	93
P2 Felds.	16	19	17	17	11	29	6
P2 Fp	6	7	2	4	5	7	1
P2 Fk	8	11	11	9	5	12	5
P2 full	2	1	4	4	1	10	0
P2 Cem.	45	44	54	41	51	32	54
P2 Fk-ov	2	2	5	4	2	1	2
P2 Carb	1	1	1	2	1	3	0
P2 Phy	15	17	13	10	19	5	30
P2 Gyp	26	24	35	25	30	23	22
P2 def.	18	19	7	15	30	7	33
P2 Ls	15	15	6	11	25	6	30
P2 Mica	3	4	1	4	5	1	3
OP (%)	8.7	9.3	12.8	25.5	13.5	25.2	8.9
K (mD)	8.02	3.8	14.5	106.7	0.9	163.0	2.7
Pore size (µm)							
>100	0.65	0.10	0.50	0.52	0.77	0.92	0.11
100--10	5.56	3.66	5.54	4.32	3.68	10.25	4.93
10--1	16.27	41.17	36.22	75.26	7.37	73.37	31.65
1--0.1	40.30	26.90	32.20	10.89	56.80	11.20	34.57
<0.1	37.22	28.17	25.53	9.00	31.38	4.26	28.74

Secondary porosity is more abundant than primary porosity with a greater variety of pore shapes and sizes (Table 2). Most of the secondary pores are the product of dissolved cements and, to a minor extent, feldspars grains (Table 2; Figure 11B). They constitute relatively isolated pores within gypsum crystals and intragranular honeycombed pores in detrital feldspars (Figure 12A, B). Phyllosilicate, carbonate cement and K-feldspar

overgrowth dissolution produces smaller pores (Figure 12C) with some of them connected to the intergranular pore network. Deformation of fragile grains may yield the formation of tiny, isolated pores within detrital lithic fragments (Figure 12D).

Both dissolution trends do not follow the facies distribution (Figure 11B) and there is no obvious relationship between cement abundance and their related dissolution values. Extent of cement dissolution in the channel area is similar in the different facies, with greater values associated to the mid-point bar, whereas feldspar dissolution is quite homogeneous. In the floodplain area, cement dissolution decreases from the upper point bar to the scroll bar whereas feldspar dissolution increases with the same pattern. Highest cement and lowest feldspar dissolution values are recognised in the chute channel. Figure 11C shows that secondary microporosity caused by deformation is mostly linked to the presence of lithic fragments (coefficient of determination $[R^2] = 0.57$).
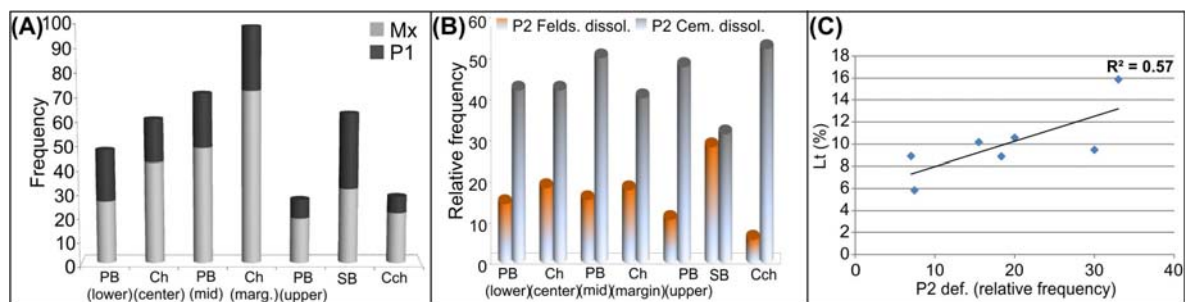
Fig. 11. Main features of primary and secondary porosity. (A) Spatial distribution of matrix content (Mx) and primary porosity (P1) according to depositional facies. Note the similar variation trend of both variables. (B) Spatial distribution of secondary porosity resulting from dissolution of detrital feldspars (P2 Felds. dissol.) and cements (P2 Cem. dissol.) showing that cement dissolution dominates over that of detrital feldspars, although there are no obvious variation patterns between them. (C) Plot of secondary microporosity (P2 def.) versus lithic fragments (Lt) showing a good and direct (coefficient of determination $[R^2] = 0.57$) correlation between lithic fragment occurrence and secondary microporosity produced by deformation. Cch = chute channel; Ch = channel; marg. = margin; PB = point bar; SB = scroll bar.

Petrophysical characterization: Open Porosity and Permeability

The MICP data show considerable differences in OP and k values between fluvial facies (Table 2). The OP values range from 8.7% to 13.5% except for the scroll bar (25.2%) and channel margin (25.5%) facies. The lowest values are at the lower point bar and in the chute channel and are 8.7% and 8.9%, respectively. Permeability values are fairly low ranging from 0.9 to 14.5 mD. The highest values are registered in the channel margin (106.7 mD) and the scroll bar facies (163 mD) whereas upper point bar and chute channel have the lowest permeability values (0.9 and 2.7 mD, respectively). Maximum and minimum values of porosity and permeability are not always directly related.

The dominant pore radius interval in the scroll bar and channel margin facies is 1-10 μm, which represents 73.37% and 75.26% of total OP, respectively (Table 2). Pore radii of less than 1 μm accounts for 15.46% and 19.89% of total OP in those facies, respectively. The scroll bar shows the highest amount of large pores (10-100 μm) with 10.25% of total OP. In the rest of analyzed facies, the differences in frequency among the pore radii are negligible, except for the upper point bar, which shows a clear predominance

of pore radius less than 1 μm (88.18% of total OP). Pore radii greater than 100 μm represent barely 1% of total OP regardless of the type of facies.
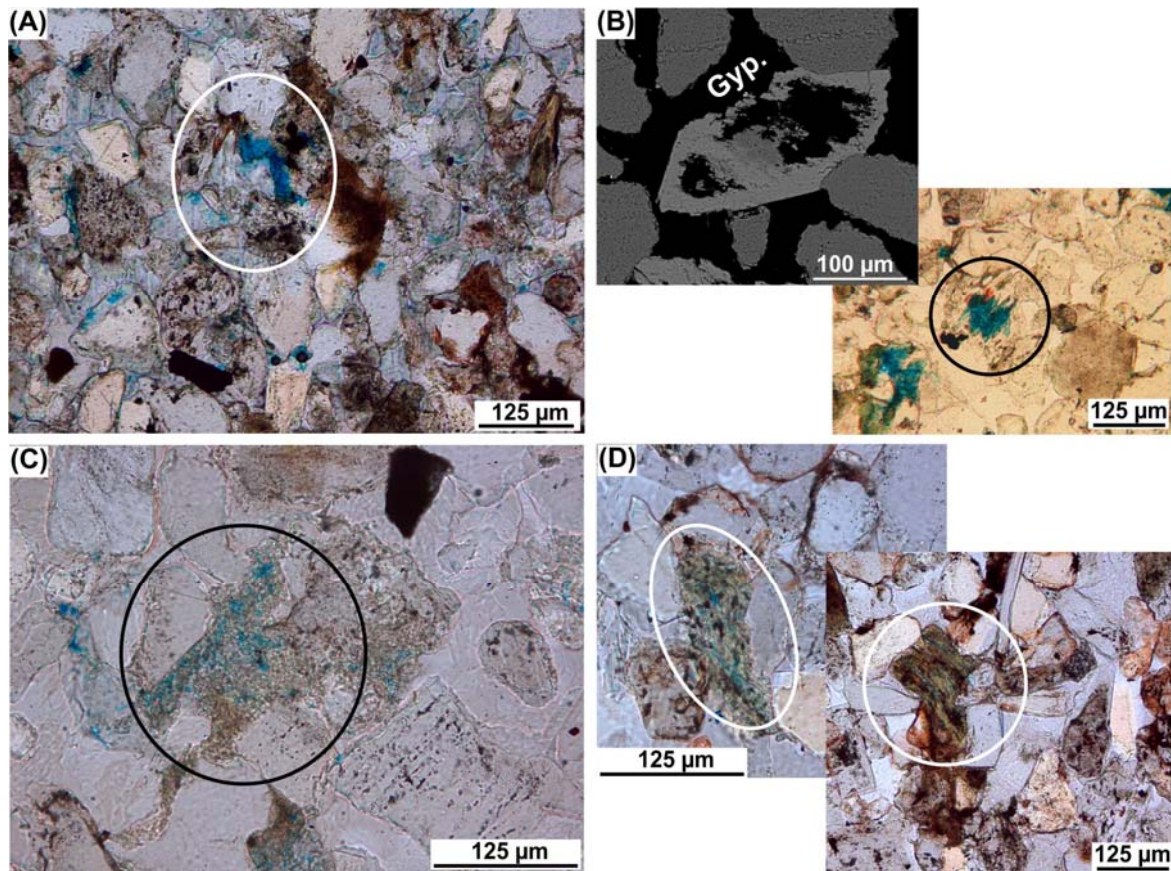
Fig. 12. Photomicrographs of secondary porosity (inside the solid circles). (A) Large isolated dissolution pore in gypsum cement (MB3, 4.25-m [14-ft] depth, plane-polarized light [PPL]). (B) Large intragranular honeycombed pores in detrital potassium (K)-feldspar grains (upper photo: MB4, 6.0-m [19.5-ft] depth, pore-filling gypsum cement [Gyp.]; lower photo: MB2, 2.4-m [8-ft] depth, PPL). (C) Microporosity within phyllosilicate pore-filling cement (MB1, 3.0-m [10-ft] depth, PPL). (D) Intragranular compaction micropores within detrital lithic fragments (upper photo: MB4, 5.8 m [19 ft] depth, PPL; lower photo: MB2, 3.15-m [10.3-ft] depth, PPL).

DISCUSSION

Origin of authigenic minerals

Despite the relatively homogeneous composition of the sandstones, cement occurrence varies by facies including the following main authigenic minerals: K-feldspar, phyllosilicates (illite and kaolinite), carbonates (Fe-rich dolomite and calcite), gypsum, Fe-oxides and quartz. Paragenetic sequence is summarized in Figure 13.

The K-feldspar overgrowths are widespread throughout the different depositional facies and are the first cement to precipitate, prior even than intense mechanical compaction, as suggested by their thick and euhedral faces. Fluvial deposits are fluxed by freshwater immediately after deposition. These meteoric waters with a low $(K^+, Na^+)/(H^+)$

71

ratio may cause early K-feldspar dissolution, leading to local source of K^+ for authigenic K-feldspar precipitation (Milliken, 1989; Rossi et al., 2002; Worden and Morad, 2003).

Petrographic analysis shows a direct relationship between the occurrence of detrital matrix and phyllosilicate cement, with similar spatial variation trends in both the channel and the floodplain areas. Kaolinite mostly represents the transformation by-product of detrital feldspars (Bjørlykke and Aagaard, 1992) so, in the presence of K^+, alteration of detrital matrix and rip-up clasts mainly causes early mesodiagenetic illite formation via mixed-layer illite/smectite (Morad et al., 2000, 2010; Worden and Morad, 2003). Such a transformation frequently results in concomitant quartz cementation (Figure 8F; McKinley et al., 2003).
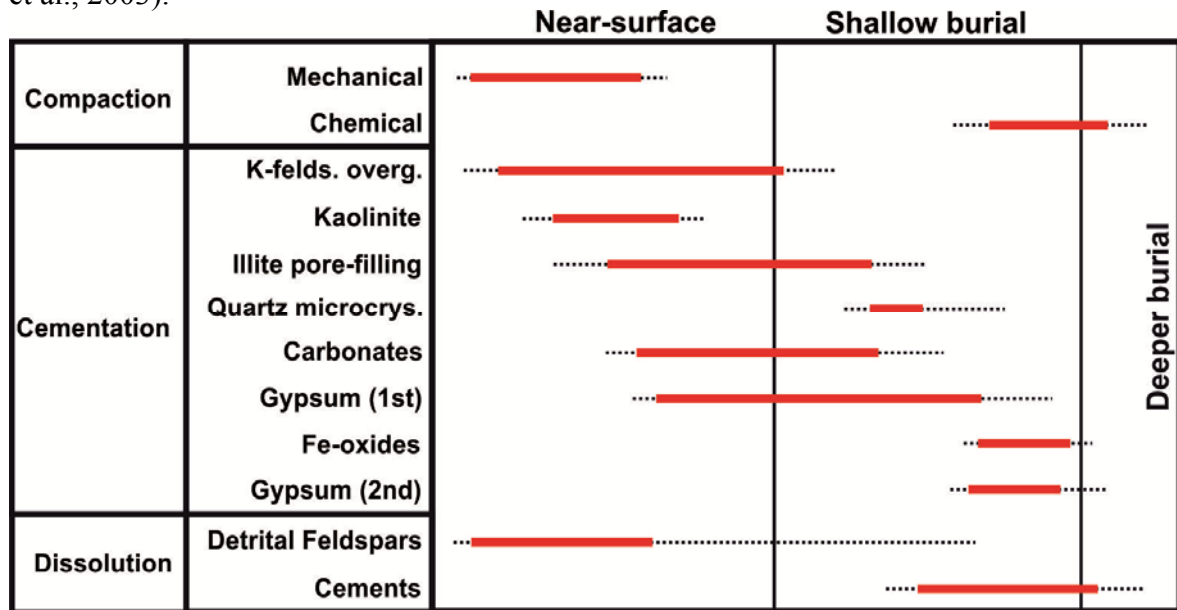
Fig. 13. Paragenetic sequence of the main diagenetic events. Solid line represents the major event of each process, whereas the associated dashed line indicates its minor or presumable occurrence. Fe = iron; K = potassium; K-felds. overg. = K-feldspar overgrowths; microcrys. = microcrystalline.

Gypsum and carbonate cements are common in semi-arid environments where they usually have a phreatic origin (Spotl and Wright 1992; Schmid et al., 2004; Khalaf, 2007). In the studied samples, preservation of high intergranular volume (IGV) and non-displacive textures in gypsum pore-filling cement as well as euhedral faces of dolomite rhombs suggest high pore-network connectivity when these minerals grow (Worden and Burley, 2003; Henares et al., 2014c). Mechanical compaction is strongly inhibited by the occurrence of these early-precipitated cements (Paxton et al., 2002; Cook et al., 2011). Gypsum and carbonates are considered to be the result of the evaporation of saline groundwaters (Talbot et al., 1994; Schreiber and El Tabakh, 2000; Schmid et al., 2006) whose composition is proven in this case by the presence of gypsum nodules and calcrete paleosols in floodplain deposits as described by Arribas et al. (1995). Carbonates precipitate slightly before gypsum as suggested by petrographic images (Figures 7E; 8E; 9B). Textural features suggest that carbonates likely form in the mixing zone between incoming fresh waters (from the reactivation of the abandoned channel during peak discharge) and saline waters (from the floodplain by capillary-driven groundwater during drying-out periods) (Morad et al., 1990; Sullivan et al., 1994). Accordingly, mixing zone may be situated in the outer part of the meandering channel coinciding with the scroll bar

facies where indeed carbonate cement is more abundant. Gypsum precipitation takes place in water-saturated sediments, presumably related to channel inactivity and maximum evaporation rates, when pore-water composition is dominantly saline due to the influence of groundwaters (Wilson and Stanton, 1994; Arribas et al., 1996). A predominance of gypsum in the center of the channel and in the upper point bar supports that interpretation. In the channel margin, occurrence of great amount of detrital matrix may hinder pervasive gypsum precipitation as well as in the scroll bar, where early carbonates also reduce the available pore space. Later generation of fractures may favour precipitation of a secondary stage of gypsum cement with drusy texture, likely sourced by weathering oxidation of unstable sulphides in the adjacent mudstones, and associated Fe-oxides, in more oxidizing conditions related to channel abandonment and subaerial exposure.

Depositional heterogeneity effect on diagenetic evolution

The fluvial deposits in this study consist of fine-grained, well sorted sandstones. Detrital matrix (silt-sized grains + clay groundmass) and other components such as heavy minerals, micas and rip-up clasts, preferentially concentrate in laminae following the sedimentary structure visible in thin section. Chuhan et al. (2002) and Bjørlykke et al. (2004) suggest that fine-grained, well-sorted sandstones, like those in the present study, should undergo less mechanical compaction but higher porosity loss by cementation than coarse-grained, poor-sorted sandstones. As shown in Figure 14A, small-scale internal heterogeneities associated with the abundance of detrital matrix affect, in large extent, the spatial distribution and magnitude of the main diagenetic processes. Thus, higher matrix contents are closely related to a higher compaction but also result in the inhibition of pore-filling cements that prevent IGV loss (Fig. 14A and B). Experimental studies of compaction have shown that relatively small amounts of detrital silty clay matrix in sandstones will cause important porosity loss by mechanical compaction (Fawad et al., 2010, 2011). Petrographic images (e.g. Figure 6A) evidence that ductile yielding of this type of matrix favours movement and rearrangement of rigid framework grains between which matrix penetrates. Pseudoplastic deformation of other ductile components (micas, rip-up clasts, phyllitic grains) also increases the effect of mechanical compaction (Fig. 14B). However, analyzed samples with abundant clay minerals (detrital and authigenic) have relatively low quantities of pore-filling gypsum and carbonates likely because (1) clay-rich matrix contains substantial void space, mostly micrometre- or nanometre scaled pores, so matrix-rich laminae can act as a baffle for cementing fluid migration (Hurst and Nadeau, 1995; Pranter et al., 2007; example given in Figure 4A), (2) there is little initial intergranular porosity in which these cements could grow (Milliken, 2001; Armitage et al., 2013; example given in Figure 4B).

Studied fluvial example corresponds to a fine-grained meandering system (according to Smith, 1987; Miall, 2006) where decimetre- or centimetre- sand-mud couplets may form on the point bar (so-called inclined heterolithic stratification). Such heterogeneity is strongly facies-dependant since it results from the interplay between transport energy and hydraulic selective sorting by grain size and grain density (Doyle et al., 1983). Accordingly, Figure 14C shows similar spatial distribution patterns throughout the meandering fluvial depositional facies of hydraulic-sorting-sensitive variables such as

detrital matrix, rip-up clasts, heavy minerals and micas. In the channel area, all of them decrease from channel margin to the center and from middle to lower point bar, except for heavy mineral content that increases in this direction. In the floodplain area, all of them increase from the upper point bar to the scroll bar except for rip-up clasts which are absent in the scroll bar. The chute channel fill shows independent behaviour with intermediate matrix content, no rip-up clasts, the highest concentration of heavy minerals and the lowest of mica.
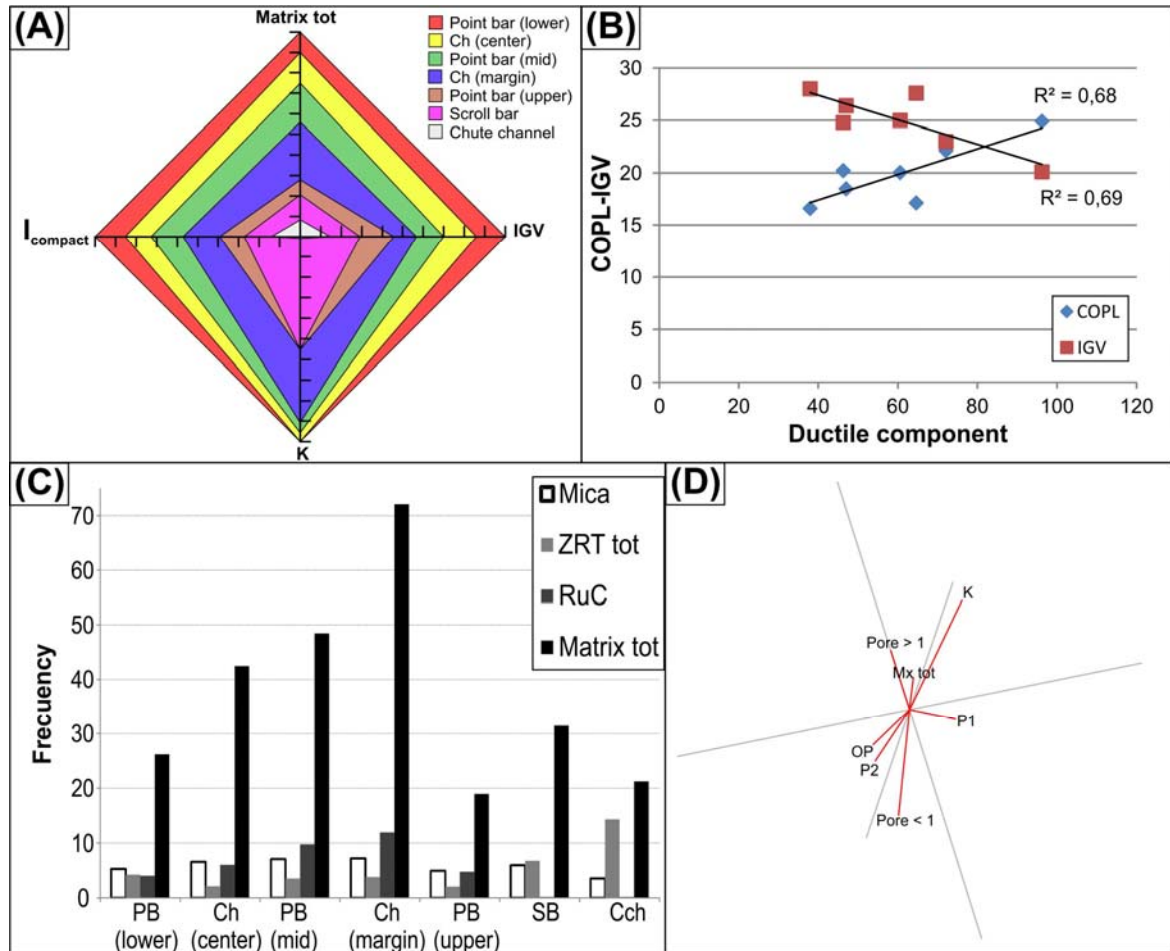
Fig. 14. (A) Spider radar chart showing the interplay between detrital matrix (Matrix tot), compaction index ($I_{compact}$), and intergranular volume (IGV) and their control on permeability (k), according to depositional facies. When matrix content, $I_{compact}$, and k show an increase, which occurs from the channel center to its margin, from the lower to midpoint bar, and from the upper point bar to the scroll bar, IGV decreases. Chute channel displays an independent behavior, with significant matrix content, similar $I_{compact}$ and IGV, and very low k. (B) Plot of compaction porosity loss (COPL) and IGV indices versus ductile component abundance (matrix + rip-up clasts + micas + phyllitic grains; point-counting data). The COPL and IGV show a good direct and inverse correlation, respectively (coefficient of determination [R^2] = 0.68; R^2 = 0.69), according to the presence of ductile components. (C) Histogram displaying similar spatial distributions of hydraulicsorting–sensitive variables throughout the meandering fluvial system. (D) Multivariate statistical graph (biplot) showing the relation between determined petrographic (matrix [Mx tot], primary porosity [P1], and secondary porosity [P2]) and petrophysical (k, open porosity [OP], pore radii > 1 mm [Pore > 1], and pore radii < 1 mm [Pore < 1]) parameters. Geometrical relationships between variables (for further explanation on biplot interpretation, cf. Caracciolo et al., 2012) indicate that matrix occurrence is directly related to preservation of large primary pores, which are the main contributors to permeability, whereas most of secondary porosity is distributed into

smaller pores, only detected by mercury injection–capillary pressure analysis. Cch = chute channel; Ch = channel; Matrix tot = detrital matrix; PB = point bar; RuC = rip-up clast; SB = scroll bar; ZRT tot = zircon + tourmaline + rutile.

Implication for reservoir properties

The reliable evaluation of reservoir properties on wellbore scale not only depends on the calculation of porosity value for an estimation of permeability, but also on the understanding of the pore network and the contribution of each type of pore to the overall properties (Loucks, 2005). As discussed above, the occurrence of clays (detrital and authigenic) favours the compaction process and hinders early pore-filling cement precipitation that helps the preservation of primary porosity. Multivariate statistical treatment of determined compositional and petrophysical data demonstrates that large (> 1 µm) and well-connected primary intergranular pores are the main contributors to permeability in matrix-rich samples (Figure 14D). However, secondary porosity, although dominant on primary porosity likely due to late dissolution of early and pervasive gypsum cement (Table 2), is mostly related to smaller (< 1 µm) pores, only detected by MICP analysis, that do not contribute to permeability enhancement (Figure 14D). Microporosity (< 0.1 µm pore size; Table 2) is also stimulated by the presence of secondary pores which result from deformation of some kind of lithic fragments.

The Reservoir Quality Index (RQI) proposed by Amaefule et al. (1993) allows for the identification of reservoir units with similar fluid-flow characteristics defined by (1) geological attributes of texture, mineralogy, sedimentary structures and nature of permeability barriers, and (2) petrophysical properties of porosity, permeability and capillary pressure. Thus, reservoir units are related to depositional facies distribution but do not necessarily coincide with facies boundaries (Amaefule et al., 1993). Figure 15 depicts the spatial distribution of reservoir properties within the meandering fluvial composite sandstone by using RQI as input in a deterministic three-dimensional facies model in Petrel®. Siltstone and claystone porosity and permeability values have been assumed from petrographic analysis and literature data (McWhorter and Sunada, 1977; Domenico and Schwartz, 1990). RQI model validation with depositional and diagenetic data reveals a good match between reservoir properties and facies distribution. Such harmony is a direct consequence of the primary control exerted by depositional features, i.e. matrix distribution, on diagenetic evolution and thus on reservoir quality. Therefore, in the channel as well as in the floodplain areas, best reservoir properties are associated to the channel margin and the scroll bar facies, respectively, where permeability is higher due to the presence of matrix that preserves primary porosity. Conversely, the channel center, upper point bar and chute channel show the most deteriorate reservoir quality because of pervasively cementation by gypsum causing permeability drop.

CONCLUSIONS

In this paper, we demonstrate that early-diagenetic porosity and permeability deterioration has a direct relation with sedimentary dynamics and, thus, with depositional features of the geobody. The observed relationships and causes of diagenetically-induced heterogeneity in this example confirm the importance of textural information for the

successful application of predictive diagenetic modelling in reservoir quality assessment. Small-scale internal porosity-permeability heterogeneity associated with the occurrence of detrital matrix and suspension settling laminae affect, to a large extent, the spatial distribution and magnitude of the main early-diagenetic processes in the way that higher matrix content favors compaction but also results in the inhibition of pervasive pore-filling cements. The spatial distribution of detrital matrix is strongly facies-related as proven by the same distribution pattern that other hydraulic sorting-sensitive variables such as rip-up clasts, heavy minerals and micas.
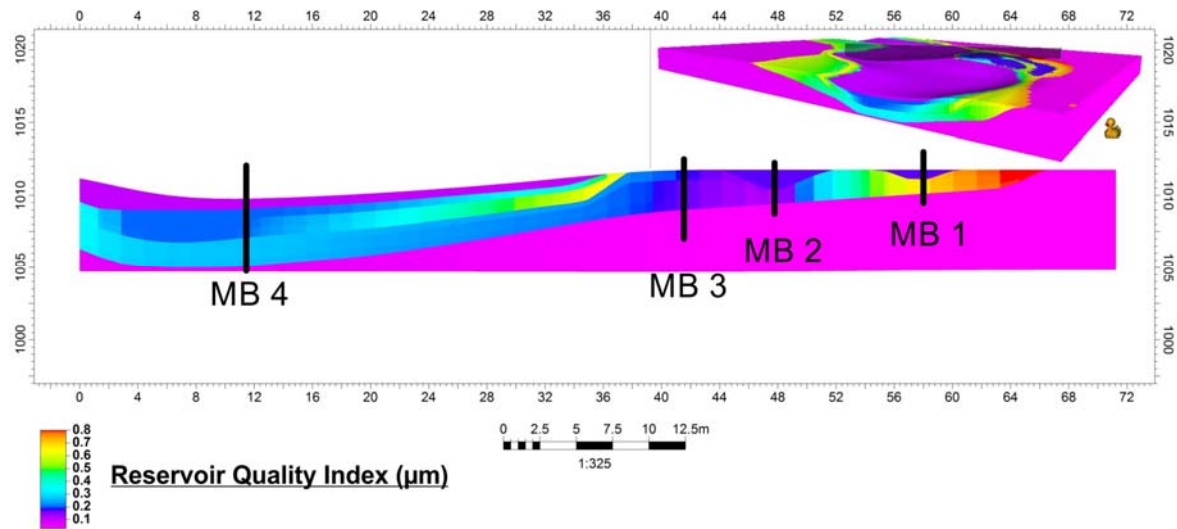
Figure 15. Reservoir quality model of the analyzed meandering composite sandstone in three-dimensional (3D) and two-dimensional (2D) views. Well position is included in 2D view. The *x*-axis is horizontal distance (meters); the *y*-axis is elevation (meters). The reservoir quality index (micrometers), ranges from 0.1 to 0.8 μm.

Multivariate statistical treatment of compositional and petrophysical data demonstrates that large (> 1 μm) and well-connected primary intergranular pores are the main contributors to permeability in the more heterogeneous samples. Secondary porosity seems to be mostly related to smaller (< 1 μm) and randomly-distributed dissolution pores.

Identification of post-depositional facies-related preferential flow pathways such as the channel margin and the scroll bar, well-represented in the RQI model, can be used to enhance recovery strategies (water or steam injection). In our view, the upward displacement of bypassed oil by water or steam injection towards the channel margins and scroll bars would improve the ultimate recovery by providing permeability connectivity with other parts of the reservoir.

Acknowledgements

4.2.2 Muddy and dolomitic rip-up clasts in Triassic fluvial sandstones: origin and impact on potential reservoir properties (Argana basin, Morocco)

S. Henares, J. Arribas, G. Cultrone and C. Viseras

Abstract

The significance of rip-up clasts as sandstone framework grains is frequently neglected in the literature being considered as accessory components in bulk sandstone composition. However, this study highlights the great value of muddy and dolomitic rip-up clast occurrence as: (a) information source about low preservation potential from floodplain deposits and (b) key element controlling host sandstone diagenetic evolution and thus ultimate reservoir quality. High-resolution petrographic analysis on Triassic fluvial sandstones from Argana Basin (T6 and T7/T8 units) highlights the significance of different types of rip-up clasts as intrabasinal framework components of continental sediments from arid climates. On the basis of their composition and ductility, three main types are distinguished: (a) muddy rip-up clasts, (b) dolomitic muddy rip-up clasts and (c) dolomite crystalline rip-up clasts. Spatial distribution of different types is strongly facies-related according to grain size. Origin of rip-up clasts is related to erosion of coeval phreatic dolocretes, in different development stages, and associated muddy floodplain sediments. Cloudy cores with abundant inclusions and clear outer rims of dolomite crystals suggest a first replacive and a subsequent displacive growth, respectively. Dolomite crystals are almost stoichiometric. This composition is very similar to that of early sandstone dolomite cement, supporting phreatic dolocretes as dolomite origin in both situations. Sandstone diagenesis is dominated by mechanical compaction and dolomite cementation. A direct correlation exits between: (1) muddy rip-up clast abundance and early reduction of primary porosity by compaction with irreversible loss of intergranular volume (IGV); (2) occurrence of dolomitic rip-up clasts and dolomite cement nucleation in host sandstone, occluding adjacent pores but preserving IGV. Both processes affect reservoir quality by generation of vertical and 3D fluid flow baffles and barriers that compartmentalize the reservoir. These findings may provide quantitative useful data for the better understanding of reservoir quality in analogous hydrocarbon-bearing basins such as the Bay of Fundy, Nova Scotia (Canada).

INTRODUCTION

Calcretes and dolocretes have been widely recognized in ancient fluvial sediments deposited under relative arid climates and saline/evaporate conditions (Goudie, 1983; Wright and Tucker, 1991; Milnes, 1992; Kraus, 1999). They may form as vadose (pedogenic) or phreatic (groundwater) mineral precipitates (Arakel, 1986; Wright, 1994; Colson and Cojan, 1996; Chen et al., 2002). Genesis of dolocretes has been attributed to similar formation mechanisms of calcretes. Several processes to generate near-surface and soil-related dolomite accumulations by increasing Mg/Ca ratio of phreatic solutions have been suggested: (1) mixing of saline brines and fresh groundwater (El-Sayed et al., 1991; Coloson and Cojan, 1996); (2) calcite precipitation from nearby groundwater resulting in Ca^{2+}-depleted but Mg^{2+}-enriched groundwater (Hutton and Dixon, 1981; Spötl and Wright, 1992; Armenteros et al., 1995); (3) fluid movements through Mg-rich clays (Pimentel et al., 1996). Examples of phreatic dolocretes in Permo-Triassic fluvial sediments have been reported in the Paris Basin (Spötl and Wright, 1992), Sherwood Sandstones in the Corrib Field (W Ireland; Schimd et al., 2004, 2006), Wessex basin (S England; Mader, 1986; McKie et al., 1998), Abo-Tubb interval (NE New Mexico, USA; Kessler et al., 2001), Orenburg region (South Urals, Russia; Kearsey et al., 2012) and Argana basin (Brown, 1980), among others.

Deposits generated above mean channel depth in fluvial systems (floodplain sediments and paleosols – calcrete and dolocretes) are prone to be incised and eroded during channel migration and base-level fall (Miall, 2006). Then, these penecontemporaneus reworked grains become part of fluvial sandstone framework as intrabasinal components, being called as "intraclast" or "rip-up clasts". They usually concentrate in particular depositional facies such as channel-lags deposits (Allen and Wright, 1989; Garzanti, 1991). Its grain size distribution, mostly greater than other framework components according to their lower density (Zuffa, 1980, 1985), may result in a significant volume of sandstone framework represented by such clasts. Thus, rip-up clast occurrence has an important significance on paleoclimatic and paleogeographic reconstructions, by testifying the existence of coeval primary dolocretes, preserving provenance signature of intrabasinal sediments (Garzanti et al., 1989; Garzanti, 1991; Odin, 1985; Zuffa, 1980, 1985; Purvis and Wright, 1991; Spötl and Wright, 1992). In addition, there are evidences of the impact exerted by these grains on diagenetic evolution of host sandstones and, eventually, on reservoir quality through: (i) favouring mechanical compaction with a consequent drastic loss of intergranular space (Rittenhouse, 1971; Pittman and Larese, 1991; Gluyas and Cade, 1997; Paxton et al., 2002; Mousavi and Bryant, 2013); and (ii) sourcing eodiagenetic carbonate cements that reduce original porosity (Burley, 1984; Schimd et al., 2004, 2006; Morad et al., 2010; De Ros and Scherer, 2012).

On the basis of the double applied interest of rip-up clasts, occurrence and abundance of different types of such grains in Triassic fluvial deposits of Argana basin (S Morocco; Fig. 1A) provides a great scenario to evaluate these questions. Thus, by coupling high-resolution petrographic and chemical analysis, this paper aims at: 1) characterizing origin and source of such clasts; 2) evaluating their impact on host sandstones postdepositional evolution by examining their behaviour during diagenesis. The proved

correlation between the Argana Basin and the hydrocarbon-bearing Bay of Fundy Basin in Nova Scotia (Canada; Smoot and Castens-Seidell, 1994; Olsen, 1997; Calder et al., 1998; Hoffman et al., 2000; Letorurneau and Olsen, 2003) reveals the relationship between spatial distribution of the different rip-up clast types and depositional facies as particularly interesting for a better understanding of fluid flow heterogeneity and reservoir compartmentalization.

GEOLOGICAL SETTING

The Triassic Argana Basin is located in the Western High Atlas of Morocco and is up to 20 km in width and extends over 85 km (Fig. 1A). It forms the eastward extension of the hydrocarbon-bearing Essaouira Basin (Medina, 1988; Broughton and Trépanier, 1993; Ellouz et al., 2003) which corresponds to the conjugate Atlantic passive continental margin of the Bay of Fundy Basin in Nova Scotia, Canada (Calder et al., 1998; Olsen et al., 2000; Letorurneau and Olsen, 2003). Both basins show remarkably similarities in sedimentary facies and stratigraphy throughout their thick Late Permian-Early Jurassic successions suggesting a predrift proximity (Fig. 1B; Smoot and Castens-Seidell, 1994; Kent et al., 1995; Olsen, 1997; Hoffman et al., 2000). In Argana Basin, estimated maximum burial depth is about 1600-2000 m with a maximum temperature at the base of the stratigraphic sequence (*ca.* 6000 m thick) ranging between 150-250ºC (Leikine et al., 1996). Hydrothermal processes are not completely discarded by some authors (Lahcen et al., 2007). Argana Basin consists on a half-graben basin with 5-30º tilted blocks towards the NW that has experimented two main phases of extension, influencing sediment distribution patterns (Brown, 1980; Medina 1991, 1995). First (pre-rifting) phase of extension only affected deposition of Late Permian sediments (Medina, 1991, 1995) whereas the second phase is considered coeval to Triassic deposition (syn-rift) by some authors (Brown, 1980; Laville and Petit, 1984; Medina 1991, 1995) or later to that time (post-rift) by others (Hofmann et al., 2000; Baudon et al., 2012).
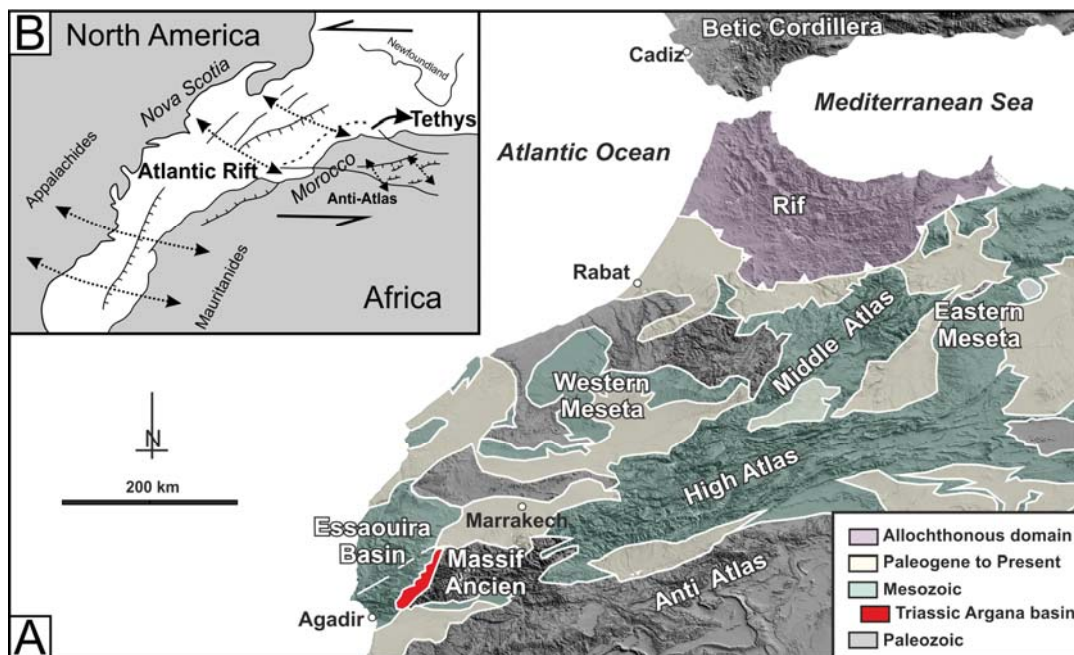
Fig. 1. A) Geological map of Western High Atlas showing present location of the study area. B) Paleogeographic map of Morocco at Triassic time (modified after Laville and Pique, 1991).

At the end of the Triassic, Argana and Fundy Basins were situated in the subtropical belt at about 20º N palaeolatitude, where deposition took place under semi-arid to arid climates (Hay et al., 1982). In the Argana Basin, a long-term change in palaeoclimate that ranges from semi-arid conditions with seasonal precipitation (Early to Middle Triassic) towards an arid, non-seasonal climate (Late Triassic) is preserved within the sedimentary cycles developed during several million years (Hofmann et al., 2000). A short-lived event of increased precipitation within the general trend of aridification is identified during the Carnian Pluvial Episode (Arche and López-Gómez, 2014 and references therein).

Stratigraphy

Continental red beds of the Argana Basin are represented by a *ca.* 5000 m-thick succession of Permo-Triassic sedimentary rocks (Tixeront, 1973, Brown, 1980) capped by the Argana basalt (205 ± 16 Ma; Fiechtner et al., 1992; Fig. 2). This stratigraphic succession is subdivided into eight lithostratigraphic units or members (namely T1 to T8; Tixeront, 1973) grouped into three formations (Brown, 1980). The lowermost Ikakern Fm (Late Permian, Brown, 1980; Jalil and Dutuit, 1996) rests unconformably on Palaeozoic basement and includes Ait Driss (T1) and Tourbihine (T2) members. It typically consists of alluvial fan conglomerates, grading vertically and laterally into cycles of conglomerate-sandstone-siltstone-mudstone from meandering rivers intercalated with floodplain deposits (Brown, 1980). The intermediate Timesgadiouine Fm (Early-Middle Triassic, Klein et al., 2011) overlies unconformably the Ikakern Fm and consists at its base on the Tanameurt Mb (T3), a volcanoclastic sheet-like conglomerate body of braided river origin (Brown, 1980). Aglegal Mb (T4) is dominated by clayey mudstones, siltstones and, in minor extent, fine-grained sandstones deposited in a flood plain/playa environment with development of vertisols and intercalations of meandering fluvial deposits (Brown, 1980; Hofmann et al., 2000). Irohalene Mb (T5) is characterized by sandstones cyclically intercalated with massive mudstones, generated on an alluvial plain setting with meandering ephemeral streams (Hofmann et al., 2000). The upper Bigoudine Fm (Late Triassic, Fiechtner et al., 1992) encompasses the Tadrart Ouadou Mb (T6) at the base, the Sidi Mansour (T7) and the Hasseine Mbs (T8) (Tixeront, 1973; Brown, 1980). The Tadrart Ouadou sandstone is interpreted as the result of the aforementioned Carnian Pluvial Event (Arche and López-Gómez, 2014) and is continuous throughout the Argana Basin. This unit consists in proximal braided river conglomerates grading upward into sand-dominated, distal braided river deposits with intercalated aeolian sandstones (Hofmann et al., 2000; Mader and Redfern, 2011). Both T7 and T8 are composed of similar, cyclically-arranged mud-rich facies difficult to be separated into two distinctive members. T7/T8 strata formed in shallow ephemeral lakes and extensive saline mudflats with periodic fluvial and aeolian inputs of sand (Hofmann et al., 2000).

Depositional Facies

For the purpose of this study, two fluvial systems are analysed: the braided system corresponding to the Tadrart Ouadou Mb (T6 unit) and a straight channel from the Sidi Mansour-Hassein interval (T7/T8 unit).

Age	Fm	Member	Log	Lithofacies	Depostional Env.
		Argana basalt		Tholeitic basalt	
Late Triassic	Bigoudine	Hasseine (T8) (300-1200m)		Mudstones with interbedded siltstones and fine-grained sandstones	Shallow ephemeral lakes Extensive saline mudflats Ephemeral streams
		Sidi Mansour (T7) (0-200m)			
		Tadrart Ouadou (T6) (0-150m)		Siltstones and mudstones	
				Basal conglomerate grading into sandstones	Braided rivers and aeolian dunes
Early-Middle Triassic	Timezgadiouine	Irohalen (T5) (200-500m)		Massive mudstones intercalated with sandstones	Alluvial plain with meandering ephemeral streams
		Aglegal (T4) (800-1500m)		Clayey mudstones, siltstones and fine-grained sandstones	Flood plain with intercalated meandering rivers
		Tanamert (T3) (0-10m)		Volcanoclastic conglomerate	Braided rivers
Late Permian	Ikakern	Tourbihine (T2) (0-1000m)		Cycles of conglomerates-sandstones-siltstones-mudstones	Meandering rivers intercalated with flood plain deposits
		Ait Driss (T1) (0-1500m)		Coarse irregulary bedded conglomerate	Alluvial fans Braided rivers

(Note: the "analyzed interval" label spans the Hasseine/Sidi Mansour/Tadrart Ouadou rows.)

Fig. 2. Simplified lithostratigraphic log for the Permian and Triassic record in Argana basin, showing the analysed stratigraphic interval (modified after Tixeront, 1973; Brown, 1980; Hofmann et al., 2000). Thicknesses are maxima.

The braided system from Tadrart Ouadou Mb was characterized in two different outcrops, 6 km apart approximately (Fig. 3A and B), to target its main depositional environments: main channel, lobate unit bars, compound bars and secondary channels. In one of the outcrops, cross-bedded sandstones with up to 2 m thick cross-bed sets are recognized with abundant rip-up clasts accumulated at the toes of cross-bedded sandstones (Fig. 3A). They correspond to foresets of megarriples and dunes developed at the tail of lobate unit bars that cover channel erosive bases (Lunt et al., 2004). Lateral and downstream accretion of lobate unit bars results in a larger-scale compound bar (Bridge et al., 1998; Lunt et al., 2004). This facies association is representative of a deep perennial braided system comprising multistorey fills with both lateral and vertical aggradation (Viseras and Fernández, 2010; Mader and Redfern, 2011). A main channel segment may become partially disconnected due to bank attachment processes, when bars migrate obliquely respect to the main current direction, being reduced to a secondary channel (Lunt

et al., 2004). Secondary channel fills are characterized by a fining upward succession comprising epsilon cross-bedded sandstone with abundant rip-up clasts at the base, to cross- and ripple-laminated sandstone with flaser and wavy structures at the top (Fig. 3A). In the other outcrop, lowermost part shows metre-thick sets of planar cross-bedded and horizontal laminated sandstones with several tens of metres in lateral extension (Fig. 3B). Top is marked by an erosional-base channelized deposit with abundant rip-up clasts (Fig. 3B). Internal architecture and the occurrence of internal erosion surfaces and rip-up clasts point out to a compound braided bar-type deposit (Viseras and Fernández, 2010) truncated by a cross-bar channel (Bridge et al., 1998).

Fluvial deposit from the T7/T8 interval is characterized by a 2 m-thick sandstone, with alternations of mudstone layers, that shows vertical aggradation (Fig. 3C). From the base to the top, a planar cross-bedding structure evolves to trough cross-bedding. Sedimentary architecture, dimension and internal structures suggest a straight channel as the fluvial depositional system (Viseras and Fernández, 2010, Viseras et al., 2011).

METHODOLOGY

A total of twelve sandstone samples from unweathered outcrop portions were analyzed which correspond to four fluvial depositional environments: (1) main braided channel (and adjacent lobate unit bars (Fig. 3A); (2) associated secondary channel (Fig. 3A), all in the first outcrop of T6 unit; (3) compound braided bar and its cross-bar channel (Fig. 3B) in the second outcrop of T6 unit; and (4) straight channel (Fig. 3C) of T7/T8 interval.

High-resolution petrographic analysis was performed including a special characterization and classification of the rip-up clasts according to their petrographic features and diagenetic behaviour. Analysis was carried out on polished thin sections and freshly broken surfaces by using optical and field emission scanning electron microscopes (FESEM Gemini of Carl Zeiss SMT) equipped with an energy dispersive X-ray spectrometer. Cold-cathodoluminescence (CL) allowed to examine textural features and relationship between rip-up clasts and carbonate cements. Samples were etched and stained with hydrofluoric acid and Na-cobaltinitrite for plagioclase and K-feldspar identification, and with alizarin red-S and potassium ferricyanide for carbonate type discrimination. Gazzi-Dickinson (600 points per thin section) (Ingersoll et al., 1984; Zuffa, 1985, 1987) and grain size (100 grains per thin section) point-countings provided qualitative and quantitative data on framework composition and interstitial component to characterize depositional and diagenetic fabrics (Table I). Intergranular volume (IGV), porosity loss by compaction and cementation (COPL and CEPL, respectively) as well as compactional index (Icompact) were calculated following established conventions (Table I; Lundegard, 1992). Chemical composition of carbonates within rip-up clast and cements was determined on selected representative samples that contain higher amount of both types. Ca, Mg, Mn, Fe, Sr, and Ba contents were obtained by using a Cameca SX100 electron microprobe operating at 15 Kv and 20 nA with an electron beam of 5 μm diameter.

RESULTS

Host sandstone detrital fabric

Grain size ranges from very-fine to medium-grained sand with moderately to well-sorted, subrounded to subangular grains. Mean grain size varies within each depositional

Fig. 3. Outcrop photointerpretations with analysed depositional facies and sample location together with photomicrographs of the main textural features (plane-polarized light, PPL). A) Main braided channel (base and top; CB1 and CB2, respectively) along with adjacent lobate unit bars (bar-head and bar-tail; Bh and Bt, respectively) and associated secondary channel (base, mid and top; CS1, CS2 and CS3, respectively). B) Compound braided bar (lower-implantation- and middle-accretion- parts; SF1 and SF2, respectively) and its cross-bar channel (SF3). C) Straight channel (base and top; PCr1 and PCr2, respectively).
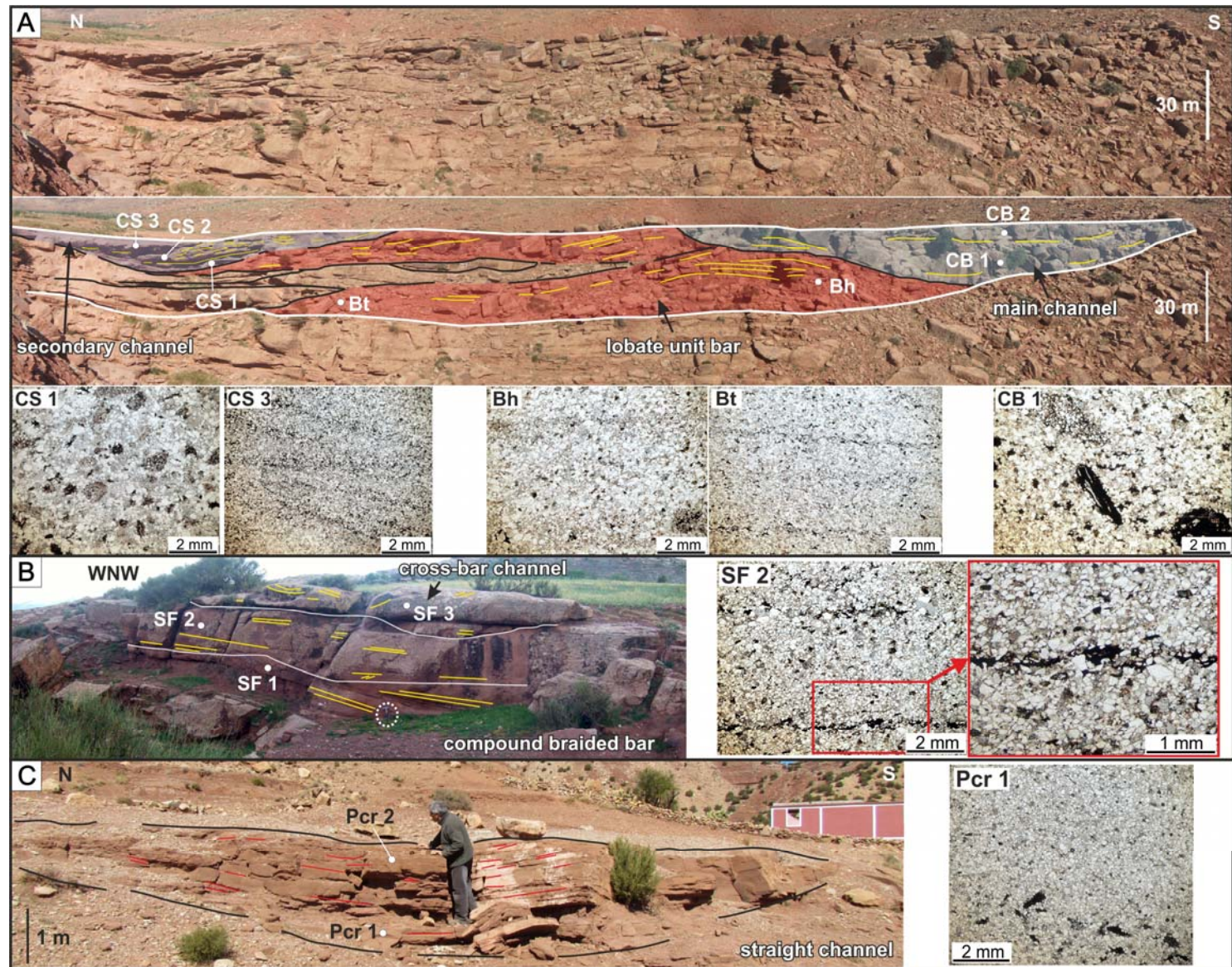
environment according to depositional facies. In the main channel and adjacent lobate unit bar, mean grain size decreases, vertically, from channel-lag deposit (0.27 mm) to channel top (0.19 mm) and, laterally, from bar-head (0.26 mm) to bar-tail (0.18 mm) (Fig. 3A). In associated secondary channel, there is a fining upward succession from basal channel-lag (0.29 mm) to epsilon cross-beds (0.25 mm) and ripple cross lamination at the top (0.1 mm) (Fig. 3A). In the compound braided bar, mean grain size increases from the base of the bar (0.2 mm) upwards (0.22 mm), being coarsest at the cross-bar channel (0.3 mm). In the straight channel, mean grain size slightly decreases upwards (from 0.18 to 0.17 mm). Depositional texture, far to be uniform at thin section scale, usually displays sedimentary structures such as parallel and ripple cross lamination highlighted by laminae with higher rip-up clast content (Fig. 3A to C) or alternation of laminae with different grain sizes (Fig. 3A Bh sample).

Compositional signature classifies sandstones mainly as extraclastic arenites (Fig. 4A; according to Zuffa (1980) with subarkosic composition in samples from braided fluvial system (average $Q_{83.8}F_{13.2}R_3$) and sublitharenitic composition in samples from straight channel (average $Q_{83.1}F_{6.7}R_{10.2}$) (Table I; Fig. 4B). Non-undulatory monocrystalline quartz is the dominant grain type followed by polycrystalline quartz without tectonic fabric and, in minor extent, inherited quartz (i.e. quartz with rounded overgrowths). Feldspars consist of K-feldspars and plagioclases in similar proportions that barely vary among different facies (total average of $Qm_{84.8}K_{8.2}P_7$ in T6 braided system and $Qm_{91.8}K_{3.9}P_{4.3}$ in T7/T8 straight channel; Fig. 4C). Rock fragments are represented in order of abundance by low-, medium-grade metamorphic (phyllites and schists) and sedimentary (sandstones and siltstones) grains. Other extrabasinal components in accessory content are micas, mainly muscovite, and silt-sized, well-rounded heavy minerals (zircon, tourmaline, rutile, epidote and opaques; 0-1.6%). Intrabasinal components may amount to an important portion of framework. They are substantially represented by different rip-up clast types (up to 29.2%; see next section for further characterization) and, subordinate, by well-rounded glauconite with similar size of other accessory host framework grains (0.2%).

Rip-up clast characterization

Rip-up clasts occur in all analysed sandstones (Fig. 4D) and their size decreases as grain size does according to depositional facies. On the basis of their petrographic features (rip-up clast composition: inclusion or not of dolomite crystals and, if so, its abundance and size) and their mechanical behaviour (ductile, semi-ductile and rigid), the following three main classes of rip-up clasts are differentiated:

1) Muddy rip-up clasts. They are dark red in colour due to Fe-oxide presence and are composed by clay minerals, mainly illite from EDX analyses (Fig. 5A). They occur in all depositional facies with a general trend of increasing abundance in coarser facies from main braided and straight channels. Opposite trend is observed in associated braided secondary channel and compound bar environments (Fig. 4D). They usually concentrate in preferential laminae according to sedimentary structure (Fig. 3B). Size ranges from 0.1 to 5 mm. This rip-up clast type displays a highly ductile behaviour during mechanical compaction which deforms and squeezes them between other rigid framework grains (Fig. 5A).

85
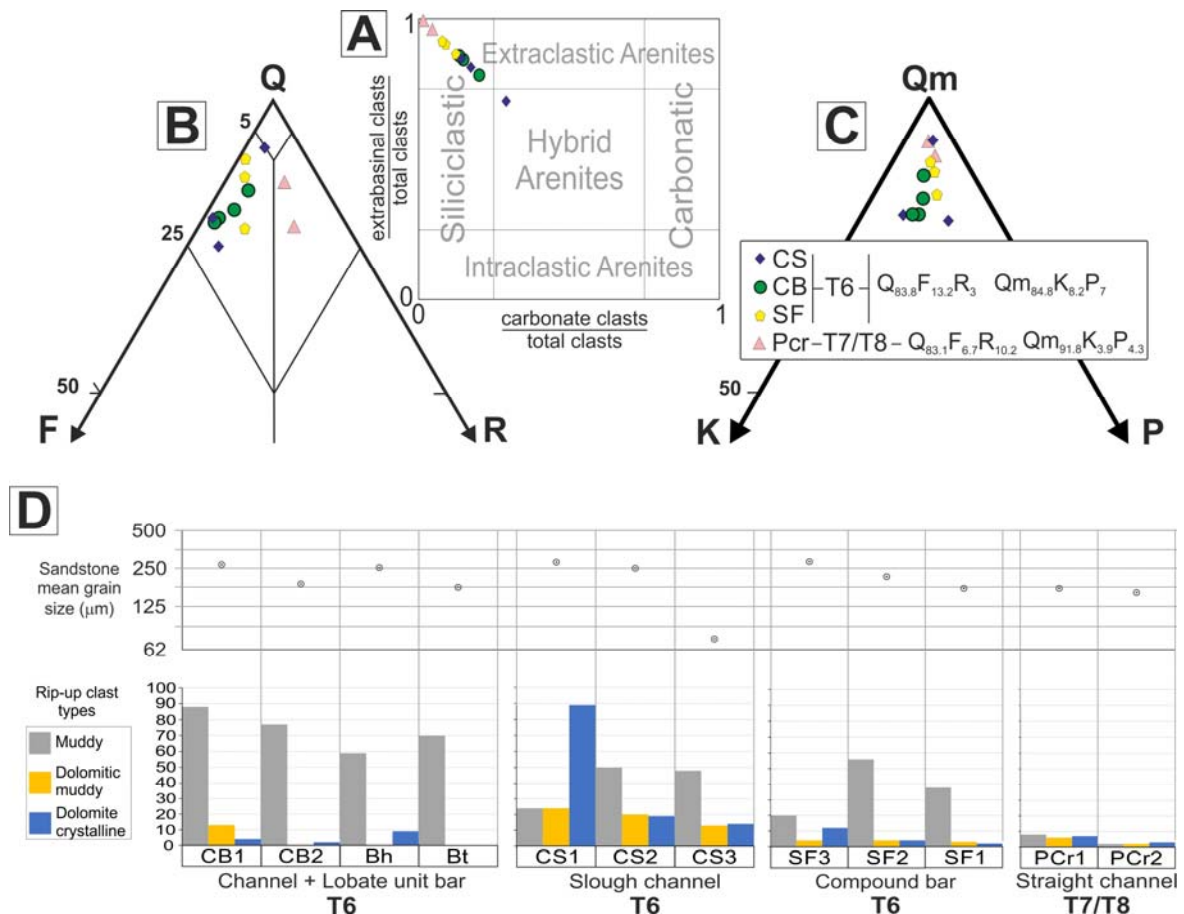
Fig. 4. Main compositional features of framework sandstones. A) Genetic (extrabasinal clasts/total clasts) versus mineralogical (carbonate clasts/total clasts) signatures (according to Di Giuglio and Valloni, 1992). B) QFR ternary diagram: Q: total quartz; F: total feldspars; R: total rock fragments (after Pettijohn et al., 1973). C) QmKP ternary diagram: Qm: total monocrystalline quartz; K: total monocrystalline K-feldspar; P: total monocrystalline plagioclase (after Dickinson, 1985). D) Abundance of different rip-up clast types according to depositional facies and grain size.

2) Dolomitic muddy rip-up clasts. They are composed by dolomite crystals embedded in a clayey matrix with similar characteristics to that of muddy rip-up clasts (Fig. 5B and C). Inclusion of silt-sized siliciclastic grains is rare. Dolomite occurs as euhedral rhombic crystals, some of them with a clean outer rim (Fig. 5B) that appears as a slight zonation at SEM (Fig. 6A and B). Most of dolomite crystals contain red-colored inclusions, some with a radial pattern from the central crystal area until the clean rim (Fig. 5B). Dolomite abundance within the clast varies between 10% and 50% of total clast volume. Crystal size is highly variable among crystals of different clasts, ranging from 0.05 to 0.1 mm, and does not show an apparent relationship with clast size (0.3-0.9 mm). Abundance of this rip-up clast type decreases according to grain size in each depositional environment, being absent in some facies of channel and adjacent lobate unit bar (Fig. 4D). Their spatial distribution does not follow sedimentary structure. These rip-up clasts display a semi-ductile behaviour during diagenesis, being partially deformed by mechanical compaction (Fig. 5B and C).

3) Dolomite crystalline rip-up clasts. They are usually composed by dolomite crystals with minor amounts of intercrystalline clayey matrix (Fig. 5D and E), similar to that of muddy rip-up clasts. In other cases, they are exclusively composed of crystalline dolomite constituting an idiotopic mosaic (Fig. 5F and G). Inclusion of siliciclastic grains is

Table I. Petrographic data base of framework and interstitial components in analysed sandstones, including main compositional and diagenetic indexes. Abbreviations: [1]RuC: rip-up clast; [2]IGV: Intergranular volume, COPL: compactional porosity loss, I_{comp}: compactional index (Lundegard, 1992); [3]Q: total quartz, F: total feldspar, R: total rock fragments (Pettijhon et al., 1973); [4]Qm: monocrystalline quartz, K: K-feldspar, P: Plagioclase (Dickinson, 1985).

Unit	T6										T7/T8	
Depositionalenv.	Channel + Lobate unit bar				Slough channel			Compound bar			Straight channel	
Sample	CB1	CB2	Bh	Bt	CS1	CS2	CS3	SF3	SF2	SF1	PCr1	PCr2
Framework												
Qm	286	320	330	309	257	296	319	305	321	353	352	371
Qp	45	42	39	52	38	43	18	52	29	54	40	40
K	42	41	27	29	8	49	27	18	24	20	13	16
K replaced by clays	1	4		6		1	3	1	3		1	1
P	21	24	14	20	9	20	43	22	27	18	8	18
Preplaced by clays	3	8	5	6	1		8	1	7	2	4	4
Phyllite	5	5	10	11	2	6	16	7	9	5	27	44
Schist	2	1	2	4	1		3	2	2	1	7	16
Siltsonte	1		5	1	1				16			
Sandstone					6			2	1	1	3	3
Muscovite	2	5	2	12	2	3	5	1	2	2	1	2
Chlorite											1	2
Opaque	4	4	6	4	2	5	2	1	3		1	6
Turmaline		2				1	2				1	
Zircon	2		1				2				1	
Rutile	1					1						
Epidote	1	2			1	1	1	2			1	2
Glauconite											1	1
Muddy RuC [1]	88	77	59	70	24	50	48	20	56	38	8	2
Dolomitic muddy RuC	13				24	20	13	4	4	3	6	2
Dolomite crystalline RuC	4	2	9		89	19	14	12	4	2	7	3
Intergranular space												
Feldspar overgrowth	2	1	1	2	2	3		1	1	2	1	3
Quartz overgrowth	40	28	37	33	29	20	6	30	47	47	20	13
Dolomite	30	24	47	15	99	55	70	61	21	30	70	30
Calcite								63	9	8	4	1
Primary porosity	3	5	6	20	5	7		5	14	17	29	18
TOTAL	596	600	600	600	600	600	600	610	600	603	607	600
IGV[2]	12,7	9,7	14,6	12,5	18,8	14,2	9,5	18,8	15,0	17,2	21,3	11,6
COPL[2]	31,3	33,6	29,7	31,4	26,1	30,1	33,7	25,9	29,4	27,5	23,7	32,1
I_{comp}[2]	0,8	0,9	0,8	0,8	0,7	0,8	0,8	0,7	0,8	0,7	0,7	0,8
Q[3]	81,7	81,5	85,3	82,4	91,5	81,7	77,1	87,1	79,7	89,6	86,2	80,1
F[3]	16,4	17,1	10,7	13,9	5,5	16,9	18,5	10,2	13,9	8,8	5,7	7,6
R[3]	2,0	1,3	4,0	3,7	3,0	1,4	4,3	2,7	6,4	1,5	8,1	12,3
Qm[4]	80,8	80,6	87,5	83,5	93,4	80,9	79,8	87,9	84,0	89,8	93,1	90,5
K[4]	12,3	11,3	7,4	9,5	2,9	13,7	7,5	5,5	7,1	5,1	3,7	4,1
P[4]	6,9	8,1	5,2	7,0	3,6	5,5	12,8	6,6	8,9	5,1	3,2	5,4
Mean grain size (mm)	0.27	0.19	0.26	0.18	0.29	0.25	0.1	0.3	0.22	0.2	0.18	0.17

common and, sometimes, abundant. Dolomite crystal habit is analogous to that of the dolomitic muddy rip-up clasts, including clear outer rims and inclusions (Fig. 5D, E and H; Fig. 6B). Subhedral and anhedral habits with nonplanar, highly irregular intercrystalline boundaries are also present (Fig. 5E). Dolomite abundance within the clast varies between 50% and 100% of total clast volume. Dolomite crystal size is highly variable between crystals from the same clast and crystals from different clasts, ranging from dolomicrite textures (Fig. 5G) up to 0.2 mm, without an apparent relationship with clast size (0.3-3 mm). These rip-up clasts are mainly equidimensional and may show organic structures filled by inherited dolomite cement (Fig. 5H). Abundance of dolomitic crystalline rip-up clasts decreases as grain size does in each depositional environment, being especially abundant as channel-lag deposits (Fig. 4D). This rip-up clast type behaves as rigid grains,

non-deformed by mechanical compaction, preserving its original grain shape (Fig. 5D to 5G).

Under CL, dolomite crystals within rip-up clasts are systematically bright orange luminescent (Fig. 6D to H). Euhedral rhombic dolomites with clear outer rims show a slight zonation from darker orange cores to brighter yellowish orange rims (Fig. 6D, E and F). Inherited dolomite cement within dolomitic crystalline rip-up clasts may present the same zonation (Fig. 6F). Bright orangish yellow luminescent inclusions are observed within dolomite crystals (Fig. 6C and D) whereas those of radial-pattern and red-colored at optical microscope luminesce darker orange (Fig. 6C to F).

Microprobe analysis indicates that dolomite crystals within rip-up clasts are approximately stoichiometric (total average CaO = 50.09 % wt.; MgO = 48.55 % wt.) with relative high Mn and Fe contents (total average Mn = 5532 ppm; Fe = 2146 ppm) (Fig. 7A and B) and low Sr (total average 358 ppm) and Ba (total average 132 ppm). Zonation in dolomite crystals, when occurs, is due to variations in Fe and Mn contents (core: Mn = 5677 ppm, Fe = 2340 ppm; rim: Mn = 5387 ppm, Fe = 1953 ppm; Fig. 7B). At SEM and under CL, clearer and brighter orange luminescent outer rims, respectively, are associated to both higher Mn and Fe contents (Fig. 6A to F). However, core-rim variation trend between these elements is highly irregular among dolomite crystals from the same rip-up clast as well as from different clasts. Combinations are variable from core to rim (Fig. 7C): Fe decreases whereas Mn increases (Fig. 6B), and vice versa, or both elements increase (Fig. 6A; Fig. 7C). Inherited dolomite cement within rip-up clasts is very similar in composition to dolomite crystals in terms of average CaO and MgO contents (50.24% and 48.12% wt.; Fig. 7A and B), with slightly higher Mn (6802 ppm), Sr (590 ppm) and Ba (510 ppm) contents but lower Fe (2308 ppm) (Fig. 7B and C).

Host sandstone diagenesis

Mechanical compaction dominates over chemical compaction and is the main porosity-reducing diagenetic process as indicated by an $I_{comp} < 0.5$ in all analysed sandstones (Lundergard, 1992). It is manifested as mechanical deformation of ductile grains such as muddy and, in minor extent, dolomitic muddy rip-up clasts (Fig. 5A to C), medium-grade metamorphic lithic fragments and micas. Mechanical compaction is partially inhibited by early diagenetic cements which preserve intergranular volume (IGV). IGV is strongly facies-related with higher IGV values systematically associated to coarser grain sizes within each depositional environment (Fig. 8A). Highest IGV (IGV=21.3%) is associated to straight channel base (PCr1 sample) whereas lowest IGV (IGV= 9.5%) is at secondary braided channel top (CS3 sample). Conversely, higher COPL values correspond mainly to finer-grained facies within each depositional environment (Fig. 8A).

The main porosity-modifying cements in sandstones include quartz (1-7.8%) and feldspar (0-0.5%) overgrowths and dolomite pore-filling cement (4-24.6%) (Fig. 9A to D). Calcite cement only occurs in compound braided bar depositional environment (SF samples; 1.3-9.8%). Feldspar overgrowths form thin and continuous euhedral prisms around detrital feldspar grains (Fig. 9A). It is the earliest cement being systematically overgrown by the rest of authigenic minerals (Fig. 8B). Dolomite replacement of this cement is common (Fig. 9A). Dolomite precipitates as: (i) coarse, euhedral, poikilotopic,

Euhedral, rhombic crystals with clean outer rims
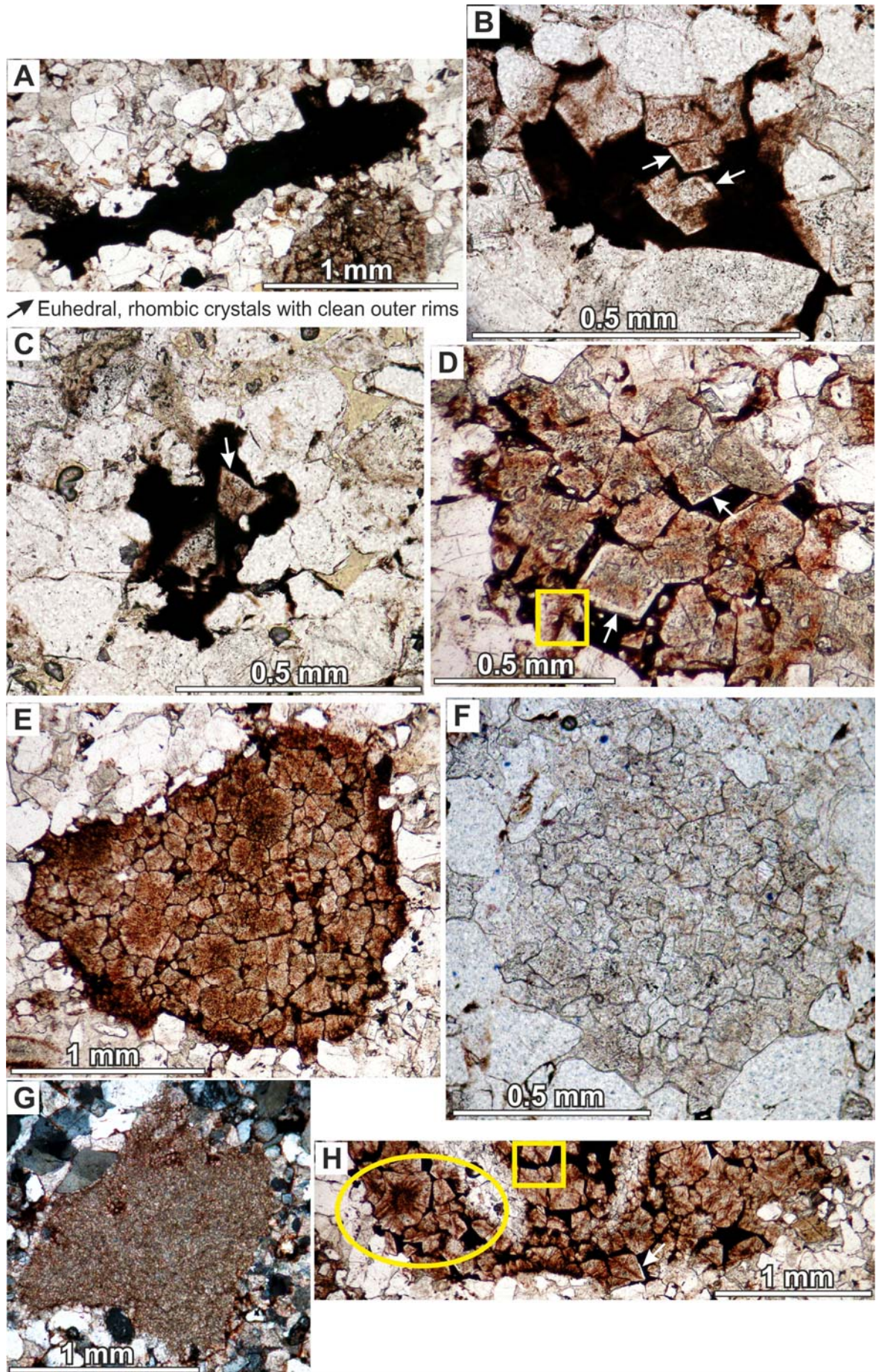
rhombic crystals (up to 3 mm; Fig. 9B) that preserve high IGV and, in some cases, inhibit quartz overgrowth formation; (ii) syntaxial dolomite that develops occluding sandstone intergranular space as overgrowths from rip-up clast dolomite crystals (Fig. 9C); (iii) fine, euhedral (up to 0.05 mm), rhombic crystals in direct contact with detrital grains that preserve primary porosity (Fig. 9D). Last dolomite textural type only occurs in T7/T8 straight channel samples (PCr samples) where represents the earliest cement that preserves highest IGV and primary porosity values (Fig. 8B). Under CL, poikilotopic and syntaxial dolomite cements show the same orange luminescent color than dolomite crystals within rip-up clasts, although slightly darker (Fig. 6D, E and F). Locally, euhedral dolomite cement may be zoned from darker cores to brighter orange luminescent rims (Fig. 6G and H). Quartz occurs as well-developed, euhedral prisms around detrital quartz grains with occasional bipyramidal habit (Fig. 9E) and, in minor amount, as microcrystalline rims (<10 μm) (Fig. 9F). Quartz, when it is not inhibited by dolomite cement, overlies dolomite crystals (Fig. 9G) and is postdated by calcite cement (Fig. 8B and 9H). Calcite forms poikilotopic pore-filling cement that systematically overlies the rest of cements (Figs. 9B and H; 8B). Under CL, calcite is dull luminescent (Fig. 6G and H). Other minor diagenetic processes encompass replacement of framework grains by carbonates (both dolomite and calcite), replacement of feldspars by phyllosilicates (mainly illite) and dedolomitization (only observed in samples from T7/T8 straight channel; Fig. 8B).

Chemical analysis of authigenic dolomite from both stratigraphic units (T6 and T7/T8) shows an important similarity in composition with dolomite crystals in terms of CaO and MgO contents (total average 50.17 % wt. and 48.49 % wt.; Fig. 7A and B). Differences with rip-up clast dolomite crystals as well as between dolomite cements from both units are mainly associated to Fe and Mn contents. Authigenic dolomite shows slightly higher Mn (6413 ppm, total average) but significantly lower Fe (1330 ppm, total average) contents than dolomite crystals within rip-up clasts (Fig. 7B and D) whereas, from braided system (T6 unit) to straight channel (T7/T8 unit), there is a general increase in both elements (T6: Mn = 5546 ppm and Fe = 592 ppm; T7T/8: Mn = 7280 ppm and Fe = 2068 ppm; Fig. 7B and D). Calcite cement is not purely stoichiometric due to MgO content (CaO = 96.67 % wt.; MgO = 3.15 % wt.). Fe, Mn and Ba are relatively low (503 ppm, 140 ppm and 48 ppm, respectively) whereas Sr content is the highest among all carbonates (600 ppm) (Fig. 7B and D).

Fig. 5. Photomicrographs showing the different rip-up clast types. A) Muddy rip-up clast strongly deformed by mechanical compaction (CB1 sample). B and C) Dolomitic muddy rip-up clasts partially deformed by mechanical compaction (CS2 and CS1 samples, respectively). Notice clean outer rims in dolomite crystals. D) Dolomite crystalline rip-up clast composed by euhedral, rhombic dolomite crystals with clean outer rims and radial-pattern inclusions, embedded in a clayey matrix (CS1 sample). Yellow box area corresponds to SEM image of Fig. 6A. E) Dolomite crystalline rip-up clast composed by dolomite crystals with nonplanar intercrystalline boundaries and radial-pattern inclusions, embedded in a clayey matrix (SF3 sample). F and G) Dolomite crystalline rip-up clasts exclusively composed by dolomite crystals constituting meso- and microcrystalline idiotopic mosaics, respectively (SF3 and Bh samples, respectively). H) Dolomite crystalline rip-up clast composed by dolomite crystals with clean outer rims and radial-pattern inclusions, embedded in a clayey matrix (CS1 sample). Organic structures within the clasts (light areas) are filled by inherited dolomite cement. Yellow box area corresponds to SEM image of Fig. 6B. Circle area corresponds to CL photomicrograph of Fig. 6F. (All photomicrographs in plane-polarized light, PPL, except G in cross-polarized light, XPL).
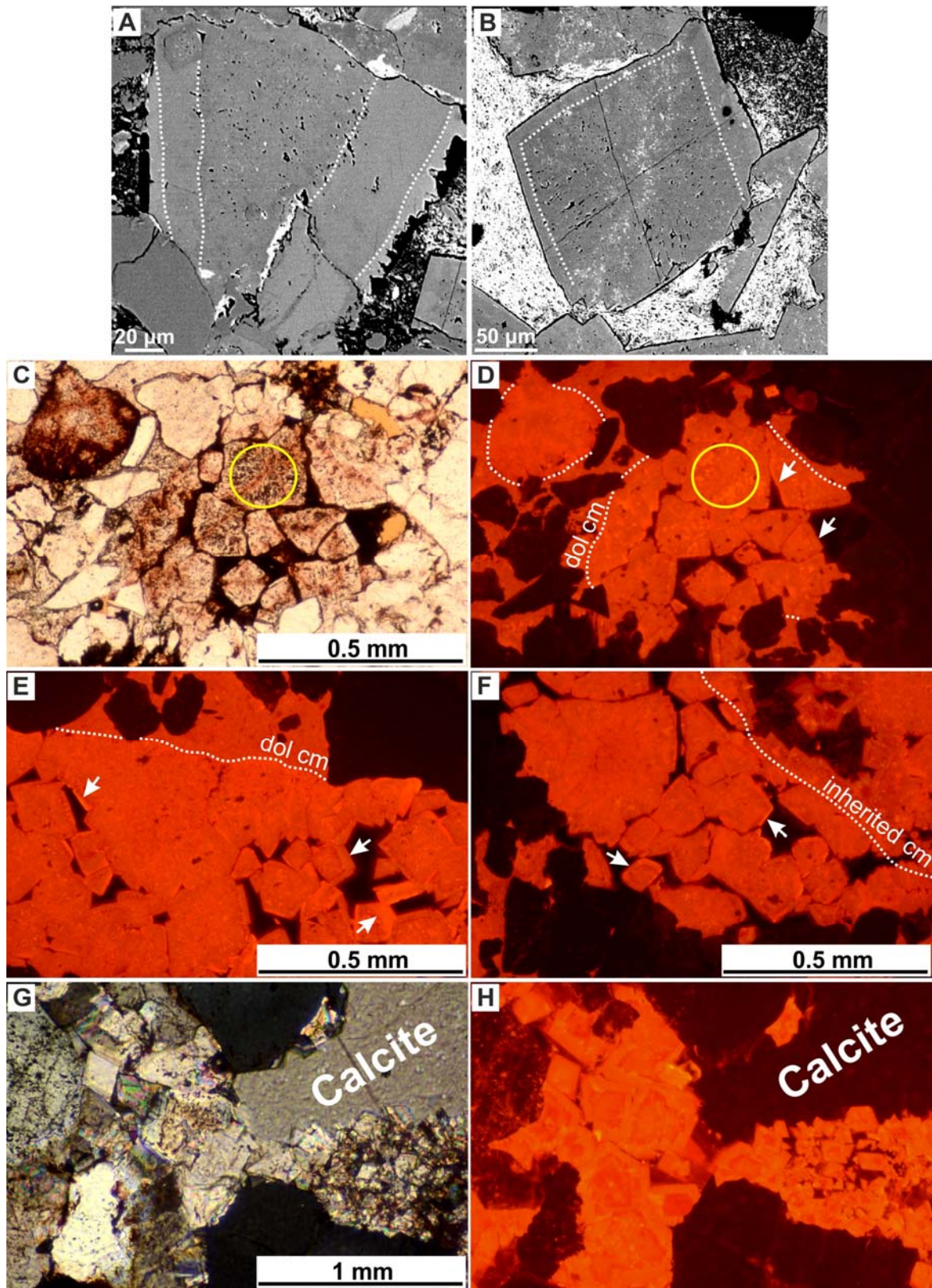
DISCUSSION

Origin of rip-up clasts

Rip-up clasts in fluvial sandstones from Argana Basin (T6 and T7/T8 stratigraphic units) have been considered as intrabasinal components according to following textural and compositional criteria (Zuffa, 1985; Garzanti, 1991): (1) grain size mostly greater than other framework grains; (2) inclusion, in a clayey matrix, of idiomorphic dolomite crystals with a wide range of crystal size and abundance; (3) inclusion, in crystalline dolomite mosaic, of finer-grained siliciclastic grains (mainly quartz) than surrounding siliciclastic framework components. In addition, frequent irregular contours in muddy-dominated grains as result of mechanical compaction denote lack of lithification and thus absence of burial diagenesis in the original source. In fluvial systems, intrabasinal detrital products derived from low preservation potential sediments are mainly associated to erosion of floodplain subenvironments (Garzanti, 1991).

Cloudy cores in dolomite crystals with abundant radial-pattern inclusions of Fe-oxides and clay minerals point out to a first-stage of replacive growth in a muddy matrix (Fig. 10A and B). Locally, a subsequent stage of displacive growth can be deduced from the presence of clean outer rims that deform muddy ground mass of host original sediments (Fig. 10C and D). Bright orange luminescence of dolomite crystals denotes slightly reducing conditions with incorporation of Mn^{2+} and Fe^{2+}. Slightly variations in chemical composition of dolomite crystals, which are approximately stoichiometric (Fig. 7A and B), suggest that dolomite does not result from dolomitization processes of previous calcite minerals (Hardie, 1987; Kupecz and Land, 1994). All these features are consistent with groundwater (phreatic) dolocretes embedded in muddy floodplain sediments as the source of different rip-up clast types (Arakel, 1986; Armenteros et al., 2003; Wright and Tucker, 1991; Spötl and Wright, 1992; Colson and Cojan, 1996; Pimentel et al., 1996). A vadose (pedogenic) origin for some of these dolocretes cannot be completely ruled out as it is suggested by the presence of organic structures with inherited dolomite cement within several dolomite crystalline rip-up clasts (Fig. 5H).

Fig. 6. A and B) SEM images of euhedral dolomite crystals with zonation from central areas to clearer outer rims, in both cases (dotted lines), and bright inclusions and clayey matrix due to the presence of Fe-oxides, in B. C and D) Same microphotograph under PPL and CL showing luminescence difference between dolomite crystal within rip-up clasts (bright orange luminescent) and poikilotopic dolomite cement (slightly darker; dol cm). Clear outer rims (arrows) luminesce brighter yellowish orange. Black-coloured inclusions under PPL are bright orangish yellow luminescent whereas those red-coloured are darker orange (solid circle) (CS1 sample). E) CL microphotograph corresponding to circle area of Fig. 9C showing luminescence difference between dolomite crystal within rip-up clasts (bright orange luminescent) and syntaxial dolomite cement (slightly darker; dol cm). Zonation of euhedral dolomite crystals from darker cores to brighter rims is also observed (arrows; CS1 sample). F) CL microphotograph showing the same zonation in inherited dolomite cement (inherited cm). Brighter yellowish orange luminescent rims (arrows) and darker orange luminescent inclusions within dolomite crystals are also recognizable. G and H)

Same microphotograph under cross-polarized light (XPL) and CL showing difference between luminescent zoned dolomite cement and dull luminescent calcite cement (SF3 sample).
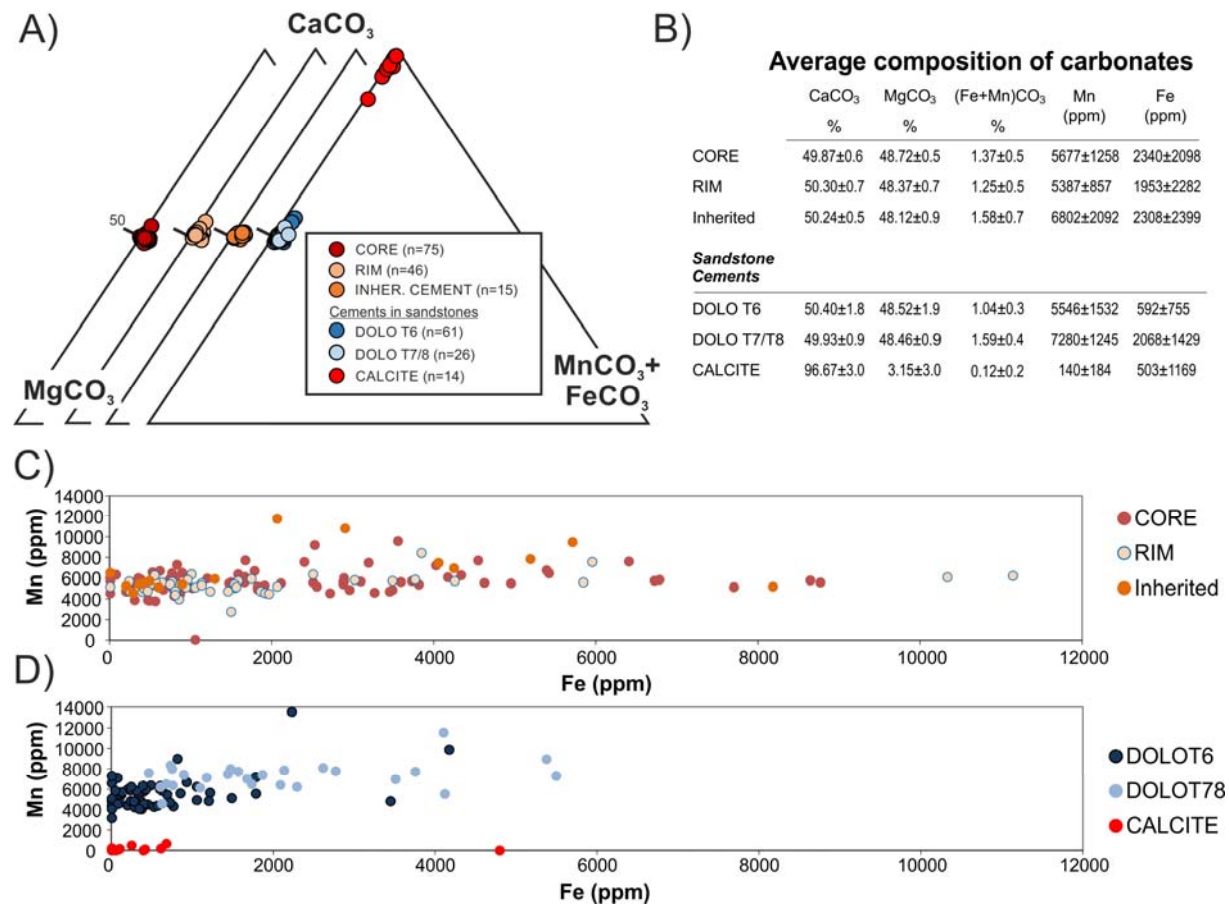
Fig. 7 – Carbonate chemical composition: CORE and RIM=core and rim of dolomite crystals within rip-up clasts, respectively; INHER. CEMENT=inherited dolomite cement within rip-up clasts; DOLO T6 and DOLO T7/T8=dolomite cements from T6 braided system sandstones and T7/T8 straight channel sandstones, respectively; CALCITE=calcite cement from T6 sandstones in compound braided bar environment (SF samples). A) $CaCO_3$-$MgCO_3$-$(Mn+Fe)CO_3$ ternary diagrams showing almost stoichiometric compositions in all cases. B) Table summarizing average composition of carbonates for major elements. C) Fe versus Mn content in dolomite within rip-up clasts. Scatter of data shows a non-constant core-rim variation trend of these elements. D) Fe versus Mn content in sandstone carbonate cements. There is an increase in both element contents from T6 to T7/T8 dolomite cement.

Fig. 8. Diagenetic evolution of host sandstones. A) Compactional (COPL) versus cementational (CEPL) porosity-loss diagrams (modified after Lundegard, 1992). B) Diagenetic sequence of main diagenetic processes as interpreted from petrographic analysis.
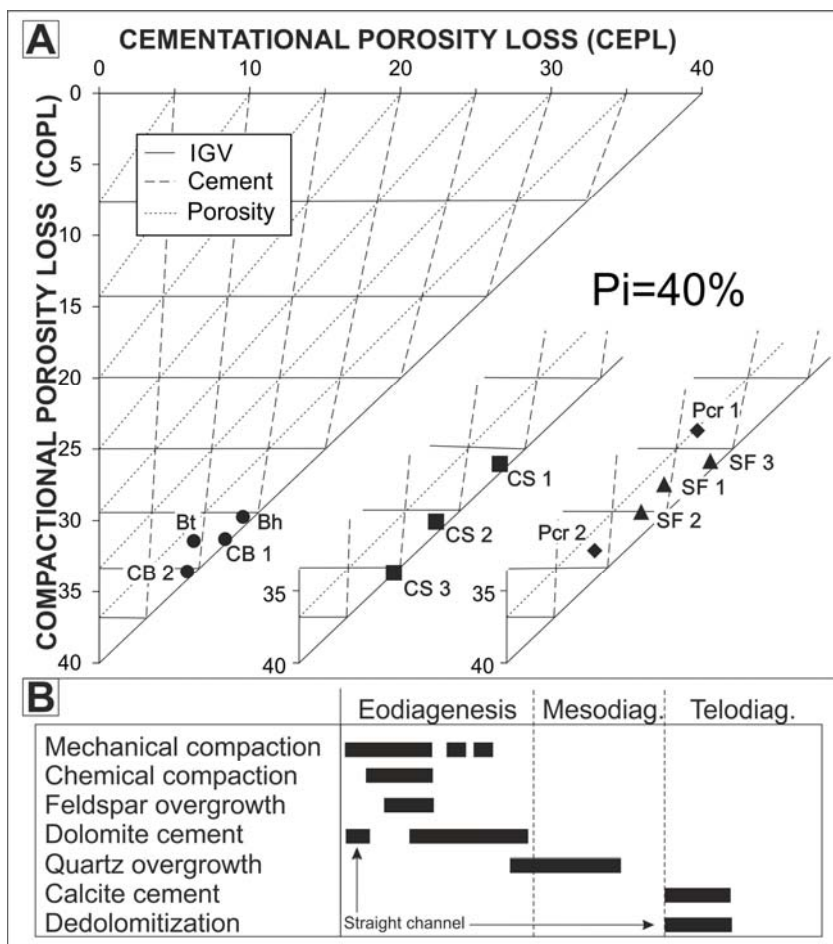
Genesis of groundwater dolocretes requires low sedimentation rates in evaporation-dominated floodplain environment (i.e. saline lakes) where groundwaters are depleted in Ca^{2+} as result of nearby calcrete formation (Andrews, 1985; Arakel, 1986; Arakel et al., 1989, 1990; Colson and Cojan, 1996; Khadkikar et al., 1998). Similar phreatic dolocretes have been documented in fluvial deposits where precipitation of evaporate minerals (gypsum) in playa-lake environment is the main factor of groundwater Ca-depletion (Arribas et al., 1996). Presence of coeval shallow ephemeral lakes and extensive saline mudflats during T6 and T7/T8 deposition have been reported by Brown (1980) and Hofmann et al. (2000).

Very early (pre-compactional), fine-grained, rhombic dolomite cement in straight channel samples (T7/T8 unit; Fig. 9D) may constitute an example of a phreatic dolocrete generated in a high porous media (Nash and McLaren, 2003). Morphology, abundance and size of dolomite crystals within dolocretes will depend on host rock lithology, porosity and permeability (Khalaf, 1990).

Similar muddy rip-clasts with dolomite crystals have been described in fluvial-aeolian sandstone reservoirs from Recôncavo Basin (Brasil) by De Ros and Scherer (2012). These authors interpret dolomite as replacement of rip-up clast during very early (pre-compactional) diagenetic stages. In the Argana basin, present study demonstrates that dolomite crystals are primary in origin and later reworked. In fact, its presence or not within rip-up clasts will have a major impact on diagenetic evolution of host sandstone.
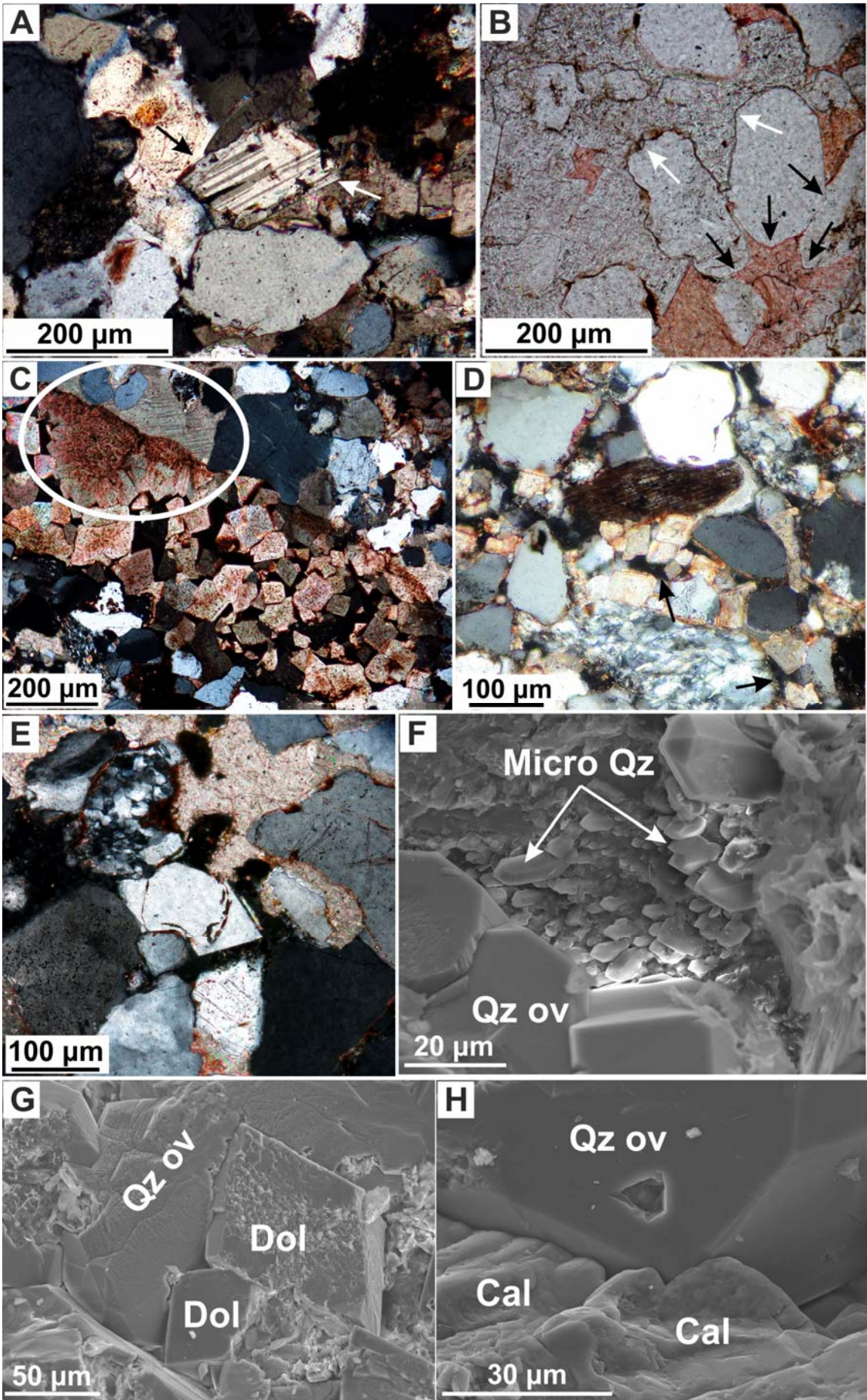
Geochemical diagenetic processes in host sandstones

K-feldspar overgrowth is interpreted as the first cementing phase, resulting from alkaline (high aK+/aH+), silica-rich eodiagenetic waters commonly associated to early diagenetic stages in arkosic redbeds (Waugh, 1978; Arribas, 1987; Morad et al., 1989). Dolomite cement, which locally replaces K-feldspar overgrowths, precipitates from alkaline phreatic waters with a high Mg/Ca ratio that may be derived from near-surface evaporitic processes during eodiagenesis (Hutton and Dixon, 1981; Spötl and Wright, 1992). This cement, in its several growth habits (poikilotopic, syntaxial and fine-grained rhombic crystals), occludes primary pores thus preventing intense mechanical compaction and predates quartz overgrowths. Silica for quartz cement may be partially released from weak chemical compaction processes during burial diagenesis. Nevertheless, alteration of K-feldspar to illite and/or transformation of smectite into illite are also encouraged as sources of Si4 (Worden and Morad, 2003) according to the sandstone framework composition and the presumable incorporation of smectitic clays in primary muddy rip-up clast composition. Both processes require high temperature diagenetic environments (130-140ºC; Bjørlykke, 1994) which is consistent with the maximum temperature data estimated for Argana Basin (150ºC; Leikine et al., 1996) without invoking hydrothermal processes (Lahcen et al., 2007). Calcite cement overlies previous authigenic minerals so postdate them. Calcite precipitation as well as dedolomitization processes are considered telodiagenetic products from flux of fresh oxidizing meteoric waters (Molenaar, 1998).

Diagenetic evolution and implications on reservoir quality

Amount and type of rip-up clasts occurring in fluvial Triassic deposits of the Argana Basin are a key first-order control over diagenetic history of host sandstones (Fig. 11). Its influence is particularly evident on mechanical compaction and dolomite cementation (Fig. 12). Both eodiagenetic processes are crucial for a thorough understanding of reservoir quality evolution.

On the one hand, mechanical compaction is strongly favoured by muddy rip-up clast occurrence (Fig. 11A and B) behaving as highly ductile grains due to intragranular microporosity (Pittman and Larese, 1991) and lack of dolomite crystals. Their presence in sandstone framework results in a significant early reduction of primary porosity and an

Fig. 9. Optical microphotographs and SEM images of main porosity-modifying cements affecting host sandstones. A) Feldspar overgrowth partially replaced by dolomite cement (white arrow) and postdated by quartz overgrowth (black arrow) (XPL, CS1 sample). B) Coarse, euhedral, poikilotopic dolomite cement inhibiting quartz overgrowth formation (white arrows). Notice the occurrence of well-developed quartz overgrowth in the same grains, postdated by calcite cement (black arrows) (PPL, SF3 sample). C) Syntaxial dolomite cement developed in adjacent intergranular space as overgrowths from rip-up clast dolomite crystals (circle area; XPL, CS1 sample). Circle area also corresponds to CL image of Fig. 6E. D) Fine, euhedral, rhombic crystals of dolomite cement preserving primary porosity (black arrows) (XPL, PCr1 sample). E) Well-developed quartz overgrowth with bipyramidal habit (XPL, SF3 sample). F) Microcrystalline rim of quartz overgrowths showing prismatic habits (Micro Qz). Coarser, euhedral quartz overgrowths are also observed (Qz ov) (CS2 sample). G) Quartz overgrowth overlaying dolomite cement (Dol) (CS1 sample). H) Quartz overgrowth postdated by calcite cement (SF2 sample).

irreversible loss of IGV which considerably deteriorates reservoir quality (Rittenhouse, 1971; Pittman and Larese, 1991; Paxton et al., 2002; Worden and Morad, 2003; Fig. 11C; Fig. 12A). From Figs. 11B and C, it can be deduced that when around 20% of sandstone framework is represented by muddy rip-up clasts, COPL increases up to around 35% whereas IGV decreases to less than a 10% remaining. Effect of other relatively ductile framework components, such as lithic fragments (phyllite and schist), is subordinated to the abundance of this rip-up clast type as demonstrated by the greater correlation between muddy rip-up clasts and COPL (Fig. 11B and D). Conversely, dolomite crystalline rip-up clasts act as rigid (non-deformed) framework grains that prevent porosity loss by mechanical compaction (Fig. 5D to H; Fig. 12C). Ductility (grade of mechanical deformation) of dolomitic muddy rip-up clasts will depend on abundance and size of dolomite crystals within the clast (see difference in clast extrusion between Fig. 5B and C; Fig. 12B).
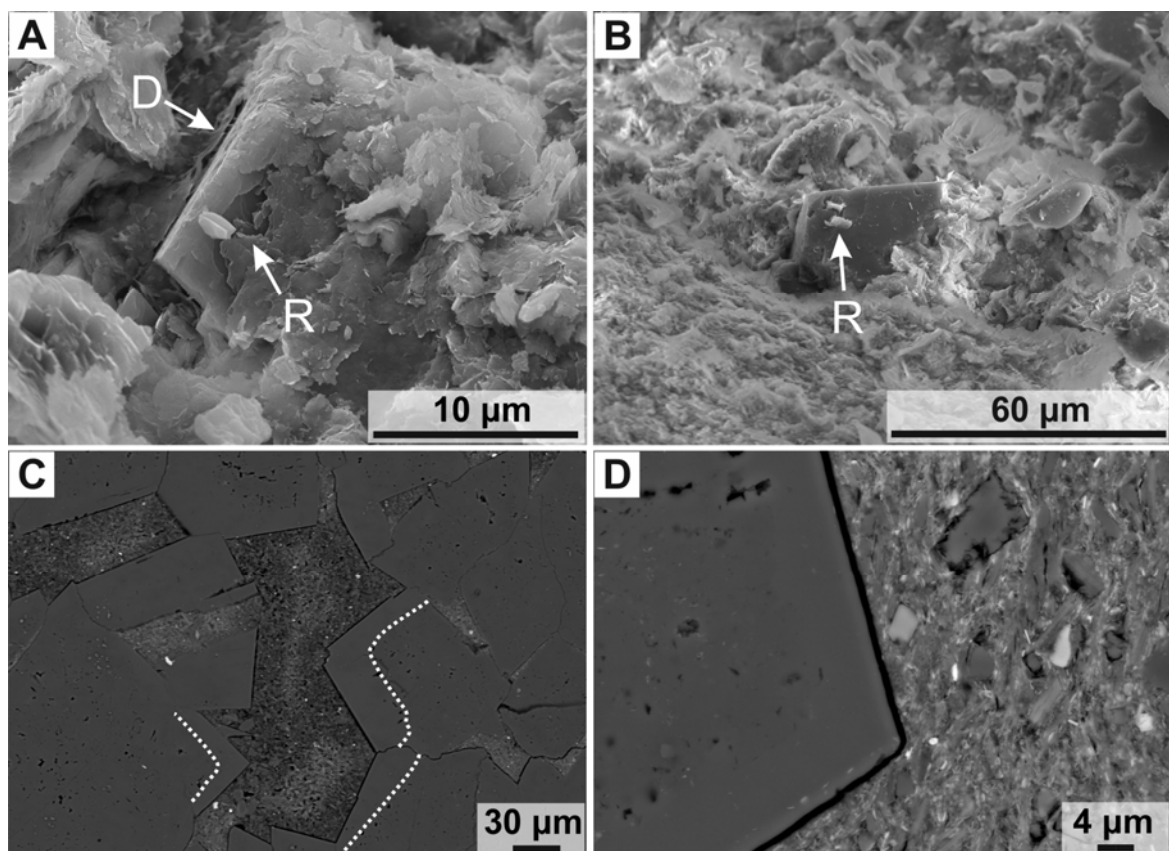
Fig. 10. SEM images of the different dolomite growth stages in a clayey matrix. A and B) Fist-stage of replacive growth of dolomite crystal incorporating illitic clays (R of replacive). In A), a clear outer rim of dolomite crystal deforms clay minerals during the last growth stage (D of displacive). C and D) Later displacive growth resulting in clear outer rims (dotted lines) that deform muddy host ground mass.

On the other hand, occurrence of dolomite crystalline and dolomitic muddy rip-up clasts has double role on eodiagenetic dolomite precipitation (Fig. 11E to H; Fig. 12B and C): 1) as nuclei for syntaxial dolomite cement to grow in adjacent interstitial space (Burley, 1984; Carvalho et al., 1995; Molenaar, 1998; Ketzer et al., 2002; Al-Ramadan et al., 2005; Fig. 9C); and 2) as local sources of dolomite cement derived from dissolution-reprecipitation processes (i.e. chemical compaction) (Arribas et al., 1996; Al-Ramadan et
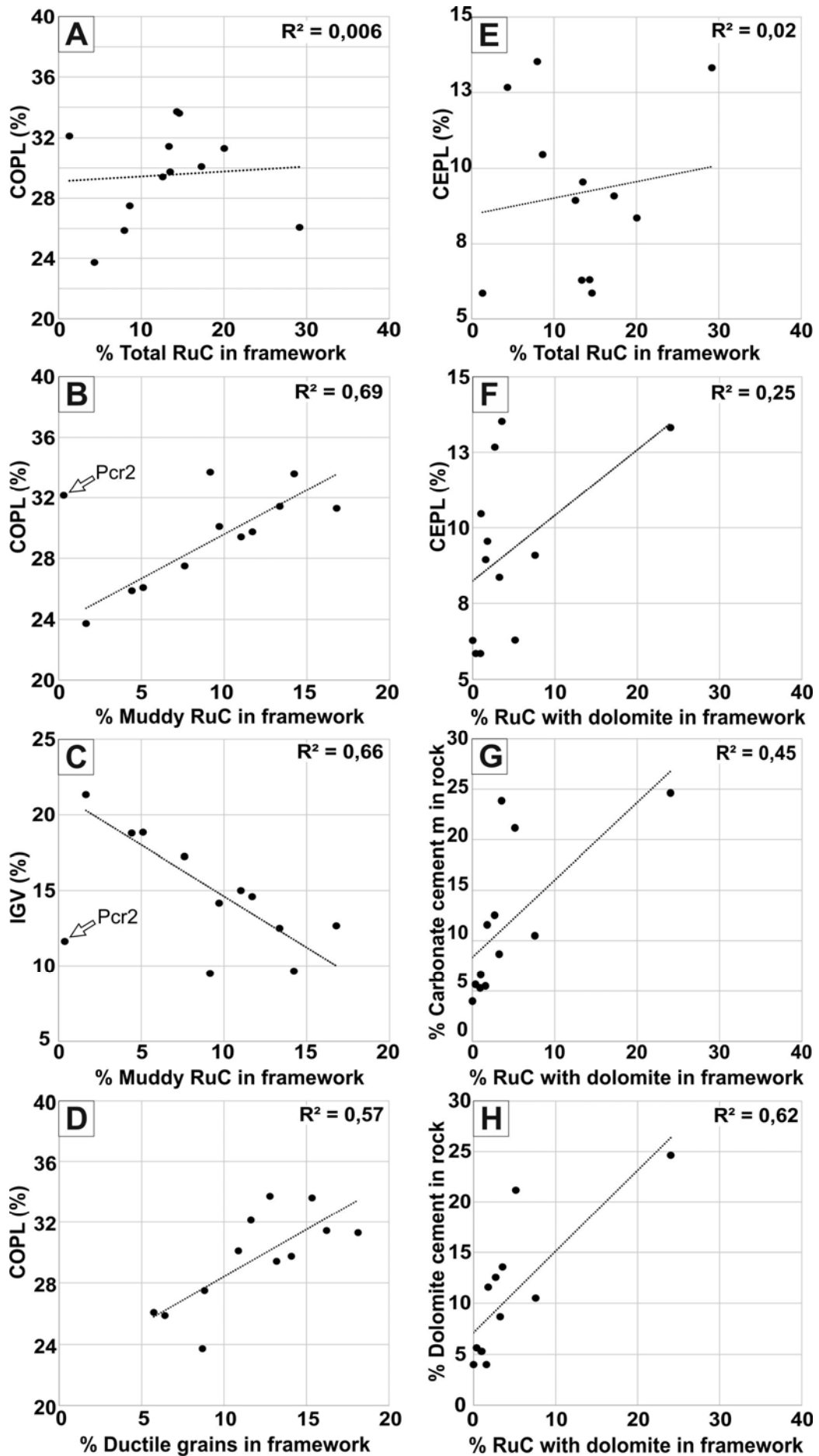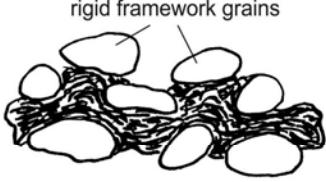
al., 2005; Morad et al., 2010; De Ros and Scherer, 2012). Petrographic evidences such as the greater correlation between this rip-up clast type and dolomite cement, compared with other cements (CEPL or total carbonate cement) (Fig. 11F to H), as well as similar chemical compositions of detrital dolomite and dolomite cements (Fig 7A) are consistent with both processes. Fig. 11H suggests that when around 10% of sandstone framework is represented by these types of rip-up clasts (dolomite crystalline and dolomitic muddy), dolomite cement only can constitute up to 25% of total rock composition (including framework, cements and pores). Typical association of dolomite crystalline and dolomitic muddy rip-up clasts with coarser-grained depositional facies may also stimulate dolomite precipitation due to higher original permeability of such facies. Early pervasive dolomite cementation occludes remnant primary porosity but partially inhibits mechanical compaction, thus preserves high IGV in host sandstones. In the case of pre-compactional, fine-grained, rhombic dolomite cement from T7/T8 straight channel samples (Fig. 9D), primary porosity is also preserved. Despite the negative effect of dolomite cementation by reducing primary porosity, preservation of IGV may considerably enhance reservoir quality by later carbonate dissolution processes (Schmidt and McDonald, 1979; Surdam et al., 1984, Bjørlykke, 1984). In addition, spatial distribution and abundance of different reported rip-up clasts are strongly facies-related according to grain size (Garzanti, 1991; Pittman and Larese; 1991). Preferential concentration of muddy rip-up clasts in continuous layers (Fig. 3B) and of dolomite crystalline rip-up clasts in specific depositional facies (e.g. channel-lags) increases porosity heterogeneity and permeability anisotropy. At pore- and depositional- scales, continuous levels of pseudomatrix blocking pore throats and intergranular pores (Fig. 12A; Bloch, 1994; Ketzer and Morad, 2006) as well as laterally extensive layers pervasively cemented by dolomite may constitute local barriers and baffles for fluid flow in-between amalgamated sandstone bodies, creating reservoir compartmentalization (Fig. 12B and C; Gibbons et al., 1993; Prosser et al., 1993).

Fig. 11. Relationship between main diagenetic processes affecting host sandstones and the abundance of rip-up clast types. A) COPL versus percentage of all rip-up clast types in sandstone framework showing no apparent correlation according to its low R^2 value. B) COPL versus percentage of muddy rip-up clasts in sandstone framework showing very high and direct correlation as indicated by the highest R^2 value. PCr2 sample (T7/T8 straight channel) is not included for correlation because of significant predominance of lithic fragments over muddy rip-up clasts mainly influence mechanical compaction. C) IGV versus percentage of muddy rip-up clasts in sandstone framework shows high but inverse correlation. Idem with PCr2 sample. D) COPL versus percentage of ductile grains (muddy rip-up clasts plus lithic rock fragments) in sandstone framework shows high and direct correlation although slightly lower that only compared with muddy rip-up content. E) CEPL versus percentage of all rip-up clast types in sandstone framework shows no apparent correlation according to its very low R^2 value. F) CEPL versus percentage of rip-up clasts with dolomite (dolomitic muddy plus dolomite crystalline rip-up clasts) in sandstone framework shows low and direct correlation. G) Percentage of carbonate cements (dolomite plus calcite) in total rock composition versus percentage of rip-up clasts with dolomite in sandstone framework still shows relative low and direct correlation, although greater than previous one. H) Percentage of rip-up clasts with dolomite (dolomitic muddy plus dolomite crystalline rip-up clasts) in sandstone framework versus percentage of only dolomite cement in rock composition (framework, cement and pores)shows high and direct correlation according to its high R^2 value.

Fig. 12. Cartoon illustrating diagenetic behaviour of the different rip-up clast types and related reservoir quality pathways. A) Muddy rip-up clasts. B) Dolomitic muddy rip-up clasts. C) Dolomite crystalline rip-up clasts.

CONCLUSIONS

Coupling high resolution petrographic and chemical data within a well-constrained depositional framework of Triassic fluvial sandstones from Argana Basin (T6 and T7/T8 units), leads to following conclusions:

(1) Rip-up clasts may represent a significant part of host sandstone framework as intrabasinal components with a spatial distribution strongly controlled by depositional facies (i.e. grain size). Importance of muddy and dolomite rip-up clasts in fluvial sandstones is proved in two fundamental ways: 1) as information sources about low preservation potential floodplain deposits for paleogeographic reconstructions; and 2) as key elements controlling host sandstone diagenetic evolution and, thus, reservoir quality.

(2) On the basis of rip-up clast composition and mechanical behaviour, three main classes are differentiated: muddy rip-up clasts without dolomite crystals; dolomitic muddy rip-up clasts with intermediate dolomite crystal proportions; dolomite crystalline rip-up clasts mainly composed by dolomite crystals.

(3) Origin of these grains is related to erosion of coeval phreatic dolocretes, in different development stages, and associated muddy floodplain sediments in an evaporation-dominated environment. Cloudy cores with radial-pattern inclusions and clear outer rims in dolomite crystals suggest a first-replacive and subsequent displacive crystal growth, respectively, in shallow environments.

101

(4) Diagenetic evolution, dominated by mechanical compaction and dolomite cementation, is strongly affected by the amount and type of rip-up clasts. Mechanical compaction of highly ductile muddy rip-up clasts results in early reduction of primary porosity and irreversible loss of IGV. High correlation ($R^2=0.69$) between COPL and this rip-up clast type indicates that when around 20% of sandstone framework is represented by muddy rip-up clasts, COPL increases up to around 35% whereas IGV decreases to less than a 10% remaining. Conversely, dolomite crystalline rip-up clasts act as rigid (non-deformed) framework grains preventing mechanical compaction. High correlation between dolomite cement and rip-clasts with dolomite crystals ($R^2=0.62$) points out that they may act as nuclei and source for dolomite cement, which can constitute up to 25% of total rock composition when these grains represent around 10% of sandstone framework. Their similar chemical compositions also support an early diagenetic origin coinciding with coeval phreatic dolocretes.

(5) Spatial distribution of rip-up clasts throughout depositional facies and associated diagenetic processes impact reservoir quality by generation of vertical and 3D fluid flow baffles and barriers that compartmentalize the reservoir.

(6) These results may be used for a better understanding of reservoir quality distribution in analogous hydrocarbon-bearing basins such as the Bay of Fundy, Nova Scotia (Canada).

Acknowledgements

Concluding remarks

In all cases, early diagenetic deterioration of primary porosity and permeability has a direct relation to sedimentary dynamics and consequently to depositional facies. Depositionally-driven hydraulic sorting effect comes out as a key first-order control on both detrital matrix and rip-up clast distribution according to facies.

Importance of textural information is highlighted in the meandering deposit by the influence of small-scale internal porosity–permeability heterogeneity associated to the occurrence of detrital matrix and suspension-settling laminae. Higher matrix content favours mechanical compaction but also inhibits pervasive pore-filling cement formation. Statistical processing of petrographic and petrophysical data demonstrates that, in these cases, primary intergranular porosity is more efficiently preserved and contributes to higher permeability values. The 3D model for the reservoir quality index fits perfectly to the distribution of depositional facies and can therefore be used to predict post depositional facies-related preferential flow pathways to improve ultimate recovery in EOR strategies.

Amount and type of rip-up clasts in braided and straight fluvial deposits have an evident influence on early mechanical compaction and dolomite cementation. Muddy rip-up clasts behave as ductile grains and their presence in sandstone framework (20%) results in a significant early reduction of primary porosity and irreversible loss of IGV (<10%). Conversely, dolomite crystalline rip-up clasts act as rigid grains against mechanical compaction but favour precipitation of early pervasive dolomite cement that occlude primary porosity and preserves IGV. When dolomite crystalline rip-up clasts represent around 10% on total sandstone framework, dolomite cement only can represent up to 25% of total rock composition. Quantitative estimation of early reduction of primary porosity by compaction and cementation on the basis of abundance of these type of grains can provide useful data for the better understanding of reservoir quality in analogous basins such as in the conjugate Atlantic margin of the Bay of Fundy (Nova Scotia, Canada).

CHAPTER **5**

Complementary Contribution

5.1 The role of detrital anhydrite in diagenesis of aeolian sandstones (Upper Rotliegend, The Netherlands): implications for reservoir-quality prediction

S. Henares, M.R. Bloemsma, M.E. Donselaar, H.F. Mijnlieff, A.E. Redjosentono, H.G. Veldkamp, G.J. Weltje

Abstract

The Rotliegend (Upper Permian) reservoir interval in the Southern Permian Basin (SPB) contains low-permeability streaks corresponding to anhydrite-cemented intervals which cause significant flow anisotropy. An integrated study of such intervals has been conducted using core, cuttings, thin sections and well-log data from a gas exploration well and two geothermal wells that target the zone of interest. The aims of this study were to understand the origin and nature of these low-permeability streaks, as well as their impact on reservoir properties, and to establish a predictive model of their spatial distribution. High-resolution XRF core-scanning analysis was carried out to extrapolate spot observations in thin sections to the entire core. The sands were subjected to grain rearrangement and mechanical compaction. The main diagenetic phases (apart from the anhydrite cement) are haematitic clay coatings, dolomite rims, quartz overgrowths, kaolinite and second-generation carbonates. Coupling of all available data reveals the detrital origin of the anhydrite/gypsum grains which were transported by wind and deposited together with the coarse-grained fraction of laminated sands in an aeolian sandflat environment. Such partially or completely dissolved grains acted as local sources of anhydrite pore-filling cement and as nuclei for precipitation, which explains its preferential occurrence in coarse-grained laminae. Thick gypscrete accumulations in the vicinity are proposed as the source of the anhydrite/gypsum grains. Partial preservation of the original detrital texture indicates a short transport distance of the ductile anhydrite/gypsum grains. A conceptual predictive model for the spatial distribution of anhydrite-cemented low-permeability intervals is proposed, which couples the locations of nearby gypscrete accumulations with the prevailing west-southwest aeolian transport direction on the southern rim of the SPB.

INTRODUCTION

The Rotliegend (Upper Permian) reservoir interval is the most prolific hydrocarbon-bearing unit in the Netherlands, both onshore and offshore. It hosts, among others, the Groningen Field, the largest producing onshore gas accumulation in Europe (2,900 x 109 m^3 or 100 Tcf GIIP; Grötsch et al., 2011). The best reservoir quality is found in Rotliegend aeolian sandstone facies which has average porosities up to 25% and permeabilities in the one Darcy range (Grötsch et al., 2011; Gaupp and Okkerman, 2011). Towards the boundary between the aeolian and the adjacent saline lake depositional environments, reservoir quality deteriorates because of progressively less favourable reservoir facies, non-permeable evaporitic sediment intercalations and early-diagenetic evaporite cementation in the sandstones. The different potential combinations of sedimentary facies, structural regimes and fluid-flow rates resulted in "diagenetic provincialism" which controls the present-day reservoir quality of the Rotliegend (Gaupp and Okkerman, 2011).

The aim of the present study is to establish a predictive model for the spatial distribution of anhydrite-cemented, low-permeability intervals in aeolian reservoir rocks of the Rotliegend on the basis of a detailed sedimentological-petrographic study of these intervals and their spatial relation with thick, isolated anhydrite bodies in the vicinity. The study was triggered by the Dutch Koekoekspolder geothermal energy production project (Fig. 1) that targeted the Rotliegend reservoir interval (Mijnlieff et al., 2014). Despite excellent data density and existing geological reservoir models of the Rotliegend, the newly-drilled geothermal wells (KKP-GT-1 and KKP-GT-2) had lower-than-predicted flow rates. Initially, skin issues were assumed to cause the low flow rates. However, after remediation of the wells the flow rates invariably remained lower than expected which prompted a refinement of existing depositional models. As a next step, the permeability heterogeneity in the reservoir interval was investigated in the dry gas-exploration well Kampen-1 (KAM-01-S1) drilled in 1969 in the same area of the geothermal wells. Core, thin sections, well-log and seismic data of all three wells were used in the present study. By broadening our understanding of reservoir heterogeneity, the results of this study will contribute to reducing the uncertainty in future geothermal energy projects in the Rotliegend reservoir interval.

REGIONAL GEOLOGICAL SETTING

The siliciclastic sandstones and conglomerates of the Upper Permian Slochteren Formation (Van Adrichem Boogaert and Kouwe 1993; Geluk 2007) are part of the fill of the Southern Permian Basin (SPB). The basin formed at the end of the Hercynian Orogeny by thermal subsidence after the Saalian tectonic phase (~ 270 Ma BP) and the start of a rifting period and associated upper mantle basalt extrusion (Gebhardt et al., 1991; Glennie, 1998). The basin is structurally bounded by the London – Brabant and Rhenish Massifs in the south and the Mid North Sea High and the Ringkøbing-Fyn High in the north (Fig. 2). It extends from the east coast of the UK to Poland with a length of more than 2000 km and a width of 300-600 km. The Texel – IJsselmeer High (TYH) is a NW-SE aligned intrabasinal high, fault-bounded to the SW and with a gently dipping flank to the NNE

107

(Fig. 2; George and Berry, 1994; Verdier, 1996; Geluk, 2005; Mijnlieff and Geluk, 2011). The Permian basin fill comprises some 2500 m of Upper Rotliegend siliciclastic and evaporitic rocks, and 2000 m of siliciclastics, carbonates and evaporite deposits of Zechstein age (Ziegler, 1990). The Rotliegend unconformably overlies the base Permian unconformity (Geluk, 2007; Gast et al., 2010). Lithostratigraphically, the sand-prone Slochteren Formation belongs to the Upper Rotliegend Group (Van Adrichem Boogaert and Kouwe, 1993) in the Dutch part of the SPB (Fig. 3).
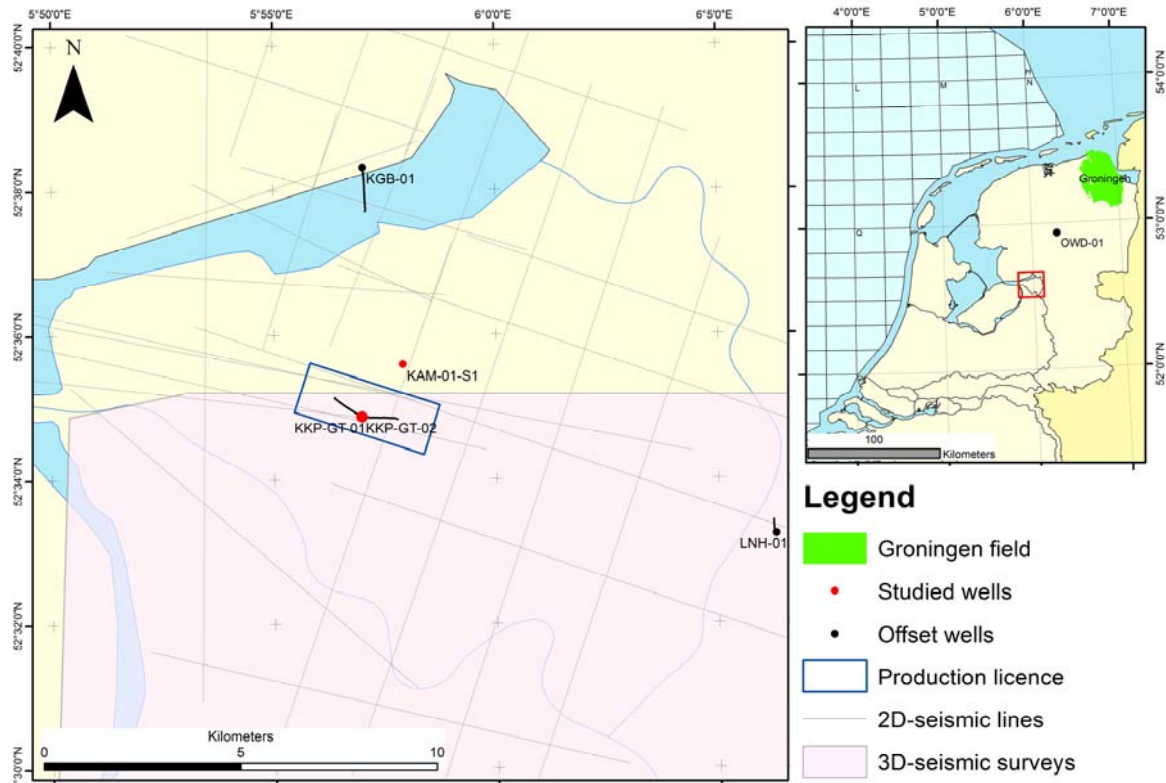
Fig. 1. Location map of the study area.
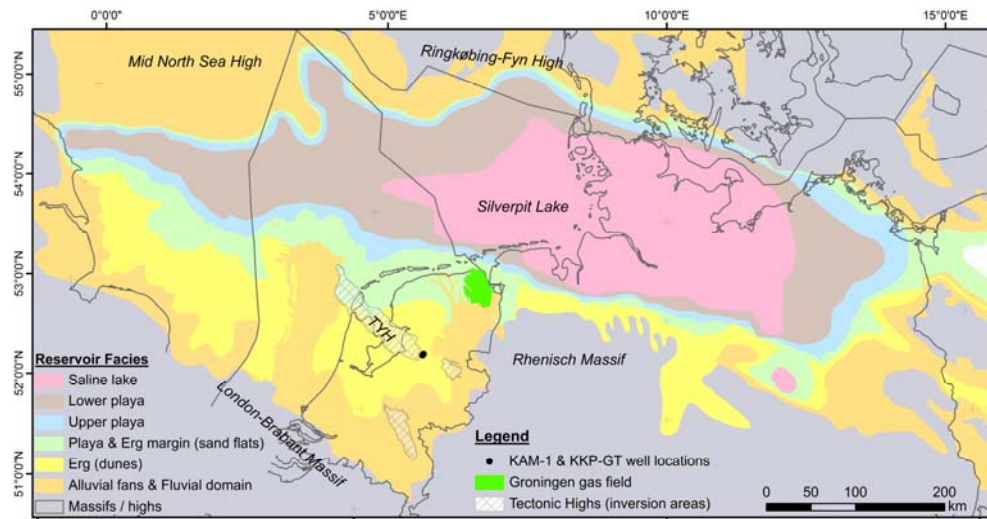
Fig. 2. Extent of the Southern Permian Basin and Upper Rotliegend palaeogeography. London-Brabant and Rhenish Massifs form part of the Variscan Mountain Range that fringes the Basin to the south. TYH: Texel-Ijsselmeer High. Compiled from maps by Gast et al. (2010); Fryberger et al. (2011).

In the Permian the SPB was situated at paleolatitudes of about 30oN, i.e., similar to the present-day North-African and Arabian deserts (Glennie, 1998). The SPB was located in the rain shadow of the Variscan Mountain Range, and could not be reached by the humid Tethyan Trade Winds from the SE. As a consequence, an arid climate prevailed at the time of deposition of the Slochteren Formation (Sweet, 1999) with north-eastern winds parallel to the Variscan Mountain Range (Verdier, 1996). Sediments of the Upper Rotliegend Group were deposited during wet/dry cycles which caused saline lake expansion and contraction (Sweet, 1999; Bailey and Lloyd, 2001; Bourquin et al., 2009). In the Netherlands, two major phases of lake expansion left prominent claystone wedges extending far towards the basin edge (Fig. 3). The lowermost claystone wedge is lithostratigrapically assigned to the Ameland Member of the clay-prone Silverpit Formation. It separates the Slochteren Formation into the Lower and Upper Slochteren members (Fig. 3). However, in the study area no claystone interval is present and thus the Rotliegend only comprises the undivided Slochteren Formation (Fig. 3). The Rotliegend basin-fill architecture is characterised by onlap. Consequently, the undivided Slochteren Formation south of the southernmost pinch-out of the Ameland Member is largely time equivalent to the Upper Slochteren Member (van Oijik et al., 2011, Mijnlieff and Geluk., 2011).
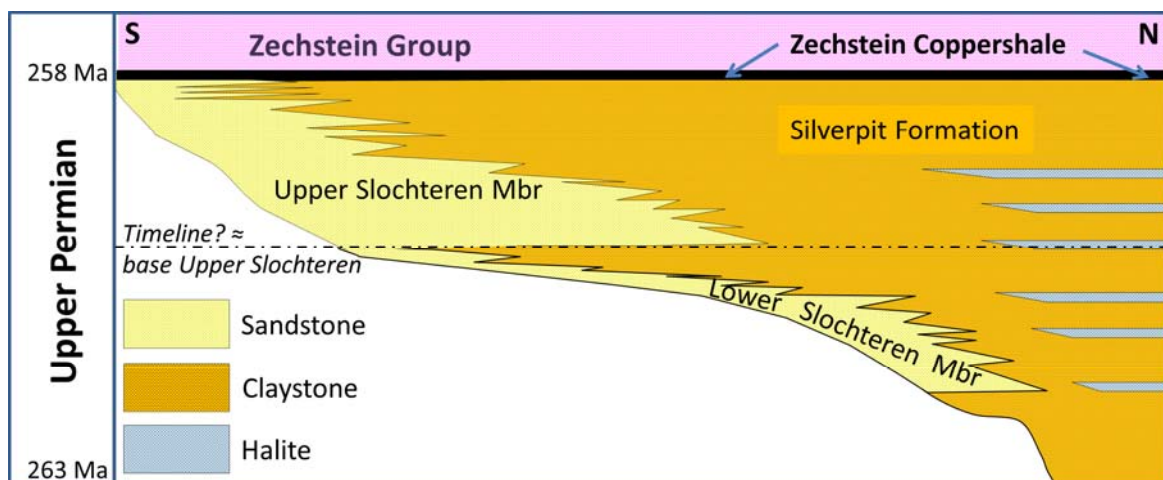
Fig. 3. Chrono-lithostratigraphic scheme of the Dutch Permian Rotliegend.

The SPB comprises a series of concentric facies belts from the southern margin to the basin centre (Fig. 2; Gast et al., 2010; Kabel, 2002; Legler and Schneider, 2008). Coarse-grained alluvial-fan and fluvial deposits occur along the margin of the London-Brabant and Rhenish Massifs. Towards the basin centre extensive sandflats with aeolian dune sand deposits pass into mudflats and perennial saline lake facies with mud and halite deposits. South-North stretching elongated fluvial fairways with conglomeratic and sandy sheetfloods, braidplain and wadi facies interfinger with sand- and mudflat facies (George and Berry, 1994; Kabel, 2002; Legler and Schneider, 2008; Fryberger et al., 2011).

The Late Permian Zechstein transgression occurred as a result of a more efficient and greater connection to the north with the proto-Atlantic (Richter-Bernburg, 1955; Verdier, 1996, Legler et al., 2005). The transgression started with the deposition of the Coppershale, a basinwide correlatable horizon at the base of the Zechstein (Fig. 3), and was followed by a number of cyclic carbonate-evaporite sequences (Legler et al., 2005).

The study area is located on the NE-flank of the TYH (Fig. 2). Regional facies maps by for example Fryberger et al. (2011) show an area dominated by aeolian sandflats and dune fields on the TYH (Fig. 2). Some 50 km to the north the aeolian facies grades into damp and wet sandflats and mudflats. Fryberger et al. (2011) describe the occurrence of gypsum and anhydrite in the saline mudflat facies.

METHODOLOGY

For this study we used core and well-log data of the gas-exploration well Kampen-1 (KAM-01-S1) drilled in 1969, and cuttings and well-logs of the two geothermal wells KKP-GT-1 and KKP-GT-2 drilled in 2012 (Fig. 1). Additionally, a 3D-seismic survey and a number of 2D-seismic lines were used to construct a 3D-subsurface model of the Rotliegend target interval.

A full macroscopic lithofacies description was made of the 26-m-long cored interval in the upper part of the Slochteren Formation (1811 to 1827 m depth) of the KAM-01-S1 well. Key sedimentary features were photographed using a high- resolution camera and focus stacking to acquire high-quality macro photos of the slabbed core surface. Extensive petrographic analysis was carried out on thin sections from the cored interval by optical microscopy, in order to characterise the textural and compositional signature of the cored interval to infer its diagenetic history. In addition, cuttings from the two geothermal wells were analyzed.

High-resolution XRF analysis was carried out on a selected core slab of KAM-01-S1 with an Avaatech X-ray Fluorescence core scanner (Jansen et al., 1998). This method yields the relative compositional variation among thinly laminated sands of KAM-01-S1 by measuring element intensities of Al, Ca, Fe, Rb, S, Si, Sr, Ti, Fe, and Zr (Richter et al. 2006; Tjallingii et al., 2007). Core slabs were measured at 10kV and 30kV with a count time of 20s and 15s, respectively, and a tube current set at 1800μA in both runs. The acquisition window (with a cross-core slit opening of 12 mm) was set to 0.3 mm in the down-core direction (down-core step size fixed at 0.3 mm). Hence, the measurements have no overlap and are in principle independent. Replicate measurements were taken every 10th core position.

The most successful calibration model for XRF-core-scanner output is based on mapping of log-ratios of intensities onto log-ratios of element concentrations (Weltje and Tjallingii, 2008; Weltje et al., 2014). According to this model, semi-quantitative interpretation of geochemical compositional variability from non-calibrated XRF-scanner-output is straightforward, because trends in log-ratios are practically the same for intensities and concentrations.

Well-logs and core plug measurements were used to obtain the porosity and permeability of the Slochteren reservoir interval. Well-log correlation between KAM-01-S1 and the two geothermal wells KKP-GT-1 and KKP-GT-2 was performed to link the occurrence of anhydrite cement in the core of KAM-01-S1 to the stratigraphic position of thick anhydrite intervals in the geothermal wells. The wells were tied to the 3D-subsurface model. Top and base of the Rotliegend reservoir were picked on the seismic data and the resulting TWT-surfaces were converted to depth surfaces. The seismic section was

flattened on the palaeo-reference horizon of the Coppershale so as to bring out possible thickness variations of the Rotliegend succession in the study area.

RESULTS

## Reservoir geology of the study area

The Rotliegend succession in the study area consists of a single, 88 to 125-m-thick stratigraphic unit characterized by a gamma-ray with a blocky pattern and continuously low values of around 30 API, overall bulk density (RHOB) in the wells of 2.2 to 2.4 g/cm3 and moderate sonic transmission times (in the order of 80 µs/ft) (Fig. 4). A seismic section through the study area (Fig. 5) shows that the thickness of the Rotliegend succession varies by about 20 m, which is confirmed in the log correlation panel (Fig. 4). The variation is caused by pre-Rotliegend palaeo-topography (Mijnlieff and Geluk 2011; Mijnlieff et al., 2014).

The poor reservoir quality in the lower part of the succession is most likely related to the Base-Permian unconformity with its associated diagenetic alterations, such as cementation (Mijnlieff et al., 2014). In both geothermal wells tight intervals are present at different depths below the top of the reservoir (Fig. 4). The tight intervals are characterised by high bulk densities of 2.75 to 2.90 g/cm3 and low sonic log values, suggesting pervasive cementation by anhydrite. The combination of high bulk density values and low gamma-ray values in well KAM-01-S1 at 1900 – 1906 m depth reveal the presence of a similar anhydrite-cemented interval (Fig. 4). Petrophysical analysis of the logs coupled with the core plug measurements in the KAM-01-S1 well and nine other offset wells indicates an average aquifer porosity of 18.5% and an average aquifer permeability of 210 mD (Fig. 6). Well-to-well correlation (Fig. 4) shows the limited lateral extent of the tight anhydrite-cemented intervals (less than the well spacing of approximately 1600 m). The top of the upper, 16-m-thick anhydrite cemented interval in well KKP-GT-1 correlates with the base of the cored interval in well KAM-01-S1 (double arrow in Fig. 4).

The tight intervals in wells KKP-GT-1 and KKP-GT-2, tied into the seismic section, show a relation between the positive (blue) reflection and the upper, 16-m-thick cemented interval in well KKP-GT-1 (Figs. 4 and 5).

Core description

The cored interval consists of a continuous succession of red-brown, very fine- to very coarse-grained sandstone characterized by the occurrence of conspicuous white laminae and by the absence of bed boundaries (Fig. 7). Parallel lamination is the dominant sedimentary structure. Occasional single sets of trough cross lamination with a set thickness up to 1 cm occur with the low-angle foreset made up of alternating coarser-finer sand laminae (Figs. 7A and 7C). Small (up to 1.2 cm wide) deep scours are filled with coarse sand grains (Fig. 7B).
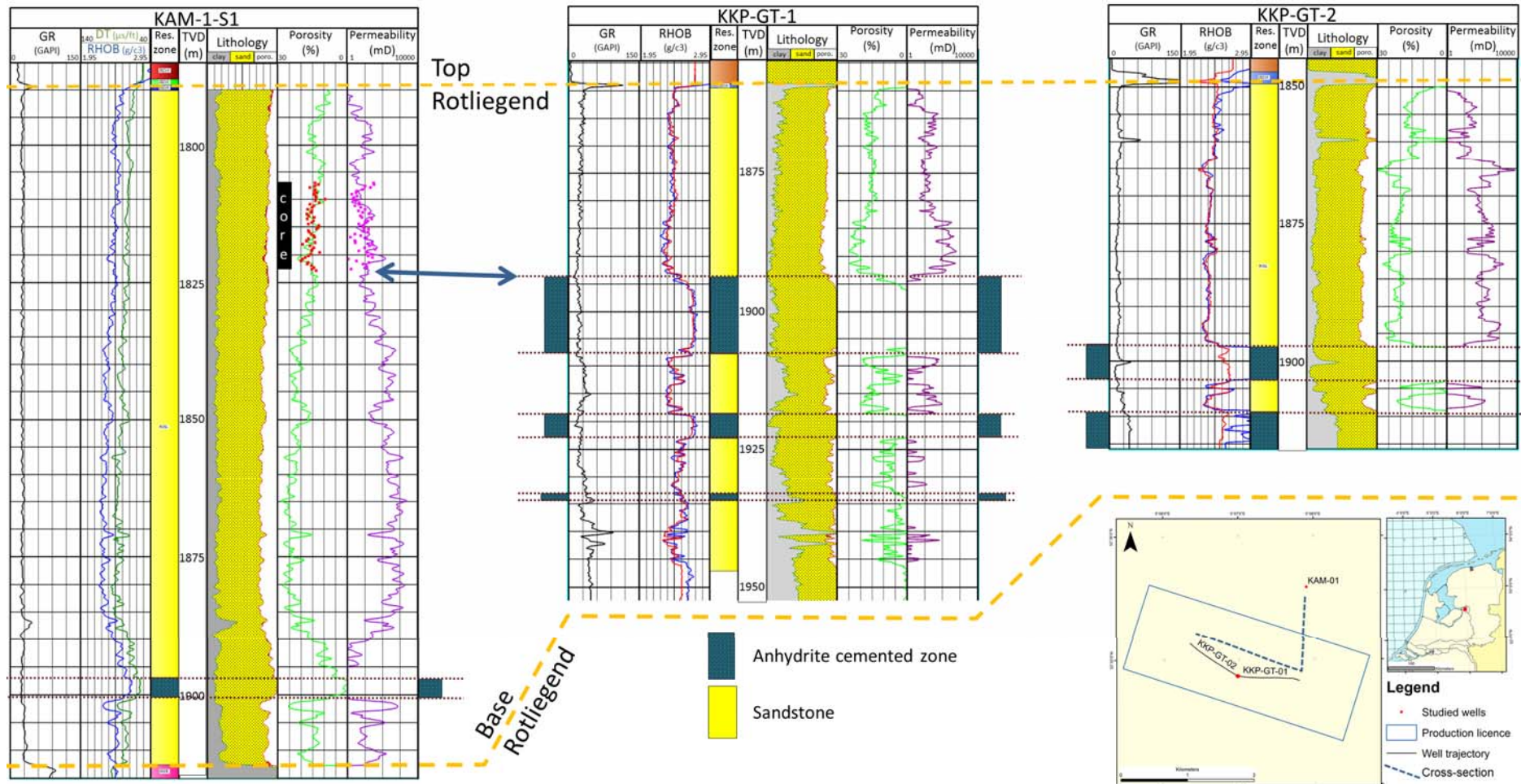
Fig. 4. Well-log correlation panel of the three wells. The section is flattened on top reservoir. Note that in KKP-GT-1 and KKP-GT-2 the base reservoir is not reached. The intervals with high density values and no porosity are rich in anhydrite. Double arrow: top of anhydrite interval in KKP-GT-1 correlates with base cored interval in KAM-1-S1.
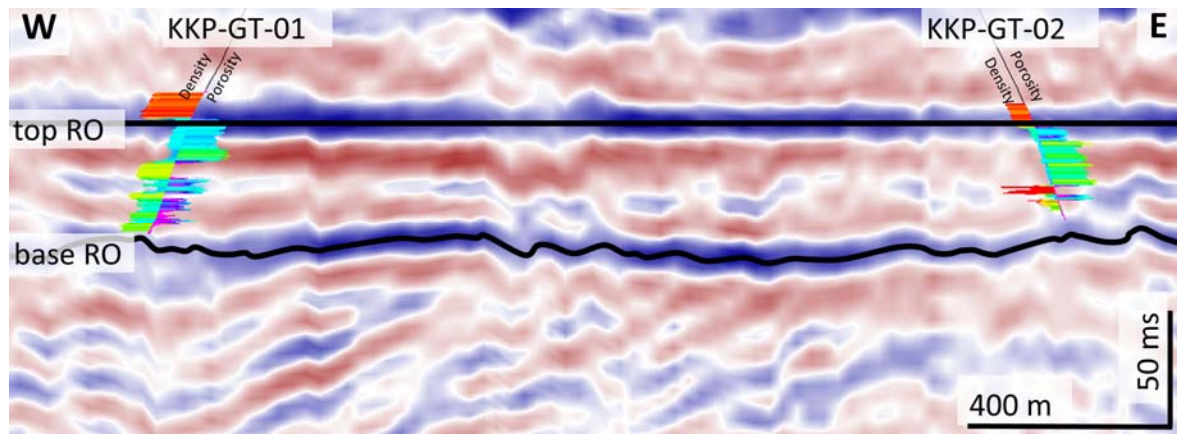
Fig. 5. Seismic section through the reservoir between geothermal wells KKP-GT-1 and KKP-GT-2. The section is flattened on top reservoir. Well-logs are tied into the section. Note that neither well reaches the base reservoir. The seismic reflection suggests a response to lithology contrasts at the KKP-GT-1 well. Well-log colour coding accentuates values. Density log: low-to high values from dark blue – yellow – red. Porosity log: low-to high values from purple – blue – green. C.f., Fig. 2 for porosity and density logs.

Fig. 6. A) Core plug porosity – permeability cross plot of KAM-01-S1 and nine offset wells.
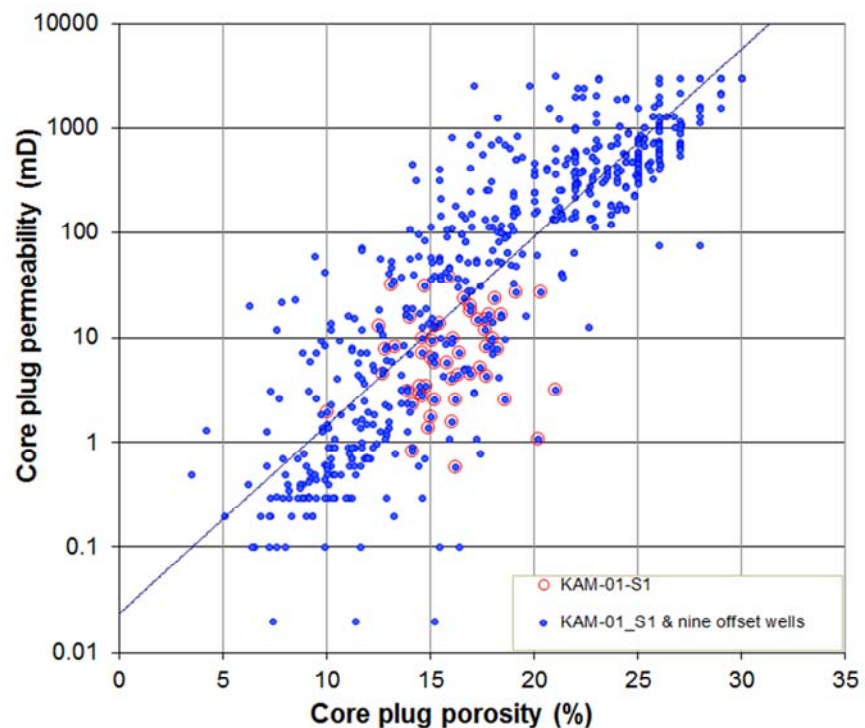
The entire succession is characterised by a bimodal grain-size distribution arranged in pairs of laminae with a total thickness of 4 to 8 mm. Each pair has a sharp flat base, whereas the boundary between the laminae is diffuse (Fig. 8). The lower lamina, usually white in colour, consists of moderately to well-sorted, rounded to well-rounded, very coarse (up to 1.3 mm), and to lesser extent, fine (up to 0.16 mm) sand grains. Within these coarse laminae, small white grains (or nodules resembling coarse grains) are abundant. The upper lamina consists of red-brown, moderately well-sorted, subrounded to rounded, dominantly fine to very-fine grained (0.25-0.06 mm) sand.

113
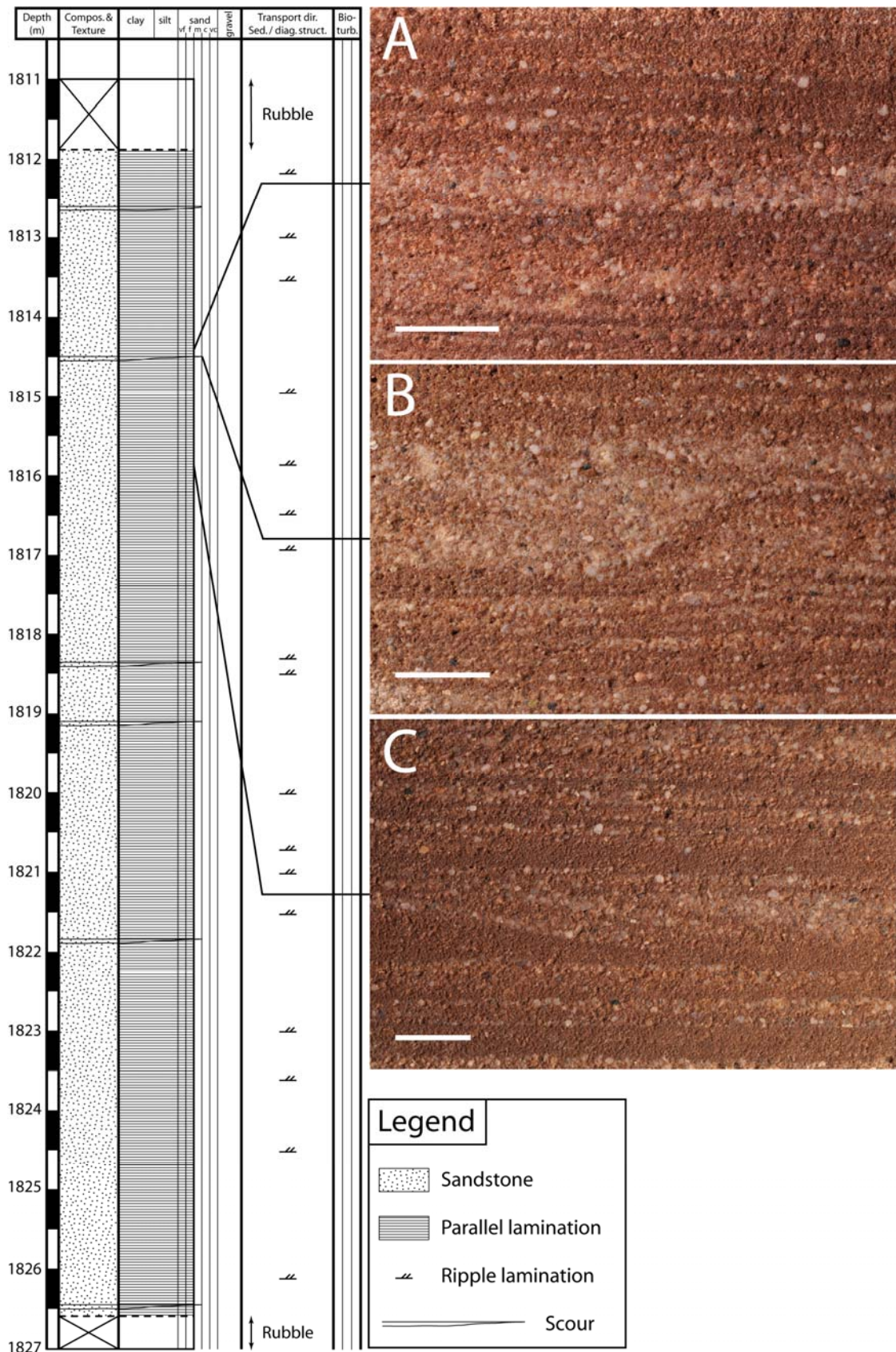
Fig. 7. Core description of the upper part of the Slochteren Formation in well KAM-01-S1. A: Alternation of coarse-grained, anhydrite-cemented (light colour) and fine-grained (red-brown colour) sand laminae. B: Small scour filled with coarse quartz sand and anhydrite grains and cement. C: Low-angle cross-laminated set. Scale bar in all three photos is 10 mm.

Fig. 8. Detail of lamina pairs.
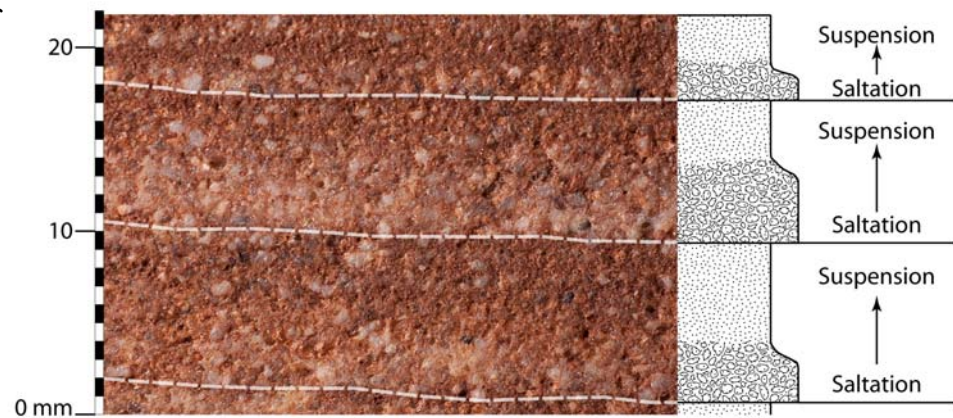
Thin section and cutting analysis

Arenite framework composition

The analysed sandstones are hybrid arenites with a quartzitic composition (Pettijohn, 1975; Zuffa, 1980), although abundances of the framework components vary slightly with grain size. Quartz is the dominant grain type (> 95%) and occurs in monocrystalline and polycrystalline forms. The latter is more abundant in coarser-grained laminae, and includes composite quartz (monomineralic, polycrystalline rock fragments of uncertain plutonic or high-grade metamorphic origin with grain size > 0.063 mm) and chert grains, whereas the monocrystalline quartz dominates in the finer laminae. Feldspar is scarce (<2%) and occurs preferentially in the finer-grained laminae. Locally, feldspars have been replaced by illite and/or kaolinite. Rock fragments are mostly concentrated in the coarser-grained laminae (2 to 3%) and are represented by low-grade metamorphic grains. Micas are absent. Detrital anhydrite grains are also present as framework components (5 to 10%) and are classified as non-carbonate intrabasinal grains (cf. Zuffa, 1980). They occur as monocrystalline grains (grain size 0.3 to 1.2 mm; Fig. 9A-C) and as composite grains made up of several anhydrite crystals and other siliciclastic grains, resembling desert-rose morphologies (grain size 1 to 3 mm; Fig. 10A-C). The first type of anhydrite grains is especially well preserved in the finer-grained laminae (Fig. 9A). In the coarser-grained laminae, these monocrystalline anhydrite grains have been partially or completely dissolved and are surrounded by pore-filling anhydrite cement with grain-boundary ghosts defined by haematite coatings (Fig. 9B) or by their optical properties such as birefringence color (Fig. 9C). Composite grains ("desert roses") are less abundant and their shape is especially clear in cutting samples from the KKP-GT-1 and KKP-GT-2 wells (Fig. 10A). In both wells, these grains appear well-rounded with lenticular anhydrite crystals and equidimensional siliciclastic particles visible at their surfaces (Fig. 10A).

Most of the quartz grains as well as other framework constituents show diffuse, inherited haematite coatings which are recognised by their occurrence at grain contacts (Fig. 9B and 9C, 11B).
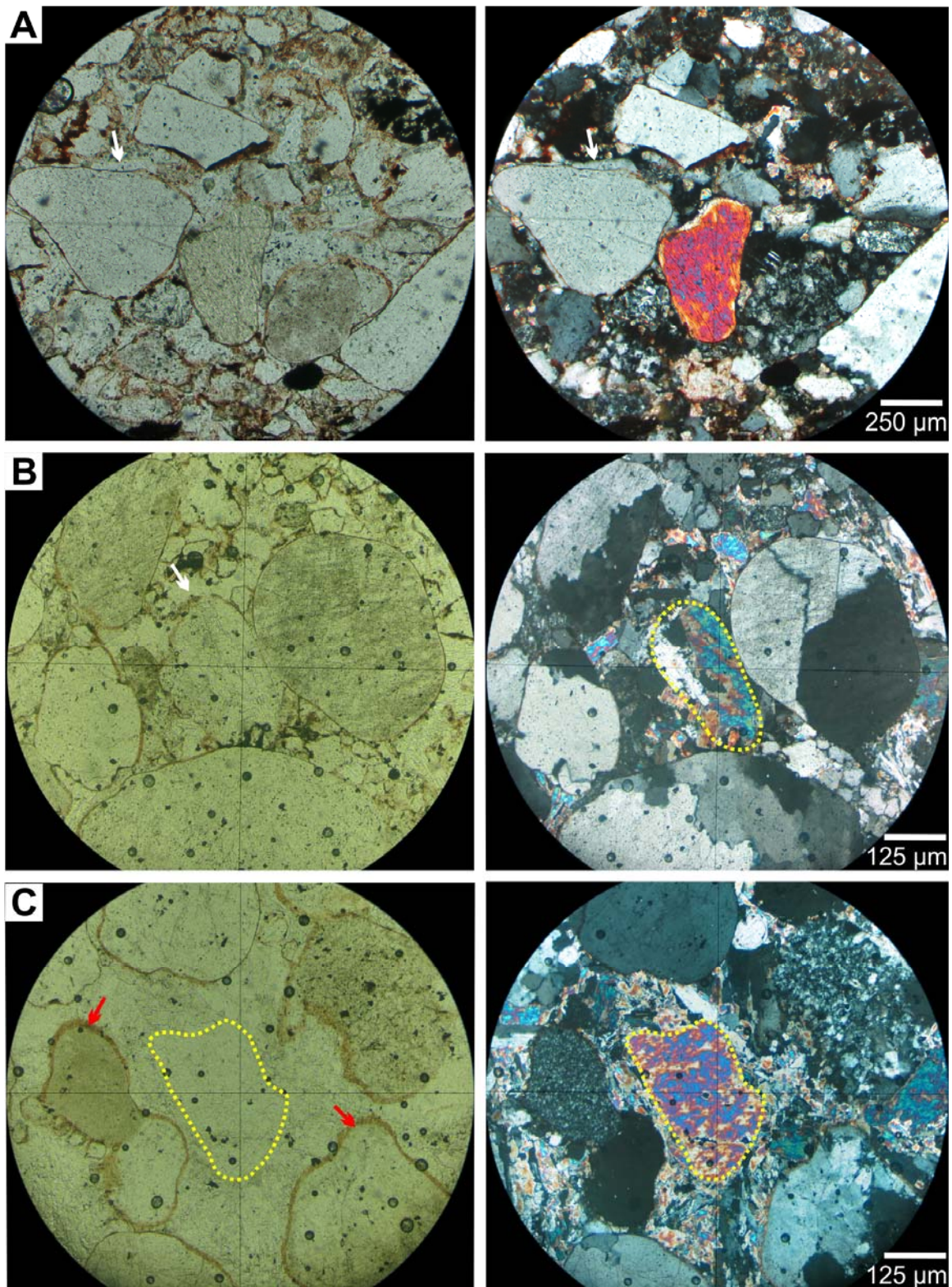
Fig. 9. Photomicrographs of: A) Monocrystalline grain of detrital anhydrite coated by haematite. White arrow indicates a quartz overgrowth postdating haematitic clay coating (1825.55 m depth); B) Grain boundary ghost of detrital anhydrite (yellow dashed line) defined by rounded haematite coating (white arrow). Grain is partially dissolved in the central part (1824 m depth); C) Grain ghost of detrital anhydrite (yellow dashed line) defined by its high birefringence violet-blue colour. Grain is partially dissolved at rims and surrounded by anhydrite cement becoming completely

unseen with one nicol. Red arrows indicate two examples of diffuse, inherited haematite coatings (1824 m depth).

Fig. 10. Detrital anhydrite composite grains at different scales. A) Example from cuttings. Notice the lenticular shape of anhydrite crystals (black arrow) and the equidimensionality of other siliciclastic particles visible at the surface of these grains (white arrows). B) and C) Examples from thin section. Yellow circle indicates the presence of an anhydrite composite grain with other siliciclastic grains included (grey arrows) (1824.55 m depth).

Diagenesis

- Compaction. Early grain rearrangement is manifested by point contacts between grains which lack early-formed haematitic clay coatings (Fig. 12A and B). Mechanical compaction is highlighted by the deformation of ductile grains such as anhydrite (Fig. 11A). This process resulted in denser sediment packing in the finer-grained laminae, whereas in coarser-grained laminae mechanical compaction was largely inhibited by early diagenetic cements. Chemical compaction generated elongate concavo-convex contacts. Pressure solution (grain-contact dissolution favoured by the presence of clay coatings) also occurred (Fig. 11B and 11C).
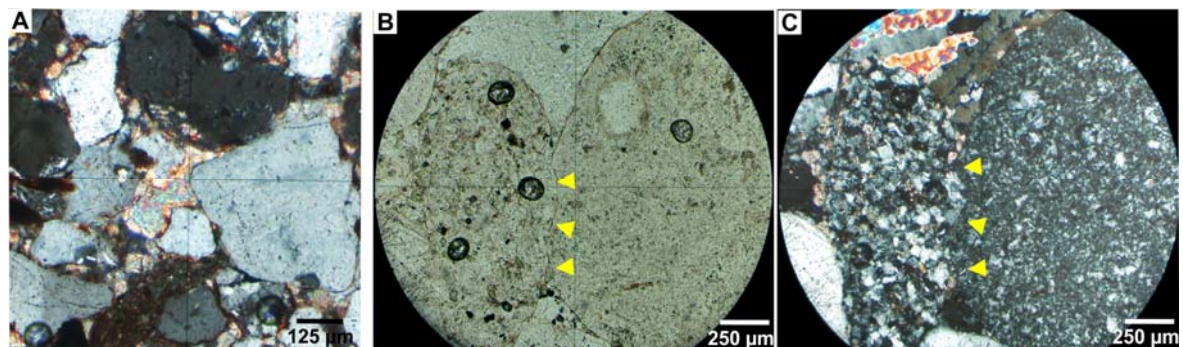
Fig. 11. Photomicrographs of mechanical and chemical compaction processes. A) Ductile deformation of a detrital anhydrite grain which is squeezed between coarser grains (1825.55 m depth). B and C) Pressure solution contact between a chert grain and a low-grade metamorphic rock fragment (yellow arrows) (1825.55 m depth).

- Cementation.

1) Haematitic clay coatings form thin and sharply outlined Fe-oxide-stained cutans that surround detrital grains with a meniscus shape at the grain contacts (Figs. 12A-B), strongly contrasting with the inherited fuzzy Fe-coatings (Figs. 9B-C) .

2) Dolomite grain rims are present as euhedral rhombs up to 0.04 mm in diameter. In coarse-grained laminae, rhombic crystals preferentially form linings around detrital grains (Fig. 12B) and are enclosed by anhydrite cement and quartz overgrowths (Fig. 12C). In fine-grained laminae, dolomite crystals are more abundant and also occur in open primary pores.

3) Quartz cement preferentially occurs in the coarse-grained laminae as thick (up to 0.03 mm) and continuous syntaxial overgrowths with euhedral faces. It postdates haematitic clay coatings and is surrounded by anhydrite cement (Figs. 9A, 12D). Locally, it occludes primary pores (Fig. 12D).

4) Anhydrite pore-filling cement with poikilotopic texture is concentrated in the coarse-grained laminae, where it completely occludes primary pores (Fig. 12E). "Floating-grain" texture is common (Figs. 12F). Dolomite crystals and kaolinite patches are usually hosted by this cement (Fig. 12G). Dissolution of anhydrite crystals (cement and grains) also occurs, generating secondary porosity (Fig. 12H).

5) Kaolinite pore-filling occurs as well-crystallized kaolinite masses that are mostly concentrated in coarse-grained laminae as erratically distributed patches. They usually occupy secondary pores and pore throats (Figs. 12G-I).

6) Carbonate pore-filling mostly occurs in the fine-grained laminae as coalescing crystals or discrete patches (0.1-0.2 mm sized). Replacement of detrital framework grains by this cement is common as well as its inclusion in anhydrite and kaolinite cements (Fig. 12J).

XRF analysis

High-resolution XRF core scanning allows for the extrapolation of spot observations on spatial compositional variability between the coarse- and fine-grained laminae to the scanned core slabs, and from there to the entire cored interval of well KAM-01-S1. To achieve this, log ratio plots of S/Si, Fe/Si, and S/Ca were used (Fig. 13). Ln{S/Si} is a measure of the abundance of S (associated with anhydrite cement and grains) relative to Si (associated with framework grains such as monocrystalline and polycrystalline quartz, rock fragments, and/or kaolinite). High values of this log-ratio are systematically associated with coarse-grained laminae, whereas fine-grained laminae show much lower values (Fig. 13). Ln{Fe/Si} illustrates the abundance of haematitic grain coatings and matrix (Fe) relative to Si. It shows high values in the fine-grained laminae versus low values in the coarse-grained laminae. Ln{S/Ca} may be interpreted as a measure of the abundance of anhydrite relative to carbonate cement (Ca). Its values are consistently low in the fine-grained laminae and high in the coarse-grained laminae.

INTERPRETATION AND DISCUSSION

Depositional setting

The deposits in the study area are located in an aeolian-dominated domain (Fig. 2). The parallel-laminated aeolian sandstone in the cored interval of well KAM-01-S1 is interpreted as an aeolian sandflat deposit. The normal grading and bimodal grain size

distribution in the horizontal laminae (Fig. 8) point to airborne sediment transport by saltation (coarse fraction) and suspension (fine fraction). This dual transport mechanism in a normally graded lamina pair is also reflected in the sharp decrease in Ln{S/Si} at the
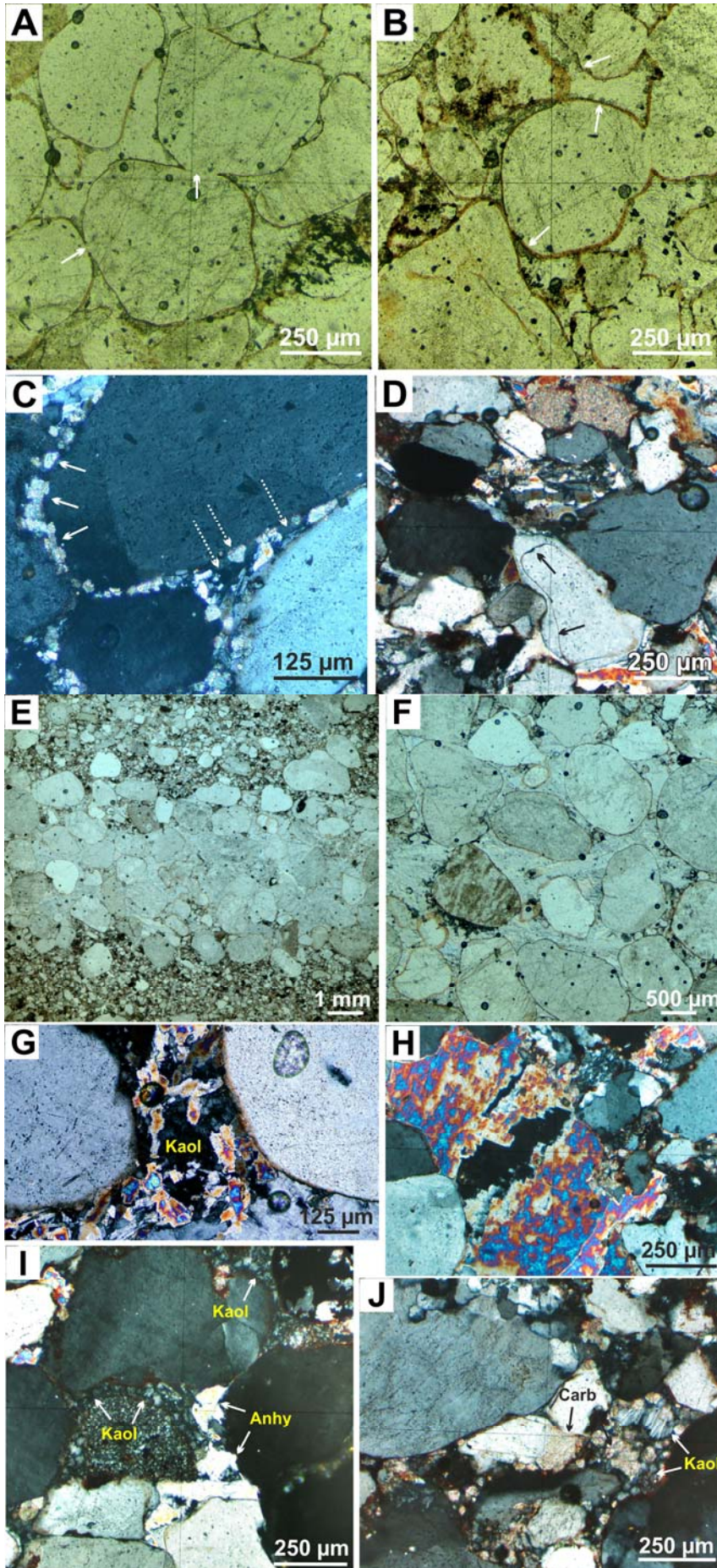
base of the lamina pair (Fig. 13, arrow at 1818.82 m depth approximately) followed by a gradual upward increase. The small scour depressions likely formed by wind eddies and the cross laminae formed by wind ripples. The absence of large-scale aeolian dune cross-bedding in the cored interval suggests that deposition of parallel-laminated sands occurred in a sheltered depression leeward of the TYH. The well-log expression of the cored interval is identical to that of the non-cored part of the Rotliegend succession (Fig. 4). We therefore propose that the lithofacies interpretation of the cored interval can be extrapolated to the entire succession in the well, with the exception of the anhydrite-cemented interval at 1900 to 1906 m depth (Fig. 4).

## Origin of detrital anhydrite/gypsum grains

The comparatively rare occurrence of haematite coatings marking the boundaries of anhydrite crystal ghosts provides evidence of their detrital origin. Their appearance suggests that they were transported together with other framework grains which also show inherited coatings. The coatings are most likely inherited because they do not uniformly cover most of the anhydrite/gypsum grains as might be expected if the coatings had formed during diagenesis. Similar haematite coatings have been observed in thin sections from well OWD-01, 50 km northeast of the study area (Fig. 1; Mijnlieff et al., 2011; their Appendix B5, p. 337). Detrital anhydrite/gypsum grains likely acted as nuclei for anhydrite cement precipitation as they are systematically surrounded by this pore-filling cement in the coarse-grained laminae. XRF results also support the detrital origin of anhydrite/gypsum grains, because high values of Ln{S/Si} in the coarse-grained laminae indicate that the vast majority of anhydrite/gypsum grains were transported and deposited together with this size fraction of the sands. This strongly size-selective nature of the anhydrite cement cannot be explained by fluid flow.

Groundwater ferricretes and/or gypscretes are common in arid climates (Wright et al., 1992). These hard surfaces have a much higher preservation potential in deserts than loose sediments. Hence, they can become an important component of the sediment (Gaupp and Okkerman, 2011; Mijnlieff et al. 2011). The source of the anhydrite/gypsum grains is

Fig. 12. Photomicrographs of the main diagenetic features of the Rotliegend sandstone in this area. A) Early grain rearrangement predating haematitic clay coatings (arrows) which locally show meniscus-shape at grain contacts (centre of the image) (1825.55 m depth; one nicol). B) Rhombic dolomite rim postdating haematitic clay coating (arrows) (1825.55 m depth; one nicol). C) Rhombic dolomite crystals forming a rim around detrital quartz (arrows) and enclosed by its overgrowths (doted arrows) (1825.55 m depth; crossed-nicols). D) Thick and continuous syntaxial quartz overgrowth, with euhedral faces, postdating haematitic clay coatings (arrow) (1824.55 m depth; crossed-nicols). E) Anhydrite poikilotopic pore-filling cement, restricted to the coarse-grained laminae (1818.80 m depth; crossed-nicols). F) Anhydrite pore-filling cement showing "floating grain" texture. Notice floating grains and point grain contacts (1818.80 m depth; crossed-nicols). G) Patch of well-crystallized kaolinite (Kaol) occupying secondary pores in anhydrite pore-filling cement (1818.80 m depth; crossed-nicols). H) Secondary porosity due to dissolution of anhydrite poikilotopic crystal (1818.80 m depth; crossed-nicols). I) Patch of well-crystallized kaolinite (Kaol) occupying pore throats and hosted by anhydrite cement (Anhy) (1824 m depth; crossed-nicols). J) Late carbonate pore-filling cement replacing quartz grain and its overgrowth as

well as carbonate patches (Carb) included in kaolinite cement (Kaol) (1818.80 m depth; crossed-nicols).

likely to have been in close proximity to the site of deposition, for these ductile grains have not been completely destroyed by mechanical impact shattering during aeolian transport (*cf*. Dutta et al., 1993). Log correlation of the three studied wells (Fig. 4) shows that the top of the 16 m thick anhydrite intervals in well KKP-GT-1 correlates with the base of the cored interval in KAM-01-S1. We suggest that the anhydrite/gypsum crusts at the location of the KKP-GT wells formed at the sediment surface, and the grains were deflated and transported over a distance of less than 2 km to the site of deposition.
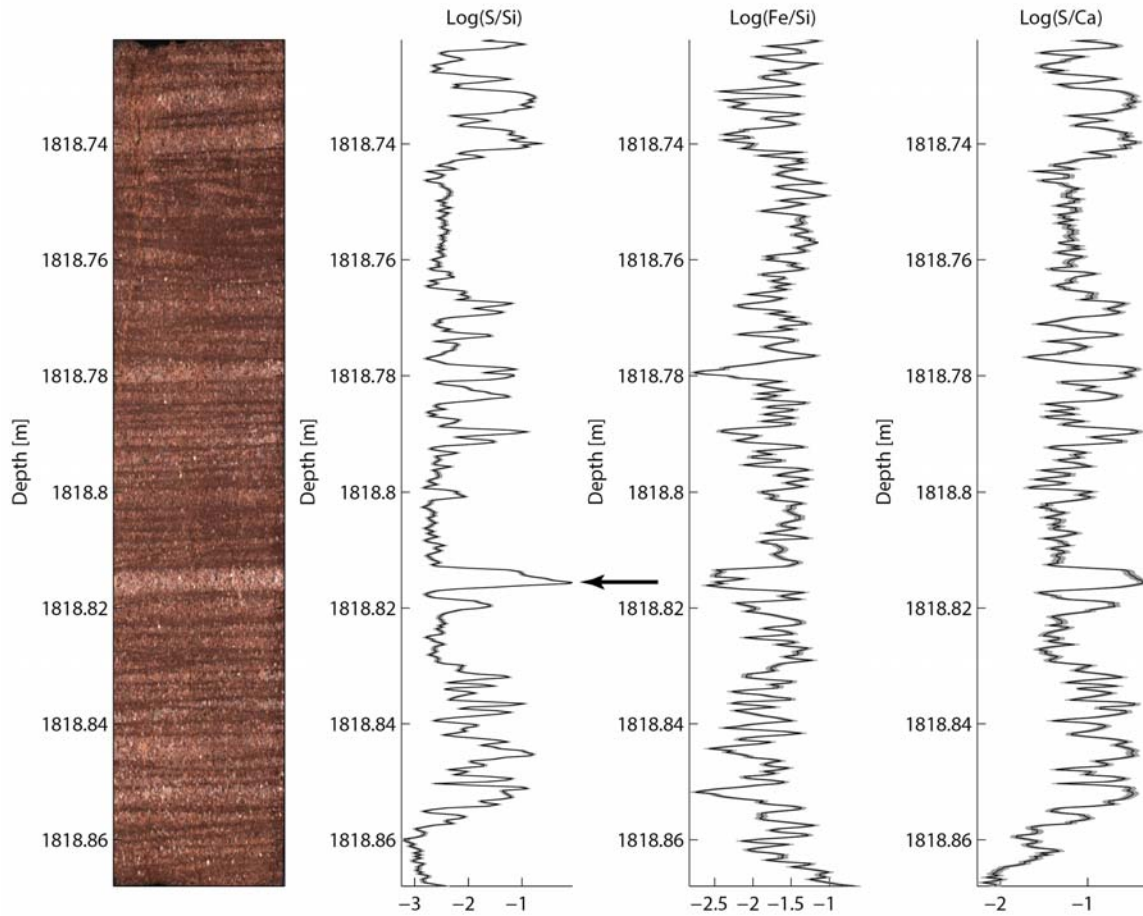

Fig. 13. Results of the core scan on a selected slab, 1818.72 – 1818.86 m depth. Grey bands: 90% or 95% confidence limits. Arrow: sharp decrease in Ln{S/Si} at the base of a lamina pair.

Timing and significance of diagenetic events

The sequence of diagenetic processes that affected the Rotliegend in this area was interpreted from the paragenetic relationships determined by petrographic analysis (Fig. 14).

The post-depositional evolution of the deposits has been controlled by near-surface and early diagenetic processes. Early compaction by grain rearrangement is highlighted by the absence of coatings at the contacts between detrital grains (Fig. 12A-B). The haematitic clay coatings which precipitated directly on the surface of the framework grains represent the first stage of cementation. This type of precipitation occurs in the vadose zone, likely

because of downward movement of meteoric water, as manifested by the observed meniscus shapes (Wright et al., 1992; Salem et al., 1998). XRF results indicate that fine-grained laminae reflect more haematitic coatings (higher Ln{Fe/Si}) relative to coarse-grained laminae, which can be explained by the relatively large specific surface area of framework grains in the fine-grained laminae, as well as the presence of Fe-rich matrix. Rhombic dolomite crystals postdate the aforementioned coatings and predate quartz overgrowths and anhydrite cement (Fig. 12C) as suggested by their inclusion in the former cements. Early dolomite can develop where the groundwater becomes progressively concentrated in cations such as Mg, among others, during downdip flow to the centre of the basin (Arakel, 1986; Metcalfe et al., 1994, Wright et al., 1992; Amthor and Okkerman, 1998). Petrographic evidence and the Ln{S/Ca} values point out the relative abundance of carbonates in the fine-grained laminae. The higher degree of compaction as well as the larger content of haematitic coatings and carbonates (presumably dolomite) in the fine-grained sandstone laminae likely inhibited the free flushing of water and favoured the preservation of detrital anhydrite grains. Well-developed quartz overgrowths suggest relatively high pore-network connectivity at the moment of its formation (Fig. 12E; Caracciolo et al., 2013; Henares et al., 2014). Furthermore, these quartz overgrowths are often covered by anhydrite cement, suggesting quartz likely precipitated shortly before the anhydrite. Early quartz cement has been reported as common in arid continental settings (Salem et al., 1998; Armitage et al., 2013). The surface temperature in deserts varies on a daily basis from subzero to more than 80ºC (Parton, 1984). Therefore, based on the timing of authigenic quartz formation and the relative scarcity of pressure solution contacts, it is likely that silica was supplied from dissolution of framework grains and dust by groundwater or dew (Waugh, 1970; McBride, 1989; McKeever, 1992; Critelli et al., 2008; Zaghloul et al., 2010; Perri et al., 2013). The anhydrite cement preserved large intergranular volumes and point contacts between grains ("floating-grain texture") which suggests precipitation soon after deposition (Fig. 12D; Seeman, 1982; Pye and Krinsley, 1986; Elias et al., 2004). XRF analysis demonstrates the predominance of this cement in the coarse-grained laminae (high Ln{S/Si}) relative to the fine-grained laminae. Petrographic observations reveal that anhydrite cement was locally sourced by partial or complete dissolution of detrital anhydrite/gypsum framework grains, whose relicts acted as nuclei for its re-precipitation as pore-filling cement. The scattered occurrence of replacive carbonates and kaolinite patches point out their late formation (Amthor and Okkerman, 1998).
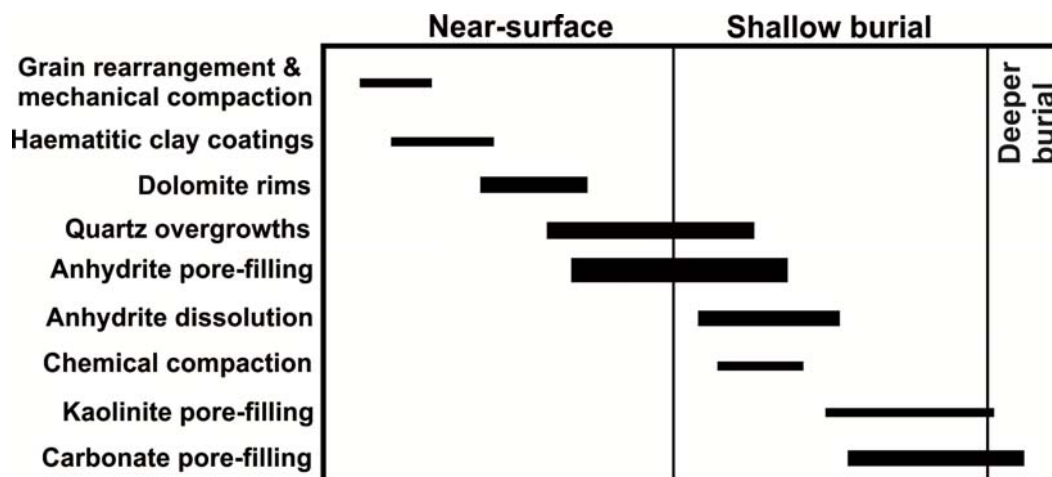
Fig. 14. Chronology of diagenetic processes, deduced by mutual textural relationships. Line length indicates approximate time extension whereas line thickness indicates intensity of each process.

Initial sediment properties

The proper recognition of anhydrite/gypsum grains as framework components has an important impact on the provenance signature and on minus-cement porosity (intergranular volume) reconstruction. Compositional signatures classify analysed sandstones as hybrid arenites with a quartzitic composition. Detrital anhydrite/gypsum grains are included in the non-carbonate intrabasinal class, and should not be considered in the traditional QFRf ternary diagram (Pettijohn, 1975; Zuffa, 1980).

In the present study as well as in other examples (Simpson and Loop, 1985; Barone et al., 2007, 2008) anhydrite/gypsum grains are volumetrically significant framework constituents, suggesting specific paleoenvironmental conditions, climate and geodynamic setting. In a sandstone classification system designed to predict diagenetic evolution, detrital anhydrite/gypsum grains should be classified as Lt, in order to stress the similarity of their diagenetic signature to that of other lithic sandstones.

The low preservation potential of anhydrite/gypsum grains (Simpson and Loop, 1985; Kendall, 1992; Kendall and Harwood, 1996; Manzi et al., 2005) and the difficult identification of their relicts introduce large uncertainties in reconstructions of their initial composition. Specifically, estimates of minus-cement porosity (intergranular volume) will be wrong if all anhydrite cement observed in our study would have been regarded as the fill of primary pores instead of local dissolution and precipitation of detrital framework grains. Such overestimation of initial porosity has a huge impact on the inferred diagenetic history (Ehrenberg, 1995; Paxton et al., 2002).

Spatial distribution of anhydrite cement in aeolian sandstone

The most likely source for the wind-transported detrital anhydrite/gypsum grains are gypscretes exposed in the close vicinity. These gypscretes usually develop desert rose morphologies and precipitate in the phreatic zone beneath ephemeral pools (Schreiber and El Tabakh, 2000). Subsequently, the gypscretes are exhumed by wind deflation and break up into rip-up clasts (Gralla, 1988) which can be entrained by air. Due to the mechanical and chemical instability of anhydrite/gypsum particles, their size is expected to decrease progressively along the aeolian transport pathway. Hence, their grain size may be used as an indicator for distance from the source (gypscrete body) as well as the location of the associated low-permeability streaks. In the sandstones analyzed, detrital anhydrite grains are mainly concentrated in the coarse sand fraction, indicating that aeolian transport was over a short distance only. Gaupp and Okkerman (2011) describe a similar occurrence of early anhydrite cement though restricted to the fine-grained sand fraction, which suggests an analogous scenario but in a more downwind position from the source (Fig. 15). Seismic and well logs from the surrounding area suggest that thick, gypsum-rich sedimentary bodies are common in the study area. Previous studies proposed a prevailing west-southwest aeolian transport direction for the southern rim of the SPB, parallel to the London-Brabant mountain range (Glennie, 1982). The results of our study, combined with the location of gypscretes and the prevailing wind direction, indicate that the spatial

distribution of anhydrite-cemented low-permeability intervals in aeolian reservoir rocks of the Rotliegend close to the interface with the Silverpit salt lake (Fig. 2) may be predicted (Fig. 15). The proposed model is valid in areas with an unconfined low-gradient palaeo-topography, as morphological irregularities may influence regional and local wind patterns.

Fig. 15. Conceptual model for the dispersion of detrital anhydrite/gypsum grains downwind of exhumed gypscrete bodies. Relative position indicated of: (1) coarse-grained, anhydrite-cemented sandstone laminae because of the occurrence of detrital anhydrite/gypsum grains in the coarse sand fraction (this study), and (2) fine-grained, anhydrite-cemented sandstone laminae (Gaupp and Okkerman, 2011) proposed in this study to have a similar origin.
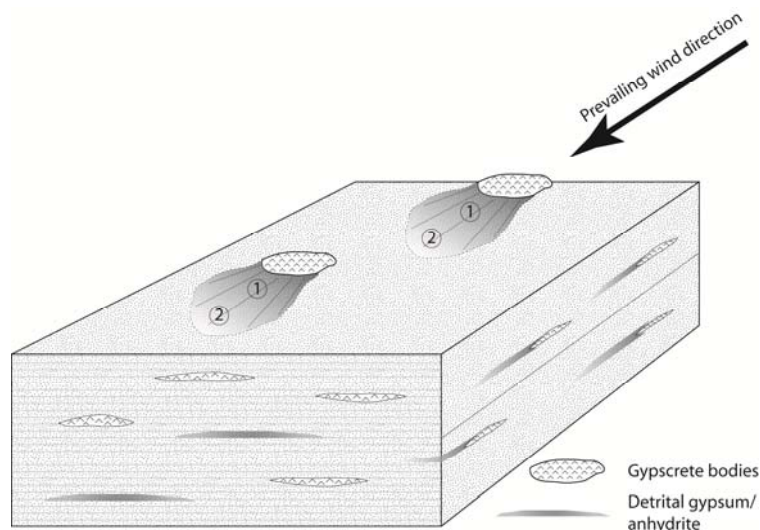
Impact on reservoir properties

Mature, well-sorted aeolian sediments are among the best potential reservoirs in the Rotliegend (Glennie et al., 1978; Walzebuck, 1993; Gaupp et al., 2005). However, the occurrence of horizontal, millimetre-thick, anhydrite-cemented, coarse-grained sandstone laminae is a contributor to high permeability anisotropy (Fig. 6A), high flow tortuosity and a low vertical-to-horizontal permeability ratio (Kv/Kh). The low-permeability streaks act as barriers or baffles in the flow pathway, causing lower-than expected flow rates and a deterioration of reservoir quality. Because similar scenarios have been reported in the literature on the Rotliegend (e.g. Gaupp and Okkerman, 2011), the proposed conceptual model may well be a generally applicable tool for predicting reservoir quality in similar settings. If anhydrite-rich layers (gypscretes) are recognised in seismic profiles or wells, downwind reservoir quality is likely to be poorer because of anhydrite cementation.

CONCLUSIONS

Our study shows that reservoir properties of Rotliegend aeolian sandstone have been negatively affected by the occurrence of extensive anhydrite-cemented intervals. An integrated approach including macroscopic and microscopic analyses of core, cuttings and well logs, combined with high-resolution XRF core scanning revealed that the anhydrite has a detrital origin. Upon partial or complete dissolution, anhydrite grains act as local source for anhydrite pore-filling cement which precipitates around the relicts of such grains. The recognition of the detrital character of the anhydrite/gypsum and its proper identification within the anhydrite pore-filling cement is crucial for the correct

interpretation of the initial framework composition (provenance) and minus-cement porosity / intergranular volume reconstructions. Along with the anhydrite cement, grain rearrangement and mechanical compaction as well as formation of haematitic clay coatings and dolomite rims represent the early (near-surface and shallow burial) diagenetic stage. Quartz overgrowths also occur, predating the formation of anhydrite cement. Kaolinite patches, chemical compaction and a second generation of carbonate cement constitute the late (deeper burial) diagenetic stage.

Detrital anhydrite/gypsum grains were transported by wind together with other framework grains and deposited on an aeolian sandflat, preferentially in the coarse fraction of normally-graded parallel-laminated sand. Transport distance of the detrital anhydrite/gypsum grains was short; otherwise the ductile grains would have completely disintegrated. Thick anhydrite intervals in the close proximity of the anhydrite-cemented sandstone are proposed as the source of the detrital anhydrite/gypsum grains. The composite anhydrite grains with desert rose appearance in cutting samples of the thick anhydrite intervals points to their formation as gypscretes by precipitation in the phreatic zone beneath ephemeral pools. Subsequent exhumation by wind deflation and weathering to rip-up clasts preceded wind transport. A conceptual predictive model is proposed for the dispersion and spatial distribution of the detrital anhydrite/gypsum, downwind of the gypscrete accumulations along the southern rim of the SPB where the prevailing west-southwest wind direction is known. The model can be used to reduce uncertainty in reservoir quality prediction of aeolian deposits in the vicinity of anhydrite accumulations.

# Acknowledgements

CHAPTER **6**

Conclusions

6. Conclusions

6.1. General Conclusions

The aim of this Thesis has been to relate depositional characteristics with the main early diagenetic processes in sandstone deposits and to evaluate their effect on petrophysical properties so that produced data can reduce uncertainty in Reservoir Quality models. For such purpose, well-constrained fluvial depositional environments have been studied from two Triassic red bed successions (TIBEM in Central SE Spain and Argana Basin in Western High Atlas, SW Morocco) that can be considered as reservoir-analogue outcrops of similar Triassic reservoirs.

Petrological study on the (from base to top) floodplain environment (overbank and channelized deposits) from Sequence II and braidplain environment from Sequence IV of the TIBEM, reveals an upward an increase in both textural (better sorting and roundness) and compositional (higher quartz content) maturity. This study coincides with the first compositional data set ever produced on the Triassic succession in the region. In addition, early diagenetic processes and resulting pore network characteristics also vary between sequences and among the different studied sedimentary deposits. In overbank deposits, a poorer sorting, a higher clay content and the confinement between gypsum-rich floodplain sediments favour greater mechanical compaction and the precipitation of poikilotopic pore-filling gypsum cement. Pore network is characterized by the smallest pore radii with OP values systematically lower than 16%. Channelized deposits in floodplain environment, which encompass meandering and straight channels, display intermediate mechanical compaction degree and variable amount and type of dominant authigenic phases depending on targeted depositional facies. The braided depositional environment is generally characterized by a better sorting, coarser grain size, lower clay content and higher content of rigid grains. Furthermore, is the one with the lowest mechanical compaction and K-feldspar overgrowths as the prevailing cementing phase. This sedimentary deposit is characterized by the greater pore radii and the highest OP values (up to 32%). Only in the gypsum-cemented slough channel facies and carbonate-cemented post-sedimentary fractures, OP values show an important reduction acting as potential barriers and/or baffles to fluid migration and compartmentalizing the potential reservoir. Analysed depositional environments can therefore be classified, from lower to greater quality as potential reservoir rocks, as follows (Fig. 1): overbank deposits (crevasse splay lobes and sheetfloods); channelized deposits (meandering and straight channels); and braided fluvial system. Despite the differences in burial history, similarities in composition, age, source area and depositional characteristics, which exert a primary control on early diagenetic porosity modification, justify satisfactorily the use of TIBEM as outcrop analogue for the TAGI reservoir.

Diagenetic differences have been reported between: sequences deposited under different allogenic factors (sequences II and IV); between depositional environments developed under the same allogenic factors (overbank and channelized deposits from sequence II); and between the different depositional facies within a given sedimentary

deposit developed under the same autogenic factors (e.g. meandering channel from sequence II).
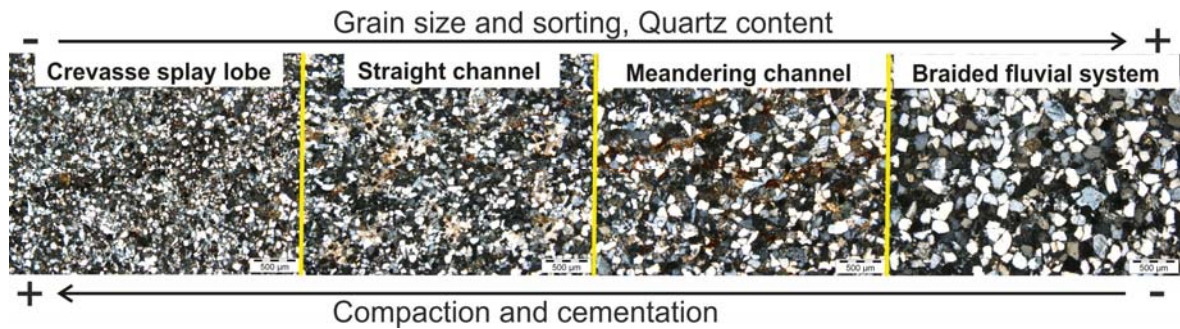
Fig. 1. Photomicrographs (XPL) showing the differences in detrital and diagenetic fabrics among some of the analysed depositional environments in the TIBEM succession.

A more exhaustive investigation on the most influential depositionally-controlled parameters in three different fluvial depositional systems – meandering system from TIBEM (Central SE Spain) as well as braided and straight systems from Argana Basin (Western High Atlas, SW Morocco) – reveals in all cases that early diagenetic deterioration of primary porosity and permeability has a direct relation to sedimentary dynamics and, thus, to depositional fabric according to facies.

In the different analysed sub-environments of the meandering fluvial example – main channel, point bar, scroll bar and chute channel – sandstone framework composition is relatively homogeneous whereas depositional fabric is highly heterogeneous with detrital matrix distribution being strongly facies-related. In the channel area, matrix is more abundant at the channel margin and decreases towards the lower point bar, whereas in the floodplain area matrix content increases from the upper point bar to the scroll bar. Differences in diagenesis are attributed to small-scale internal heterogeneities in matrix content whose occurrence favours mechanical compaction and inhibits early pervasive cement formation. Multivariate statistical processing of petrographic and petrophysical data demonstrates that, in matrix-rich facies, large (> 1 µm) and well-connected primary intergranular pores are more efficiently preserved which contributes to higher permeability values. Secondary porosity, which does not show obvious relationship with facies distribution, is mostly related to smaller (< 1 µm) pores that do not contribute to permeability enhancement. The spatial distribution of detrital matrix is mainly controlled by hydraulic sorting effect as proven by the same distribution pattern that other hydraulic sorting-sensitive variables such as rip-up clasts, heavy minerals and micas. Furthermore, reservoir quality distribution 3D model perfectly fits to depositional facies distribution so it can be used to predict postdepositional, facies-related preferential-flow pathways that improve ultimate recovery of EOR strategies in similar fluvial siliciclastic reservoirs.

Application of O/BO characterization workflow in the former example results in a better quantification and more accurate modelling of stratal geometries and petrophysical properties distribution thus contributing to depositional model refinement. By contrasting depositional and diagenetic features in well-exposed outcrop and behind-outcrop cores, the processing of subsurface data (e.g. well logs) is encouraged by extrapolation from microscale anisotropies of porosity and permeability to mesoscale heterogeneity.

Depositional fabric in studied braided and straight fluvial systems is characterized by the occurrence of three different types of rip-clasts, classified according to its composition and mechanical behaviour as: muddy rip-up clasts without dolomite crystals; dolomitic muddy rip-up clasts with intermediate dolomite crystals proportions; and dolomite crystalline rip-up clasts mainly composed by dolomite crystals. These intrabasinal components result from the erosion of coeval phreatic dolocretes and associated muddy floodplain sediments and shows a spatial distribution strongly controlled by depositional facies (i.e. grain size). Intense mechanical compaction of highly ductile muddy rip-up clasts (up to 20% of sandstone framework) results in early reduction of primary porosity and irreversible loss of IGV which can decrease up to less than a 10% remaining. Conversely, dolomite crystalline rip-up clasts behave as rigid (non-deformed) framework grains. However, they act as local source of dolomite cement and as nuclei for early dolomite precipitation which occludes remnant primary porosity but partially inhibits mechanical compaction, thus preserving IGV. When around 10% of sandstone framework is represented by these type of rip-up clasts, dolomite cement only can constitute up to 25% of total rock composition. Preservation of IGV may considerably enhance reservoir quality by later carbonate dissolution processes. At pore-and depositional-scales, spatial distribution of rip-up clasts in continuous layers (e.g. muddy rip-up clasts) or in specific depositional facies (e.g. dolomite crystalline rip-up clasts) and their associated diagenetic processes may impact reservoir quality by generation of vertical and 3D fluid flow barriers and baffles that compartmentalize the reservoir. These results have direct application for better understanding of reservoir quality distribution in analogous hydrocarbon-bearing basins such as in the conjugate Atlantic margin of the Bay of Fundy (Nova Scotia, Canada).

The complementary study carried out on the aeolian depositional facies from the Rotliegend (Upper Permian; The Netherlands) geothermal reservoir also emphasize the importance of depositional controls, such as intrabasinal components and depositional texture, on both early diagenetic processes and reservoir quality distribution. In this case, depositional texture is characterized by alternating very fine- and very coarse-grained sandstone laminae, with the latter systematically cemented by anhydrite pore-filling cement as demonstrated by combined thin-section and XRF core scanning analysis. Occurrence of detrital anhydrite/gypsum grains may act as local source for anhydrite cement precipitation preferentially in the more (primary) permeable, coarser-grained laminae. These horizontal, mm-thick, anhydrite-cemented sandstone laminae contribute to higher permeability anisotropy and higher flow tortuosity causing lower-than expected flow rates and thus reservoir quality deterioration. Due to the mechanical and chemical instability of anhydrite/gypsum detrital particles, their grain size may be used as an indicator of source distance, interpreted as nearby gypscretes recognized in seismic and well-logs. These results combined with the prevailing west-southwest aeolian transport direction for the southern rim of the SPB lead to the proposal of a conceptual predictive model for low-permeability streak distribution that reduce uncertainty in reservoir quality prediction.

The multidisciplinary analytical workflow developed in this Thesis highlights the significance of diagenetic studies in reservoir quality prediction models. By using of outcrop-derived data, diagenetic analysis can be stressed to utmost when placed in a well-

131

constrained depositional framework maximizing its use as input in upscaling reservoir properties.

6.2. Conclusiones Generales

El objetivo de esta Tesis ha sido el de relacionar las características deposicionales con los principales procesos diagenéticos temprano en depósitos de areniscas así como evaluar su efecto sobre las propiedades petrofísicas de manera que los datos producidos puedan reducir la incertidumbre en los modelos de calidad de almacén (*reservoir quality*). Con tal propósito, se ha seleccionado ambientes deposicionales fluviales bien caracterizados sedimentológicamente procedentes de la sucesión triásica de la parte SE del centro de España (aquí referida como TIBEM) así como en la cuenca de Argana (Alto Atlas occidental, SW de Marruecos) los cuales se pueden considerar como análogos de afloramiento ideales de una serie de conocidos almacenes triásicos entre los que se incluyen los depósitos del TAGI (Trias Argilo-Gréseux Inférieur) por todo el norte de África así como los depósitos triásicos en Bay of Fundy (Nova Scotia, Canadá).

El estudio petrológico (de base hacia techo) en la llanura de inundación (que incluye depósitos de desbordamiento y canalizados) de la secuencia II y en el ambiente de llanura trenzada de secuencia IV del TIBEM revela un significante incremento de madurez tanto textural (mejor granoselección y redondeamiento) como composicional (mayor contenido en cuarzo) hacia arriba en la sucesión. Este estudio aporta el primer conjunto de datos composicionales producido hasta la fecha en el triásico de esta región. Además, los procesos diagenéticos tempranos y el sistema de poros resultante también varían entre las distintas secuencias y entre los diferentes depósitos sedimentarios estudiados. Los depósitos de arenisca de desbordamiento, una peor granoselección, un mayor contenido en arcilla y el confinamiento entre sedimentos finos de la llanura de inundación ricos en yeso favorecen una mayor compactación mecánica y la precipitación de cemento de yeso poiquilotópico. El sistema de poros se caracteriza por los menores tamaños de poro y valores de porosidad abierta sistemáticamente inferiores a 16%. Los depósitos canalizados de la llanura de inundación, que incluyen sistemas fluviales de estilo meandriforme y rectilíneo, muestran grados de compactación mecánica intermedia así como cantidades y tipo de fase autigénica dominante variables en función de las facies deposicional. La llanura trenzada se caracteriza por una mejor granoselección, mayor tamaño de grano, menor contenido en arcilla y mayor contenido de granos rígidos. Más aún, este ambiente es el que presenta la menor compactación con el recrecimiento de feldespato potásico siendo la principal fase cementante. Este depósito sedimentario presenta los mayores tamaños de poro así como los valores de porosidad abierta más elevados (hasta 32%). Sólo en las facies de canal abandonado cementadas por yeso así como de fracturas postdeposicionales cementadas por carbonato, los valores de porosidad abierta muestra una importante reducción actuando así como potenciales barreras o bafles para la migración de fluidos las cuales pueden compartimentar el almacén. Los ambientes deposicionales analizados pueden entonces clasificarse, de menor a mayor calidad como potencial roca almacén, como sigue (Fig. 1): depósitos de desbordamiento (lóbulos de crevasse y sheetfloods), depósitos canalizados (sistemas fluviales meandriforme y rectilíneo) y llanura trenzada. A pesar de las diferencias en la historia de enterramiento, las similitudes en composición, edad, área fuente y características deposicionales, lo cual ejerce un control primario sobre

la reducción diagenética temprana de la porosidad, justifican satisfactoriamente el uso de TIBEM como análogo de afloramiento del almacén del TAGI.

Se ha identificado diferencias diagenéticas entre: secuencias depositadas bajo diferentes factores alogénicos (secuencia II y IV); entre ambientes deposicionales desarrollados bajo los mismo factores alogénicos (depósitos de desbordamiento y depósitos canalizados de la secuencia II); así como entre diferentes facies deposicionales dentro de un mismo deposito sedimentario desarrollado bajo los mismos factores autogénicos (p.e. canal meandriforme de la secuencia II).

Una investigación más exhaustiva sobre la relación entre los parámetros más influyentes controlados deposicionalmente y la distribución espacial y temporal de los procesos diagenéticos desarrollada en tres sistemas deposicionales diferentes - depósitos de canal meandriforme del TIBEM (parte SE del centro de España) así como en los depósitos de los sistemas fluviales trenzado y rectilíneo de la cuenca de Argana (Alto Atlas occidental, SW de Marruecos) – pone de manifiesto en todos los casos que el deterioro diagenético temprano de la porosidad y la permeabilidad tiene una relación directa con la dinámica sedimentaria y por tanto con la fábrica deposicional según las facies.

En los diferentes sub-ambientse analizados el ejemplo meandriforme - canal, barra de meandro (*point bar*), barra de *scroll* y canal de chute- la composición de la arenisca es relativamente homogénea mientras que la fábrica deposicional es altamente heterogénea con la distribución de la matriz detrítica fuertemente controlada por las facies. En el área de canal, la matriz es más abundante en el margen del canal y decrece hacia la barra de meandro inferior, mientras que en el área de la llanura de inundación el contenido en matriz aumenta desde la barra de meandro superior hasta la barra de scroll. Diferencias en la diagénesis son atribuidas a heterogeneidades internas de pequeña de escala relacionadas con el contenido en matriz, el cual favorece la compactación mecánica pero inhibe la precipitación temprana de cementos. El procesamiento estadístico multivariante de los datos integrados demuestra que los poros primarios intergranulares, mejor interconectados y de mayor tamaño (>1 µm) son los principales contribuyentes de la permeabilidad en las muestras más ricas en matriz. La porosidad secundaria no parece estar relacionada con la distribución de facies y parce estar más asociada con poros de menor tamaño (<1 µm) e irregularmente distribuidos los cuales no mejoran la permeabilidad. La distribución de la matriz está controlada principalmente por procesos de selección hidráulica como prueban similares patrones de distribución de otras variables sensibles a este proceso tales como rip-up clasts, minerales pesados y micas. Más aún, el modelo 3D de distribución de calidad del almacén encaja perfectamente con la distribución de facies deposicionales con lo que puede ser utilizado para identificar potenciales trayectorias postdeposicionales preferentes de fluidos y ser aplicado con éxito en las estrategias de recuperación mejora de petróleo en almacenes siliciclásticos similares.

La aplicación del flujo de trabajo para la caracterización O/BO en el ejemplo anterior ha resultado en una mejor cuantificación y un modelado más preciso de las geometrías de estratos y de la distribución de propiedades petrofísicas lo cual contribuye al refinamiento del modelo deposicional. Mediante el contraste de los rasgos deposicionales y diagenéticos entre afloramiento y testigos de tras-afloramiento, se optimiza el procesado de los datos de subsuelo (p.e. registros de pozos) a través de la extrapolación de las

anisotropías de porosidad y permeabilidad a microescala a las heterogeneidades a mesoescala.

En los depósitos fluviales trenzado y rectilíneo de la cuenca de Argana, la presencia y abundancia de diferentes tipos de *rip-clasts* tiene un control directo y sustancial sobre la evolución diagenética temprana y el consecuente deterioro del almacén. Una clasificación propia de estos granos de acuerdo a su composición y comportamiento mecánico resulta en tres tipos principales denominados: rip-clasts arcillosos, rip-clasts arcilloso-dolomíticos y rip-clasts dolomíticos cristalinos. Los rip-clasts arcillosos se comportan como granos dúctiles y su presencia en el esqueleto de la arenisca (hasta un 20%) resulta en una reducción temprana importante de la porosidad primaria con una pérdida irreversible del volumen intergranular (*IGV*) (menos del 10% restante). Contrariamente, los rip-clasts dolomíticos cristalinos actúan como granos rígidos contra la compactación mecánica pero favorecen la precipitación de cemento temprano de dolomita el ocluye la porosidad primaria pero preserva el IGV. Cuando alrededor del 10% del esqueleto de la arenisca está representado por estos granos, sólo el cemento de dolomita puede llegar a reprsentar el 25% de la composición total de la roca. A escala deposicional y de poro, la distribución espacial de los rip-clasts en láminas continuas (p.e. los rip-clasts arcillosos) o en facies deposicionales específicas (p.e. los rip-clasts dolomíticos cristalinos) junto con sus procesos diagenéticos asociados pueden afectar a la calidad del almacén mediante la generación de barreras o bafles para la migración de fluidos, verticales y 3D, provocando así su compartimentación. Las estimaciones cuantitativas obtenidas sobre la reducción de la porosidad primaria por compactación y cementación en función de la abundancia de estos tipos de granos proporcionan datos útiles para un mejor entendimiento de la calidad del almacén en cuencas análogas como el margen conjugado atlántico en la Bay of Fundy (Nova Scotia, Canada).

Un caso de estudio adicional se presenta como parte de esta Tesis, en el cual se sigue el mismo enfoque de relación entre rasgos deposicionales y procesos diagenéticos tempranos para predecir su impacto en la calidad del almacén. Este estudio estuvo motivado por la necesidad de entender unas tasas de producción más bajas de lo esperado en un pozo geotérmico en facies eólicas del almacén del Rotliegend (Pérmico Superior, Holanda). En este caso, el estudio diagenético incorpora datos petrofísicos y de fluorescencia de rayos-X de alta resolución en escaneo de testigos y se integra en un sólido marco sedimentológico caracterizado mediante sísmica, registros de pozo y testigos de subsuelo. La textura deposicional fue caracterizada a escala de testigo y de lámina delgada consistiendo en una alternancia de láminas de grano muy fino y grueso, con estas últimas sistemáticamente cementadas por anhidrita. La identificación de granos detríticos de anhidrita/yeso apunta a éstos como la potencial fuente local para el cemento de anhidrita el cual habría precipitado las láminas de mayor tamaño de grano y por tanto más permeables. Debido a la inestabilidad de las partículas de anhidrita/yeso, su tamaño de grano puede usarse como indicador de distancia hasta el área fuente, en este caso interpretada como unas gypsicretas cercanas. Mediante la combinación de estos resultados con la dirección oeste-suroeste preferente de transporte eólico, se propone un modelo conceptual predictivo para la distribución de estas láminas de baja permeabilidad el cual ayuda a reducir la incertidumbre en la predicción de la calidad del almacén.

El flujo de trabajo multidisciplinar desarrollado en esta Tesis pone de relieve la importancia de los estudios diagenéticos en los modelos de predicción de calidad de almacenes. Mediante el uso de datos derivados de afloramiento, los análisis diagenéticos pueden ser exprimidos al máximo cuando se enmarcan dentro de un contexto deposicional bien caracterizado maximizando así su uso como datos de entrada para el *upscaling* de las propiedades del almacén.

6.3. Forthcoming research

Besides the extensive fieldwork, detailed core description and exhaustive sample analysis for determining the relationships between depositional controls and diagenetically-induced heterogeneities, other approaches are being used that complement and constrain the results presented in this Thesis and lay the foundation for future research. This new perspective includes: chemostratigraphy and automated mineralogy developed in collaboration with Chemostrat Ltd. (service company for the oil industry), University of Geneva (Prof. Andrea Moscariello). A brief description of the rationale for the use of this techniques and the results obtained to date are reported below:

Chemostratigraphy

The technique of elemental chemostratigraphy uses changes in elemental composition, determined from whole rock inorganic geochemistry, to define stratigraphic frameworks. However, its use in the oil and gas industry has proliferated over the past decade (Pearce et al., 2005a, b; Ratcliffe et al., 2006; Hildred et al., 2010; Ratcliffe et al., 2010) as a result of the growing realization of the independent and objective characterization and correlation it can provide. Because of that objectivity and independence, it is commonly employed to provide an alternative solution where other stratigraphic methods are providing conflicting models. Resultant elemental data set is then used to model changes in geological features such as sediment provenance (Armstrong et al., 2004; Pearce et al., 2005a, b), paleoclimate (Retallack, 1997; Armstrong et al., 2004; Ratcliffe et al., 2010), basin anoxia (English, 1999; Algeo et al., 2004; Ratcliffe et al., 2012a; Sano et al., 2013), fluctuations in terrigenous input (Davies et al., 2014) or simple lithological variations. However, despite the numerous studies and their proposed geological interpretations, there is still very little literature (North et al., 2005; Davies et al., 2014) dealing with validation of chemostratigraphic correlations against physical chronostratigraphic correlations.

Cooperation rationale between the University of Granada and Chemostrat Ltd. lies on test the integration of high precision inorganic geochemistry with high resolution petrographic analysis to link sediment compositional signatures to sediment physical properties (e.g. preferential concentrations of chemical elements and correspondent petrographic classes to depositional facies). The key steps of the workflow adopted are (i) sample preparation and analysis, (ii) data processing and (iii) data modelling. Cooperation with Chemostrat Ltd. (UK Office) started in October 2014 and, from this moment, it has materialized through 5 stays (two weeks/each). The preliminary results of this cooperation have been already presented at the AAPG Conference "Siliciclastic Reservoirs of Middle

East" (Caracciolo et al., 2015) and the 31st IAS Meeting in Sedimentology (Caracciolo et al., 2015) and are now to be submitted to Journal of Marine and Petroleum Geology:

(i)   Samples were disaggregated and subsequently ground in agate to produce a homogeneous powder which was then prepared for geochemical analyses by employing the lithium metaborate (alkali) fusion procedure advocated by Jarvis & Jarvis (1992a, b). Following this, each sample was subjected to analysis via accredited inductively-coupled plasma optical emission spectrometry (ICP-OES) and inductively-coupled plasma mass spectrometry (ICP-MS) instruments with quantitative data being acquired for fifty elements. The 50 elements quantitatively acquired include: 10 major element oxides (e.g., Al_2O_3, SiO_2, TiO_2, Fe_2O_3, MnO, MgO, CaO, Na_2O, K_2O and P_2O_5), 26 trace elements (e.g., Ba, Be, Co, Cr, Cs, Cu, Ga, Hf, Mo, Nb, Ni, Pb, Rb, S, Sc, Sn, Sr, Ta, Th, Tl, U, V, W, Y, Zn and Zr), and 14 rare earth elements (REEs; e.g., La, Ce, Pr, Nd, Sm, Eu, Gd, Tb, Dy, Ho, Er, Tm, Yb and Lu). In addition, REEs have been categorised as light (LREEs - La, Ce, Pr and Nd), middle (MREEs - Sm, Eu, Gd, Tb and Dy) and heavy rare earth elements (HREEs - Ho, Er, Tm, Yb and Lu).

The precision of the geochemical data acquired by the ICP analyses has been determined by replicate analyses of multiple preparations of certified rock standard reference materials (SRMs), together with duplicate preparations of three unknown samples, which have been analysed on a routine basis along with each of the samples. For this study, precision error for the major element data is found to be better than 2% overall and is around 3% for the high abundance trace element data, such as the Sr, Ba, Zr and Cr data. The ICP-MS analyses acquire data for trace elements and REEs - these data generally are less precise (ca. 5% precision error) - as such elements tend to occur in very low concentrations, sometimes close to the detection limit. Precision error for the W, Tl and Sn data ranges from 10% to 20%, thus these data have not been included in any later interpretations. With reference to the SRMs, the absolute accuracy of all the data are generally considered to lie within the range of error achieved for multi-determinations of the same sample.

For the high resolution petrographic analysis, petrographic dataset, methodology and general conclusions about controlling factors on diagenetic heterogeneity are the same included in Henares et al. (2016a).

(ii)   Information from petrographic analysis has been integrated into the chemostratigraphic dataset by means of multivariate statistical analysis. Preliminary results reveal the link between REEs, as Cs, Ga, Rb and La, with the presence of mud intraclasts and high matrix concentrations. Ga/Rb vs K_2O/Rb were extremely useful in identifying the presence of K-feldspar overgrowths while Al_2O_3/SiO_2 signature perfectly fits variations in grain size, recognizing even finning-upwards successions. The gypsum cement occurrence is strongly connected to S concentration whereas CaO concentration is not fully related to the amount of carbonate cements. A-CN-K, CaCO3-(MnO)FeCO3-MgCO3 plots provide insight on the origin of carbonate cementing phases. Results demonstrate how a combined petrographic-chemical multidisciplinary approach nourishes the characterization of microscale attributes for its use in RQ prediction models.

(iii)   Chemical signatures are currently being modelled for its validation it with the published 3D facies and RQI models. (Henares et al., 2016a).

Automated mineralogy

QEMSCAN® is an automated petrography system based around a SEM. The addition of EDX spectroscopy detectors and an extensive mineral database enables the identification of minerals and other compounds in-situ. The sample surface is scanned along a grid pattern, where each node is identified as a mineral, other compound or as pore space. The selected grid resolution defines a mineral map as a matrix of pixels each containing detailed chemical information.

The automated mineralogy system produces rich digital petrography data, including:

- Bulk chemistry and mineralogy
- Grain counts and size distribution
- Precise measures of porosity
- Morphology of rock matrix and pore space
- Clay and cement volumes
- Mineral association data
- 2D spatial mineral and porosity maps

Despite the advances in instrumentation and associated quantification techniques, mineral analysis methods are prone to a range of uncertainties. For instance, data derived from traditional mineralogical analytical methods may be subject to potentially large errors; optical analysis can be controlled by grain-size and the experience of the petrographer whilst X-ray diffraction (XRD) can be influenced by the presence of phases with variable or poor crystallinity and may be sensitive to differences in sample preparation. On the other hand, QEMSCAN® technology (Fig. 1) is designed to characterise and visualise the distribution of detrital and diagenetic phases and porosity in cuttings, core and outcrop samples based on the analytical reproducibility and the reference to baseline geochemical data from X-ray fluorescence analyses. Still, in case of clay-rich or pyroclastic-rich reservoir rocks, QEMSCAN® technology is routinely supplemented by XRD and SEM studies in order to have a better definition on mineral phases having similar chemistry but different crystallographic characteristics (e.g. clay minerals, zeolites, some inosilicates).

The QEMSCAN® analysis has been performed on 19 samples recovered from a fully-cored, 22-m-depth, behind-outcrop well targeting the entire K2 unit (braidplain of sequence IV). Previous works (Henares et al., 2014a) on outcrop samples include petrographic analysis and petrophysical measurements. Through the comparison of compositional/petrophysical information from both sources (surface and subsurface) within a well-constrained sedimentological framework, a comprehensive O/BO characterization will be produce in the near future. Objectives of the QEMSCAN® study performed in cooperation with the University of Geneva are:

- Generate true mineralogical vertical log with minerals quantified to be used to validate petrophysical log evaluations
- Evaluate the nature and quantify pore-occluding minerals

- Generate an independent density curve based on true mineralogy used to calibrate and validate existing wireline logs.
- Generation of an independent 2D porosity vertical log which can give a fair indication of reservoir properties variability in absence of wireline logs or conventional core analyses.

Automated mineral and textural characterization was performed using a FEI QEMSCAN® Quanta 650F facility at the Department of Earth Sciences (University of Geneva/Switzerland). Mineral phase identification relies on the combination of back-scattered electron (BSE) brightness values, low-count energy-dispersive X-ray spectra (EDS) and X-ray count rate giving information on the elemental composition. Following the acquisition, individual X-ray spectrum is compared against a library of known spectra and a mineral name is assigned to each individual acquisition point. The X-ray EDS spectra library is provided by FEI Company and has been further developed in-house using different natural standards. Measurements were performed on the carbon-coated samples at high vacuum conditions using an acceleration voltage of 15 kV and probe current of 10 nA. The X-ray acquisition time was 10 ms per pixel with a point-spacing of 5 μm. Up to 122 individual fields were measured in each sample whereby the size of single field was 1.5 x 1.5 mm.

The preliminary results highlight important changes in mineralogy especially regarding the interstitial components. Framework composition is constant throughout the analysed succession with quartz and K-feldspar being the most abundant minerals. The most important indication provided by the automated mineralogy approach is that the lower and upper parts experienced a different diagenetic history which triggered to different reservoir quality. Samples from the lower part are fine-grained sandstone, with low intergranular volume, moderate compaction and interstitial component being mostly represented by K-feldspar overgrowth and illite (partially recrystallized). Samples from the upper part display considerably higher intergranular volume due to the early precipitation of gypsum cement and, to a lesser extent, of calcite-dolomite cements. According to QEMSCAN® data porosity values vary from an average of $\geq 20\%$ porosity for samples from the lower part of the succession to $\leq 10\%$ for those from the upper part (Fig. 1). Porosity trends from both outcrop and core samples are very similar remarking the potential of the QEMSCAN® technique and the useful applicability of reservoir-analogue outcrop studies for reservoir quality distribution models.
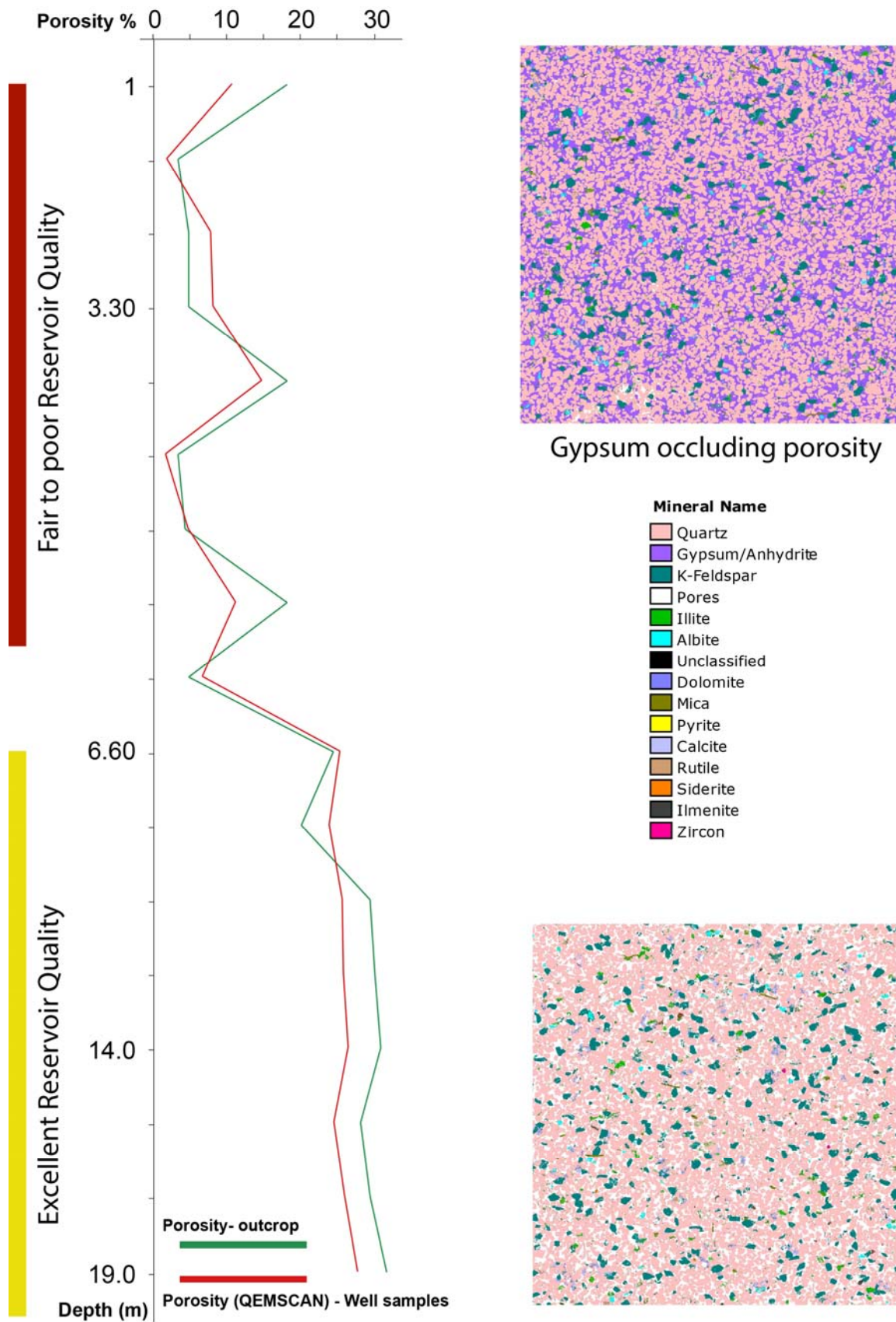
Fig. 1. Preliminary results of QEMSCAN® analysis in 22-m-depth, behind-outcrop well targeting the entire K2 unit (braidplain of sequence IV).

REFERENCES

Aitchison, J., 1997. The one hour course in compositional data analysis of compositional data analysis is simple. In: Pawlowsky, G.V. (ed.), Proceedings of IAMG '97 – The Third Annual Conference of the International Association for Mathematical Geology. International Center for Numerical Methods in Engineering (CIMNE), Barcelona, 3–35.

Ajdukiewicz, J.M., Lander, R.H., 2010. Sandstone reservoir quality prediction: the state of the art. AAPG Bulletin 94, 1083-1091.

Allen, J.R.L., Wright, V.P., 1989. Paleosols in siliciclastic sequences. University of Readings, PRIS Short Course Notes 1.

Al-Ramadan, K., Morad, S., Proust, J.N., Al-Aasm, I.S., 2005. Distribution of diagenetic alterations in siliciclastic shoreface deposits within a sequence stratigraphic framework: Evidence from the Upper Jurassic, Boulonnais, NW France. Journal of Sedimentary Research 75, 943–959.

Amaefule, J.O., Altunbay, M., Tiab, D., Kersey, D.G., Keelan, D.K., 1993. Enhanced reservoir description using core and log data to identify hydraulic flow units and predict permeability in uncored intervals/wells. Society of Petroleum Engineers 88th Annual Technical Conference and Exhibition, 205-220.

Amthor, J.E., Okkerman, J., 1998. Influence of early diagenesis on reservoir quality of Rotliegend sandstones, Northern Netherlands. AAPG Bulletin 82, 2246-2265.

Andrews, J.E., 1985. The sedimentary facies of a late Bathonian regressive episode: the Kilmaluag and Skudiburgh Formations of the Great Estuarine Group, Inner Hebrides, Scotland. Journal of the Geological Society of London 142, 1115–1137.

Arakel, A.V., 1986. Evolution of calcrete in palaeodrainages of the Lake Narpperby area, Central Australia. Palaeogeography, Palaeoclimatology, Palaeoecology 54, 283-303.

Arakel, A.V., Jacobson, G., Lyons, W.B., 1990. Sediment-water interaction as a control on geochemical evolution of playa lake systems in the Australian arid interior. Hydrobiology 197, 1-12.

Arakel, A.V., Jacobson, G., Salehi, M., Hill, C.M., 1989. Silicification of calcrete in palaeodrainage basins of the Australian arid zone. Australian Journal of Earth Sciences 36, 73-89.

Arche, A., López-Gómez, J., 2014. The Carnian Pluvial Event in Western Europe: new data from Iberia and correlations with the Western Neotethys and Eastern North America-NW Africa regions. Earth Science Reviews 128, 196-231.

Arche, A., López-Gómez, J., García-Hidalgo, J.F., 2002. Control climático, tectónico y eustático en depósitos del Carniense (Triásico Superior) del SE de la Península Ibérica. Journal of Iberian Geology 28, 13-30.

Armenteros, I., Ben Brahim, M., Blanco, J.A., Huerta, P., Suárez, M., 2003. Costras carbonatadas en la sucesión aluvial distal eocena de la Formación Hamada de Boudenib II al sur del Alto Atlas (Marruecos). Geogaceta 34, 199-202.

Armenteros, I., Bustillio, M.A., Blanco, J.A., 1995. Pedogenic and groundwater processes in a closed Miocene basin (northern Spain). Sedimentary Geology 99, 17–36.

Armitage, P.J., Worden, R.H., Faulkner, D.R., Aplin, A.C., Butcher, A.R., Espie, A.A., 2013. Mercia Mudstone Formation caprock to carbon capture and storage sites: petrology and petrophysical characteristics. Journal of the Geological Society 170, 119-132.

Arribas, J. 1987. Origen y significado de los cementos en las areniscas de las facies Buntsandstein (Rama Aragonesa de la Cordillera Ibérica). Cuadernos de Geología Ibérica 11, 535-556.

Arribas, J., 1984. Sedimentología y diagénesis del Buntsandstein y Muchelkalk de la Rama Aragonesa de la Cordillera Ibérica (provincias de Soria y Zaragoza). PhD dissertation, Universidad Complutense de Madrid, Spain, 354 pp.

Arribas, J., Díaz Molina, M., Tortosa, A., 1996. Ambientes de Sedimentación, procedencia y diagénesis de depósitos de ríos meandriformes desarrollados sobre playa-lakes. Mioceno de la Cuenca de Loranca (provincias de Cuenca y Guadalajara). Cuadernos de Geología Ibérica 21, 319-343.

Arribas, J., Gómez-Gras, D., Rosell, J., Tortosa, A., 1990. Estudio comparativo entre las areniscas paleozoicas y triásicas de la isla de Menorca: evidencias de procesos de reciclado. Revista de la Sociedad Geológica de España 3, 105-116.

Arribas, M.E., Doval, M., Díaz Molina, M., 1995. Petrological and mineralogical characterization of lutitic deposits in a fluvial dominated depositional system. Upper Oligocene-Lower Miocene, Loranca Basin (Central Spain). Revista de la Sociedad Geológica de España 8, 149-160.

Arts, R., Chadwick, A., Eiken, O., Thibeau, S., Nooner, S., 2008. Ten years' experience of monitoring CO_2 injection in the Utsira Sand at Sleipner, offshore Norway. First Break 26, 65-72.

Ashmore, P., 1982. Laboratory modelling of gravel briaded stream morphology. Earth Surface Processes and Landforms 7, 201-225.

Bailey, R.J., Lloyd, D.A., 2000. A log correlation of the Rotliegend of the northern Cleaver Bank High: the search for controls on reservoir sand distribution. Petroleum Geoscience, 7, 351-358.

Barone, M., Dominici, R., Muto, F., Critelli, S., 2008. Detrital modes in a late Miocene wedge-top basin, northeastern Calabria, Italy: compositional record of wedge-top partitioning. Journal of Sedimentary Research 78, 693-711.

Barone, M., Dominici, R., Stefano, L., 2007. Interpreting gypsarenites in the Rossano basin (Calabria, Italy): a contribution to the characterization of the Messinian salinity crisis

in the Mediterranean. In: Arribas, J., Critelli S., Johnsson, M.J. (eds.), Sedimentary Provenance and Petrogenesis: Perspectives from Petrography and Geochemistry. Geological Society of America Special Paper 420, 135-148.

Baudon, C., Redfern, J., Van Den Driessche, J., 2012. Permo-Triassic structural evolution of the Argana Valley, impact of the Atlantic rifting in the High Atlas, Morocco. Journal of African Earth Sciences 65, 91-104.

Beard, D.C., Weyl, P.K., 1973. Influence of texture on porosity and permeability of unconsolidated sand. AAPG Bulletin 57, 349-369.

Bennion, D.B., Bachu, S., 2008. Drainage and imbibition relative permeability relationships for supercritical CO_2/brine and H_2S/brine systems in intergranular sandstone, carbonate, shale, and anhydrite rocks. SPE Reservoir Evaluation and Engineering, Paper SPE 99326, 487-496.

Bjørlykke, K. 1994. Fluid-flow processes and diagenesis in sedimentary basins. In: Parnell, J. (ed.), Geofluids: Origin, migration and evolution of fluids in sedimentary basins. Geological Society Special Publication 78, 127-140.

Bjørlykke, K., 1984. Formation of secondary porosity: how important is it?. In: McDonald, D.A., Surnam, R.C. (eds.), Clastic diagenesis. AAPG Memoir 37, 277-286.

Bjørlykke, K., 2014. Relationships between depositional environments, burial history and rock properties. Some principal aspects of diagenetic process in sedimentary basins. Sedimentary Geology 301, 1-14.

Bjørlykke, K., Aagaard, P., 1992. Clay minerals in North Sea sandstones. In: Houseknecht, D.W., Pittman, E.P. (eds.), Origin, diagenesis and petrophysics of clay minerals in sandstones. SEPM Special Publication 47, 65-80.

Bjørlykke, K., Chuhan, F., Kjeldstad, A., Gundersen, E., Lauvrak, O., Høeg, K., 2004. Modelling of sediment compaction during burial in sedimentary basins. In: Stephansson, O., Hudson, O., King, L. (eds.), Coupled Thermo-Hydro-Mechanical-Chemical Processes in Geo-systems. Fundamentals, Modelling, Experiments and Applications. Geo-Engineering Book Series 2, London, Elsevier, 699-708.

Bjørlykke, K., Jahren, J., 2010. Sandstones and sandstone reservoirs. In: Bjørlykke, K. (ed.), Petroleum geoscience: from sedimentary environments to rock physics. Springer-Verlag, Berlin, 113-140.

Bloch, S., 1991. Empirical prediction of porosity and permeability in sandstones. AAPG Bulletin 75, 1145-1160.

Bloch, S., 1994. Effect of detrital mineral composition on reservoir quality. In: Wilson, M.D. (ed.), Reservoir Quality Assessment and Prediction in Clastic Rocks. SEPM Short Course 30, 161–182.

Bloch, S., McGowen, J.H., 1994. Influence of depositional environment on reservoir quality prediction. In: Wilson, M.D. (ed.), Reservoir quality assessment and prediction in clastic rocks. SEPM Short Course 30, 41-58.

Boogaart, K.G.v.d., Tolosana-Delgado, R., 2008. "Compositions": a unified R package to analyze compositional data. Computer and Geosciences 34, 320-338.

Bourquin, S., Guillocheau, F., Péron, S., 2009. Braided river within an arid alluvial plain (example from the early Triassic, western German Basin): criteria of recognition and expression of stratigraphic cycles. Sedimentology 56, 2235-2264.

Brayshaw, A.C., Davies, G.W., Corbett, P.W.M., 1996. Depositional controls on primary permeability and porosity at the bedform scale in fluvial reservoir sandstones. In: Carling, P.A., Dawson, M.R. (eds.), Advances in Fluvial Dynamics and Stratigraphy. Chichester, England, John Wiley & Sons, 373–394.

Brewer, R., 1964. Fabric and mineral analysis of soils. Wiley, New York, 482 pp.

Bridge, J.S., Collier, R.E.Ll., Alexander, J., 1998. Large-scale structure of Calamus river deposits revealed using ground-penetrating radar. Sedimentology 45, 977–985.

Broughton, P., Trépanier, P., 1993. Hydrocarbon generation in the Essaouira basin of western Morocco. AAPG Bulletin 77, 999-1015.

Brown, R.H., 1980. Triassic rocks of the Argana Valley, sourthern Morocco, and their regional structural implications. AAPG Bulletin 64, 988-1003.

Bryant, I.D., Flint, S.S., 1993. Quantitative clastic reservoir geological modelling: problems and perspective. In: Flint, S.S., Bryant, I.D. (eds.), The geological modelling of hydrocarbon reservoirs and outcrop analogues. International Association of Sedimentologists Special Publication 15, 3-20.

Burley, S.D., 1984. Patterns of diagenesis in the Sherwood Sandstone Group (Triassic), United Kingdom. Clay Minerals 19, 403–440.

Burley, S.D., Kantorowicz, J.D., Waugh, B., 1985. Clastic diagenesis. Geological Society of London Special Publication 18, 189-226.

Burt, R.A., 1993. Ground-water chemical evolution and diagenetic processes in the Upper Florida Aquifer, Southern South Carolina and Northeastern Georgia. U.S. Geological Survey water-supply paper, 2392, 76 pp.

Calder, J.H., Boehner, R.C., Brown, D.E., Gibling, M.R., Mukhoppadhyay, P.K., Ryan, R.J., Skilliter, D.M., 1998. Classic Carboniferous sections of the Minas and Cumberland Basins in Nova Scotia with special reference to organic deposits. Society for Organic Petrology Annual Meeting Field Trip, 29-30 July. Nova Scotia Natural Resources Open File Report ME 1998-5.

Cant, D.J., Walker, R.G., 1978. Fluvial processes and facies sequences in the sandy braided South Saskatchewan River, Canada. Sedimentology 25, 625-648.

Caracciolo, L., Arribas, J., Ingersoll, R.V., Critelli, S., 2013. The diagenetic destruction of porosity in plutoniclastic petrofacies: the Miocene Diligencia and Eocene Maniobra formations, Orocopia Mountains, southern California, USA. Geological Society of London Special Publications 386, 1-14.

Caracciolo, L., Arribas, J., Ingersoll, R.V., Critelli, S., 2014. The diagenetic destruction of porosity in plutoniclastic petrofacies: The Miocene Diligencia and Eocene Maniobra formations, Orocopia Mountains, southern California, USA. In: Scott, R., Morton, A. (eds.), Provenance analyses in hydrocarbon exploration. Geological Society of London Special Publication 386, 49-62.

Caracciolo, L., Eynatten, H. von, Tolosana-Delgado, R., Critelli, S., Manetti, P., Marchev, P., 2012. Petrological, geochemical and statistical analysis of Eocene-Oligocene sandstones of the Western Thrace Basin, Greece and Bulgaria. SEPM 82, 482-498.

Carvalho, A.S.G., Dani, N., De Ros, L.F., Zambonato, E.E., 2014. The impact of early diagenesis on the reservoir quality of pre-salt (Aptian) sandstones in the Espirito Santo basin, Eastern Brazil. Journal of Petroleum Geology 37, 127-142.

Carvalho, M.V.F., De Ros, L.F., Gomes, N.S., 1995. Carbonate cementation patterns and diagenetic reservoir facies in the Campos Basin Cretaceous turbidites, offshore eastern Brazil. Marine and Petroleum Geology 12, 741–758.

Chayes, F., 1952. Notes on the staining of potash feldspar with sodium cobaltnitrite in thin section. American Mineralogist 37, 337-340.

Chen, X.Y., McKenzie, N.J., Roach, I.C., 2002. Distribution in Australia: calcrete landscapes. In: Chen, X.Y., Lintern, M.J., Roach, I.C. (eds.), Calcrete: Characteristics, Distribution and Use in Mineral Exploration. Cooperative Research Centre for Landscape Environments and Mineral Exploitation. Perth, Western Australia, 110-138.

Choquette, P.W., Pray, L.C., 1970. Geologic nomenclature and classification of porosity in sedimentary carbonates. AAPG Bulletin 54, 207-250.

Chuhan, F.A., Kjeldstad, A., Bjørlykke, K., Høeg, K., 2002. Porosity loss in sand by grain crushing − experimental evidence and relevance to reservoir quality. Marine and Petroleum Geology 19, 39-53.

Clearly, E.J., Connolly, J.R., 1974. Distribution and genesis of quartz in a piedmont-coastal plain environment. Geological Society of America Bulletin 82, 2755-2766.

Colson, J., Cojan, I., 1996. Groundwater dolocretes in a lake-marginal environments: an alternative model for dolocrete formation in continental settings (Danian of the Provence Basin, France). Sedimentology 43, 175-188.

Cook, J.E., Goodwin, L.B., Boutt, D.F., 2011. Systematic diagenetic changes in the grain-scale morphology and permeability of a quartz-cemented quart arenite. AAPG Bulletin 95, 1067-1088.

Critelli, S., Mongelli, G., Perri, F., Martin-Algarra, A., Martin-Martin, M., Perrone, V., Dominici, R., Sonnino, M., Zaghloul, M.N., 2008. Sedimentary evolution of the Middle Triassic-Lower Jurassic continental redbeds from Western-Central Mediterranean Alpine Chains based on geochemical, mineralogical and petrographical tools. Journal of Geology 116, 375-386.

Dabrio, C., Fernández, J., 1986. Evolución del estilo alluvial en el Triásico de Alcaraz (Albacete). Cuadernos de Geología Ibérica 10, 173-206.

De Ros, L.F., 1998. Heterogeneous generation and evolution of diagenetic quartzarenites in the Silurian-Devonian Furnas Formation of the Parana Basin, southern Brazil. Sedimentary Geology 116, 99-128.

De Ros, L.F., Morad, S., Paim, P.S.G., 1994. The role of detrital composition and climate on the diagenetic evolution of continental molasses: evidence form the Cambro-Ordovician Guaritas Sequence, southern Brazil. Sedimentary Geology 92, 197-228.

De Ros, L.F., Scherer, C.M.S., 2012. Stratigraphic controls on the distribution of diagenetic processes, quality and heterogeneity of fluvial-aeolian reservoirs from the Reconcavo Basin, Brazil. International Association of Sedimentologists Special Publication 45, 105-132.

Di Giulio, A., Valloni, R., 1992. Analisi microscopica delle areniti terrigene: parametri petrologici e composición modali. Acta Naturalia di "L´Ateneo Parmese" 28, 55-101.

Dickinson, W.R., 1970. Interpreting detrital modes of graywacke and arkose. Journal of Sedimentary Petrology 40, 695-707.

Dickinson, W.R., 1985. Interpreting provenance relations from detrital modes of sandstones. In: Zuffa, G.G. (ed.), Provenance of arenites. NATO-ASI Series, Reidel Publishing Company, Dordrecht, Netherlands, 333-361.

Dickson, J.A.D., 1965. A modified staining technique for carbonates in thin section. Nature 205, p. 587.

Domenico, P.A., Schwartz, F.W., 1990. Physical and chemical hydrogeology. New York, John Wiley and Sons, 824 pp.

Donselaar, M.E. Schmidt, J.M., 2005. Integration of outcrop and borehole image logs for high-resolution facies interpretation: Example from a fluvial fan in the Ebro Basin, Spain. Sedimentology 52, 1021-1042.

Dott, R., 1964. Wacke, greywacke and matrix-what approach to immature sandstone classification?. Journal of Sedimentary Petrology 34, 625-632.

Dowey, P.J., Hodgson, D.M., Worden, R.H., 2012. Pre-requisites, processes, and prediction of chlorite grain coatings in petroleum reservoirs: a review of subsurface examples. Marine and Petroleum Geology 32, 63–75.

Doyle, L.J., Carder, K.L. Steward, R.G., 1983. The hydraulic equivalence of mica. Journal of Sedimentary Petrology 53, 643-648.

Dutta, P.K., Suttner, L.J., 1986. Alluvial sandstone composition and paleoclimate, II. Authigenic mineralogy. Journal of Sedimentary Petrology 56, 346-358.

Dutta, P.K., Zhou, Z., dos Santos, P.R., 1993. A theoretical study of mineralogical maturation of eolian sand. In: Johnsson, M.J., Basu, A. (eds), Processes Controlling

the Composition of Clastic Sediments. Geological Society of America Special Paper 284, 203-210.

Dutton, S.P, White, C.D., Willis, B.J., Novakovic, D., 2002. Calcite cement distribution and its effect on fluid flow in a deltaic sandstone, Frontier Formation, Wyoming. AAPG Bulletin 86, 2007-2021.

Dutton, S.P., 2008. Calcite cement in Permian deep-water sandstones, Delaware Basin, west Texas: origin, distribution, and effect on reservoir properties. AAPG Bulletin 92, 765-787.

Ehrenberg, S.N., 1989. Assessing the relative importance of compaction processes and cementation to reduction of porosity in sandstones: discussion; compaction and porosity evolution of Pliocene sandstones, Ventura Basin, California. AAPG Bulletin 73, 1274-1276.

Ehrenberg, S.N., 1995. Measuring sandstone compaction from modal analyses of thin sections: How to do it and what the results mean. Journal of Sedimentary Research, A65, 369-379.

Ehrenberg, S.N., 1997. Influence of depositional sand quality and diagenesis on porosity and permeability: examples form Brent group reservoirs, Northern North Sea. Journal of Sedimentary Research 67, 197-211.

El Arabi, E.H., Díez, J.B., Broutin, J., Essamoud, R., 2006. Prémière characterisation palynologique du Trias moyen dans le Haut Atlas: implications pour l'initiation du rifting tethysien au Atlas. Comptes Rendus Geosciciences 338, 641–649.

Elias, A.R.D., De Ros, L.F., Mizusaki, A.M.P., Anjos, S.M.C., 2004. Diagenetic patterns in eolian/coastal sabkha reservoirs of the Solimoes Basin, northern Brazil. Sedimentary Geology 169, pp. 191-217.

El-Khatri, F., El-Ghali, M.A.K., Mansurberg, H., Morad, S., Ogle, N., Kalin, R.M., 2015. Diagenetic alterations and reservoir quality evolution of Lower Cretaceous fluvial sandstones: Nubian Formation, Sirt Basin, North-Central Libya. Journal of Petroleum Geology 38, 1-23.

Ellouz, N., Patriat, M., Gaulier, J.-M, Bouatmani, R., Sabounji, S., 2003. From rifting to Alpine inversion: Mesozoic and Cenozoic subsidence history of some Moroccan basins. Sedimentary Geology 156, 185-212.

El-Sayed, M.I., Fairchild, I.J., Spiro, B., 1991. Kuwaiti dolocretes: petrology, geochemistry, and groundwater origin. Sedimentary Geology 73, 59–75.

Eschard, R., Doligez, B. (eds.), 1993. Subsurface characterization from outcrop observations. Proceedings of the 7th IFP Exploration and Production Research Conference, Scarborough, April 12-17, 1992. Éditions Technip, Paris, France, 189 pp.

Fawad, M., Mondol, N.H., Jahren, J., Bjørlykke, K., 2010. Microfabric and rock properties of experimentally compressed silt-clay mixtures. Marine and Petroleum Geology 27, 1698-1712.

Fawad, M., Mondol, N.H., Jahren, J., Bjørlykke, K., 2011. Mechanical compaction and ultrasonic velocity of sands with different texture and mineralogical composition. Geophysical Prospecting 59, 697-720.

Fernández, J., 1977. Sedimentación triásica en el borde Sureste de la Meseta. PhD dissertation, Universidad de Granada, 173 pp.

Fernández, J., Bluck, B.J., Viseras, C., 1993. The effects of fluctuating base level on the structure of alluvial fan and associated fan delta deposits: an example from the Tertiary of the Betic Cordillera, Spain. Sedimentology 40, 879-893.

Fernández, J., Dabrio, C., 1985. Fluvial architecture of the Buntsandstein facies redbeds in the Middle to Upper Triassic (Ladinian-Norian) of the Southeastern edge of the Iberian Meseta (Southern Spain). In: Mader, D. (ed.), Aspects of fluvial sedimentation in the Lower Triassic Buntsandstein of Europe. Springer-Verlag, Berlin, 113-140.

Fernández, J., Dabrio, C., Pérez-López, A., 1994. El Triásico de la región Siles-Alcaraz (Cordillera Bética). IV Meeting of Spanish Permian and Triassic, Field Guide, Cuenca, 47 pp.

Fernández, J., Gil, A., 1989. Interpretación sedimentaria de los materiales triásicos de facies Buntsandstein en las Zonas Externas de las Cordilleras Béticas y en la Cobertura Tabular de la Meseta. España. Revista de la Sociedad Geológica de España 2, 114-124.

Fernández, J., Pérez-López, A., 2004. Triásico de la Cordillera Bética y Baleares. In: Vera, J.A. (ed.), Geología de España. SGE-IGME, Madrid, 365-366.

Fernández, J., Viseras, C., 2004. Geometría de cuerpos sedimentarios y análisis de facies en las areniscas de red beds triásicas del extremo SE de la Meseta Ibérica. Field Guide (REPSOL YPF-UGR, eds.), 50 pp.

Fernández, J., Viseras, C., Dabrio, C., 2005. Triassic fluvial sandstones (Central South Spain): an excellent analogue for the TAGI reservoir of Algeria. In: Fernández, J., Viseras, C., Dabrio, C. (eds.). 67th European Association of Geoscientists and Engineers, Field Guide F1, 18 pp.

Fiechtner, L., Friedrichsen, H., Hammerschmidt, K., 1992. Geochemistry and geochronology of Early Mesozoic tholeiites from Central Morocco. International Journal of Earth Sciences 81, 45-62.

FitzPatrick, E.A., 1984. Micromorphology of soils. Chapman and Hall, London and New York, 433 pp.

Friend, P.F., 1983. Towards the field classification of alluvial architecture or sequence. In: Collinson, J.D., Lewin, J. (eds.), Modern and ancient fluvial systems. International Association of Sedimentologists Special Publication 6, 345-354.

Friend, P.F., Slater, M.J., Williams, R.C., 1979. Vertical and lateral building of river sandtone bodies, Ebro basin, Spain. Journal of the Geological Society of London 136, 39-46.

Frizon de Lamotte, D., Zizi, M., Missenard, Y., Hafid, M., El Auzzoui, M., 2008. The Atlas system. In: Michard, A., Saddiqui, O., Chalouan, A., Frizon de Lamotte, D. (eds.), Continental Evolution: The Geology of Morocco. Springer, 133–202.

Fryberger, S.G., Knight, R., Hern, C., Moscariello, A., Kabel, S., 2011. Rotliegend facies, sedimentary provinces, and stratigraphy, southern Permian Basin UK and the Netherlands: A review with new observations. In: Grötsch, J., Gaupp, R. (eds.), The Permian Rotliegend in the Netherlands. SEPM Special Publication 98, 51-88.

Garzanti, E., 1991. Non-carbonate intrabasinal grains in arenites: their recognition, significance, and relationship to eustatic cycles and tectonic setting. Journal of Sedimentary Petrology 61, 959-975.

Garzanti, E., Haas, R., Jadoul, F., 1989. Irostones in the Mesozoic passive margin sequence of the Thetys Himalaya (Zanskar, Northen India: sedimentology and metamorphism. In: Young, T.P., Taylor, W.E.G. (eds.), Phanerozoic irosntones. Geological Society of London, 229-244.

Gast, R.E., Dusar, M., Breitkreuz, C., Gaupp, R., Schneider, J.W., Stemmerik, L., Geluk, M.C., Geissler, M., Kiersnowski, H., Glennie, K.W., Kabel, S., Jones, N.S., 2010. Rotliegend. In: Doornenbal, J.C., Stevenson, A.G. (eds.), Petroleum Geological Atlas of the Southern Permian Basin Area. EAGE Publications, Houten, 101–121.

Gaupp, R., Okkerman, J.A., 2011. Diagenesis and reservoir quality of Rotliegend sandstones in the Northern Netherlands - a review. In: Grötsch, J., Gaupp, R. (Eds.), The Permian Rotliegend in the Netherlands. SEPM Special Publication 98, 193-226.

Gaupp, R., Solms, M., Baunack, C. Pudlo, D., Oncken, O., Krawczyk, C., Tanner, D., Littke, R., Schwarzer, D., Trappe, H., Schubarth-Engelschall, J., Samiee, R., 2005. Paleo oil- and gasfields in the Rotliegend of the North German basin: effects upon hydrocarbon reservoir quality. Final Report: Deutsche Wissenschaftliche Gesellschaft für Erdöl, Erdgas und Kohle e.v. (DGMK) Research Project 593-8, 210 p., Hamburg.

Gazzi, P., Zuffa, G.G., Gandolfi, G., Paganelli, L., 1973. Provenienza e dispersione litoranea delle sabbie delle spiagge adriatiche fra le foci dell'Isonzo e del Foglia: inquadramento regionale. Memoria della Società Geologica Italiana 12, 1-37.

Gebhardt, U., Schneider, J.W., Hoffmann, N., 1991. Modelle zur Stratigraphie und Beckenentwicklung im Rotliegend der Norddeutschen Senke. Geologisches Jahrbuch A-127, 405–427.

Geehan, G.W., Underwood, J., 1993. The use of length distributions in geological modelling. In: Flint, S.S., Bryant, I.D. (eds.), The geological modelling of hydrocarbon reservoirs and outcrop analogues. International Association of Sedimentologists, Special Publications 15, 205–212.

Geluk, M.C., 2005. Stratigraphy and tectonics of Permo-Triassic basins in the Netherlands and surrounding areas. Published Doctorate Thesis, Utrecht University.

Geluk, M.C., 2007. Permian. In: Wong, Th.E., Batjes, D.A.J., De Jager, J. (Eds.), Geology of the Netherlands. Amsterdam, Royal Netherlands Academy of Arts and Sciences, 63–83.

George, G.T., Berry, J.K., 1994. A New Palaeogeographic and Depositional Model for the Upper Rotliegend, Offshore The Netherlands. First Break 12, 147-158.

Gibbons, K., Hellem, T., Kjemperud, A., Nio, S.D., Vebenstad, K., 1993. Sequence architecture, facies development and carbonate-cemented horizons in the Troll Field reservoir, offshore Norway. In: Ashton, M. (ed.), Advances in reservoir geology. Geological Society of London Special Publication 69, 1-31.

Gil, A., Fernández, J., López-Garrido, A.C., 1987. Evolución de facies en el Trias de la zona Prebética y borde de la Meseta - Transversal Orcera-Puente Génave (Prov. Jaén). Cuadernos de Geología Ibérica 11, 403-420.

Giles, M.R., 1997. Diagenesis: A quantitative perspective. Dordrecht, Kluwer Academic Publishers, 526 pp.

Glennie, K.W., 1982. Early Permian (Rotliegendes) palaeowinds of the North Sea. Sedimentary Geology 34, 245–265.

Glennie, K.W., 1998. Lower Permian – Rotliegend. In: Glennie, K.W. (ed.), Petroleum Geology of the North Sea, Fourth Edition. Blackwell Science (Oxford), 137–174.

Glennie, K.W., Mudd, G.C., Nagtegaal, P.J.C., 1978. Depositional environment and diagenesis of Rotliegend sandstones in the Leman Bank and Sole Pit area of the U.K. southern North Sea. Geological Society of London 135, 25-34.

Gluyas, J., Cade, C.A., 1997. Prediction of porosity in compacted sands. In: Kupecz, J.A., Gluyas, J., Bloch, S. (eds.), Resevoir quality prediction in sandstones and carbonates. AAPG Memoir 69, 19-27.

Goudie, A.S., 1983. Calcrete. In: Goudie, A.G., Pye, K. (eds.), Chemical Sediments and geomorphology: precipitates and residua in the near-surface environment. Academic Press, London, 93-131.

Goy, A., Yébenes, A., 1977. Características, extensión y edad de la formación Dolomías tableadas de Imón. Cuadernos de Geología Ibérica 4, 375-384.

Gralla, P., 1988. Das Oberrotliegenden in NW Deutschland – Lithostratigraphie und Faziesanalyse. Geol. Jb. A 106, 3-59.

Grötsch, J., Sluijk, S., Van Ojik, K., De Keijzer, M., Graaf, J., Steenbrink, J., 2011. The Groningen Gas Field: Fifty years of exploration and gas production from a Permian dryland reservoir. In: Grötsch, J., Gaupp, R. (eds.), The Permian Rotliegend in the Netherlands. SEPM Special Publication 98, 11-33.

Haq, B.U., Hardenbol, J., Vail, P.R., 1987. Chronology of fluctuating sea levels since the Triassic. Science 235, 1156-1167.

Hardie, L.A., 1987. Perspectives on dolomitization: a critical view of some currents views. Journal of Sedimentary Petrology 57, 166-183.

Hartkamp-Bakker, C.A., Donselaar, M.E., 1993. Permeability patterns in point bar deposits: Tertiary Loranca Basin, central Spain. In: Flint S.S., Bryant, I.D. (eds.), The

geological modelling of hydrocarbon reservoirs and outcrop analogs. International Association of Sedimentologists Special Publication 15, 157-168.

Hartmann, D.J., Beaumont, E.A., 1999. Predicting reservoir system quality and performance. In: Beaumont, E.A., Foster, N.H. (eds.), Treatise of petroleum geology/Handbook of petroleum geology: exploring for oil and gas traps. AAPG Special Volumes, chapter 9, 1-154.

Hay, W.W., Behensky Jr., J.F., Barron, E.J., Sloan, J.I., 1982. Late Triassic palaeoclimatology of the proto-central North Atlantic rift system. Palaeogeography, Palaeoclimatology, Palaeoecology 40, 13-30.

Heins, W.A., Kairo, S., 2007. Predicting sand character with integrated genetic analysis. In: Arribas, J., Critelli, S., Johnsson, M.J. (eds.), Sedimentary provenance and petrogenesis: perspectives from petrography and geochemistry. Geological Society of America Special Paper 420, 345–379.

Hemming, N.G., Meyers, W.J., Grams, J.C., 1989. Cathodoluminescence in diagenetic calcites: the roles of Fe and Mn as deduced from electron probe and spectrophotometric measurements. Journal of Sedimentary Petrology 59, 404-411.

Henares, S., Arribas, J., Cultrone, G., Viseras, C., 2016b. Muddy and dolomitic rip-up clasts in Triassic fluvial sandstones: origin and impact on potential reservoir properties (Argana basin, Morocco). Sedimentary Geology (http://dx.doi.org/10.1016/j.sedgeo.2016.03.020).

Henares, S., Bloemsma, M.R., Donselaar, M.E., Mijnlieff, H.F., Redjosentono, A.E., Veldkamp, H.G., Weltje, G. J., 2014b. The role of detrital anhydrite in diagenesis of aeolian sandstones (Upper Rotliegend, The Netherlands): implications for reservoir-quality prediction. Sedimentary Geology 314, 60-74.

Henares, S., Caracciolo, L., Cultrone, G., Fernández, J., Viseras, C., 2014a. The role of diagenesis and depositional facies on pore system evolution in a Triassic outcrop analogue (SE Spain). Marine and Petroleum Geology 51, 136-151.

Henares, S., Caracciolo, L., Viseras, C., Fernández, J., Yeste, L.M., 2016a. Diagenetic constraints on heterogeneous reservoir quality assessment: a Triassic outcrop analogue of meandering fluvial reservoirs. AAPG Bulletin (doi: 10.1306/04041615103).

Henares, S., Viseras, C., Fernández, J., Lizarazo, N., 2014c. Point bar deposit characterization with preliminary subsurface data: a case from the Triassic of the Iberian Meseta. Geogaceta 54, 7-10.

Henares, S., Viseras, C., Fernández, J., Pla-Pueyo, S., Cultrone, G., 2011. Triassic Red Beds in SE Spain: evaluation as potential reservoir rocks based on a preliminary petrological study. AAPG Search and Discovery Article, #50541.

Hernando, S., 1977a. Pérmico y Triásico de la region Ayllón-Atienza. Seminarios Estratigrafía 2, 1–408.

Hernando, S., 1977b. Aspectos estratigráficos del Keuper en el borde SW de la Rama Castellana de la Cordillera Ibérica (provincias de Segovia, Soria y Guadalajara). Cuadernos de Geología Ibérica 4, 385–398.

Hofmann, A., Tourani, A., Gaupp, R., 2000. Cyclicity of Triassic to Lower Jurassic continental red beds of the Argana Valley, Morocco: implications for palaeoclimate and basin evolution. Palaeogeography, Palaeoclimatology, Palaeoecology 161, 229-266.

Horbury, A.D., Adams, A.E., 1989. Meteoric phreatic diagenesis in cyclic late Dinantian carbonates, northwest England. Sedimentary Geology 65, 319-344.

Howell, J.A., Martinius, A.W., Good, T.R., 2014. The application of outcrop analogues in geological modelling: a review, present status and future outlook. In: Martinius, A.W., Howell, J.A., Good, T.R. (eds.), Sediment-Body Geometry and Heterogeneity: Analogue Studies for Modelling the Subsurface. Geological Society of London Special Publications 387, 1–25.

Hurst, A., Nadeau, P.H., 1995. Clay microporosity in reservoir sandstones: an application of quantitative electron microscopy in petrophysical evaluation. AAPG Bulletin 79, 563-573.

Hutton, J.T., Dixon, J.C., 1981. The chemistry and mineralogy of some South Australian calcretes and associated soft carbonates and their dolomitization. Journal of Geological Society of Australia 28, 71-79.

Ingersoll, R.V., Bullard, T.F., Ford, R.L., Grimm, J.P., Pickle, J.D., Sares, S.W., 1984. The effect of grain-size on detrital modes: a test of the Gazzi-Dickinson point-counting method. Journal of Sedimentary Petrology 49, 103-116.

Issautier, B., Viseur, S., Audigane, P., Le Nindre, Y-.M., 2014. Impacts of fluvial reservoir heterogeneity on connectivity: Implications in estimating geological storage capacity for CO_2. International Journal of Greenhouse Gas Control 20, 333-349.

Jalil, N.E., Dutuit, J.-M., 1996. Permian captorhinid reptiles from the Argana formation, Morocco. Palaeontology 39, 907-918.

Jansen, J.H.F., Van der Gaast, S.J., Koster, B., Vaars, A.J., 1998. CORTEX, a shipboard XRF scanner for element analyses in split sediment cores. Quaternary Research 151, 143–153.

Johnsson, M.J., Stallard, R.F., Meade, R.H., 1988. First-cycle quartz arenites in the Orinoco River basin, Venezuela and Colombia. Journal of Geology 96, 263-277.

Kabel, A.B.E.T., 2002. Overview of the Upper Rotliegend gas play in the Southern Permian Basin: EPNL Special Issue – Palaeozoic Plays of NW Europe, May 2002. EP 2002-7023.

Katz, A.J., Thompson, A.H., 1987. Prediction of rock electrical conductivity from mercury injection measurements. Journal of Geophysical Research 92, 599-607.

Kearsey, T., Twitchett, J.R., Newell, A.J., 2012. The origin and significance of pedogenic dolomite from the Upper Permian of the South Urals of Russia. Geological Magazine 149, 291-307.

Kendall, A.C., 1992. Evaporites. In: Walker, R.G., James, N.P. (Eds.), Facies Models: Response to Sea-Level Changes. Geoscience Canada Reprint Series 1, pp. 259–296.

Kendall, A.C., Harwood, G.M., 1996. Marine evaporites: arid shorelines and basins. In: Reading, H.G. (ed.), Sedimentary Environments: Processes, Facies and Stratigraphy. Blackwell Science, 281–324.

Kent, D.V., Olsen, P.E., Witte, W.K., 1995. Late Triassic-Earliest Jurassic geomagnetic polarity sequence and paleolatitudes from drill cores in Newark rift basin, eastern North America. Journal of Geophysical Research 100, 14065-14998.

Keogh, K.J., Martinius, A.W., Osland, R., 2007. The development of fluvial stochastic modelling in the Norwegian oil industry: a historical review, subsurface implementation and future directions. Sedimentary Geology 202, 249-268.

Kessler, J.L.P., Soreghan, G.S., Wacker, H.J., 2001. Equatorial aridity in western Pangea: Lower Permian loessite and dolomitic paleosols in northeastern New Mexico, USA. Journal of Sedimentary Research 71, 817-832.

Ketzer, J.M., Morad, S., 2006. Predictive distribution of shallow marine, low-porosity (pseudomatrix-rich) sandstones in a sequence stratigraphic framework – example from the Ferron sandstone, Upper Cretaceous, USA. Marine and Petroleum Geology 23, 29-36.

Ketzer, J.M., Morad, S., Evans, R., Al-Aasm, I., 2002. Distribution of diagenetic alterations in fluvial, deltaic, and shallow marine sandstones within a sequence stratigraphic framework: Evidence from the Mullaghmore Formation (Carboniferous), NW Ireland. Journal of Sedimentary Research 72, 760–774.

Khadkikar, A.S., Merh, S.S., Malik, J.N., Chamyal, L.S., 1998. Calcretes in semi-arid alluvial systems: formative pathways and sinks. Sedimentary Geology 116, 251–260.

Khalaf, F.I., 1990. Occurrence of phreatic dolocrete within Tertiary clastic deposits of Kuwait, Arabian Gulf. Sedimentary Geology 68, 223-239.

Khalaf, F.I., 2007. Occurrences and genesis of calcrete and dolocrete in the Mio-Pleistocene fluviatile sequence in Kuwait, northeast Arabian Peninsula. Sedimentary Geology 199, 129–139.

Khalifa, M.A., Morad, S., 2015. Impact of depositional facies on the distribution of diagenetic alterations in the Devonian shoreface sandstone reservoirs, Southern Ghadamis Basin, Libya. Sedimentary Geology 329, 62-80.

Klein, H., Voigt, S., Saber, H., Schneider, J., Hminna, A., Fisher, J., Lagnaoui, A., Brosig, A., 2011. First occurrence of a Middle Triassic tetrapod ichnofauna from the Argana basin (Western High Atlas, Morocco). Palaeogeography, Palaeoclimatology, Palaeoecology 307, 218-231.

Kolodzie, Jr.S., 1980. Analysis of pore throat size and use of the Waxman-Smits equation to determine OOIP in Spindle field, Colorado. Society of Petroleum Engineers 55th Annual Fall Technical Conference, p. 10.

Kraus, M.J., 1999. Paleosols in clastic sedimentary rocks: their geologic applications. Earth Science Reviews 47, 41-70.

Kulkarni, M.M., Rao, D.N., 2005. Experimental investigation of miscible and immiscible Water-Alternating-Gas (WAG) process performance. Journal of Petroleum Science and Engineering 48, 1-20.

Kupecz, J.A., Land, L.S., 1994. Progressive recrystallization and stabilization of early-stage dolomite: Lower Ordovician Ellenberger Group, west Texas. International Association of Sedimentologists Special Publication 21, 255-279.

Labrecque, P.A., Hubrard, S.M., Jensen, J.L., Nielsen, H., 2011. Sedimentology and stratigraphy architecture of a point bar deposit, Lower Cretaceous McMurray Formation, Alberta, Canada. Bulletin of Canadian Petroluem Geology 59, 147-171.

Lahcen, D., Brahim, O., Fida, M., 2007. Facteurs de contrôle et signification génétique des assemblages minéralogiques argileux du Trias-Lias d'Argana (Haut Atlas Occidental, Maroc). Comunicações Geológicas 94, 145-159.

Lai, J., Wang, G., Ran, Y., Zhou, Z., 2015. Predictive distribution of high-quality reservoirs of tight gas sandstones by linking diagenesis to depositional facies: evidence from Xu-2 sandstones in the Penglai area of the central Sichuan basin, China. Journal of Natural Gas Science and Engineering 23, 97-111.

Lander, R.H., Bonnell, L.M., Larese, R.E., 2008. Toward more accurate quartz cement models: The importance of euhedral versus noneuhedral growth rates. AAPG Bulletin 92, 1537–1563.

Laville, E., Petit, J.-P., 1984. Role of synsedimentary strike-slip faults in the formation of Moroccan Triassic basins. Geology 12, 424-427.

Laville, E., Pique, A., 1991. La distension crustale atlantique et atlasique au Maroc au début du Mésozoïque: le rejeu des structures hercyniennes. Bulletin de la Societe Géologique de France 162, 1161–1171.

Lee, M.R., Harwood, G.M., 1989. Dolomite calcitization and cement zonation related to uplift of the Raisby (Zechtstein carbonate), northern England. Sedimentary Geology 65, 285-305.

Legler, B., Gebhardt, U., Schneider, J.W., 2005. Late Permian non-marine-marine transitional profiles in the central Southern Permian Basin, northern Germany. International Journal of Earth Sciences (Geologische Rundschau) 94, 851-862.

Legler, B., Schneider, J.W., 2008. Marine ingressions into the Middle/Late Permian saline lake of the Southern Permian Basin (Rotliegend, Northern Germany) possibly linked to sea-level highstands in the Arctic rift system: Palaeogeography, Palaeoclimatology, Palaeoecology 267, 102–114.

Leikine, M., Medina, F., Ahmamou, M., 1996. Lack of low-grade metamorphism in the Triassic formations of the Argana basin, Morocco: an illite crystallinity re-evaluation. Journal of African Earth Sciences 22, 565-573.

Letourneau, P.M., Olsen, P.E., 2003. The Great Rift Valleys of Pangea in Eastern North America. Volume one: Tectonics, structure and volcanism. Columbia University Press, 214 pp.

López Garrido, A.C., 1971. Geología de la Zona Prebética al NE de la Provincia de Jaén. PhD dissertion, Universidad de Granada, 371 pp.

Loucks, R.G., 2005. Revisiting the importance of secondary dissolution pores in Tertiary sandstones along the Texas Gulf Coast. The Gulf Coast Association of Geological Societies Transactions 55, 447-455.

Lundegard, P. D. 1992. Sandstone porosity loss. A 'big picture' view of the importance of Compactation. Journal of Sedimentary Petrology 62, 250–260.

Lunt, I.A., Bridge, J.S., Tye, R.S., 2004. Development of a 3-D depositional model of braided river gravels and sands to improve aquifer characterization. In: Bridge, J.S., Hyndman, D. (eds.), Aquifer Characterization. SEMP Special Publication 80, 139–169.

Luo, J.L., Morad, S., Salem, A., Ketzer, J.M., Lei, X.L., Guo, D.Y., Hlal, O., 2009. Impact of diagenesis on reservoir-quality evolution in fluvial and lacustrine-deltaic sandstones: evidence from Jurassic and Triassic sandstones form the Ordos Basin, China. Journal of Petroleum Geology 32, 79-102.

MacGregor, D.S., 1998. Giant fields, petroleum systems and exploration maturity of Algeria. In: MacGregor, D.S., Moody, R.T.J., Clark-Lowes, D.D. (eds.), Petroleum geology of North Africa. Geological Society of London Special Publication 132, 79-96.

Mader, D., 1986. Braidplain, floodplain and playa-lake, alluvial fan, aeolian and palaeosol facies composing a diversified lithogenetical sequence in the Permian and Triassic of south Devon (England). In: Mader, D. (ed.), Aspects of Fluvial Sedimentation in the Lower Triassic Buntsandstein of Europe (Lecture Notes in Earth Sciences, Vol. 4). Springer, Berlin, 15–64.

Mader, N.K., Redfern, J., 2011. A sedimentological model for the continental Upper Triassic TadrartOuadou sandstone member: recording an interplay of climate and tectonics (Argana Valley, South-west Morocco). Sedimentology 58, 1247-1282.

Maia, A.M.S. Borsali, R., Balaban, R.C., 2009. Comparison between a polyacrylamide and a hydrophobically modified polyacrylamide flood in a sandstone core. Materials Science and Engineering C 29, 505-509.

Manzi, V., Lugli, S., Ricci Lucchi, F., Roveri, M., 2005. Deep-water clastic evaporite deposition in the Messinian Adriatic foredeep (northern Apennines, Italy): did the Mediterranean ever dry out?. Sedimentology 52, 875–902.

Martin Ramos, J.D., 2004. XPowder. A software package for powder X-ray diffraction analysis. Legal Deposit GR 1001/04.

Martin-Algarra, A., Vera, J.A., 2004. Evolución de la Cordillera Bética. In: Vera, J.A. (ed.), Geología de España. SGE-IGME, Madrid, 437-444.

McBride, E.F., 1989. Quartz cement in sandstones: a review. Earth Science Review 26, 69-112.

McKeever, P.J., 1992. Petrography and diagenesis of the Permo–Triassic of Scotland. In: Parnell J. (Ed.), Basins on the Atlantic seaboard: petroleum geology, sedimentology and basin evolution. Geological Society Special Publication 62, pp. 71-96.

McKie, T., Aggett, J., Hogg, A.J., 1998. Reservoir architecture of the Upper Sherwood Sandstone Wytch Farm. In: Underhill, J.R. (ed.), Development, Evolution and Petroleum Geology of the Wessex Basin. Geological Society Special Publication 133, 399–406.

McKie, T., Williams, B., 2009. Triassic palaeogeography and fluvial dispersal across the northwest European Basins. Geological Journal 44, 711-741.

McKinley, J.M., Atkinson, P.M., Lloyd, C.D., Ruffell, A.H., Worden, R.H., 2011. How porosity and permeability vary spatially with grain size, sorting, cement volume and mineral dissolution in fluvial Triassic sandstones: the value of geostatistics and local regression. Journal of Sedimentary Research 81, 844-858.

McKinley, J.M., Worden, R.H., Ruffell, A.H., 2003. Smectite in sandstones: a review of the controls on occurrence and behaviour during diagenesis. In: Worden, R.H., Morad, S. (eds.), Clay Mineral Cements in Sandstones. International Association of Sedimentologists Special Publication 34, 109-128.

McWhorther, D.B., Sunada, D.K., 1977. Ground-water hydrology and hydraulics. Colorado, Water Resources Publications, 304 pp.

Medina, F., 1988. Tilted-blocks pattern, paleostress orientation and amount of extension, related to Triassic early rifting of the central Atlantic in the Amzri area (Argana basin, Morocco). Tectonophysics 148, 229-233.

Medina, F., 1991. Superimposed extensional tectonics in the Argana Triassic formations (Morocco), related to the early rifting of the central Atlantic. Geological Magazine 128, 525-536.

Medina, F., 1995. Syn- and postrift evolution of the El Jadida-Agadir basin (Morocco): constraints for the rifting models of the central Atlantic. Canadian Journal of Earth Sciences 32, 1273-1291.

Metcalfe, R., Rochelle, C.A., Savage, D., Higgo, J.W., 1994. Fluid-rock interactions during continental red bed diagenesis: implications for theoretical models of mineralization in sedimentary basins. In: Parnell J. (ed.), Geofluids: origin, migration and evolution of fluids in sedimentary basins. Geological Society of London Special Publication 78, 301-324.

Miall, A. D., 2006. The Geology of fluvial Deposits. Sedimentary facies, Basin Analysis, and Petroleum Geology. Springer-Verlag, Berlin Heidelberg, 585 pp.

Miall, A.D., 1988. Reservoir heterogeneities in fluvial sandstones: lessons from outcrop studies. AAPG Bulletin 72, 682– 697.

Mijnlieff, H.F., Bloemsma, M.R., Donselaar, M.E., Henares, S., Redjosentono, A.E., Veldkamp, J.G., Weltje, G.J., 2014. The Permian Rotliegend reservoir architecture of the Dutch Koekoekspolder Geothermal doublet. Abstract 76th EAGE Conference & Exhibition, Amsterdam, NL, 16-19 June 2014.

Mijnlieff, H.F., Geluk, M., 2011. Palaeotopography-governed sediment distribution - a new predictive model for the Permian Upper Rotliegend in the Dutch sector of the southern Permian Basin. In: Grötsch, J., Gaupp, R. (eds.), The Permian Rotliegend in the Netherlands. SEPM Special Publication 98, 147-159.

Mijnlieff, H.F., Van Ojik, K., Nortier, J., Okkerman, J.A., Gaupp, R., Grötsch, J., 2011. The Permian Rotliegend of the Netherlands: Core Atlas. In: Grötsch, J., Gaupp, R. (eds.), The Permian Rotliegend in the Netherlands. SEPM Special Publication 98, 281-370.

Milliken, K.L., 1989. Petrography and composition of authigenic feldspars, Oligocene Frio Formation, South Texas. Journal of Sedimentary Petrology 59, 361-374.

Milliken, K.L., 2001. Diagenetic heterogeneity in sandstone at the outcrop scale, Breathitt Formation (Pennsylvanian), eastern Kentucky. AAPG Bulletin 85, 795-815.

Milnes, A.R., 1992. Calcrete. In: Martine, I.P., Chesworth, W. (eds.), Weathering, Soils and Paleosols, Development in Earth Surface Processes 2. Elsevier, Amsterdam, 309-347.

Molenaar, N., 1998. Origin of low-permeability calcite-cemented lenses in shallow marine sandstones and CaCO3 cementation mechanisms: An example from the Lower Jurassic Luxemburg Sandstone, Luxemburg. In: Morad, S. (ed.), Carbonate cementation in sandstones. International Association of Sedimentologists Special Publication 26, 193–211.

Morad, S., Al-Aasm, I.S., Ramseyer, K., Marfil, R., Aldahan, A.A., 1990. Diagenesis of carbonate cements in Permo-Triassic sandstones from the Iberian Range, Spain: evidence from chemical composition and stable isotopes. Sedimentary Geology 67, 281-295.

Morad, S., Al-Ramadan, K., Ketzer, J.M., De Ros, L.F., 2010. The impact of diagenesis on the heterogeneity of sandstone reservoirs: a review of the role of depositional facies and sequence stratigraphy. AAPG Bulletin 94, 1267-1309.

Morad, S., Ketzer, J.M., De Ros, L.F., 2000. Spatial and temporal distribution of diagenetic alterations in siliciclastic rocks: implications for mass transfer in sedimentary basins. Sedimentology 47, 95-120.

Morad, S., Ketzer, J.M., De Ros, L.F., 2013. Linking diagenesis to sequence stratigraphy: an integrated tool for understanding and predicting reservoir quality distribution. In:

Morad, S., Ketzar, J.M., De Ros, L.F. (eds.), Linking diagenesis to sequence stratigraphy. International Association of Sedimentologists Special Publication 45, 1-36.

Morad, S., Marfil, R. De la Peña, J.A., 1989. Diagenetic K-feldspar pseudomorphs in the Triassic Buntsandstein sandstones of the Iberian Range, Spain. Sedimentology 36, 635-650.

Morad, S., Marfil, R., Al-Aasm, I.S., Gómez-Gras, D., 1992. The role of mixing-zone dolomitization in sandstone cementation: evidence from the Triassic Buntsandstein, the Iberian Range, Spain. Sedimentary Geology 80, 53-65.

Mousavi, M.A., Bryant, S.L., 2013. Geometric models of porosity reduction by ductile grain compaction and cementation. AAPG Bulletin 97, 2129-2148.

Nash, D.J., McLaren, S.J., 2003. Kalahari valley calcretes: their nature, origins and environmental significance. Quaternary International 111, 3-22.

Odin, G. S., 1985. Significance of green particles (glaucony, berthierine, chlorite) in arenites. In: Zuffa, G.G. (ed.), Provenance of Arenites, 148. D. Reidel, NATO Advanced Study Institute, Dordrecht, Netherlands, 279-307.

Olivarius, M., Weibel, R., Hjuler, M., Kristensen, L., Mathiesen, A., Nielsen, L.H., Kjøller, C., 2015. Diagenetic effects on porosity-permeability relationship in red beds of the Lower Triassic Bunter sandstone formation in the North German Basin. Sedimentary Geology 321, 139-153.

Olsen, P.E., 1997. Stratigraphic record of the Early Mesozoic breakup of Pangea in the Laurasia-Gondwana rift system. Annual Review of Earth and Planetary Sciences 25, 337-401.

Olsen, P.E., Kent, D.V., Fowell, S.J., Schlische, R.W., Withjack, M.O., LeTourneau, P.M., 2000. Implications of a comparison of the stratigraphy and depositional environments of the Argana (Morocco) and Fundy (Nova Scotia, Canada) Permian-Jurassic basins. In: Oujidi, M., Et-Touhami, M. (eds.), Le Permien et le Trias du Maroc. Acte de la Premiere Reunion du Groupe Marocain de Permien et du Trias, Oujda, 165-183.

Øren, P.-E., Bakke, S., Arntzen, O.J., 1998. Extending predictive capabilities to network models. Society of Petroleum Engineers Journal 3, 324-336.

Ortí-Cabo, F., 1974. El Keuper del Levante español: litoestratigrafía, petrología y paleogeografía de la cuenca. PhD dissertation, Universidad de Barcelona, 174 pp.

Parton, W. J., 1984. Predicting soil temperatures in short grass steppe. Soil Science 138, pp. 93-101.

Paxton, S.T., Szabo, J.O., Ajdukiewicz, J.M., Klimentidis, R.E., 2002. Construction of an intergranular volumen compaction curve for evaluating and predicting compaction and porosity loss in rigid-grain sandstone reservoirs. AAPG Bulletin 86, 2047-2067.

Pérez-López, A., Sanz de Galdeano, C., 1994. Tectónica de los materiales triásicos en el sector central de la Zona Subbética (Cordillera Bética). Revista de la Sociedad Geológica de España 7, 141-153.

Perri, F., Critelli, S., Martin-Algarra, A., Martin-Martin, M., Perrone, V., Mongelli, G., Zattin, M., 2013. Triassic redbeds in the Malaguide Complex (Betic Cordillera - Spain): petrography, geochemistry and geodynamic implications. Earth Science Reviews 117, 1-28.

Pettijohn, F.J., 1975. Sedimentary rocks. Harper and Brothers Publisher, New York, 3rd edition, 618 pp.

Pettijohn, F.J., Potter, P.E., Siever, R., 1973. Sand and Sandstones. Springer-Verlag, Berlin, 617 pp.

Pickup, G.E., Ringrose, P.S., Corbett, P.W.M., Jensen, J.L., Sorbie, K.S., 1995. Geology, geometry and effective flow. Petroleum Geoscience 1, 37-42.

Pimentel, N.L., Wright, V.P., Azevedo, T.M., 1996. Distinguishing early groundwater alteration effects from pedogenesis in ancient alluvial basins: examples from the Palaeogene of Portugal. Sedimentary Geology 105, 1-10.

Pittman, E.D., 1992. Relationship of porosity and permeability to various paremeters derived from mercury injection-capillary pressure curves for sandstones. AAPG Bulletin 76, 191-198.

Pittman, E.D., 2001. Estimating pore throat size in sandstones from routine core-analysis data. Search and Discovery Article 40009: http:/www.searchanddiscovery.net/documents/pittman/index.htm.

Pittman, E.D., Larese, R. E., 1991. Compaction of lithic sands: experimental results and applications. AAPG Bulletin 75, 1279–1299.

Pranter, M.J., Ellison, A.I., Cole, R.D., Patterson, P.E., 2007. Analysis and modeling of intermediate-scale reservoir heterogeneity based on a fluvial point-bar outcrop analog, Williams Fork Formation, Piceance Basin, Colorado. AAPG Bulletin 91, 1025-1051.

Pringle, J.K., Clarke, J.D., Drinkwater, N.J., Westerman, A.R. 2004. 3D high- resolution digital models of outcrop analogue study sites to constrain reservoir model uncertainty: an example from Alport Castles, Derbyshire, UK. Petroleum Geoscience 10, 343–352.

Pringle, J.K., Howell, J.A., Hodgetts, D., Westerman, A.R., Hodgson, D.M., 2006. Virtual outcrop models of petroleum reservoir analogues: a review of the current state-of-the-art. First Break 24, 33-42.

Prosser, D.J., Daws, J.A., Fallick, A.E., Williams, B.P.J., 1993. Geochemistry and diagenesis of stratabound calcite cement layers within the Rannoch Formation of the Brent Group, Murchison Field, North Viking Graben (northern North Sea). Sedimentary Geology 87, 139-164.

Purvis, K., Wright, V.P., 1991. Calcretes related to phreatophytic vegetation from the Middle Triassic Otter Sandstone of South West England. Sedimentology 38, 539–551.

Putnis, A., Mauthe, G., 2001. The effect of pore size on cementation in porous rocks. Geofluids 1, 37-41.

Pye, K., Krinsley, D.H., 1986. Diagenetic carbonate and evaporite minerals in Rotliegend eolian sandstones of the southern North Sea: their nature and relationship to secondary porosity development. Clay Minerals 21, 443-457.

Ratcliffe, K.T., Martin, J., Pearce, T.J., Hughes, A.D., Lawton, D.E., Wray, D.S., Bessa, F., 2006. A regional chemostratigraphically-defined correlation framework for the late Triassic TAG-I Formation in Blocks 402 and 405a, Algeria. Petroleum Geosciences 12, 3-12.

Richter, T.O., Van der Gaast, S., Koster, B., Vaars, A., Gieles, R., De Stigter, H., De Haas, H., van Weering, T.C.E., 2006. The Avaatech XRF core scanner: technical description and applications to NE Atlantic sediments. In: Rothwell, R.G. (Ed.), New Techniques in Sediment Core Analysis. Geological Society London, Special Publication 267, 39–50.

Richter-Bernburg, G., 1955. Statigraphische Gliederung des deutschen Zechsteins. Zeitschrift der deutschen geologischen Gesellschaft 105, 593-645.

Ringrose, P., Bentley, M., 2015. Reservoir model types. In: Ringrose, P., Bentley, M., (eds.), Reservoir model design: a practitioner's guide. Dordrecht, Springer, 173-231.

Rittenhouse, G., 1971. Mechanical compaction of sands containing different percentages of ductile grains: a theoretical approach. AAPG Bulletin 55, 92–96.

Rossi, C., Kälin, O., Arribas, J., Tortosa, A., 2002. Diagenesis, provenance and reservoir quality of Triassic TAGI sandstones from Ourhoud field, Berkine (Ghadames) Basin, Algeria. Marine and Petroleum Geology 19, 117-142.

Salem, A.M., Abdel-Wahab, A., McBride, E.F., 1998. Diagenesis of shallowly buried cratonic sandstones, southwest Sinai, Egypt. Sedimentary Geology 119, 311-335.

Salem, A.M., Morad, S., Mato, L.F., Al-Aasm, I.S., 2000. Diagenesis and reservoir-quality evolution of fluvial sandstones during progressive burial and uplift: evidence from the Upper Jurassic Boipeba Member, Recôncavo Basin, Northeastern Brazil. AAPG Bulletin 84, 1015-1040.

Sánchez-Moya, Y., Arribas, J., Gómez-Gras, D., Marzo, M., Pérez-Arlucea, M., Sopeña, A., 2004. Primera fase de rifting intracontinental Pérmico Superior-Triásico. In: Vera, J.A. (ed.), Geología de España. SGE-IGME, Madrid, 484-485.

Scarciglia, F., Pulice, I., Robustelli, G., Vecchio, G., 2006. Soil chronosequences on Quaternary marine terraces along the northwestern coast of Calabria (Southern Italy). Quaternary International 156-157, 133-155.

Schimdt, V., McDonald, D.A., 1979. The role of secondary porosity in the course of sandstone diagenesis. SEPM Special Publication 26, 209-225.

Schmid, S., Worden, R.H., Fisher, Q., 2006. Sedimentary facies and the context of dolocrete in the Lower Triassic Sherwood Sandstone group: Corrib Field west of Ireland. Sedimentary Geology 187, 205-227.

Schmid, S., Worden, R.H., Fisher, Q.J., 2004. Diagenesis and reservoir quality of the Sherwood Sandstone (Triassic), Corrib Field, Slyne Basin, west of Ireland. Marine and Petroleum Geology 21, 299–315.

Schowalter, T.T., 1979. Mechanics of secondary hydrocarbon migration and entrapment. AAPG Bulletin 63, 723-760.

Schreiber, B.C., El Tabakh, M., 2000. Deposition and early alteration of evaporites. Sedimentology 47, 215-238.

Schulz-Rojahn, J., Ryan-Grigor, S., Anderson, A., 1998. Structural controls on seismic-scale carbonate cementation in hydrocarbon-bearing Jurassic fluvial and marine sandstones from Australia: a comparaison. In: Morad, S. (ed.), Carbonate Cementation in Sandstones. International Association of Sedimentologists Special Publication 26, 327-362.

Seeman, U., 1982. Depositional facies, diagenetic minerals and reservoir quality of Rotliegend sediments in the southern Permian Basin (North Sea): a review. Clay Minerals 17, 55-67.

Sharp, J.M., Mingjuan, S., Galloway, W.E., 2003. Heterogeneity of fluvial systems; control on density-driven flow and transport. Environmental and Engineering Geosciences 9, 5-17.

Simpson, E.L., Loop, D.B., 1985. Amalgamated interdune deposits, White Sands, New Mexico. Journal of Sedimentary Petrology 55, 361-365.

Slatt, R.M., Buckner, N., Abousleiman, Y., Sierra, R., Philp, P., Miceli-Romero, A., Portas, R., O'Brien, N., Tran, M., Davis, R., Wawrzyniec, T., 2011. Outcrop/behind outcrop (quarry), multiscale characterization of the Woodford Gas Shale, Oklahoma. In: Breyer, J. (ed.), Shale reservoirs-Giant resources for the 21st century. AAPG Memoir 97, 1-21.

Smith D.G., 1987. Meandering river point bar lithofacies models: modern and ancient examples compared, in F. G. Ethridge, R. M. Flores, and M. D. Harvey, eds., Recent developments in fluvial sedimentology. SEPM Special Publication 39, 83-91.

Smoot, J.P., Castens-Seidell, B., 1994. Sedimentary features produced by efflorescent salt crusts, Saline Valley and Death Valley, California: sedimentology and geochemistry of modern and ancient Saline Lakes. In: Renaut, R.W., Last, W.M. (eds.), sedimentology and geochemistry of modern and ancient Saline Lakes. SEPM Special Publications 50, 73-90.

Sneider, R.M., 1990. Introduction: reservoir description of sandstones. In: Barwis, J.H., McPherson, J.G., Studlick, R.J. (eds.), Sandstone petroleum reservoirs. Springer-Verlag, 584 pp.

Spötl, C., Wright, V.P., 1992. Groundwater dolocretes form the Upper Triassic of the Paris Basin, France: a case study of an arid, continental diagenetic facies. Sedimentology 39, 1119-1136.

Stanley, K.O., Jorde, K., Raestad, N., Stockbridge, C.P., 1989. Stochastic modelling of reservoir sand bodies for input to reservoir simulation, Snorre Field, northern North Sea, Norway. In: Buller A.T. et al. (eds.), North Sea Oil and Gas Reservoirs II. Proceedings of the North Sea Oil and Gas Reservoirs Conference, Graham and Trotman, 91–101.

Stear, W.M., 1983. Morphological characteristics of ephemeral strem cannel and overbank splay sandstone bodies in the Permian Lower Beaufort Group, Karoo Basin, South Africa. In: Collinson, J.D., Lewin, J. (eds.), Modern and ancient fluvial systems. International Association of Sedimentologists Special Publication 6, 405-420.

Strobl, R.S., Yuan, L.P., Muwais, W.K., 1991. Reservoir geological modelling of the McMurray Formation, Alberta. Bulletin of Canadian Petroleum Geology 39, 225-225.

Suárez-Alba, J., 2007. La Mancha Triassic and Lower Lias stratigraphy, a well-log interpretation. Journal of Iberian Geology 33, 55–78.

Sullivan, M.D., Haszeldine, R.S., Boyce, A.J., Rogers, G., Fallick, A.E., 1994. Late anhydrite cements mark basin inversion: isotopic and formation water evidence, Rotliegend sandstone, North Sea. Marine and Petroleum Geology 11, 46-54.

Surdam, R.C., Boese, S.W., Crossey, L.J., 1984. The chemistry of secondary porosity. In: McDonald, D.A., Surnam, R.C. (eds.), Clastic diagenesis. AAPG Memoir 37, 127-149.

Suttner, L.J., Basu, A., Mack, G.H., 1981. Climate and the origin of quartz arenites. Journal of Sedimentary Petrology 51, 1235-1246.

Swanson, B.F., 1981. A simple correlation between permeabilities and mercury capillary pressures. Journal of Petroleum Technology 33, 2498-2504.

Sweet, M.L., 1999. Interaction between aeolian, fluvial and playa environments in the Permian Upper Rotliegend Group, UK southern North Sea. Sedimentology 46, 171-187.

Talbot, M.R., Holm, K., Williams, M.A.J., 1994. Sedimentation in low gradient desert margin systems: A comparison of the Late Triassic of northwest Somerset (England) and the Late Quaternary of east–central Australia. In: Roson, M.R. (ed.), Paleoclimate and basin evolution of playa systems. Geological Society of America Special Paper 289, 97–117.

Taylor, T.R., Giles, M.R., Hathon, L.A., Diggs, T.N., Braunsdorf, N.R., Birbiglia, G.V., Kittridge, M.G., Macaulay, C.I., Espejo, I.S., 2010. Sandstone diagenesis and reservoir quality prediction: models, myths and reality. AAPG Bulletin 94, 1093-1132.

Teles, V., de Marsily, G., Perrier, E., 1998. A new approach for modelling sediment deposition in an alluvial plain in order to display its heterogeneity. Comptes Rendus de L'Academie des Sciences Serie IIA, Earth and Planetary Sciences 327, 597-606.

Theting, T.G., Rustad, A.B., Lerdahl, T., Stensen, J.Å., Boassen, T., Øren, P.-E., Bakke, S., Ringrose, P., 2005. Pore-to-field multi-phase upscaling for depressurization. 13th European Symposium on Improved Oil Recovery, Budapest.

Tixeront, M., 1973. Lithostratigraphie et minéralisations cuprifères et uranifères stratiformes syngénétiques et familières des formations détritiques permo-triasiques du couloir d'Argana (Haut-Atlas occidental, Maroc). Notes du Service Géologique du Maroc 33, 147-177.

Tjallingii, R., Röhl, U., Kölling, M., Bickert, T., 2007. Influence of the water content on X-ray fluorescence core-scanning measurements in soft marine sediments. Geochemistry, Geophysics, Geosystems 8. Q02004.

Tourani, A., Lund, J.J., Bennaouiss, N., Gaupp, R., 2000. Stratigraphy of the Triassic syn-rift deposits in Western Morocco. In: Bacman, G.H., Larche, I. (eds.), Epicontinental Triassic, Zentralbl. Geol. Palaeontol., 1193–1215.

Tuncay, K., Ortoleva, P., 2004. Quantitative basin modeling: Present state and future developments toward predictability. Geofluids 4, 23–39.

Turner, P., Pilling, D., Walker, D., Exton, J., Binnie, J., Sabaou, N., 2001. Sequence stratigraphy and sedimentology of the late Triassic TAG-I (Blocks 401/402, Berkine Basin, Algeria). Marine and Petroleum Geology 18, 959-981.

Uphoff, T.L., 2005. Subsalt (pre-Jurassic) exploration play in the northern Lusitanian Basin of Portugal. AAPG Bulletin 89, 699–714.

Van Adrichem Boogaert, H.A., Kouwe, W.F.P., 1993. Stratigraphic nomenclature of the Netherlands; revision and update by RGD and NOGEPA. Mededelingen Rijks Geologische Dienst 50, 1-40.

Van Ojik, K., Böhm, A.R., Cremer, H., Geluk, M.C., De Jong, M.G.G., Mijnlieff, H.F., Nio, S.D., 2011. The rationale for an integrated stratigraphic framework of the Upper Rotliegend II depositional system in the Netherlands. In: Grötsch, J., Gaupp, R. (eds.), The Permian Rotliegend in the Netherlands. SEPM Special Publication 98, 37-50.

Verdier, J.P., 1996. The Rotliegend sedimentation history of the southern North Sea and adjacent countries. In: Rondeel, H.E., Batjes, D.A.J., Nieuwenhuijs, W.H. (Eds.), Geology of Gas and Oil under the Netherlands. Dordrecht, Netherlands, Kluwer Academic Publishers, 45–56.

Viseras, C., Fernández, J., 1994. Channel migration patterns and related sequences in some alluvial fan systems. Sedimentary Geology 88, 201-217.

Viseras, C., Fernández, J., 2010a. Sistemas aluviales de alta sinousidad. In: Arche, A. (ed.), Sedimentología: del proceso físico a la cuenca sedimentaria. Madrid, CSIC, 261-298.

Viseras, C., Fernández, J., 2010b. Triassic braidplain deposits and their potential as reservoir rocks. Examples from Spain and Morocco. In: Schwarz, E., Georgieff, S.,

Piovano, E., Ariztegui, D. (eds.). Sedimentology at the foot on the Andes, 18th International Sedimentological Congress, Mendoza, Argentina, p. 908.

Viseras, C., Fernández, J., Henares, S., Cuéllar, N., 2011. Facies architecture in outcrop analogues for the TAGI reservoir. Exploratory interest. AAPG Search and Discovery Article, AAPG International Conference and Exhibition, Milan, Italy, #90135.

Viseras, C., Henares, S., Fernández, J., Jaimez, J., 2013. Outcrop/behind outcrop characterization in onshore Western Mediterranean basins of Southern Iberia. AAPG European Regional Conference, April, 8-10, Barcelona, Spain, 2013. Search and Discovery Article #41175.

Viseras, C., Henares, S., Yeste, L.M., Pla-Pueyo, S., Jaimez, J., Teixido, T., Peña, J.A., 2015. Integration of outcrop and subsurface stratigraphic methods for the characterization of reservoir rocks. In: Muñoz-García, B., Martín-Chivelet, J. (eds.), Stratigraphy: New Trends. Spanish Association for Earth Sciences Teaching Special Volume 23, 192-205.

Walderhaug, O., 2000. Modeling quartz cementation and porosity in Middle Jurassic Brent Group sandstones of the Kvitebjorn field, northern North Sea. AAPG Bulletin 84, 1325–1339.

Walzebuck, J.P., 1993. Ranking of geological factors controlling the well productivity in Rotliegend Gas Field of the Dutch off-shore area. AAPG Bulletin, abstract, 77, p. 1675.

Waugh, B., 1970. Petrology, provenance and silica diagenesis of the Penrith Sandstone (Lower Permian) of northwest England. Journal of Sedimentary Petrology 40, 1226-1240.

Waugh, B., 1978. Authigenic K-feldspar in British Permo-Triassic sandstones. Journal of the Geological Society 135, 51-56.

Weber, K.J., 1986. How heterogeneity affects oil recovery. In: Lake, L.W., Carroll Jr., H.B. (eds.), Reservoir Characterization. Academic Press, Inc., 487–544.

Weibel, R., 1999. Effects of burial on the clay assemblages in the Triassic Skagerrak Formation, Denmark. Clay Mineralogy 34, 619-635.

Weltje, G.J., 2006. Ternary sandstone composition and provenance: an evaluation of the 'Dickinson model'. In: Buccianti, A., Mateu-Figueras, G., Pawlowsky-Gahn, V. (eds.), Compositional data analysis in the geosciences: from theory to practice. Geological Society of London Special Publication 264, 79-99.

Weltje, G.J., Bloemsma, M.R., Tjallingii, R., Heslop, D., Röhl, U., Croudace, I.W., 2014. Prediction of geochemical composition from XRF-core-scanner data: A new multivariate approach including automatic selection of calibration samples and quantification of uncertainties. In: Rothwell, R.G., Croudace, I.W. (eds.), Micro-XRF scanning of sediment cores. Developments in Paleoenvironmental Research (DPER) Special Publication.

Weltje, G.J., Tjallingii, R., 2008. Calibration of XRF core scanners for quantitative geochemical logging of sediment cores: Theory and application. Earth and Planetary Science Letters 274, 423-438.

Wentworth, C.K., 1922. A scale of grade and class terms for clastic sediments. The Journal of Geology 30, 377-392.

Wilson, M.D., Stanton, P.T., 1994. Diagenetic mechanisms of porosity and permeability reduction and enhancement. In: Wilson, M.D. (ed.), Reservoir quality assessment and prediction in clastic rocks. SEPM Short Course 30, 59-118.

Worden, R.H., Burley, S.D., 2003. Sandstone diagenesis: the evolution of sand to stone, in S. D. Burley and R. H. Worden, eds., Sandstone diagenesis: recent and ancient. International Association of Sedimentologists Special Publication Series 4, 3-47.

Worden, R.H., Morad, S., 2003. Clay minerals in sandstones: controls on formation, distribution and evolution. In: Worden, R.H., Morad, S. (eds.), Clay Mineral Cement in Sandstones. International Association of Sedimentologists Special Publication 34, 3-41.

Wright, V.P., 1994. Losses and gains in weathering profiles and duripans. In: Parker, A., Sellwood, B.W. (Eds.), Quantitative diagenesis: recent developments and applications to reservoir geology. NATO ASI Series, Series C: Mathematical and physical sciences 453, pp. 95-123.

Wright, V.P., Sloan, R.J., Garces, B.V., Garvie, L.A.J., 1992. Groundwater ferricretes from the Silurian of Ireland and Permian of the Spanish Pyrenees. Sedimentary Geology 77, 37-49.

Wright, V.P., Tucker, M.E., 1991. Calcretes: an introduction. In: Wright, V.P., Tucker, M.E. (eds.), Calcretes. IAS Reprint Series, vol. 2. Blackwell Scientific Publications, Oxford, 1-22.

Zaghloul, M.N., Critelli, S., Mongelli, G., Perri, F., Perrone, V., Tucker, M., Aiello, M., Sonnino, M., Ventimiglia, C., 2010. Depositional systems, composition and geochemistry of Triassic rifted-continental margin redbeds of Internal Rif Chain, Morocco. Sedimentology 57, 312-350.

Zhang, Y., Pe-Piper, G., Piper, D.J.W., 2015. How porosity and permeability vary with diagenetic minerals in the Scotian Basin, offshore eastern Canada: implications for reservoir quality. Marine and Petroleum Geology 63, 28-45.

Ziegler, P.A., 1990. Geological Atlas of Western and Central Europe, Second Edition. Geological Society of London, 239 pp.

Zuffa, G.G., 1980, Hybrid arenites: their composition and classification. Journal of Sedimentary Petrology 50, 21-29.

Zuffa, G.G., 1985. Optical analyses of arenites: influence of methodology on compositional results. In: Zuffa, G.G. (ed.), Provenance of Arenites. NATO-ASI Series, Redsel Publishing Company, Dordrecht, Netherlands, 165-189.

Zuffa, G.G., 1987. Unravelling hinterland and offshore palaeogeography from deep-water arenites. In: Legget, J.K., Zuffa, G.G. (eds.), Deep-marine clastic sedimentology: concepts and case studies. Graham and Trotman, London, 39-61.

ACKNOWLEDGEMENTS

del mundo que ha enriquecido sin duda la mía y su inestimable consejo en temas de software sin los cuales esta tesis hubiese sido mucho más difícil.

A MI FAMILIA. Gracias, Gracias y Gracias. A mis padres Saturnina y Manuel que han creído en mi desde el primer momento y me han apoyado incondicionalmente en todos los aspectos de mi vida. A mi hermana Carmen que ha sido mi más fiel compañera durante estos largos y duros últimos cuatro años. A mi tía Carmen y mi primo Javi por su ayuda tanto personal como "técnica" en los momentos necesarios. Y, en general, a todos los que formáis parte del núcleo que me ha sostenido desde mi niñez hasta el día de hoy.

Y, como se suele decir, por último pero no menos importante, a ti, Luca, mi compañero, mi colega, mi amigo, mi guía, mi inspiración, el amor de mi vida. Gracias por los mejores años en los que me has ayudado a mejorar como científica con tu experiencia, ayuda y consejo, y como persona con tu apoyo absoluto día tras día. Gracias por creer en mí y ser mi roca.

Universidad
de Granada

Programa Doctorado
Ciencias de la Tierra

SEDIMENTARY
RESERVOIRS
WORKGROUP